Coupling the mechanics and energetics of bird and insect flight

Alexander Nicholas Evans

Submitted in accordance with the requirements for the degree of
Doctor of Philosophy

The University of Leeds
School of Biomedical Science
Faculty of Biological Sciences

May 2018

Intellectual property statements

The candidate confirms that the work submitted is his own and that appropriate credit has been given where reference has been made to the work of others.

This copy has been supplied on the understanding that it is copyright material and that no quotation from the thesis may be published without proper acknowledgement.

Declaration

In Chapter 2, the optimal muscle length changes and electrical stimulation parameters for in vitro mechanical power generation by the mouse soleus were provided by GA.

In Chapter 3, the budgerigar pectoralis muscle length changes and activity patterns during flight were determined in vivo across a range of flight speeds and provided by GA.

In Chapter 4, the avian accelerometer harness was designed and constructed in collaboration with Saul Avery (SA), who also assisted with the accelerometry experiments. SA also helped to develop the analytical approach for the data analysis and extracted the video-derived kinematic data discussed in this chapter.

In Chapter 5, the glycerol extracted *Lethocerus indicus* carcasses were provided by Belinda Bullard, University of York.

Acknowledgements

Firstly, I would like to thank Dr Graham Askew for his supervision and support through this project; I have learned so much and gained experience in a variety of new and exciting techniques. I'd also like to thank Prof Stuart Egginton for additional support through my transfer stages and guidance through the rest of my PhD.

Thank you to everyone in the Askew lab, especially Dr Laura McFarlane, Dr Thomas Neil and Dr Roger Kissane, as well as honorary lab members Dr Yazi Al'joboori and Dr Pip Warren, for their help all throughout my PhD. Additional thanks to the online science community, and especially to Dr Michelle Reeve for her help and support through the final months of the project.

Special thanks to my parents and sister, as well as Sharon and Chris, for their encouragement and support. Thanks most of all to Ellie for her unwavering support during my PhD; it's been a long and bumpy road and I couldn't have crossed the finish line without her.

Thanks to Neil, Stan and the rest of the CBS staff for taking care of the birds. Finally, I owe enormous thanks to all the animals I have worked with during my PhD; this project would not have been possible without them.

Dedicated to Conor.

"Birds don't just fly, they fall down and get up. Nobody learns without getting it wrong." -- Shakira*, Try Everything*

Abstract

Humanity has long been fascinated by the mysteries of bird and insect flight, but only recently have we developed the technologies required to understand the complex mechanisms at work. These mechanisms range from molecular interactions to the interactions between whole organisms, encompassing a great number of mechanical and energetic processes. Research into animal flight has made great progress over the past half-century thanks to developments in technology and methodology, allowing for greater insights into the metabolic, mechanical and aerodynamic processes central to animal flight. Currently, there is a good understanding of several of these components but the topic of animal flight has been explored with a rather piecemeal approach and a more integrative understanding of the mechanics and energetics of animal flight is required. The research presented in this thesis aims to bridge our understanding of the often separately analysed mechanical and energetic aspects of animal flight and address key gaps in the existing knowledge.

Many volant bird species exhibit asymmetrical wingbeat cycles such that the flight muscles spend relatively more time shortening than lengthening. Through the simultaneous determination of mechanical work generation and energy consumption in the mouse soleus during in vitro contraction cycles with asymmetrical length trajectories, we reveal that mechanical power production can be increased by increasing the proportion of the cycle spent shortening without sacrificing net muscle efficiency. These experiments also served to validate a methodology for estimating the net muscle efficiency of the avian pectoralis muscle.

The following experiments determined the mechanical power generation, muscular costs of contraction and muscle efficiency of the budgerigar pectoralis during a range of simulated flight speeds. The efficiency of avian flight muscle was previously unknown and unsubstantiated values had been used in common predictive models of flight energetics. It was found that avian

flight muscle efficiency is approximately 21% during the downstroke and remains constant with flight speed, with muscular energy consumption and power generation sharing characteristics with whole-animal metabolic and mechanical power-speed relationships. The consequences of these findings for the estimation of energetic flight costs are discussed.

While respirometry serves as the gold standard for measuring metabolic expenditure during activity, accelerometry affords the potential for estimating the energetic costs of flight in birds in the field. However, there has been no calibration of the relationship between body acceleration and energy expenditure. By measuring energy consumption via respirometry and dynamic body acceleration in masked lovebirds during wind tunnel flights at a range of speeds, we determine the metabolic requirements of flight for a new avian species and validate the use of accelerometry for estimating energy expenditure and flight kinematics.

Finally, we examined the previously unexplored relationship between myoplasmic calcium ion concentration, contraction frequency, mechanical power and myofibrillar efficiency in asynchronous insect flight muscles. There is increasing evidence to suggest that calcium plays an important role in the modulation of mechanical power during flight in insects with asynchronous flight muscles. By simultaneously measuring mechanical power generation and ATPase activity of flight muscles from giant waterbugs (*Lethocerus*), we reveal a positively shifting relationship between increasing calcium concentrations and optimal frequency for generating power, but with no evidence of a shift in optimal frequency for muscle efficiency.

This research demonstrates scientific impact by improving our understanding of the factors that affect muscle efficiency, refining the models used to predict wild animal metabolism during flight, developing and validating existing experimental techniques for determining the costs of flight, and improving our understanding of how both mechanical and physiological factors can affect the mechanical and energetic performance of bird and insect flight muscles.

Table of Contents

List of Tables

List of Figures

List of Appendices

List of Abbreviations

A	Muscle activating solution containing Ca^{2+}
$A_\%$	Diluted activating solution containing a percentage of A
ADP	Adenosine diphosphate
α	Wingspan
ANOVA	Analysis of variance test
ATP	Adenosine triphosphate
ATPase	Class of enzymes that catalyse the decomposition of ATP
$ATPase_{extra}$	Rate of ATP consumption above $ATPase_{iso}$ during oscillations
$ATPase_{iso}$	ATP consumption under isometric conditions
$ATPase_{gross}$	Rate of ATP consumption during oscillations
BMR	Basal metabolic rate
BP	Barometric pressure
C	Curve coefficient
Ca^{2+}	Calcium ion
$[Ca^{2+}]$	Calcium ion concentration
CO_2	Carbon dioxide
DA	Dynamic acceleration
DAx, DAy, DAz	Dynamic acceleration in x, y and z axes
D	Total aerodynamic drag
ΔO_2	Change in oxygen content before and after work-generating contraction cycles
D_{ind}	Induced aerodynamic drag
DLM	Dorsal longitudinal muscle
DLW	Doubly-labelled water method

D_{par}	Parasite aerodynamic drag
PIV	Particle Image Velocimetry
D_{pro}	Profile aerodynamic drag
E	Extinction coefficient for NADH at 340 nm
EE	Energy expenditure
ε_i	Initial mechanical efficiency
ε_{fm}	Mechanical efficiency of the avian pectoralis muscle
EMG	Electromyography
EO_2	Energetic equivalent of oxygen consumed during oxidative phosphorylation
ε_{net}	Net mechanical efficiency
η_{net}	Net thermodynamic efficiency
η_{app}	Apparent myofibrillar efficiency
η_{fm}	Thermodynamic efficiency of the avian pectoralis muscle
η_{gross}	Gross myofibrillar efficiency
F_0	Calcium-activated force
F_e	Incurrent airflow into respirometry mask
FG	Fast glycolytic
F_i	Excurrent flow out of respirometry mask
FOG	Fast oxidative-glycolytic
$f\mathrm{H}$	Heart-rate
FFT	Fast Fourier transformation
F_{SA}	Stretch-activated force
G	Gibb's free energy
g	Acceleration due to the Earth's gravity (9.80665 m s^{-2})
GLM	Generalized linear model

I_0	Intensity of the 340 nm beam with no NADH present
I_t	Intensity of the 340 nm beam at time t
IFM	Insect flight muscle
l	Light-beam path length
L	Length
LDH	Lactate dehydrogenase
L_0	Optimal length generating maximum twitch or tetanus force
LDH	Lactate dehydrogenase
k_{pos}	Postural costs of flight
M_m	Muscle mass
M_b	Body mass
MC	Mechanochemical coefficient
MC_{app}	Apparent mechanochemical coefficient using $ATPase_{extra}$
MC_{gross}	Gross mechanochemical coefficient using $ATPase_{gross}$
n	Sample size
NAD^+	Oxidised nicotinamide adenine dinucleotide
NADH	Reduced nicotinamide adenine dinucleotide
O_2	Oxygen
ODBA	Overall Dynamic Body Acceleration
P	Force
P_{mech}	Mechanical power
P_{met}	Metabolic power
$P_{met,pec}$	Metabolic power of the pectoralis
P_0	Maximum isometric force
P_i	Inorganic phosphate
pCa	Negative base-10 logarithm of the calcium concentration

PCr	Phosphocreatine
PEP	Phosphoenolpyruvate
pH	Negative base-10 logarithm of the hydrogen concentration
PK	Pyruvate kinase
PO_2	Partial pressure of oxygen
q	Quantity of NADH
R_0	Intensity of the reference beam with no NADH present
R_t	Intensity of the reference beam at time t
ρ	Density of muscle
Q_{10}	Temperature coefficient
SA	Static acceleration
Saw%	Sawtooth contraction cycle with a percentage of the contraction cycle spent shortening
SEM	Standard error of the mean
SO	Slow oxidative
SP	Standard pressure
SR	Sarcoplasmic reticulum
RER	Respiratory exchange ratio
RFD	Relative flapping duration
RFD_{acc}	Accelerometer-derived relative flapping duration
RFD_{vid}	Video-derived relative flapping duration
RMR	Resting metabolic rate
RQ	Respiratory quotient
t	Time
T	Temperature
T_a	Ambient temperature

T_b	Body temperature
T_s	Standard temperature
V	Velocity
V_{act}	Actual airflow velocity
VeDBA	Vectorial Dynamic Body Acceleration
V_{std}	Standard airflow velocity
$\dot{V}_c$	Corrected airflow velocity
$\dot{V}CO_2$	Volumetric rate of carbon dioxide production
$\dot{V}O_2$	Volumetric rate of oxygen consumption
$\dot{V}_u$	Uncorrected airflow velocity
V_{sol}	Volume of solution in the insect flight muscle chamber
W_{net}	Net mechanical work
W_{short}	Shortening work
Wf	Wingbeat frequency
Wf_{acc}	Accelerometer-derived wingbeat frequency
Wf_{vid}	Video-derived wingbeat frequency
WTS	Wingtip spacing
WTS_{opt}	Optimal wingtip spacing for upwash exploitation
WVP	Water vapour pressure

Chapter 1
General introduction

Locomotion is an important and often essential activity for animal life, and in order to move through the Earth's environments, animals have evolved a range of anatomical, physiological and behavioural adaptations that suit the requirements of their ecological niche. Driven by processes of natural and sexual selection, these adaptations commonly include specialised anatomical structures that enable organisms to move through different physical media such as air, earth and water. The ability for animals to fly requires a great number of adaptations but ultimately provides a powerful means of traversing their environment, whether to hunt prey, escape predators, locate reproductive mates or migrate to different climates.

To fully understand all aspects of animal flight, there are four main areas of research to be considered: biomechanics, aerodynamics, energetics and behavioural ecology. Biomechanics concerns the anatomical systems that allow mechanical motion in biological systems, aerodynamics concerns the consequences of moving through physical media, energetics concerns the translocation and transformation of energy, and behavioural ecology concerns the natural and sexual selective pressures and environmental interactions that influence the ability of animals to move. Each of these areas are integrally linked and we can only fully comprehend the whole picture by working towards an integrated and unified understanding of these topics.

1.1 The structure and function of flight muscles

While some animals exhibit passive flight mechanisms that harvest the energy required to stay airborne from the environment, the majority of volant animal species actively produce their own momentum through the force-generating contractions of striated muscle.

1.1.1 Structure of striated muscle

Striated muscles consist of numerous muscle fascicles contained within the epimysium, a fibrous tissue envelope. These fascicles consist of bundles of muscle fibres contained within the sarcolemma, a plasma membrane. These muscle fibres consist of myofibrils interspersed with mitochondria and sarcoplasmic reticulum (SR). The myofibrils consist of overlapping thick and thin filaments, which produce the striated appearance of the muscle under a microscope (Huxley, 1969).

The thick and thin filaments within the myofibrils constitute the contractile apparatus of the muscle, responsible for making up the individual contractile units called sarcomeres. The thick filament consists largely of myosin, a complex protein composed of two heads and a tail domain, whereas the thin filament largely consists of three proteins: actin, troponin and tropomyosin (Huxley, 1969, Barclay, 2015). Each myosin head possesses two important binding sites; one for ATP and one for actin.

1.1.2 Excitation-contraction coupling

For vertebrate striated muscle, excitation-contraction coupling is the principle process of instigating muscle activation. This occurs when the membranes of muscle cells become depolarised and generate action potentials that enter the muscle fibre's network of transverse tubules (T-tubules). Depolarisation of the T-tubules prompts the release of calcium ions (Ca^{2+}) from the SR into the myoplasm. Myoplasmic Ca^{2+} binds to the troponin-C subunit of the troponin molecule on the thin filament and produces conformational changes in the troponin and tropomyosin molecules. These changes expose binding sites for the myosin heads to attach to actin which allows cross-bridges to form, producing muscular contraction and generating force (Woledge et al., 1985). These contractions may occur with no change in muscle length (isometric), or may occur during muscle shortening (concentric) or muscle lengthening (eccentric) (Fenwick et al., 2017).

In the absence of activation, Ca^{2+} is actively pumped back into the SR, which causes the troponin and tropomyosin proteins to undergo conformational changes and block the binding sites, which inhibits cross-bridge formation and detaches the thin and thick filaments. This causes the muscle to relax and brings about a decline in force (Woledge et al., 1985). The ability of the SR to bring about rapid changes in intracellular Ca^{2+} and act as a 'switch' for modulating muscle force is crucial for vertebrate muscle contraction.

1.1.3 Cross-bridge cycling

According to the widely accepted "sliding filament" theory of muscle contraction (Huxley, 1969), the generation of muscular force is the result of molecular cross-bridges repeatedly forming and disassociating between the thick and thin filaments. During muscle shortening, the myosin heads projecting from the thick filaments briefly attach to active binding sites on the actin molecules situated on the thin filaments that are exposed in the presence of Ca^{2+} during calcium cycling. This forms a cross-bridge that undergoes a "power stroke" and exerts a force which slides the thin filaments over the thick filament (Smith et al., 2005). During this process, adenosine triphosphate (ATP) is bound to the myosin head and is hydrolysed into adenosine diphosphate (ADP) and inorganic phosphate (Pi), which releases the energy required for the power stroke. When ATP binds to a myosin head, it detaches from actin, freeing the myosin head and allowing it to bind to a new actin molecule. This brings the cross-bridge cycle back to the starting position and ready to begin the next cycle.

1.1.4 Energetic costs of contraction

The generation of force by the muscles requires the energy released by ATP hydrolysis. ATP is the only energy source capable of directly fuelling cross-bridge cycling and calcium cycling due to the ATP-specific binding sites on the myosin heads and the SR Ca^{2+} pumps (Barclay, 2017). Despite this critical need for ATP, myoplasmic concentrations of ATP are relatively low. For example, the myoplasmic ATP concentration within the human quadriceps is

~8 mM (Kemp et al., 2007), but the average rate of ATP turnover during knee-extension exercise is ~24 mM min^{-1} (Cannon et al., 2014), meaning that ATP must be rapidly regenerated in order to sustain the exercise beyond short bouts. To fuel this ATP resynthesis, phosphocreatine (PCr) serves as a store of high-energy phosphates for recycling the hydrolysed ATP and is found at myoplasmic concentrations approximately four-fold greater than ATP (Barclay, 2015).

The majority of the energy required for muscle contraction is consumed in the form of ATP during cross-bridge cycling (Barclay, 2017) but the cycling of calcium in and out of the SR also represents a significant energetic investment and can consume up to 30-40% of the total energetic costs of muscle contraction (Barclay, 2015).

1.1.5 Muscle fibre type

Depending on the physical requirements of the muscle tissue, the composition of the muscle fibres and distribution of blood vessels within the muscle will differ to suit those requirements. Typically, these types of fibres are differentiated into three categories based on their relative densities of myoglobin, mitochondria and capillaries, as well as their contraction times, fatigue resistance, oxidative capacity and ability to generate force (Rosser and George, 1986). These three major fibre types are referred to as slow oxidative (SO / Type 1), fast oxidative-glycolytic (FOG / Type 2a) and fast glycolytic (FG / Type 2b).

The pectoralis muscle of small bodied birds with high frequency wingbeats tend to consist exclusively or predominantly of FOG fibres (Rosser and George, 1986, Welch and Altshuler, 2009) while larger birds that regularly use passive flight strategies, such as soaring and gliding, tend to have relatively high proportions of SO fibres in their pectoralis (Rosser and George, 1986, Rosser et al., 1994). The fibre type of the wing muscles (e.g. biceps, triceps) may be more heterogeneous to fit a wider variety of roles than the pectoralis

and supracoracoideus muscles, but there is a lack of data concerning these muscles (Welch and Altshuler, 2009).

1.1.6 Insect flight muscles

In contrast to vertebrate locomotor muscles, insect locomotor muscles have no internal endoskeleton for attachment and a chitinous exoskeleton acts as the attachment framework for the flight musculature (Vigoreaux, 2007). Cuticular ingrowths called apodemes serve as attachment sites for locomotor muscles and phragma are the specialised apodemes for anchoring insect flight muscles. Apodemes in locusts have been found to be stronger and stiffer than vertebrate tendons, but also capable of substantial elastic energy storage when stretched (Bennet-Clark, 1975).

There are two major distinct types of insect flight muscle (IFM): direct and indirect. Direct IFMs are only present in the Paelaeopterans, which includes the mayflies, dragonflies and damselflies. Direct IFMs are antagonistic pairs of vertical muscles that insert directly at the hinged wing bases. During contraction of the elevator muscles, the wing bases are pulled down in order to lift the wings upwards, while contraction of the depressor muscles pulls the wings downwards. All other winged insects, collectively called the Neopterans, possess indirect IFMs. Instead of attaching directly to the basal structure of the wings, indirect IFMs are antagonistic pairs of vertical (tergosternal) and horizontal (dorsal longitudinal) muscles that contract in turn to deform the thoracic cavity. As the wings are an extension of the exoskeleton, these thoracic deformations move the wings (Figure 1.1).

1.1.6.1 Asynchronous flight muscles

The flight muscles of many insect species can contract repeatedly at incredibly high frequencies, reaching even as high as 1000 Hz in midges (*Forcipomyia*) (Sotavalta, 1953). While synchronous muscles contract in a 1:1 ratio with neural impulses, asynchronous muscles can contract and relax multiple times per neural impulse (Josephson et al., 2000a). Asynchronous muscles are also referred to as "fibrillar" muscle in the literature due to their conspicuously large

and readily separable myofibrils (Pringle, 1977). Instead of relying on electrical stimulation to initiate contraction, asynchronous muscles utilise stretch-activation and shortening-deactivation in order to generate delayed force at a rapid rate (Glasheen et al., 2017). Interestingly, while asynchronous IFM is capable of incredibly rapid contractions, it is classed as a "slow" muscle type due to its cellular composition and slow-twitch isometric properties (Josephson et al., 2000a).
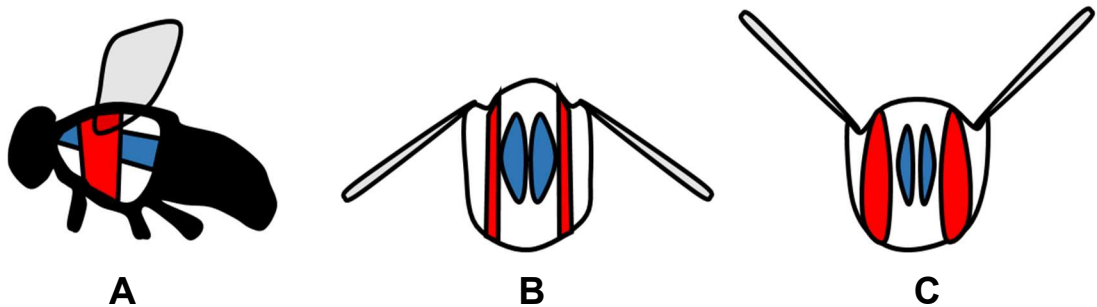
Figure 1.1 **Diagram of indirect power-generating insect flight muscles.** Vertical muscles indicated in red and horizontal muscles in blue. (A) Sagittal view of insect with a focus on the thoracic cavity. (B) Indirect IFMs at peak downstroke. (C) Indirect IFMs at peak upstroke. Adapted from Hill et al., 2012.

1.2 Muscle mechanics

1.2.1 Force, work and power

The mechanical force generated by a muscle depends on the number of cross-bridges formed and maximal force can be achieved at sarcomere lengths with an optimal overlap between thick and thin filaments (Gordon et al., 1966). Mechanical work is calculated as the product of force generated and length change undergone by the muscle during contraction. Mechanical power (P_{mech}) is the rate of work generation per second and is a commonly used determinant of muscle performance in comparative biomechanics and energetics. The mechanical power generated over the course of a contraction cycle represents the net sum of the power generated during muscle shortening and lengthening, which can be determined separately to better understand the functional role of the muscle (Holt and Askew, 2012).

1.2.2 Isometric force properties

Muscles contract isometrically when their sarcomeres shorten during contraction without undergoing an overall length change (Gordon et al., 1966, James et al., 1996). The isometric properties of a muscle can be determined in vitro by the analysis of twitch and tetanus forces. When a brief electrical stimulus is applied to a muscle held at constant length, force will quickly rise in a "twitch" contraction and then fall back to a resting level. If multiple stimuli are applied rapidly, the muscle will contract maximally in a tetanic contraction and force will reach a plateau before falling to a resting level. The force-generating and temporal properties of these isometric contractions can reveal a lot of information about the physical performance of the muscle and are often used to determine muscle fibre quality and assess power-generating performance during in vitro experiments (James et al., 1996, Askew and Marsh, 1997).

1.3 Flight muscle energetics

In accordance with the laws of thermodynamics, the generation of mechanical work by locomotor muscles requires the transformation of chemical energy into kinetic energy (Kleiber, 1961, Kushmerick and Davies, 1969). Understanding the chain of energy transformations required for powered flight is essential for determining the role of metabolic changes in major ecological facets of bird and insect life, such as the energy requirements to undergo activities such as migration and reproduction, as well as predicting energy-efficient speeds and styles of flight. The metabolic rate of an organism during flight represents a summary of all the underlying metabolic processes at work, but much of this metabolic energy expenditure is likely to reflect the energy consumed by the locomotor muscles as they contract and produce the forces that drive locomotion (Ellerby et al., 2005).

The process of converting chemical energy from metabolic fuel into useful mechanical work in the environment can be broken down into a number of underlying steps (Figure 1.2). At each stage, energy is lost due to inefficiencies in the energy transfer mechanisms and the overall efficiency of locomotion is

determined by the efficiencies of each of the underlying steps. In avian flight, several components of the energy transduction chain have been studied. For example, whole-animal flight energy expenditure (Tucker, 1972, Ward et al., 2004, Morris et al., 2010) and the mechanical performance of the major flight muscles (Biewener et al., 1992, Dial et al., 1997, Askew and Ellerby, 2007) have been studied in a range of bird species and the transfer of mechanical energy to the environment has been quantified (Spedding, 1987b, Hedenström et al., 2006, Warrick et al., 2012), but wholly integrative studies are currently lacking.
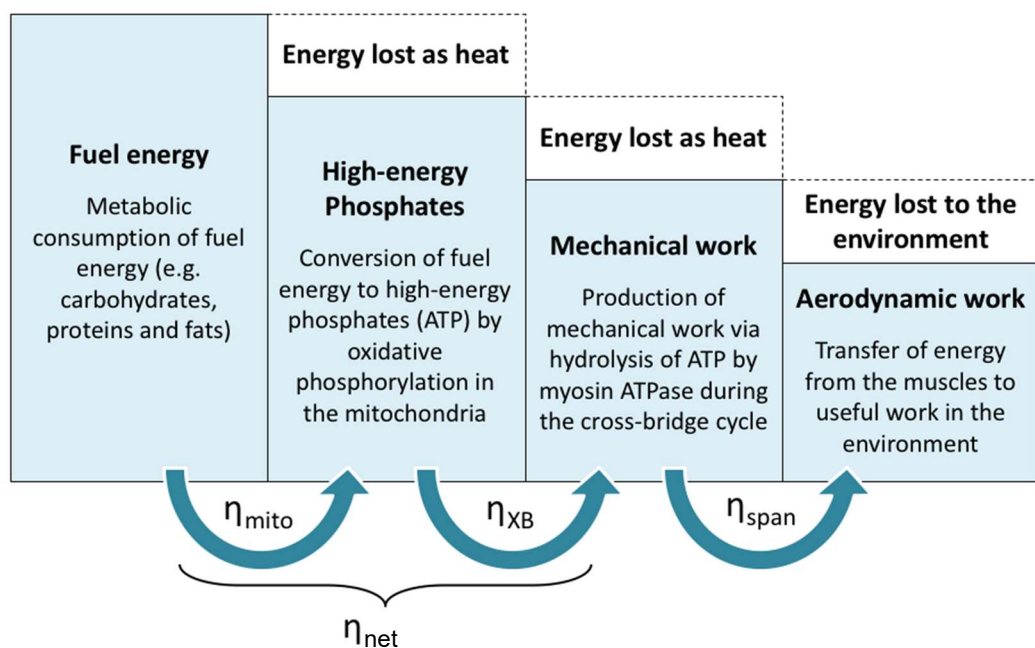
Figure 1.2 **Energy transduction chain during animal flight.** η_{mito} is the mitochondrial efficiency, η_{XB} is the cross-bridge efficiency and η_{span} is the span or aerodynamic efficiency. The product of η_{XB} and η_{mito} is the net muscle efficiency (η_{net}).

1.4 Muscle efficiency

The mechanics and energetics of locomotor muscles are tightly linked by the mechanochemical conversion of energy. Generally speaking, locomotor muscles are thermodynamically inefficient machines that convert only a small amount of the available metabolic energy to useful work and releasing the rest as heat (Smith et al., 2005). A small amount of this energy is inevitably lost

due to entropy but the majority of the remaining available energy (G, Gibb's free energy) that is lost is due to inefficiencies in the force-generating and recovery processes within the muscle.

There are many definitions of muscle efficiency that refer to different thermodynamic, biochemical or mechanical aspects of muscular work generation, but the "net" muscle efficiency is one of the definitions most valuable to whole animal locomotion studies as it represents the proportion of available metabolic energy that is successfully transferred to mechanical power by a muscle (Equation 1.1).

$$\eta_{net} \approx \varepsilon_{net} = \frac{P_{mech}}{P_{met}} \qquad [1.1]$$

where η_{net} is net thermodynamic muscle efficiency (work / G), ε_{net} is the net mechanical muscle efficiency (work / total enthalpy), P_{mech} is the rate at which work is undergone by the locomotor muscles and P_{met} is the rate at which fuel energy is consumed (Norberg, 2002). Net efficiency values include the costs of recovery metabolism but exclude the costs of resting metabolism (Smith et al., 2005). While η_{net} represents the true ratio between work generation and energy consumption, changes in G cannot be measured directly from intact muscle, but ε_{net} should be similar to η_{net} because the G (2810 KJ mol^{-1}) and enthalpy (2870 KJ mol^{-1}) of glucose oxidation are approximately equal (Gibbs and Barclay, 1995, Barclay and Weber, 2004, Smith et al., 2005), allowing ε_{net} to be measured experimentally in intact muscle fibres.

1.4.1 Experimental estimates of muscle efficiency

There are two popular methods of determining the muscle efficiency of isolated muscle tissue. Both methods involve the measurement of mechanical work production and the simultaneous measurement of muscular energy expenditure; either by the oxygen consumed by the muscle during oxidative metabolism (Heglund and Cavagna, 1987, Josephson and Stevenson, 1991, Harwood et al., 2002) or by the heat produced as a result of thermodynamic

processes (Curtin and Woledge, 1996, Barclay and Weber, 2004, Holt and Askew, 2012).

1.4.2 Factors affecting muscle efficiency

The efficiency of muscle has been found to be affected by a range of contractile factors. Reduced muscle efficiencies have been observed when oscillating muscles are subjected to sub-optimal strains (Curtin and Woledge, 1993, Barclay, 1994) and frequencies (Askew et al., 2010, Holt and Askew, 2012). Interestingly, Barclay and Weber (2004) observed that while a slow-twitch muscle from a mouse hindlimb had a greater initial mechanical efficiency than a fast-twitch muscle, there was no difference in the net efficiency. Temperature has predominately been found to have very little effect on the efficiency of isolated muscle preparations in mammals (Barclay et al., 2010) and amphibians (Gibbs and Chapman, 1974), but a study by Seebacher et al. (2014) did observe higher energetic costs per unit of work performed by isolated *Xenopus laevis* at 15 °C compared to 25 °C, suggesting that muscle efficiency may not be independent of temperature in all cases. Differences in experimental methodology may also play a role in these discrepancies.

1.4.3 Avian flight muscle efficiency

Almost nothing is currently known about the efficiency of avian flight muscles, and previous studies of whole-animal flight energetics and aerodynamic power requirements have assumed values that range anywhere between 10% and 25% (Biewener, 1998, Rayner, 1999, Ward et al., 2001). If flight muscle efficiency is constant across different flight speeds, then metabolic power should equal a fixed multiple of mechanical power (Norberg, 1996). However, (Morris et al., 2010) presented evidence from whole-organismal metabolism to suggest the pectoralis muscle efficiency of cockatiels (*Nymphicus hollandicus*) may change as a factor of flight speed. They predicted an approximately U-shaped relationship with estimated flight muscle efficiencies between 6.9% (recorded at 8 m s^{-1}) and 11.2% (recorded at 13 m s^{-1}). This partly agrees with Rayner's aerodynamic theory (1999), which predicted that muscle efficiency

would increase linearly with flight speed, but more informed estimates of avian muscle efficiency are currently lacking.

1.5 Aerodynamics of avian flight

The aerodynamic principles that permit birds to fly consist of complex physical interactions between animals and their environmental medium. These interactions have been examined both theoretically and experimentally to improve our understanding of animal flight.

1.5.1 Aerodynamic modelling

The fundamental aerodynamic forces generated for avian flight are "thrust" to overcome drag and propel the bird forwards, and "lift" to overcome the bird's mass and keep the bird airborne. The generation of these forces requires a significant amount of mechanical power output (P_{mech}) from the major flight muscles. The mechanical power requirements for flight can be calculated using aerodynamic models (Equation 1.2).

$$P_{mech} = DV \qquad [1.2]$$

where D is the total drag on the bird and V is the flight velocity (Pennycuick, 1968a). The total drag generated during flight is comprised of three constituent measures (Equation 1.3).

$$D = D_{ind} + D_{par} + D_{pro} \qquad [1.3]$$

where D_{ind}, D_{par} and D_{pro} represent lift-induced drag, parasite drag and profile drag respectively. In order to overcome these aspects of drag, P_{mech} also comprises of three measures: parasite power to overcome drag on the body, profile power to overcome drag on the wings and induced power to transfer air in a downwash in order to produce lift and thrust (Pennycuick, 1968a, Rayner, 1979a). From these measures, it is possible to produce a theoretical mechanical power curve that represents the total power required for flight as a

factor of flight speed (Figure 1.3). When each coefficient is plotted individually as a factor of speed, it is clear that induced power is highest when at low speeds and reduces rapidly with increasing speed due to increased air movement around the wing which reduces the power required for lift (Alexander, 2002). In contrast, profile and parasite power are both lowest when stationary and increase gradually with increasing speed in response to increased drag on the wings and body respectively (Ellington, 1991). When combined, the expected mechanical power curve produces a U-shape with the highest power required at low and high flight speeds (Rayner, 1982).
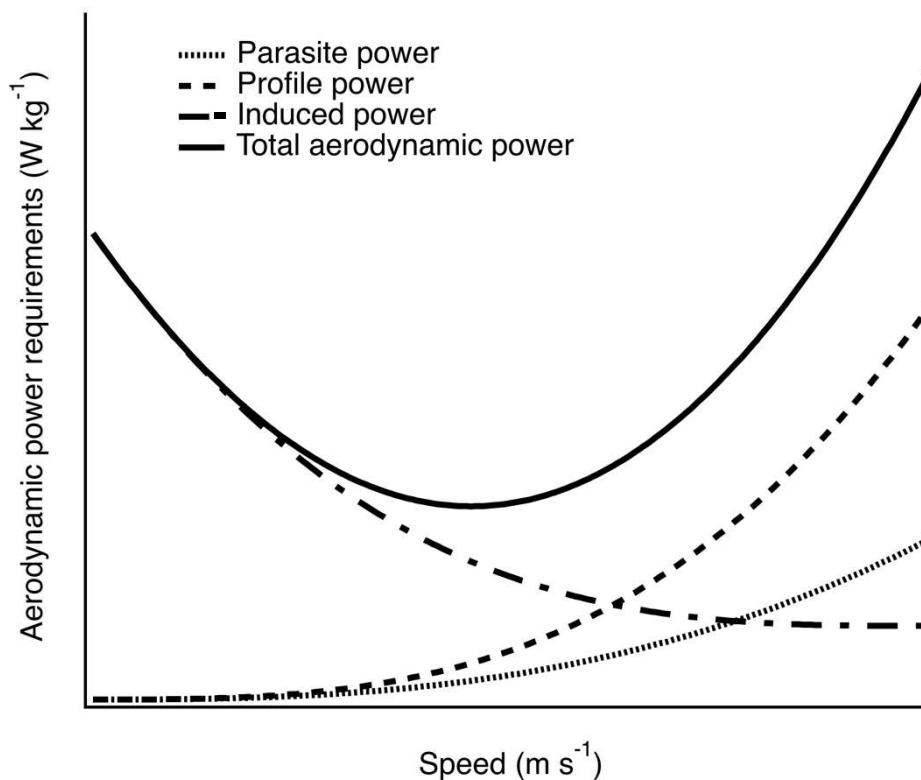
Figure 1.3   Theoretical aerodynamic power requirements. Total aerodynamic power and the three constituent parts: parasite, profile and induced power. Adapted from Rayner (1999).

1.5.1.1 Wake structure analysis

The wake structure produced by the movement of the air during flight is an important aspect of quantifying the energy transfer from the organism to the environment to produce momentum. The efficiency with which mechanical

work is transferred into useful aerodynamic work is known as span efficiency, and this is an area in which little work has been done. Limited span efficiency estimates have been produced for birds including pied flycatchers (*Ficedula hypoleuca*) and blackcaps (*Sylvia atricapilla*) (Muijres et al., 2012) but further studies combining physiological mechanical power estimates and wake structure analysis could reveal more information about the factors affecting span efficiency.

Rayner (1979b) was one of the first to use aerodynamic theory to predict that different flight styles and speeds would produce different wake structures in birds. Following on from these theoretical studies, the first series of empirical wind-tunnel experiments by Spedding (1986, 1987a, b) were significant in visualising the wake structures produced by jackdaws (*Corvus monedula*) and kestrels (*Falco tinnunculus*) at different flight speeds and styles. As predicted by Rayner's aerodynamic calculations (Rayner, 1979b), it was shown that there were characteristically different flight "gaits" for gliding and flapping flight, as well as for slow and fast flight. The wake produced by gliding flight was accurately predicted by fixed-wing lifting-line theory (Rayner, 1979b), characterised by a bound vortex around the wing, where air circulated around the wing edge and becoming a "horseshoe vortex" at the wingtips (Beaufrere, 2009). Also in accordance with aerodynamic theory, slow flapping flight was found to generate discontinuous ring vortices due to the inactive upstroke phase, while medium and fast flapping flight was found to generate a pair of continuous undulating wingtip vortices due to the active upstroke (Norberg, 2002).

Spedding's basic wake visualisation experiments used helium-filled soap bubbles and flash photography to produce visual patterns of the vortex wakes (Spedding, 1986), while more recent advancements in technology over the past two decades have allowed researchers to study the intricate vortex wakes of bird flight in more detail through Particle Image Velocimetry (PIV) (Spedding et al., 2003, Hedenström et al., 2006, Warrick et al., 2012). When used in tandem with mechanical power output measurements, PIV can be used to

measure the proportion of energy transferred to the environment in order to estimate span efficiency. In the past two decades, PIV has been used to visualise vortex wakes in thrush nightingales (*Luscinia luscinia*) (Spedding et al., 2003) and robins (*Turdus migratorius*) (Hedenström et al., 2006), revealing that in contrast to the discrete flight gaits recorded for kestrels, these species appeared to have a more gradual transition between flight styles.

1.6 Biomechanics of avian flight

1.6.1 Flight muscle mechanics

The biomechanics of flight are integrally linked to the production of mechanical power by the flight muscles (Biewener, 2011). In birds, the pectoralis muscle is the primary source of the power required for flight, accounting for approximately 16% of a bird's body mass and contributing the power for the downstroke phase during flight by performing cyclical contractions and depressing the wing bones at the shoulder (Greenewalt, 1975). In comparison, the supracoracoideus muscle contributes the power required for the upstroke phase and makes up approximately 2% of a bird's body mass (Greenewalt, 1975). The remaining wing muscles, such as the biceps and triceps, modify the shape and angle of the wings during flight for stability and kinematic flexibility (Biewener, 2011).

1.6.2 Mechanical power requirements of avian flight

The mechanical power requirements of flight have been calculated using theoretical aerodynamic models (Rayner, 1999) and estimated empirically through indirect metabolic rate estimations (Tucker, 1966), estimates of force production (Biewener et al., 1992, Dial and Biewener, 1993, Dial et al., 1997) and measurements of dynamic pressure (Usherwood et al., 2003, Usherwood et al., 2005). As mechanical work is the product of muscle length change and force production, several methods have been developed to measure these factors both in vivo and in vitro to estimate the mechanical power requirements of flight.

1.6.3 Quantifying the mechanical power requirements of flight

Sonomicrometry is a technique used for measuring in vivo muscle fascicle length change during activity (Hedrick et al., 2003). By implanting piezo-electric transducing crystals that can transmit and receive ultrasonic signals through muscle tissue, the muscle length change can be calculated from the time taken for the signal to travel between crystals if the speed of ultrasound through muscle tissue is known (Griffiths, 1987). When these measurements are combined with force measurements, the mechanical power generated by the muscle can be calculated. Forces produced during flight have also been estimated in vivo by implanting strain gauges on the deltopectoral crest of the humerus in starlings, pigeons and magpies (Biewener et al., 1992, Dial and Biewener, 1993, Tobalske, 2000, Hedrick et al., 2003, Soman et al., 2005). These measured forces can be multiplied by the estimated or measured muscle length change to find the work done per cyclical contraction, which can then be multiplied by wingbeat frequency to calculate the mechanical power output of the muscle. Using this method, Dial and Biewener (1993) estimated the mass-specific power of a pigeon pectoralis to be 51 W kg^{-1} during flight at 8 m s^{-1} 104 W kg^{-1} during flight at 13.7 m s^{-1} and later found that power was significantly higher during take-off (Biewener, 1998). When repeated at various speeds, this method can produce a mechanical power curve that is approximately comparable to the one predicted by aerodynamic theory (Figure 1.3), but establishing a link between bone strain and muscle force can be difficult as Hedrick et al. (2003) found a differing relationship between the two measurements at different speeds.

Muscle activation patterns can be measured in vivo through electromyography (EMG), which records the activation and intensity of electrical stimulation of skeletal muscles (Adams et al., 1992). Multiple studies have reported a strong positive relationship between EMG intensity, which represents recruitment of motor units, and force production (Hedrick et al., 2003, Tobalske et al., 2010). The highest EMG intensities have been reported during slow and fast flight speeds (Dial, 1992). EMG studies were also used to demonstrate how the pectoralis is activated late in the upstroke, and the supracoracoideus muscle

is activated late in the downstroke (Biewener et al., 1992); allowing for a stable deceleration of the wings (Beaufrere, 2009). However, a single EMG electrode only collects information from a small area of muscle, and it is common for multiple EMG electrodes to be placed across several locations of a large muscle, such as the avian pectoralis, in order to measure differences in intra-muscular activation (Boggs and Dial, 1993).

1.6.3.1 The work loop technique

The in vitro work loop technique can be used to estimate muscle power output by subjecting isolated muscle to muscle length changes and activity patterns recorded in vivo (Figure 1.4) (Ellerby and Askew, 2007a) allowing muscle function during flight to be simulated while conducting in vitro mechanical or energetic analysis. For example, Askew and Marsh (2001) used the work loop technique to predict the average mass-specific power output of a blue-breasted quail (*Coturnix chinensis*) wingstroke during take-off to be approximately 350 W kg^{-1} using in vivo EMG and sonomicrometry recordings (Askew and Marsh, 2001).
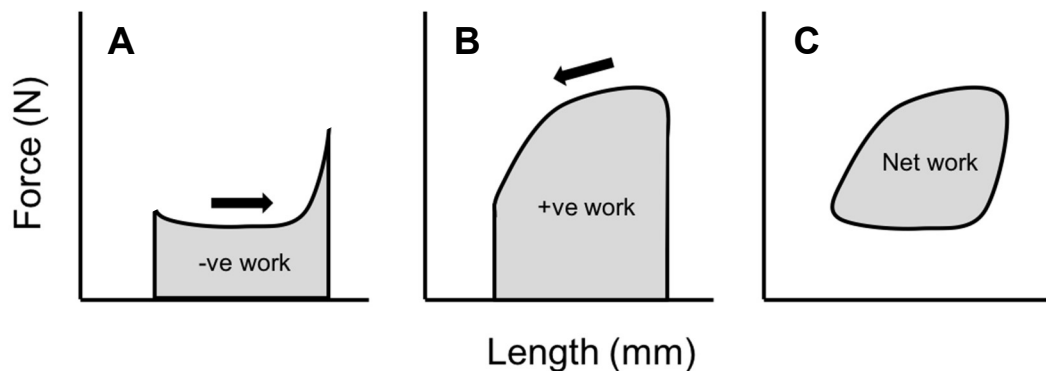
Figure 1.4   **Muscle work calculated using the work loop technique.**
Work is indicated by the shaded area. (A) Negative work is done on the muscle during lengthening. (B) Positive work is done by the muscle during shortening. (C) Complete counter-clockwise work loop generating net positive work.

1.6.4 Mechanical power-speed relationship

The U-shaped relationship between the aerodynamic power requirements for flight and flight speed have been established experimentally for many species over a range of speeds using the previously mentioned physiological

estimation methods (Figure 1.5) as well as aerodynamic theory (Rayner, 1982, Dial et al., 1997, Tobalske et al., 2003b, Askew and Ellerby, 2007, Morris and Askew, 2010b). Unfortunately, these measurements have predominantly been made independently of metabolic input measurements and there is a need for more integrative studies between the mechanics and energetics of flight at the organismal level.
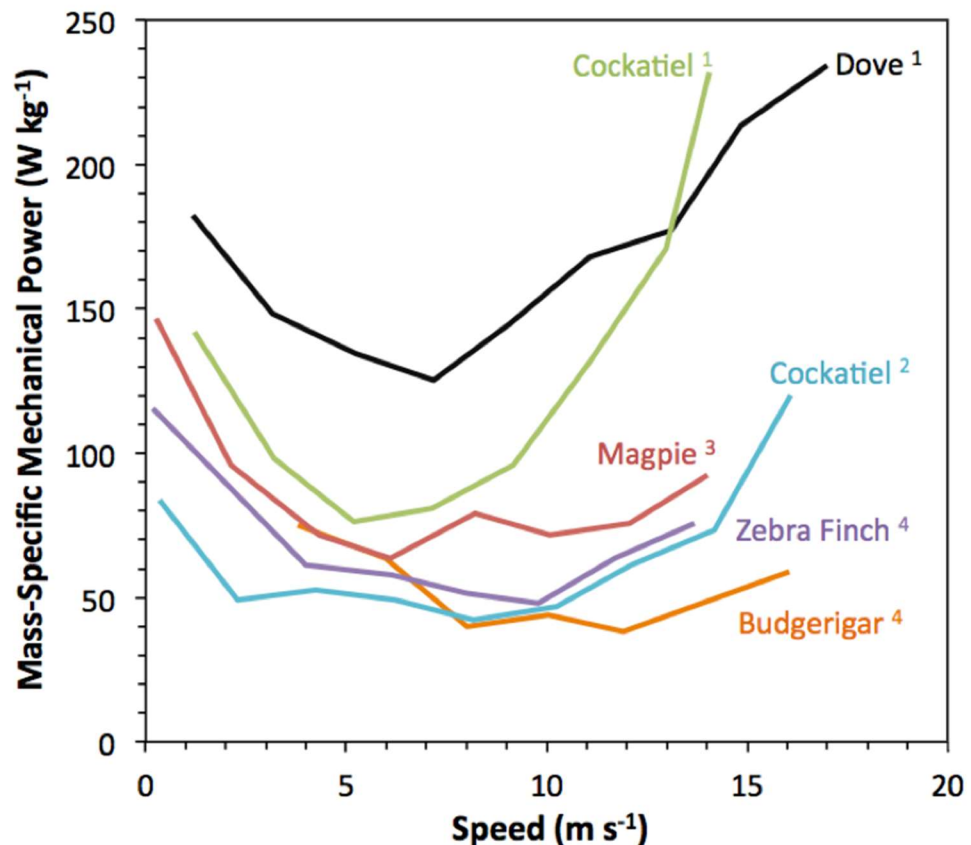
Figure 1.5 **Experimentally-derived examples of the mechanical power-speed relationship in flying birds.** Data from [1] Tobalske and Dial (2003); [2] Morris and Askew (2010); [3] Dial et al. (1997) and [4] Askew and Ellerby (2007).

1.7 Energetics of avian flight

Metabolic power (P_{met}) is the rate at which chemical energy is consumed during exercise and metabolic flight costs during flight are considered to be approximately 10 to 20 times the basal metabolic rate (BMR) (Norberg, 1996). Relative to running and swimming, flapping flight is an incredibly energetically expensive mode of locomotion if measured as the energy cost per unit of time;

however, due to the high velocities achieved through flight, the cost of transport (energy cost per unit of distance travelled) for flying is relatively low compared to running and only slightly higher than swimming (Alerstam, 1991). These metabolic flight costs are predominantly a reflection of the metabolic energy consumed by the locomotor muscles, but also include the energy consumed by the cardio-respiratory system, and other systems not directly involved in locomotion such as the digestive and renal systems. For example, the energy consumed by the locomotor muscles in running birds represents approximately 70% of the total metabolic energy consumption (Ellerby et al., 2005). This suggests that the flight muscles are likely to account for most of the energy expenditure in flying birds, but the actual distribution of energy consumption amongst flight muscles is currently unknown. Increases of energy expenditure in flight muscles other than the pectoralis and all non-muscular systems are often referred to as the 'postural' costs of flight (Morris et al., 2010). However, it is difficult to estimate the contribution of postural costs from metabolic studies and an unsubstantiated value of 10% is often assigned (Ward et al., 2001), assuming that the cardiovascular and respiratory systems each consume 5% of the total metabolic energy required for flight (Ward et al., 2001).

1.7.1 Quantifying the energetic costs of flight

The metabolic power required for flight is difficult to measure by direct calorimetry and so indirect calorimetry methods are used. These most commonly include metabolic measurements through respirometry, isotope elimination and heart rate recordings. Metabolic power is also commonly estimated from aerodynamic calculations of mechanical power (Pennycuick, 1968a), but these estimates are difficult to validate as they rely on untested assumptions about muscle efficiency and the postural costs of flight.

1.7.1.1 Respirometry

Respirometry is an indirect calorimetry technique that is used to estimate the metabolic rate of organisms by determining their rate of oxygen consumption ($\dot{V}O_2$) and carbon dioxide production ($\dot{V}CO_2$). In flying organisms, it is usually performed using either a respirometry chamber or a flow-mask system

(Bernstein et al., 1973). Flow-mask studies typically take place in specially-constructed wind-tunnels. Wind tunnels are useful tools that allow the energetics and kinematics of avian flight to be studied in a controlled environment where parameters such as flight speed and duration can be manipulated and repeated with multiple individuals (Pennycuick, 1968b, Tucker, 1968, Rayner, 1994, Dial et al., 1997, Askew and Ellerby, 2007). However, wind tunnel studies are only approximate representations of natural flight and it has been proposed that wind tunnels create close boundary effects that may interrupt airflow as well as physically and psychologically stressful conditions for birds, which may distort metabolic estimates (Rayner, 1994).

The advantage of respirometry is that it directly measures gas exchange, which allows metabolic rate to be estimated with a high level of confidence (Welch Jr, 2011). However, there are certain complications to consider when measuring the oxygen consumption of birds. Primarily, the respiratory mask and tubing increase the parasite drag that the bird has to overcome, which is likely to increase metabolic energy expenditure above that of a non-instrumented bird (Rothe et al., 1987, Ward et al., 2004). In addition to this, respirometry is only representative of aerobic metabolism and cannot be used to estimate anaerobic metabolic rate when flying at extremely physically demanding speeds unless lactate production is monitored (Butler et al., 1977).

The respiratory exchange ratio (RER) can be calculated from the amount of O_2 consumed and the amount of CO_2 produced by an organism during activity. Typically, values of RER range from 0.71 to 1 during aerobic exercise (Withers, 1977) and RER values of 1 or above indicate that more CO_2 is being produced than O_2 is being consumed. This is a signal of anaerobic energy metabolism, typically brought on by high intensity exercise. As respirometry is used to estimate energy costs of aerobic exercise, it is unreliable at RER values of 1 or above. The respiratory quotient (RQ) is a similar measure of gas exchange, but applies at the cellular level instead of the organismal. The RQ can be used as an indicator of which fuel is being metabolised to provide the energy

required for certain activities, but cannot be actively determined at the organismal level during flight (Kosan and Burton, 1966).

1.7.1.2 Isotope elimination

Isotope elimination methods rely on the elimination of known heavy isotopes introduced into the bird's bloodstream to measure the removal of oxygen from the body through respiration (Lefebvre, 1964). Currently two isotope elimination methods have been established: doubly-labelled water and labelled bicarbonate. Doubly-labelled water estimates use heavy hydrogen and oxygen isotopes, commonly $H_2^{18}O$ and D_2O. Whereas ^{18}O leaves the body through exhaled CO_2 and water loss (urine and sweat), D_2 only leaves the body through the latter, and so the relative differences in concentration between ^{18}O and D_2 represents the oxygen exhaled as CO_2. Alternatively, Hambly and Voigt (2011) more recently established the use of ^{13}C-labelled bicarbonate for accurate isotope elimination measurements over short periods of activity due to the rapid equilibration of ^{13}C as bicarbonate in the bird's body. An advantage of isotope elimination as a proxy of energetic consumption is that the birds are not restricted by the masks or chambers used in respirometry. As in respirometry, isotope elimination studies are limited to aerobic metabolism, but they have an added disadvantage in that they require long periods of exercise to measure reasonable changes in metabolism, making them only suitable for longer-duration studies (Butler et al., 2004).

1.7.1.3 Heat transfer modelling

During locomotion, the majority of P_{met} is released as heat as a fundamental thermodynamic consequence of mechanical work production. Using infra-red thermal imaging, this heat can be quantified and modelled as a component of metabolic energy consumption (Ward et al., 2004, Mccafferty et al., 2011, Hill et al., 2014). Infra-red imaging technology has significantly improved in the last two decades, and high-resolution thermal images can now even be captured using devices mounted on mobile phones (Cao et al., 2017). Total heat transfer is the sum of heat released from the surface of an animal by three processes: radiation, convection and evaporation (Ward et al., 2004). However, the use of

heat transfer modelling to estimate P_{met} relies on assumptions of muscle efficiency and is sensitive to the changes in ambient air temperature (Ward et al., 2001, Ward et al., 2004).

1.7.1.4 Heart-rate method

Although not a direct measurement of energy expenditure, heart rate measurements have also been increasingly used as a predictor of metabolic rate. Multiple studies have found strong linear relationships between heart rate and metabolic rate, measured as oxygen consumption, in both running (Bevan et al., 1994) and flying birds (Bishop et al., 2002). A review by Green (2011) concluded that heart rate can provide a useful estimation of metabolic power, but this method requires accurate and simultaneous calibration of heart rate and metabolic rate in order for any predictive relationship to be produced. Radiotelemetry has allowed researchers to take readings of heart-rate in free-flying birds to gain a more natural representation of flight performance, but a study by Gessaman and Nagy (1988) indicated that pigeons back-mounted with radio-transmitters expended up to 50% more oxygen per hour than unburdened birds. Further studies have reported that leg-mounted transmitters may be less costly for large flying birds (Elliott et al., 2013b).

1.7.1.5 Predictive modelling

Using measured values of mechanical power, estimates of basal metabolism and physiological constants, P_{mech} has been used to predict P_{met} based on the close relationship between the generation of mechanical work and energetic expenditure (Equation 1.4; Rayner, 1999).

$$P_{met} = \frac{k_{pos}}{\eta_{fm}} P_{mech} + P_{bas} \qquad [1.4]$$

where η_{fm} is the thermodynamic efficiency of the flight muscles, P_{bas} represents the basal metabolic rate and k_{pos} represents the postural costs of flight. The Pennycuick model (Pennycuick, 1989, Pennycuick, 2008) is the most commonly used predictive model of avian flight costs using aerodynamic

inputs. While this model provides reasonable predictions of the mechanical power requirements of flight (Dial et al., 1997, Tobalske et al., 2003b), it may be unreliable at predicting the metabolic costs due to the undetermined efficiency of the avian flight muscles (Morris et al., 2010). By selecting a constant efficiency for all bird species and flight styles, this model may under- or over-estimate the costs of flight and ignore important factors that may generate variations in mechanochemical energy conversion (Elliott, 2016).

1.7.1.6 Metabolic power-speed relationship

Metabolic power measurements estimated using respirometry and other methods have appeared to produce the U-shaped power-speed curve predicted by the mechanical power requirements assuming constant muscle efficiency (Tucker, 1968, Tobalske et al., 2003b, Askew and Ellerby, 2007, Bundle et al., 2007, Morris et al., 2010) but have also produced L-shaped (Dial et al., 1997) and J-shaped curves (Bernstein et al., 1973, Rothe et al., 1987, Ward et al., 2001, Ward et al., 2002, Ward et al., 2004) and some completely linear relationships (Tucker, 1972, Torre-Bueno and Larochelle, 1978, Ward et al., 2001) (Figure 1.6).

Aerodynamic theory dictates that higher energy consumption would be required to fly at the lowest and highest of available flying speeds but flat, L and J-shaped curves do not adhere to this expectation. It has been suggested that these non-U curves may be due to a possible under-representation of the true minimum and maximum available flight speeds for each species, which when measured, would only produce a certain fraction of the U-shaped curve (Ellington, 1991); although most authors express that they flew their birds at the minimum and maximum of voluntary flight speeds. Hummingbirds are the only birds that can hover and fly at very slow speeds aerobically (Warrick et al., 2012), which is why studies have been able to record a peak of their metabolic power requirements at the lowest end of the speed-power curve, but not for other species. If muscle efficiency changes between flight speeds, as has been hypothesised in cockatiels (Morris et al., 2010), then this may also help explain the discrepancies in metabolic power-speed curves from

mechanical power predictions. Many of these metabolic measurements have been made in isolation of mechanical power measurements, and a comparative investigation will help uncover more information about the relationship and efficiency of energy transfer between the two measurements.
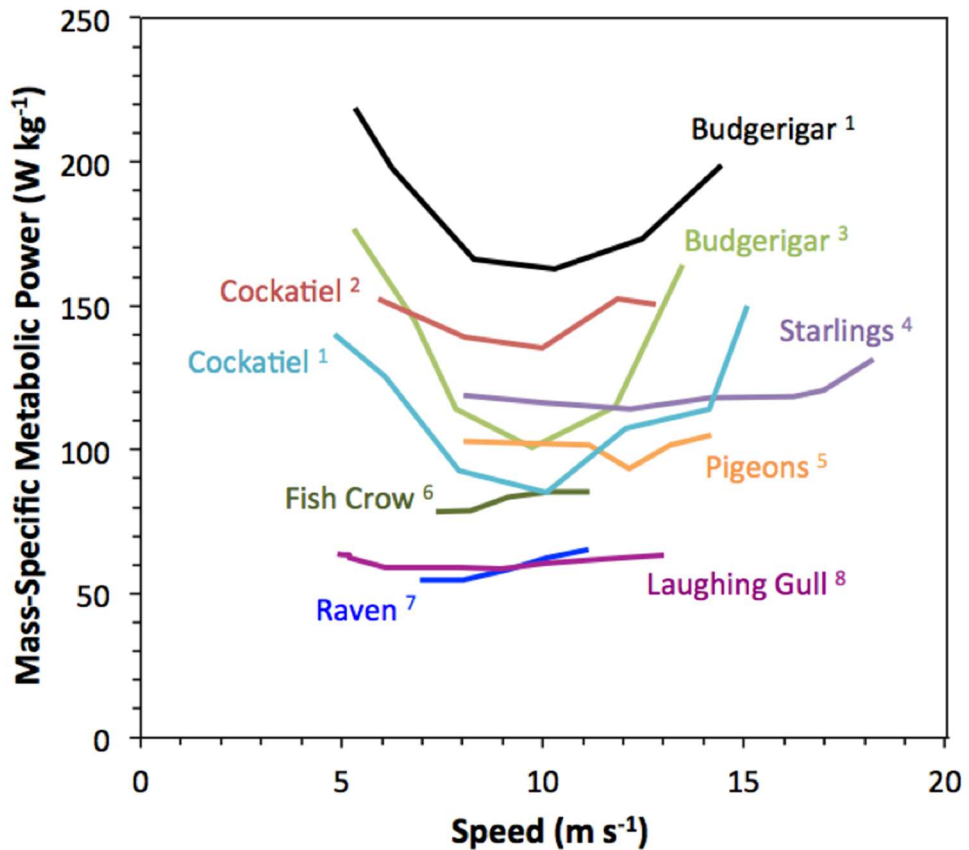
Figure 1.6 **Experimentally-derived examples of the metabolic power-speed relationship in flying birds.** Data from [1] Bundle et al. (2007); [2] Morris et al. (2010); [3] Tucker (1968); [4] Ward et al. (2001); [5] Rothe et al. (1987); [6] Bernstein et al. (1973); [7] Hudson (1983) and [8] Tucker (1972).

1.8 Energy saving strategies in avian flight

It is energetically beneficial for birds to reduce the costs of flight when possible and consequently birds have adapted a number of physiological and behavioural energy-saving strategies. For example, a number of larger bird species have evolved with particularly high-aspect wings, which provide a better lift-to-drag ratio. This in turn improves the bird's ability to glide and

makes efficient use of localised thermals for soaring (Akos et al., 2010). Birds can also gain energy savings by flying close to the ground or water surface. The effect of gaining lift and decreased drag on airfoils by flying close to a fixed surface is known as the "ground effect" (Hainsworth, 1988) in which the inboard-wing downwash produced by the wingtip cortices is interrupted by the ground and birds are able to save energy and glide for longer distances.

1.8.1 Formation flight

Individual energy-saving locomotion strategies are abundant in nature, but group strategies are also common, including strategies such as schooling in fish (Herskin and Steffensen, 1998), queue-formation travel in spiny lobsters (Bill and Herrnkind, 1976) and perhaps formation flight in birds (Weimerskirch et al., 2001). The topic of formation flight has been much discussed by ecologists, aerodynamicists and mathematical modelers, but the definitive reasons for its benefits are still empirically unproven. It is important to investigate the true qualitative and quantitative benefits of formation flight, as the knowledge can be applied to both animal and human aviation (Dimock and Selig, 2003). There are currently two central hypotheses for the adaptation of formation flight: the most supported theory is that there are energetic benefits gained by flying in the vortex wake of a leading bird (Lissaman and Shollenberger, 1970). A second theory suggests that formation flight improves communication and navigation between participants (Gould and Heppner, 1974). In the past, authors have argued for or against the two hypotheses separately, but the current understanding is that these two hypotheses can be mutually inclusive, and that a combined model should help explain the varied flight patterns commonly observed (Hummel, 1983).

1.8.1.1 Energy-saving hypothesis

Formation flight may help improve the overall efficiency of flapping flight by reducing the mechanical power transferred from the bird to the environment. Aerodynamic theory predicts that birds flying in the wake produced from the wingtips of a preceding bird will gain an upwash effect that may reduce the required power for flight (Hummel, 1983, Bajec and Heppner, 2009) (Figure

1.7). As stated previously, gliding flight produces a horseshoe vortex, with two trailing wingtip vortices that roll-up in from the wingtips towards the centre of the wing (Kshatriya, 1990). It is agreed that the optimal energetic benefits will be gained from flying at the roll-up point, as the wingtip vortices will eventually dissipate at increasing distances from the bird (Speakman and Banks, 1998).

1.8.1.2 Theoretical studies

Lissaman and Shollenberger (1970) first produced an equation of energy savings through flight formation, stating that a group of 25 large birds flying in a V could have an increase of 71% on their flight range over solo flyers due to the reduction in momentum imparted to the air. This equation was centered on the lateral wing-tip spacing (WTS) between the leading and following birds (Figure 1.7). There has been some criticism of this equation due to its assumption of fixed-wing aerodynamics, but large birds such as geese have a relatively slow wing-beat when cruising at a steady speed and so most subsequent studies have used Lissaman's fixed-wing equation and assumed minimal wing movement (Hummel, 1983, Hainsworth, 1987). Theoretically, the greatest energy saving will occur when the wing of a trailing bird overlaps laterally with the leading birds, which is described as the optimal wingtip spacing (WTS_{opt}), where α is wingspan (Equation 1.5).

$$WTS_{opt} = \frac{0.78\alpha - \alpha}{2} = -0.11\alpha \qquad [1.5]$$

Subsequent studies have followed a similar methodology of comparing observed WTS with WTS_{opt} and calculating predicted energy savings using Lissaman's equation (Appendix 1). The majority of these studies have found that birds fly with an average WTS in the region of WTS_{opt} but with very large variation. The majority of this variation appears to favour flying slightly outbound of WTS_{opt}, which would help prevent collisions and would theoretically give more of an energetic benefit than flying slightly inbound, where the wing of the trailing bird might overlap with the downwash of the leading bird (Cutts and Speakman, 1994, Speakman and Banks, 1998). It has

been observed that maintaining a stable formation can be difficult (Weimerskirch et al., 2001) and while the greatest energy-savings are likely to occur at constant optimal positioning, there may be other ecological reasons as to why birds are not utilising the full energetic benefits of formation flight (Hummel, 1983). As well as WTS, the number of participating birds in a formation is thought to be important, with theoretical energy savings predicted to be optimal with an infinite number of birds (Lissaman and Shollenberger, 1970, Kshatriya, 1990).
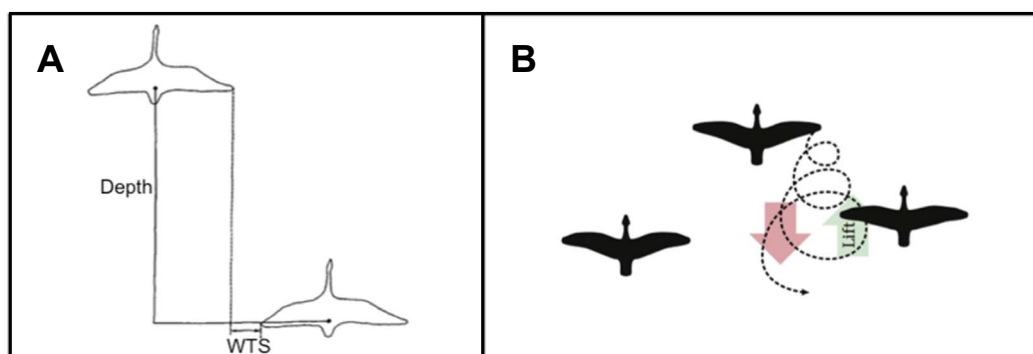
Figure 1.7 **Visual analysis of formation flight.** (A) Visual descriptions of the depth and wingtip spacing (WTS) used for estimating energy savings during formation flight. (B) Diagram depicting the upwash outbound of the wingtip vortex. Adapted from Hainsworth (1987) and Bajec and Heppner (2009).

1.8.1.3 Empirical studies

Currently, the only empirical energetic evidence for the energy-saving hypothesis comes from a study by Weimerskirch et al. (2001), who compared the heart-rate and wing-beat frequency of white pelicans (*Pelecanus onocrotalus*) flying solo and flying in formation. They found that birds participating in formation flight had significantly lower wing-beat frequencies and heart-rates than solo flyers, with a proposed average total energy saving of 11.4-14% (Appendix 1). Bejan and Marden (2006) speculated that this may be due to the fact that pelicans are typically social flyers, and forced solo flight may induce solitary-stress related increases in heart-rate that have been observed in lab mice. In order to quantify the energy-saving benefits of

formation flight, it is imperative to take further metabolic estimates of multiple birds in formation.

1.8.1.4 Formation shape and organisation

Bird flight formations are traditionally considered to be V-shaped, but Canada geese (Gould and Heppner, 1974) and pelicans (O'Malley and Evans, 1982) have been observed flying in echelons, swept U-shaped and asymmetric J-shaped formations much more frequently than in V-shaped formations. U-shaped formations are predicted to even the energy saving distribution by reducing energy savings compared to V-formations for all birds except the leader, who may gain increased lift from a slight upwash preceding the trailing birds (Hummel, 1973). Andersson and Wallander (2004) suggest that V-shaped flight formations are more like to occur in groups that have individuals willing to lose their energetic savings, such as migrating family units subject to kin selection or altruistically reciprocating adults. Likewise, formation flight may also allow older birds with migratory experience to act as navigators for trailing birds.

1.8.1.5 Wingbeat synchronicity

It has been proposed that the energetic benefits of formation flight are only effective if leading and following birds have a synchronous wingbeat. The results of observation studies were mixed on this topic, with Nachtigall (1970) finding a synchronous phase relationship in wingbeats but a similar study by Berger (1972) finding no relationship. However, a recent study by Portugal et al. (2014) that used data-loggers to monitor the positioning and wing-beat relationships between northern bald ibises (*Geronticus eremita*) flying in formation was a significant advancement in the field as they constantly and accurately monitored the birds for an extended period of time instead of relying solely on photography to determine bird positioning. Portugal et al. (2014)'s study found a strong wingbeat phase relationship between individuals in the formation, with wingbeats corresponding to the optimal placement to exploit upwash and avoid downwash that strongly suggested energetic savings.

1.8.1.6 Scaling effects of formation flight

A recurring theme in the literature regarding formation flight appears to question why smaller migrating birds are not observed flying in V-formations if the proposed energy savings and organizational benefits are true for larger birds. The issues appear to lie in the wake-formation of smaller birds, which is more complex than that of larger birds (Kokshaysky, 1979) as they have more complicated wing kinematics and a higher wing-beat frequency. Hummel (1983) predicts that the current theories for energetic benefits only applies to formations of large birds and that it is unlikely that these current models will apply to smaller birds. It may be the case that smaller birds are able to save energy in ways more effective than formation flight. Canada geese have a relatively high wing loading, and it has been suggested that they fly in formation as they are less likely to gain effective energy savings from gliding and soaring (Badgerow, 1988).

1.9 Summary of work

Presented in this thesis are a series of experiments designed to further our understanding of avian and insect flight by elucidating key gaps in the literature and by coupling the often separately analysed mechanics and energetics of animal flight with the goal of contributing towards a more integrated understanding of avian and insect flight. This is achieved by examining how the asymmetrical muscle length trajectories, commonly observed to be used in avian flight, affect net efficiency in the mouse hindlimb muscle (Chapter 2), determining how the mechanical efficiency of the avian pectoralis varies with flight speed (Chapter 3), examining how accelerometry can be used as a proxy for estimating the metabolic costs of flight by conducting respirometry experiments with masked lovebirds in a wind tunnel (Chapter 4) and finally by examining how the myoplasmic calcium ion concentration affects the optimal wingbeat frequency for power generation and myofibrillar efficiency in asynchronous insect flight muscles (Chapter 5). All of these experiments are connected to each other through their coupled measurements of flight mechanics and energetics, either at the muscular or organismal level.

Chapter 2
The effects of asymmetrical length trajectories on the net efficiency of the mouse soleus muscle

2.1 Abstract

Many volant bird species exhibit wingbeat cycles with asymmetrical contraction cycles that spend relatively more time shortening than lengthening. These asymmetric contraction cycles been found to increase the mechanical power output of skeletal muscles involved in mouse locomotion and frog vocalisations as well as avian flight. Previous in vitro work has demonstrated that this increased mechanical power comes without a trade-off with initial mechanical muscle efficiency in the mouse soleus. However, it is unknown how asymmetrical length trajectories may affect net muscle efficiency, which incorporates the energetic costs of metabolic recovery and represents a more ecologically relevant measure of efficiency. By simultaneously measuring O_2 consumption and net work production during a series of cyclical contractions, this study investigated the effects of varying the proportion of the cycle spent shortening on the net muscle efficiency of the mouse soleus muscle. In vitro sawtooth cycles where the shortening duration represented 25% (Saw25%), 50% (Saw50%) or 75% (Saw75%) of the total cycle duration were imposed on the muscle at a cycle frequency of 5 Hz using the work loop technique, with the timing and duration of stimulation optimised to maximise net power output. The net muscle efficiency ranged from 4.76% for Saw25% to 11.7% for Saw50% and 9.48% for Saw75% cycles, suggesting that contraction cycles that spend less than 50% of the cycle shortening operate with a lower net efficiency than those that spend 50% or more of the cycle shortening. Therefore, it is possible to enhance muscle power output during Saw75% cycles without an effect on net efficiency. The reduction in net efficiency during Saw25% is proposed to be due to several factors relating to proportionally larger energy expenditure during non-shortening processes. These results are likely not unique to mouse muscles and may be representative of other vertebrate muscles, including the avian pectoralis muscle.

2.2 Introduction

Animal locomotion is an energetically expensive activity, with the majority of the associated metabolic energy expenditure reflecting the energy consumed by the locomotor muscles as they contract and produce forces to transport the animal through the environment (Ellerby et al., 2005). However, vertebrate locomotor muscles are demonstrably thermodynamically inefficient, so small relative changes to muscle efficiency can have large absolute effects on the costs of locomotion for animals. It is therefore important to determine the effects that different contraction parameters, such as strain, cycle frequency and length trajectory, have on muscle energetics and muscle efficiency in order to provide us with a better comprehension of locomotor muscle function and performance.

Asymmetrical contraction cycles, during which more time is spent shortening than lengthening, are typically associated with activities that require high levels of mechanical power. Such asymmetrical cycles have been recorded from the avian pectoralis using sonomicrometry in vivo during horizontal flights in multiple bird species including starlings (54% of cycle spent shortening; *Sturnus vulgaris*) (Biewener et al., 1992), pigeons (63%; *Columba livia*) (Biewener et al., 1998, Robertson and Biewener, 2012), quails (69.6%; *Coturnix chinensis*) (Askew and Marsh, 2001), mallards (67%; *Anas platyrhynchos*) (Williamson et al., 2001), cockatiels (49.6-61.5%) (Hedrick et al., 2003, Morris and Askew, 2010b) and zebra finches (66.9%; *Taeniopygia guttata*) (Tobalske et al., 2005), as well as take-off flights in quails (69.1%) (Askew and Marsh, 2001) and four species of phasianids (55.8-64.4%) (Tobalske and Dial, 2000). Subsequent studies have also simulated these asymmetrical contractions in vitro and have found that longer relative shortening durations produce higher net mechanical power outputs than symmetrical contraction cycles in the vocal muscles used for calling in tree frogs (*Hyla versicolor* and *H. chrysoscelis*) (Girgenrath and Marsh, 1999), in the mouse soleus muscle (Holt and Askew, 2012) and in the quail pectoralis during flight (Askew and Marsh, 2001). It has been suggested that these

increases in mechanical power may be due to the increased period of stimulation that results in a more complete activation of muscle leading to increased cross-bridge formations and the generation of greater muscular force (Marsh, 1999). These asymmetrical cycles can be especially beneficial for increasing power generated during the movement of limbs in a particular direction, such as the downstroke during avian flight (Marsh, 1999). While the mechanical benefits of asymmetrical length trajectories have been investigated, their effects on the energy requirements and efficiency of muscle contraction are less well understood.

Simultaneous measurements of muscular energy consumption and mechanical power generation using the work loop technique allows for investigations into the effect of various contraction parameters, such as cycle frequency and length trajectory, on the mechanical and energetic aspects of muscle contraction, including the efficiency of the muscle (Josephson, 1985, Askew et al., 1997). Muscular energy use has previously been estimated through measurements of O_2 consumption by isolated muscles (Kushmerick and Paul, 1976, Harwood et al., 2002) or net enthalpy production as indices of energetic costs (Barclay and Weber, 2004, Holt and Askew, 2012). Measurements of O_2 consumption during and following muscle contraction represent the energetic costs of consuming and resynthesizing metabolites such as ATP and PCr at the mitochondria to pre-contraction resting levels in a process called oxidative recovery (Barclay and Weber, 2004). Measuring O_2 consumption is considered to provide a good reflection of the metabolic energy used to produce mechanical work during muscle contractions due to the O_2 required for aerobic metabolism, and has been measured numerous times with success in skeletal and cardiac muscles from mammals (Heglund and Cavagna, 1987), fish (Harwood et al., 2002), amphibians (Kushmerick and Paul, 1976) and insects (Josephson and Stevenson, 1991).

Current evidence suggests that increased mechanical power correlates with increased muscle efficiency in animal (Barclay, 1994, Harwood et al., 2002, Holt and Askew, 2012) and human (Reger et al., 2012) locomotion but other

studies have suggested the existence of a trade-off between generating high mechanical power and high efficiencies (Curtin and Woledge, 1996). It may be that the power-efficiency relationship varies between species and the contraction parameters applied to the muscle in vitro compared to in vivo contractions, and this trade-off may be subject to the separate priorities and demands of different modes of locomotion.

The initial mechanical efficiency (ε_i) and the net efficiency (ε_{net}) of the mouse soleus have been determined using measurements of total enthalpy and O_2 consumption alongside measurements of mechanical work generation. The ε_i of the mouse soleus has been determined to be approximately 30% (Barclay and Weber, 2004), while the ε_{net} is approximately 12% (Barclay and Weber, 2004), but contraction parameters such as strain and cycle frequency have been shown to affect these values (Barclay, 1994, Holt and Askew, 2012). Only Holt and Askew (2012) determined the effects of asymmetrical length trajectories on the ε_i of this muscle, finding that there was no trade-off in high mechanical work generation during contraction cycles at 5 Hz that spent 50% or greater of the cycle shortening (~25%), but that ε_i was reduced (~7%) during cycles that spent only 25% of the cycle shortening. However, this study only investigated the ε_i of the mouse soleus and did not investigate the ε_{net} since the oxidative recovery process was not investigated and the basal metabolism of the muscle was not deducted. The net efficiency represents a more valuable piece of information as it more directly corresponds to the total in vivo energy consumption during locomotion. As the ε_i is thought to be approximately twice the ε_{net} (Smith et al., 2005), the values of ε_{net} at different length trajectories can be roughly predicted, but work by Askew et al. (2010) on the flight muscles of apid bees suggested that, at least inter-specifically, the efficiency of oxidative recovery may not always be constant and this may change what was previously thought about the relationship between ε_i and ε_{net}. Novel work investigating the effect of length trajectories on ε_{net} is needed to support or amend these predictions.

In the present study, we investigated the effects of altering length trajectories on the ε_{net} by determining the metabolic energy consumption and net mechanical power output (net P_{mech}) from mouse soleus muscles performing a series of in vitro cyclical work loops at both symmetrical (Saw50%) and asymmetrical (where shortening represented 25% or 75% of the total cycle duration: Saw25% and Saw75%, respectively) sawtooth length trajectories. Based on the results of Holt and Askew (2012), we hypothesised that net P_{mech} power would increase with increasing duration spent shortening and that the net efficiency of the mouse soleus would be constant during cycles with 50% or greater of the cycle spent shorting, but would be lower with relatively shorter shortening durations (e.g. Saw25%).

The conclusions of this experiment are unlikely to be unique to the mouse soleus muscle and the relationship between asymmetrical length trajectories and muscle efficiency may be applicable to other vertebrate muscle, including the major flight muscles of birds where asymmetrical length trajectories have been determined in vivo. Muscles from mice were selected not because they are likely to undergo asymmetrical the selected length trajectories in vivo, but rather that their mechanical and energetic properties are well recorded (Askew and Marsh, 1997, Askew et al., 1997, Holt and Askew, 2012) and the mouse soleus is an important postural muscle with a highly oxidative fibre type (approx. 66-76% Type I [SO], 24-34% Type IIa [FOG], 0% Type IIb [FG]) (Crow and Kushmerick, 1982, Askew and Marsh, 1997), which makes it suitable for measures of muscular oxygen consumption during contraction cycles (Barclay, 1994).

2.3 Materials and Methods

2.3.1 Animals and muscle dissection

Adult female mice (*Mus musculus* [CD1 strain], Linnaeus, 1758, n = 10) aged 5-9 weeks old were housed in a licenced facility and killed by cervical dislocation in accordance with Schedule 1 requirements. The skin was removed from the hindlegs and both limbs were removed at the hip using a

scalpel and placed in oxygenated Krebs-Henseleit solution at room temperature (approximately 23°C). The soleus muscle and proximal and distal tendons were then carefully dissected out from one leg, ensuring a small piece of femur was still attached at the proximal tendon and a small piece of calcaneus was attached at the distal tendon.

2.3.2 Oxygen electrode and muscle chamber setup

Oxygen consumption by the mouse soleus was determined polarographically using respirometry in a closed, glass chamber (Rank Bros Ltd., Cambridge). A glass chamber was selected as it is chemically inert and effectively impermeable to oxygen. The lid of the chamber was constructed using Kel-F, a plastic that has near-zero moisture absorption and extremely low outgassing of oxygen (<0.01% O_2 in 24h) (Stevens, 1992). A conical depression in the inner surface of the lid facilitated the removal of air bubbles from the chamber via a hole in the centre of the lid following injection of fresh Krebs-Henseleit solution. The volume of the chamber with the lid in place was calculated to be 2.15 ml by incrementally injecting water into the chamber via a syringe until the chamber was full.

A small PTFE-coated stir bar was used in conjunction with the magnet under the oxygen electrode to thoroughly mix the Krebs-Henseleit solution (Figure 2.1). While a glass stir-bar was preferable due to its relatively smaller oxygen consumption, the oxygen traces produced with the glass stir-bar were noticeably more erratic, which reduced the ability to detect small changes in oxygen consumption. The muscle chamber was filled with oxygenated Krebs-Henseleit solution (concentrations in mmol l^{-1}: 117 NaCl, 4.7 KCl, 2.5 $CaCl_2$, 1.2 $MgSO_4$, 24.8 $NaHCO_3$, 1.2 KH_2PO_4 and 11.1 glucose, pH 7.59 at 39°C when bubbled with 95% O_2 and 5% CO_2) (Burton, 1975). A temperature of 39°C was chosen to simulate physiological conditions of mouse muscle (*Mus musculus* body temp approximately 37-39°C) (Habicht, 1981). This temperature is slightly higher than used in the Holt and Askew (2012) study (35°C) but 10°C temperature changes have been found to have negligible effects on ε_i in isolated mouse muscle preparations (Barclay et al., 2010) so

temperature differences between studies are unlikely to affect the conclusions drawn. The temperature of the Krebs-Henseleit solution and the oxygen chamber were maintained around 39°C (recorded values ranged between 38.9°C and 39.3°C) using a refrigerated water bath unit (Model TC120, Grant Instruments Ltd., Cambridge) that circulated temperature controlled water through the chamber's water jacket.
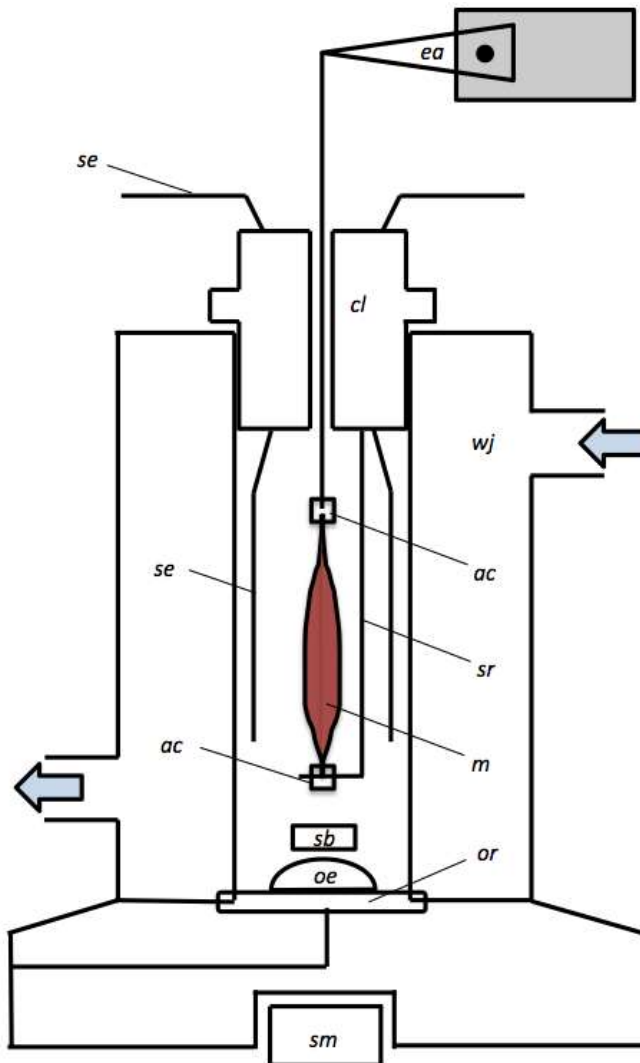
Figure 2.1 **Technical diagram of the mammalian muscle chamber and ergometer setup.** Components include stirring magnet (sm), oxygen electrode (oe), O-ring (or), stir-bar (sb), aluminium foil clips (ac), muscle (m), support rod (sr), silver stimulating electrodes (se), water-jacket (wj), chamber lid (cl) and the ergometer arm (ea).

A Clark-type oxygen electrode (Rank Bros Ltd., Cambridge; Figure 2.1) built into the base of the muscle chamber was used for these experiments. The oxygen electrode consisted of an outer silver-silver chloride ring reference electrode and a smaller platinum disc electrode that acted as the cathode and was used to detect changes in the oxygen content of the solution in the chamber. The chamber and lid were washed daily with 100% ethanol and rinsed with distilled water before a period of experimentation to remove microorganisms. The platinum and silver-silver chloride electrodes were soaked with 3M KCl to act as the electrolyte for the electrode and a semi-permeable PTFE membrane was placed across the electrodes through which oxygen could reach the electrode but which prevented mixing of the electrolyte and the Krebs-Henseleit solution in the chamber. The oxygen electrode was calibrated before each experimental period by ensuring the electrode's control box (Digital Model 10, Rank Bros Ltd., Cambridge) was outputting zero volts when disconnected from the electrode and that the sensitivity of the control box was adjusted to output a value of 95% when the 95% O_2, 5% CO_2 Krebs-Henseleit solution first entered the chamber. The polarization voltage of the electrode was 0.6 V.

The chamber was tightly sealed except for a thin aperture (approximately 1.2 mm) in the lid through which a stainless steel rod that connected the muscle to the ergometer which could be used to impose length changes on the soleus muscle. A second aperture (approximately 1.2 mm) in the lid was used to flush the chamber with oxygenated Krebs-Henseleit solution and through which a thermocouple (Type T Model BAT-12, Physitemp, NJ, USA) could be inserted (when solution changes were not taking place) into the chamber to monitor temperature. The electrode's output in response to changes in oxygen concentration would stabilise within approximately 30 seconds following the injection of 10 ml of oxygenated Krebs-Henseleit solution through the aperture in the lid.

An ergometer (Model 300B-LR; Aurora Scientific Inc., Ontario, Canada) was used to control muscle length and to measure the force and muscle length

changes during the contraction cycles. The ergometer rod and affixed support rod built into the underside of the chamber lid were used to secure the muscle in the chamber and to facilitate the manipulation of muscle length via the ergometer (Figure 2.1). The ergometer arm was attached to a vertically-movable platform (C. F. Palmer, London) which was adjusted to remove slack from the muscle and to position it at an in vitro resting length of approximately 12 mm. The horizontal position of the ergometer was also adjusted to align the stainless-steel rod connected to the muscle directly down the centre of the hole in the chamber lid to minimise interference with force measurements.

Aluminium foil clips were secured on to each tendon in order to mount the muscle in the oxygen chamber. One tendon was attached to the support rod that was attached to the chamber lid, and the other tendon was secured on to a hooked rod that was attached to the arm of the ergometer. All air bubbles were carefully removed from the chamber prior to placement of the lid. The chamber lid and mounted muscle were then lowered into the chamber and fitted securely. Once the muscle was secure in the chamber, it was left for a period of 30 minutes to recover from the dissection and to thermoequilibriate. The contralateral leg remained in ice-chilled oxygenated Krebs-Henseleit solution until the measurements on the muscle from the first limb had been completed.

The muscle chamber was re-oxygenated prior to each experimental run by flushing approximately 10 ml of Krebs-Henseleit solution bubbled with 95% O_2 and 5% CO_2 at 39°C to ensure the muscle had sufficient exogenous oxygen for recovery metabolism. Excess Krebs-Henseleit solution exited the chamber through the aperture with the ergometer rod and was captured with tissue paper to prevent any contact between the solution and the electrical components of the electrode.

The high temperature conditions of the muscle chamber and the radius of the muscle limited the diffusion of oxygen to the centre of the muscle. According to Barclay (2005), it can be estimated that the centre of these soleus muscles

(mean radius 0.39 mm) would have become anoxic after 8-15 seconds of continuous contraction cycles. Additionally, the proportion of the cycle spent shortening is inversely related to the time taken for an anoxic area to form at the centre of the muscle (Barclay, 2005). To mitigate this, exogenic PO_2 at the muscle surface was kept above 70% at all times, all contraction cycle series were limited to a maximum of 6 seconds and muscles were left for at least 10 minutes between contraction sequences to facilitate full metabolic recovery. The contribution of anaerobic metabolism to the production of energy during the contractions is assumed to be negligible based on the findings that anaerobic metabolism (calculated by measurement of accumulated lactate, pyruvate and alanine in a similar muscular respiration chamber) contributed a maximum of 5% of the energy consumed for a strenuous 15 second tetanus in the mouse soleus in Krebs-Henseleit solution with a high PO_2 at 20°C (Crow and Kushmerick, 1982).

2.3.3 Mechanical power measurements

2.3.3.1 Isometric contractile properties

Following the 30 minute recovery period after dissection, a series of isometric twitches were conducted using a supramaximal stimulus with a pulse width of 0.2 ms at increasing muscle lengths (increments of 0.5 mm) to determine the maximum isometric twitch force for the muscle and the associated optimal muscle length (L_0). L_0 was used for all subsequent experimental contractions. Muscle fibre length was calculated as 85% of the L_0 (Askew and Marsh, 1997) and this value was used when calculating strain trajectories. A 400 ms burst of stimuli at 150 Hz was used to elicit an isometric tetanus (Askew and Marsh, 1997), which was used to determine the peak isometric force of the muscle. Maximal isometric tetanic stress was determined from the peak isometric force (P_0), L_0 and muscle mass (determined at the end of experiments) assuming a muscle density of 1060 kg m^{-3} (Mendez and Keys, 1960).

The muscle was stimulated (applied by a Model S48G Stimulator, Grass Medical Instruments, MA, USA via a Stimulus Isolation Unit, Type 236, Hugo
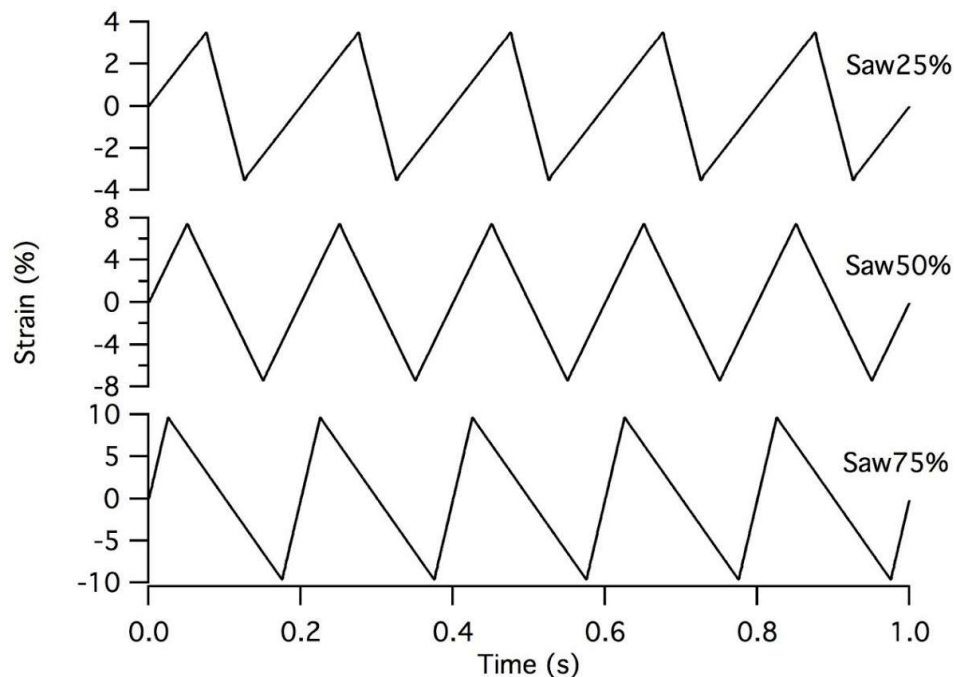
**Figure 2.2   Examples of sawtooth length trajectories and strains used
for five contraction cycles.** All cycles performed at a
frequency of 5 Hz.

Sachs Elektronik, March-Hugstettem, Germany) by the two chlorided silver
electrodes inserted into the chamber through the lid. The direction of current
flow was alternated by changing the polarity of the electrodes with each
stimulus to prevent electrolysis and the evolution of oxygen at the stimulating
electrodes. A series of control stimulated cycles without a muscle in the
chamber were performed to ensure electrolysis was not affecting the oxygen
content in the chamber. The muscle length changes and forces produced by
muscle contractions were logged to a PC via a 12-bit A/D converter (DAS-
1801AO, Keithley Metrabyte, OH, USA) and recorded at a rate of 1000 Hz
using TestPoint software for calculations of mechanical work (TestPoint
Version 7, Capital Equipment Corp, MA, USA).

Control isometric twitches performed immediately before each set of work
loops were used to monitor any decline in the muscle's performance. Work
loops performed while the muscle was below 80% of peak twitch performance
were not used in the analysis. The decline in muscle performance was
assumed to be linear (Askew and Marsh, 1997) but the muscle preparations

were not corrected for the decline in force in order to maintain the relationship with O_2 consumption. A recovery period of 1 minute was allotted following each twitch and 5 minutes following each tetanus to allow for metabolic recovery.

2.3.3.2 Sawtooth contraction cycles

The work loop technique (Josephson, 1985, Askew et al., 1997) was used to subject the isolated muscle to cyclical muscle length changes and stimulation patterns in order to generate mechanical work under semi-realistic conditions. These work measurements allowed the calculation of net work (W_{net}) and net mechanical power (net P_{mech}) output. To determine the effects of different proportions of time spent shortening during a cycle on net muscle efficiency, the muscles were contracted using three different sawtooth length trajectories, with 25% (Saw25%), 50% (Saw50%) and 75% (Saw75%) of the cycle spent shortening (Figure 2.2). These experiments were all carried out at a cycle frequency of 5 Hz as this has previously yielded the maximal mechanical power output in these muscles (Askew and Marsh, 1997, Holt and Askew, 2012). Stimulation parameters (phase, duration, frequency) and strains

Table 2.1   Muscle strains and stimulation parameters for each sawtooth waveform.

Sawtooth Cycles	Saw25%	Saw50%	Saw75%
Cycles	20	20	20
Total duration (s)	4	4	4
Strain (±%)	3.3	7.0	9.1
Phase (ms)	-15	-15	-5
Stim duration (ms)	40	60	90

Duration = Total time duration between the start and end of contractions

Strain = Amplitude of length change from longest to shortest peak length expressed as a percentage of L_0

Phase = Timing of stimulation, relative to peak length

Stim duration = Duration of stimulation per cycle

previously found by Holt and Askew (2012) to maximise net P_{mech} were used for the sawtooth cycles (Table 2.1).

Each run consisted of 20 cycles as preliminary experiments determined that this was maximum number of cycles that could be performed before net P_{mech} decreased below 80% of its starting value, while providing a quantifiable level of O_2 consumption. Following the completion of the work loops or when the performance of a muscle had declined significantly, the muscle was removed from the chamber and the tendons were removed from either end of the muscle. The muscle was then blotted lightly with tissue paper before being weighed using an analytical balance (Sartorius, Germany).

2.3.4 Correction for electrode oxygen absorption and leak

When experimental conditions were tested without a muscle present, the oxygen concentration of the chamber decreased over time due to oxygen absorption at the oxygen electrode, potential absorption by materials held within the chamber (e.g. the stir-bar and O-ring) and leak through the chamber lid. There were two narrow holes in the chamber lid through which oxygen could leak and the non-glass components also absorbed oxygen, which resulted in an exponential decline in the oxygen concentration of the chamber over time. This asymptote represents the point at which the combined rate of oxygen decline through chamber leak and oxygen absorption of the electrode equals the rate of oxygen entering the system.

A correction to account for this background oxygen absorption was produced (Equation 2.1) by generating a series of oxygen decline curves in the chamber without a muscle and determining the mean coefficients for a double-exponential curve (n=6).

$$Corrected\ PO_2 = C_1 + C_2 e^{(-C_3 \cdot t)} + C_4 e^{(-C_4 \cdot t)} \qquad [2.1]$$

where C_1, C_2, C_3 and C_4 are curve coefficients and t represents the time in minutes from the point of stabilisation at 95% O_2 following re-oxygenation of

the chamber. A double-exponential equation most appropriately fitted the data, as a single-exponential equation appeared to deviate substantially for the lowest and highest values of t. All results refer to the corrected data.

2.3.5 Quantifying O_2 consumption

The metabolic cost of the mechanical work performed by the muscle during the work loops was determined by measuring the O_2 consumed by the muscle during oxidative recovery metabolism. The oxygen concentration in the chamber was continuously sampled at a rate of 20 Hz using LabChart software (LabChart, Version 5.5.6, AD Instruments, Oxford) via a PowerLab data acquisition system (PowerLab Model 4/25, AD Instruments, Oxford). Once the muscle had been secured in the oxygen chamber, the oxygen concentration was measured for at least 10 minutes to obtain a reliable baseline that represented the resting metabolic rate of the muscle preparation. Following completion of the work loops, the muscles were left for a period of
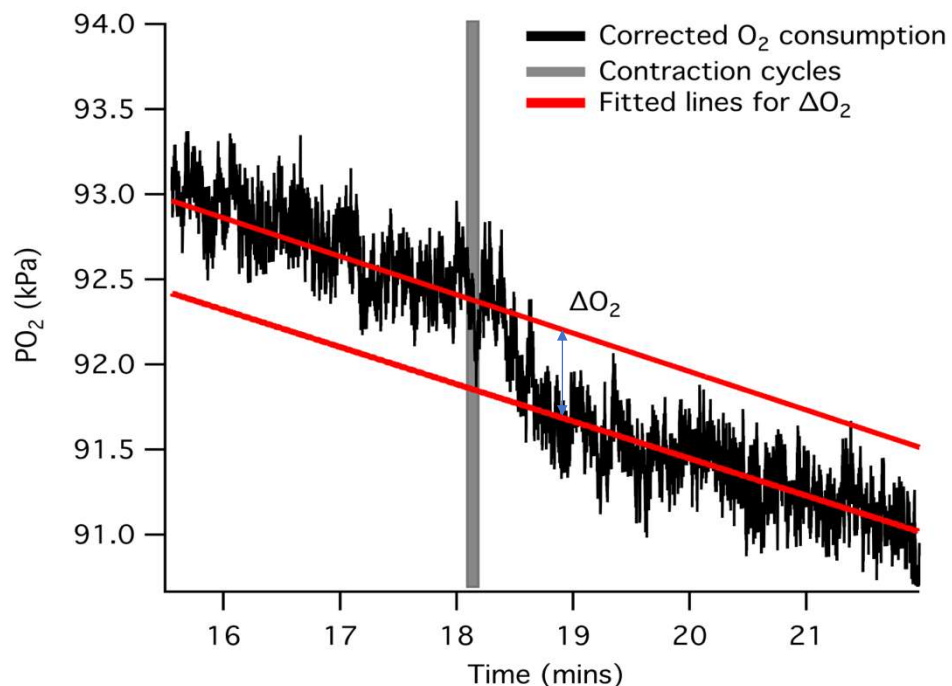
Figure 2.3   **Representative example of the corrected oxygen consumption trace.** A smoothed trace (black trace) is displayed as well as the corrected PO_2 data (grey trace) for clarity. The blue arrow indicates the difference between the pre-contraction and post-contractions values used to determine ΔO_2. The light grey block indicates the period of stimulated contraction cycles.

approximately 5 minutes to fully record the period of recovery oxygen consumption and to ensure a stable resting baseline had been reached.

Once the correction for chamber leak and oxygen consumption by the electrode had been applied, linear regressions were fitted to the baselines preceding stimulation and following the completion of oxidative recovery as determined by a period of 10 minutes with a stable rate of O_2 consumption (Figure 2.3). The change in the oxygen content of the Krebs-Henseleit solution (ΔO_2) was calculated as the distance between the two regression lines at an approximated central point between the start and end of recovery oxygen consumption. This mid-point value provided an estimate of active oxygen consumption above basal metabolism that would aptly represent the net oxygen consumed (Trinh and Syme, 2007). ΔO_2 was then multiplied by the chamber volume (2.15 ml) and the oxygen solubility of the Krebs-Henseleit solution (994.342 nmol O_2 ml^{-1} at a salinity of 8 ‰ at 39°C), which was determined using a standard dissolved oxygen solubility table to obtain the molar oxygen consumption, assuming standard atmospheric pressure (760 Torr / 101.325 kPa) (Cameron, 1986). To standardise the measurements of metabolic and mechanical energy, the oxygen consumption values were converted to Joule equivalents at a rate of 4.79 x10^{-4} J nmol^{-1} O_2 (or 20.1 J ml^{-1} O_2). Glucose was the only exogenous fuel source available to the muscle, so a respiratory quotient (RQ) of 1 was assumed (Crow and Kushmerick, 1982). The Joule equivalents of measured oxygen consumption were normalised for muscle mass and expressed as J kg^{-1}.

2.3.6 Work loop analysis and efficiency calculations

Using force and muscle length measurements from the ergometer, instantaneous mechanical power output was determined for each cycle as the product of force and velocity (IGOR Pro Version 5.01; Wavemetrics, OR, USA). Velocity was determined as the mathematical derivative of muscle length changes over time. The cycle-average net P_{mech} output was calculated as the average value of each instantaneous power value for each cycle in the series. Total net work (W_{net}) was calculated by multiplying the cycle-average net P_{mech}

by the duration of the cycle series. Work loops were produced by plotting force against muscle length. The net efficiency of the muscle was determined using Equation 2.2:

$$\varepsilon_{net} = \frac{W_{net}}{EO_2} \qquad\qquad [2.2]$$

where ε_{net} is the net muscle efficiency, EO_2 is the energetic equivalent of oxygen consumed above basal metabolism and W_{net} is the net mechanical work performed.

2.3.7 Statistical analysis

One-way ANOVAs were used to test for differences in cycle-average net P_{mech} between the different sawtooth length trajectories. Bonferroni post-hoc tests were used to identify significant differences between factor categories. GLMs were used to check for linear relationships between the proportion of the cycle spent shortening and the W_{net} performed and energetic equivalent of oxygen consumption. Statistical analysis was performed in SPSS (Version 20.1, IBM).

2.4 Results

2.4.1 Muscle properties

The contractile properties of the muscles used in these experiments are displayed in Table 2.2. The peak isometric stresses of these muscles are comparable to those previously recorded for mouse soleus at similar temperatures (22.4 N cm^{-2} at 35°C, James et al., 1995; 21.2 N cm^{-2} at 37°C, Askew and Marsh, 1997; 47.1 N cm^{-2} at 37°C, Holt and Askew, 2012).

2.4.2 Mechanical power and net work

Net P_{mech} was found to increase with increasing proportions of the contraction cycle spent shortening (Figure 2.4). Saw25% cycles produced an average net P_{mech} output of 18.6 ± 1.94 W kg^{-1}, Saw50% produced 35.7 ± 2.29 W kg^{-1} and Saw75% produced 67.4 ± 4.07 W kg^{-1}. There was a significant effect of length

trajectory on net P_{mech} output ($F_{2,19}$ = 78.4, P < 0.001) with significant differences between each combination of Saw25%, Saw50% and Saw75% cycles (P < 0.001).

Table 2.2   Muscle properties and mean isometric stresses.

Property	Mean ± SEM (n = 13)
Muscle mass [M_m] (mg)	5.96 ± 0.16
Optimal resting length [L_0] (mm)	11.9 ± 0.2
Muscle Radius[1] (mm)	0.39 ± 0.01
Peak Isometric Stress (N cm^{-2})	29.5 ± 1.6

[1]Muscle radius was determined using the equation $\sqrt{(\frac{M_m}{\pi \times L_O \times \rho})}$ from Barclay, 2005, where ρ is the density of muscle (1060 kg m^{-3})
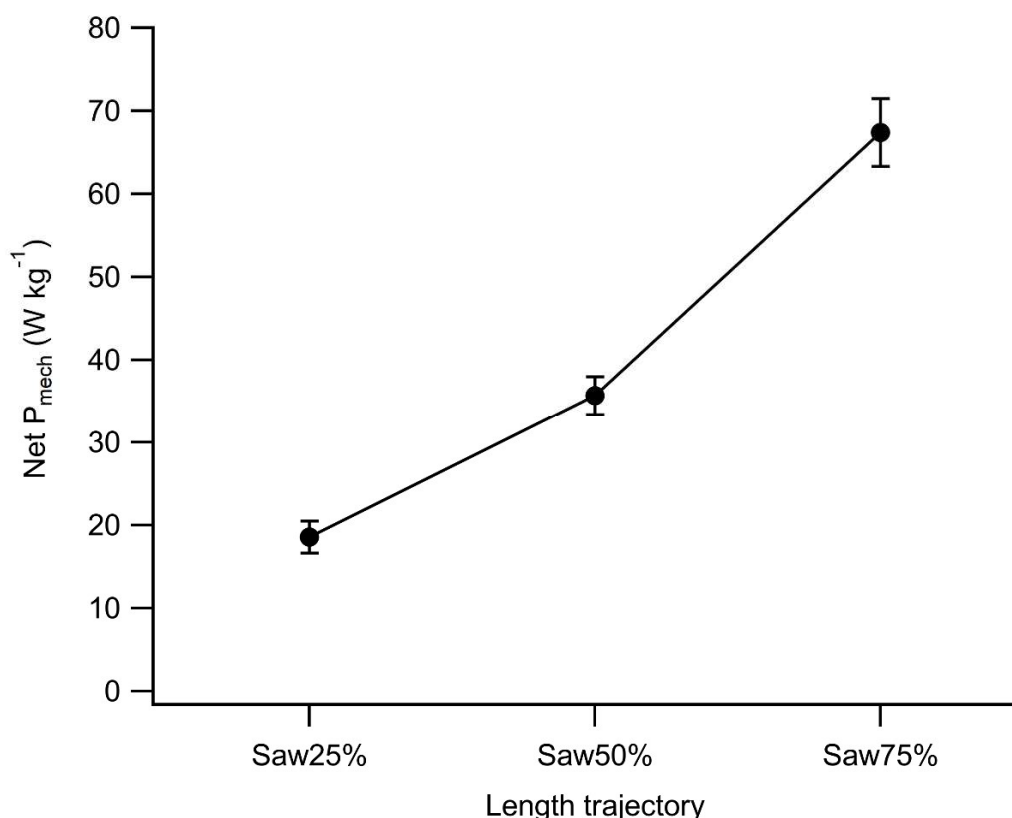
Figure 2.4   Relationship between net P_{mech} and length trajectory. Data presented as mean ± SEM. n = 8, 8 and 6 for Saw25%, Saw50% and Saw75% length trajectories respectively.
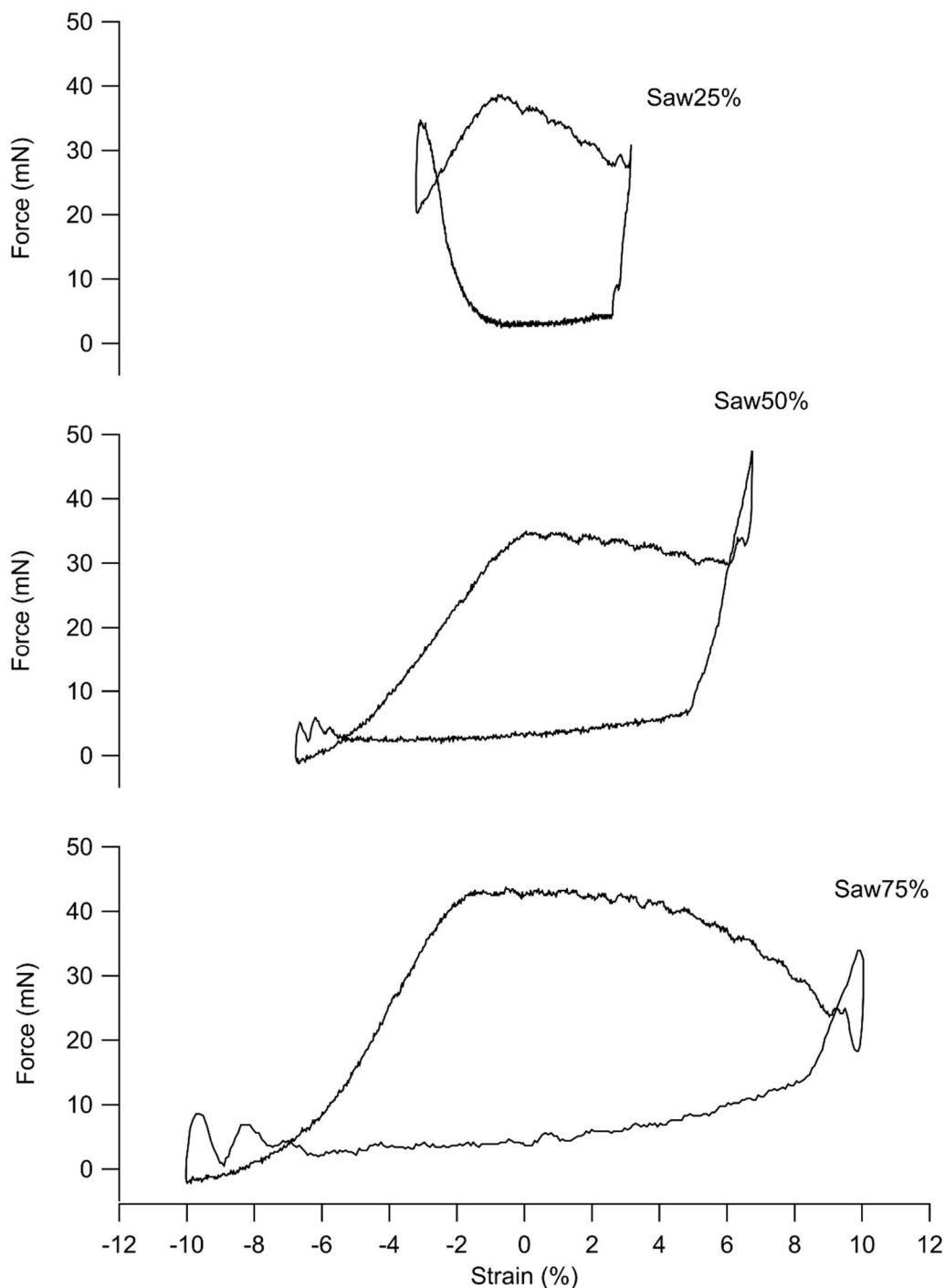
Figure 2.5   Representative work loops. Each work loop is representative of the net work generated over a whole cycle for each length trajectory.

W_{net} values were calculated from the net P_{mech} measurements. Saw25% cycles produced an average W_{net} per cycle of 0.74 ± 0.08 J kg^{-1}, Saw50% produced 1.49 ± 0.07 J kg^{-1} and Saw75% produced 2.7 ± 0.16 J kg^{-1}. There was a significant effect of length trajectory on the W_{net} generated per cycle ($F_{2,19}$ =

88.65, P < 0.001) with significant differences between each combination of Saw25%, Saw50% and Saw75% cycles (P < 0.001) as shown in Figure 2.6. Representative work loops are presented in Figure 2.5.

2.4.3 O_2 consumption

The average resting oxygen consumption of a muscle in Krebs-Henseleit solution at 39°C was 335 ± 35 J min^{-1} kg^{-1}. This equates to 16.7 ml O_2 min^{-1} kg^{-1}. These values are similar to those previously reported for mouse soleus muscles (270 J min^{-1} kg^{-1} extrapolated from 20°C using a Q_{10} of 2; Crow and Kushmeric 1982) and rat soleus muscles (320 J min^{-1} kg^{-1} extrapolated from 20°C using a Q_{10} of 2; Heglund and Cavagna 1987).
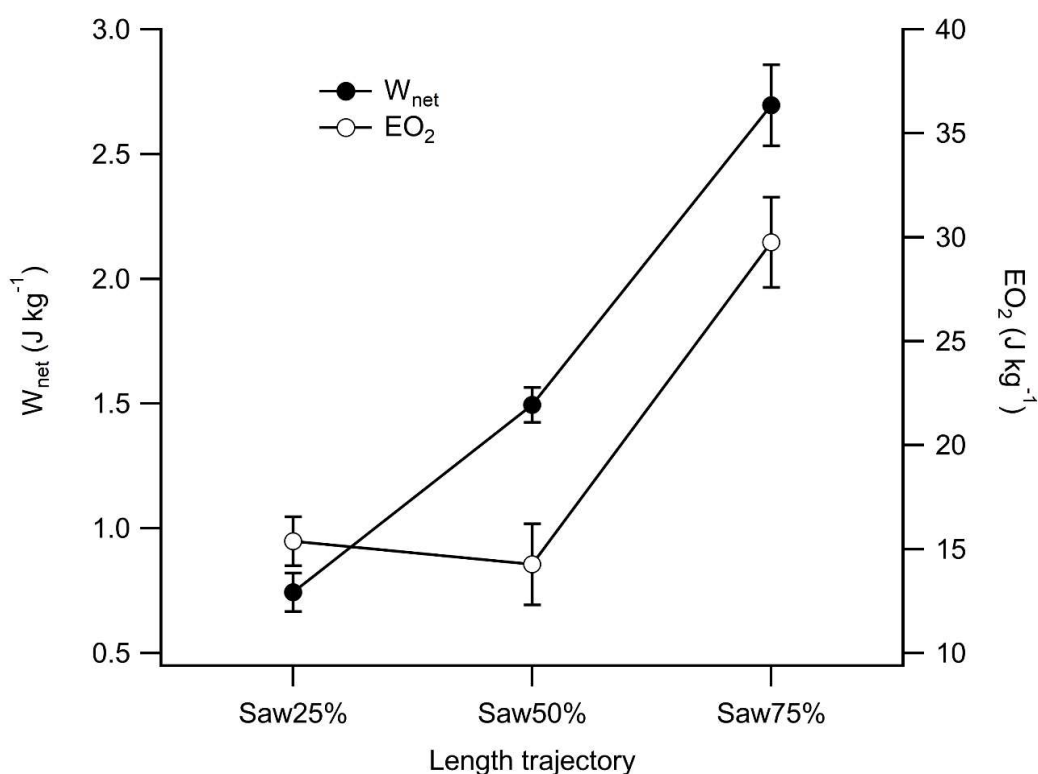
Figure 2.6　**Relationships between W_{net} (filled circles) and EO_2 (empty circles) and length trajectory.** Data presented as mean ± SEM. n = 8, 8 and 6 for Saw25%, Saw50% and Saw75% length trajectories respectively.

PO_2 declined at this resting rate prior to stimulation, after which the rate of oxygen consumption increased, after a delay of between 1 and 10 seconds.

This delay is believed to be due to the time it takes for oxygen to diffuse into the muscle for metabolic recovery (Heglund and Cavagna, 1987). Following the conclusion of oxidative recovery metabolism, the rate of oxygen consumption returned to the same resting oxygen consumption rate as prior to stimulation in most instances. Linear regressions were applied to the oxygen trace before and after oxygen recovery to determine the amount of O_2 consumed during the active consumption period. An experimental recording of O_2 consumption is displayed in Figure 2.3.

The mean active oxygen consumption following stimulation was 15.38 ± 1.17 J kg^{-1} per cycle for Saw25%, 14.27 ± 1.96 J kg^{-1} per cycle for Saw50% and 29.8 ± 2.2 J kg^{-1} per cycle for Saw75%. The relationship between the proportion of the cycle spent shortening and the energetic equivalent of the oxygen consumption (EO$_2$) does not appear to be linear ($F_{2,19}$ = 21.9, R^2 = 0.42, $P > 0.1$) as shown in Figure 2.6. There was a significant effect of length
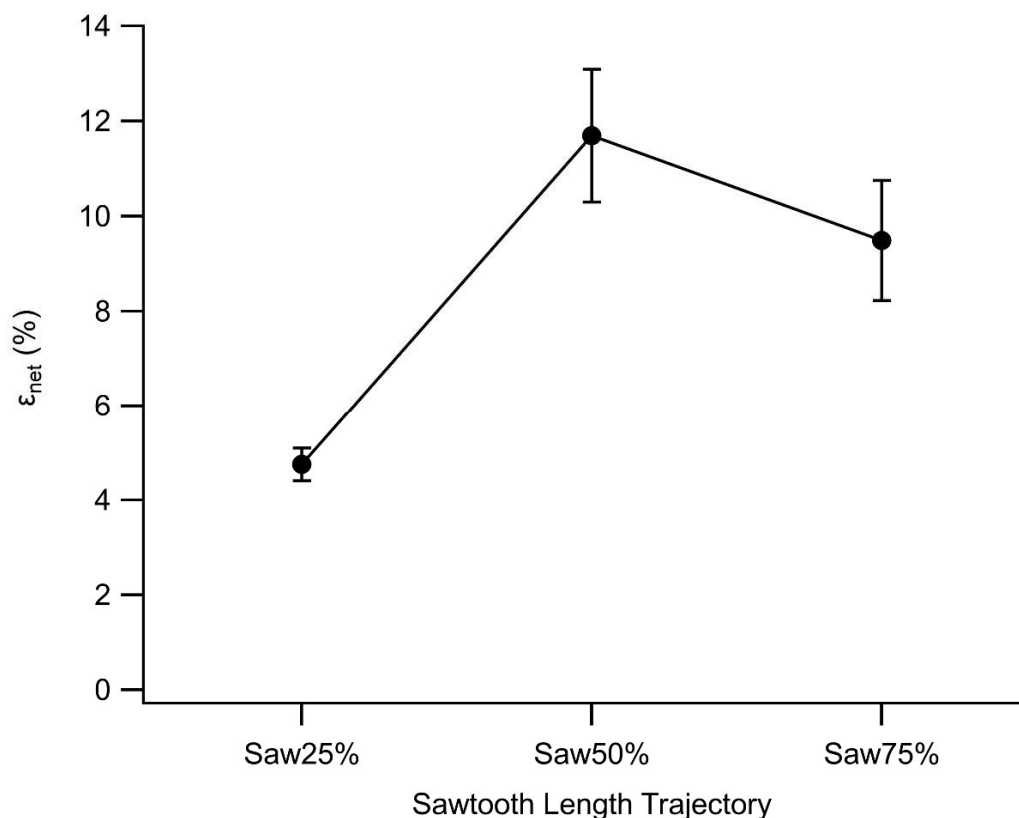
Figure 2.7 Relationship between ε$_{net}$ and length trajectory. Data presented as mean ± SEM. n = 8, 8 and 6 for Saw25%, Saw50% and Saw75% length trajectories respectively.

trajectory on the oxygen consumption per cycle ($F_{2,19}$ = 21.5, P < 0.001) with significant differences between Saw25% and Saw75% (P < 0.001) and between Saw50% and Saw75% (P < 0.001) but not between Saw25% and Saw50%.

2.4.4 Net efficiency

The mean ε_{net} ranged from 4.76 ± 0.34% for Saw25% to 11.7 ± 1.4% for Saw50% and 9.48 ± 1.3% for Saw75% (Figure 2.7). There was a significant effect of length trajectory on the ε_{net} ($F_{2,19}$ = 11.5, P < 0.01) with a Bonferonni post-hoc test finding significant differences between Saw25% and Saw50% (P < 0.01) and between Saw25% and Saw75% (P < 0.05) but not between Saw25% and Saw50% or Saw75%.

2.5 Discussion

2.5.1 Effects of asymmetric length trajectories on mechanical power output

In support of our hypotheses, both net P_{mech} output (Figure 2.4) and the W_{net} generated per cycle (Figure 2.6) increased with an increasing proportion of the cycle spent shortening. Our net P_{mech} values are similar but slightly lower than the values reported by Askew and Marsh (1997) and Holt and Askew (2012) which is likely due to the effects of muscle fatigue developed over sequential contraction cycles. The experimental runs in the Askew and Marsh (1997) and Holt and Askew (2012) studies were all limited to 5 cycles, while the experimental runs in this study consisted of 20 cycles, presenting a greater opportunity for the development of muscle fatigue and subsequent reduction in net P_{mech} during the later cycles (Askew et al., 1997). From our assessment of mechanical performance, we can determine that the muscles used in these experiments are mechanically similar to those used in previous studies of mouse soleus performance and therefore appropriate for comparative energetic studies.

The positive linear relationship between net P_{mech} and the proportion spent shortening isn't unexpected as previous research has demonstrated the positive consequences of increased relative shortening durations on mechanical power generation (Askew and Marsh, 1997, Marsh, 1999, Holt and Askew, 2012). There are several factors that contribute to this increase in mechanical power, including increasing optimal strain amplitudes that generate more work per cycle, longer durations over which to fully activate the muscle and generate force, and faster stretch velocities during lengthening which allows for rapid force development and greater net P_{mech} (Askew and Marsh, 1997).

2.5.2 Effects of asymmetric length trajectories on O_2 consumption and net efficiency

This study presents the first ε_{net} values for skeletal muscles contracting at Saw25% (4.76%), Saw50% (11.7%) and Saw75% (9.48%) sawtooth length trajectories (Figure 2.7). O_2 consumption per cycle increased with the proportion of the cycle spent shortening and also increased with the W_{net} generated per cycle (Figure 2.6). The relationship between ε_{net} and increasing proportion of the cycle spent shortening does not appear to be linear, as the ratio of W_{net} performed to molecules of O_2 consumed during the Saw25% cycles is much lower than the Saw50% and Saw75% cycles, resulting in a lower net efficiency.

These results demonstrate that it is possible to enhance muscle power output during asymmetrical cycles by increasing the proportion of the cycle spent shortening without significantly reducing the net muscle efficiency. However, contraction cycles that spend less than 50% of the cycle shortening suffer a reduced net efficiency by up to 6% compared to symmetrical cycles, which supports the findings of Holt and Askew (2012) for initial mechanical efficiency. They suggest that this reduction may be caused in part by several factors related to non-shortening processes: (1) the reduced period spent shortening may result in a less complete activation of the muscle fibres, which would reduce the force production during cross-bridge cycling (Biewener et al.,

1998), (2) spending a higher proportion of the available metabolic energy on producing negative work during the proportionally longer period of lengthening (Proske and Morgan, 1999), and (3) a higher proportion of the total muscle energy expenditure is spent on non-force generating processes such as Ca^{2+} ion pumps (Alexander, 1991). These conclusions are supported by the work of Curtin and Woledge (1996), which showed that stimulation that continues longer into shortening increases the metabolic energy consumption during lengthening. In this study, the proportion of shortening spent being stimulated was higher (80%) in the Saw25% cycles than in both the Saw50% and Saw75% cycles (60%).

Assuming that the initial mechanical efficiency of a muscle is expected to be approximately twice the value of net efficiency (Smith et al., 2005), the net efficiency values presented in this study are similar to those predicted from the initial mechanical efficiency values estimated by Holt and Askew (2012) for Saw25% (~4%), Saw50% (~13%) and Saw75% (~13%), indicating that metabolic recovery efficiency remains constant between asymmetrical length trajectories. The Saw75% value we measured is slightly lower than predicted by this assumption, suggesting that there may be a slight reduction in efficiency at the expense of higher mechanical power when more than 50% of the cycle is spent shortening, but this value is not significantly different from the net efficiency value observed during the Saw50% cycles.

Our Saw50% and Saw75% net efficiency values are also similar to the net efficiency values for mouse muscle during work-generating contractions between 0.5 and 4.5 Hz as estimated by Barclay and Weber (2004) using enthalpy measurements at 35 °C. Their study estimated a net efficiency value of 12.6% for a contraction protocol that was optimised for maximum efficiency by minimizing the contributions to net enthalpy during lengthening, whereas the contraction parameters used in this study maximised mechanical power output for each length trajectory. This may explain the slightly lower net muscle efficiency values observed in this study compared to theirs.

In conclusion, the results of this study suggest that an increased proportion of the cycle spent shortening can enhance mechanical power output without a substantial reduction in net muscle efficiency, but also that a reduced proportion of the cycle spent shortening can significantly reduce net muscle efficiency. This reduction may be due to energy expenditure during non-shortening processes rather than during shortening. It is thought that this relationship between net muscle efficiency and length trajectory will not be unique to the mouse soleus and are likely to be similar in the skeletal muscles of other organisms.

2.5.3 Validation of method for avian flight muscles

As well as examining the role of asymmetric length trajectories on the net efficiency of vertebrate muscle, these experiments also served to test and validate the use of this methodology with isolated preparations of avian pectoralis in order to examine the currently unknown avian muscle efficiency. While there are intraspecific differences in the optimal contractile parameters between mouse soleus and avian pectoralis, the fundamental mechanical and energetic processes will remain the same. The predominantly oxidative fibre type of pectoralis muscles in small birds (Welch and Altshuler, 2009) and high-power generation capabilities during in vitro experiments (Ellerby and Askew, 2007a) make it likely that simultaneous work and O_2 consumption measurements can be used to estimate avian muscle efficiency.

Chapter 3

The mechanical efficiency of the pectoralis muscles in budgerigars (*Melopsittacus undulatus*) during flight

3.1 Abstract

Flight is an energetically expensive activity for volant birds with a substantial portion of this energy being consumed by the major locomotor muscles to generate mechanical work to move the wings and transfer energy to the air. The mechanical power requirements of the flight muscles are known to change with flight speed in order to overcome different aerodynamic requirements, but there are currently no empirical estimates of the metabolic costs of flight at the muscular level. The metabolic power of the pectoralis muscle has previously been estimated using predictive models based on mechanical power and assumed values of muscle efficiency and the postural costs of flight. However, the muscle efficiency of the avian pectoralis has not yet been determined and previous predictions of how muscle efficiency may change with flight speed have been largely theoretical. By simultaneously measuring the generation of work from isolated muscle fibre bundles undergoing contraction cycles and the change in O_2 consumption relative to resting muscle as an indicator of the energetic costs associated with stimulated contractions, we calculated the net flight muscle efficiency of the budgerigar (*Melopsittacus undulatus*) pectoralis across three flight speeds. Mean net flight muscle efficiency ranged between 19.1% and 24.8% but did not change significantly between the flight speeds of 4 and 16 m s^{-1}. This helps to unify our understanding of flight mechanics and energetics by revealing one of the two previously unknown values in estimates of metabolic flight costs calculated from mechanical power. While these results may be valid for similar sized birds, other species may possess different muscle contractile properties, which may affect their muscle efficiencies and also their relationship with flight speed.

3.2 Introduction

Flight is an energetically expensive form of locomotion (Alexander, 1999), but it is essential for the survival and reproduction of volant birds. These energetic costs encompass a number of metabolic processes that transform the energy gained from food into mechanical work generated by the flight muscles to power the wings in order to overcome drag and generate momentum through the air. A substantial portion of this metabolic energy is thought to be consumed by the major flight muscles, the pectoralis muscle and the supracoracoideus muscle, which power the downstroke and upstroke phases of the wingbeat, respectively (Tobalske, 2007, Biewener, 2011), but energy is also consumed by the wing muscles to control the wing shape and angle during flight (Biewener, 2011). Together with increases in energy use by physiological systems such as circulatory and respiratory systems above the basal metabolic rate, these non-pectoralis energetic costs constitute the postural costs of flight (Morris et al., 2010), which contribute towards the total metabolic costs of flight.

The total metabolic costs of flight have been calculated using a number of experimental methods. Whole-animal metabolic measurements have been taken from birds flying in specially constructed wind-tunnels using indirect calorimetry techniques, such as respirometry (Tucker, 1966, Ward et al., 2002, Ward et al., 2004, Morris et al., 2010) and doubly-labelled water isotope elimination (Tatner and Bryant, 1986, Butler et al., 2004, Ward et al., 2004). However, calculating accurate metabolic costs from respirometry can be complicated as the imposed drag of the mask and tubing is likely to increase the metabolic costs of flight above those in free-flying birds (Ward et al., 2002, Morris et al., 2010) and doubly-labelled water studies usually require at least two hours of flight to get useful results (Butler et al., 2004), making it largely impractical for investigating short constant-speed flights. A more economic and time-efficient way of estimating the metabolic costs of flight is to calculate estimations from mechanical flight power using aerodynamic models. Past

studies (Pennycuick, 1968a, Tucker, 1973, Pennycuick, 2008) have used the Equation 3.1 to estimate flight metabolic energy expenditure.

$$P_{met} = \frac{k_{pos}}{\epsilon_{fm}} P_{mech} + P_{bas} \qquad [3.1]$$

where P_{met} is the metabolic power, k_{pos} are the postural costs, ϵ_{fm} is the mechanical efficiency of the avian pectoralis muscle, P_{mech} is the measured or calculated mechanical power and P_{bas} is the basal metabolic costs of the bird at rest. Whilst values for the in vivo metabolic (Tucker, 1968, Tucker, 1972, Bernstein et al., 1973, Bundle et al., 2007) and mechanical (Dial et al., 1997, Askew and Ellerby, 2007, Morris and Askew, 2010b) power requirements of flight have been collected by experimental methods for multiple bird species, both the muscle efficiency of the pectoralis and the postural costs are unknown and estimated values are used with little empirical basis. In order to produce meaningful estimates of metabolic flight costs in wild birds using these models, these two unknown values must be determined.

The net efficiency of avian flight muscle (net ϵ_{fm}) is calculated as the ratio of mechanical power output produced by the pectoralis muscle during downstroke to the muscular energy expenditure above the basal metabolic rate (Smith et al., 2005) and is used as a representative measure of how much of the metabolic energy intake is usefully transformed into work to move the bird through the environment. Generally, skeletal muscle is thermodynamically inefficient, transforming only a small proportion of the available metabolic energy into useful work and releasing the majority as heat (Hill, 1938). Measured estimates of net muscle efficiency vary between 5-35% across different animal taxa including mammals (Barclay, 1996, Barclay et al., 2010), reptiles (Woledge, 1968), amphibians (Heglund and Cavagna, 1987), fish (Curtin and Woledge, 1996) and insects (Josephson and Stevenson, 1991). However, the net efficiency of avian flight muscle is currently unknown and estimates of the metabolic costs of flight calculated from aerodynamic models and mechanical power measurements in flying birds have used

uncorroborated values of 10-23% (Pennycuick, 1968a, Tucker, 1973). The most commonly used values are towards the higher end of this range (19-23%) but there is little validation for these values.

It is also unknown how flight muscle efficiency may vary with flight speed and previous predictions have been largely theoretical. When calculating the metabolic power of avian flight from aerodynamic models of mechanical power, Tucker (1973) and Pennycuick (1973) assumed a constant pectoralis muscle efficiency value of 23% across flight speeds. Contrary to this assumption, theoretical and whole-animal metabolic work from Rayner (1979b, 1999) and Ward et al. (2001) has suggested that flight muscle efficiency may be likely to increase with flight speed, whilst other predictions have suggested the efficiency-speed relationship may be U-shaped (Tucker, 1968). More recent work from Morris et al. (2010) also supports the prediction that the flight muscle efficiency of cockatiels should either increase linearly with flight speed or take the form of a U-shaped relationship when mechanical power values from different studies are used. By demonstrating how muscle efficiency predictions can be heavily affected by variance in the values of mechanical and metabolic power, they concluded that simultaneous measurements of the mechanical work and metabolic costs of the flight muscles need to be determined in order to obtain accurate estimates of flight muscle efficiency.

In the present study, we investigated the effects of varying flight speed on the net efficiency of the budgerigar (*Melopsittacus undulatus*) pectoralis muscle and present the first direct measurements of avian flight muscle efficiency by determining the metabolic energy consumption and mechanical power output from isolated pectoralis muscle fibres undergoing a series of realistic in vitro cyclical work loops. Estimating muscular energy use in combination with the work loop technique (Josephson, 1985, Askew et al., 1997) allows us to examine the effects of flight speed on net muscle efficiency by subjecting the muscles to realistic contraction cycles using stimulation parameters and strain patterns recorded from flying budgerigars (Askew and Ellerby, 2007).

Measuring O_2 consumption is considered to provide a good reflection of the metabolic energy used to produce mechanical work under aerobic conditions during muscle contractions and has been reproduced numerous times with success in skeletal and cardiac muscles from mammals (Heglund and Cavagna, 1987), fish (Harwood et al., 2002), amphibians (Kushmerick and Paul, 1976) and insects (Josephson and Stevenson, 1991). The pectoralis muscle (primary contributor of the power required for flight) of the budgerigar was selected for this study as the mechanical properties have previously been reported (Ellerby and Askew, 2007b), as well as data on whole-organism metabolic consumption (Tucker, 1968, Bundle et al., 2007), and it is primarily fuelled by oxidative metabolism, making it suitable for measurements of O_2 consumption (Barclay, 1994).

3.3 Materials and Methods

A considerable amount of the methodology for these experiments is shared with those already detailed in Chapter 2, but there are a number of subtle and important changes involved throughout and so the full methodology is included.

3.3.1 Oxygen electrode and muscle chamber setup

Muscle oxygen consumption was determined polarographically using respirometry in a closed, glass chamber (Rank Bros Ltd., Cambridge; Figure 3.1). A glass chamber was selected, as it is chemically inert and effectively impermeable to oxygen. The lid of the chamber was constructed using Kel-F, a plastic that has near-zero moisture absorption and extremely low outgassing of oxygen (<0.01% O_2 in 24h; Stevens, 1992). A conical depression in the inner profile of the lid facilitated the removal of air bubbles from the chamber via a hole in the centre of the lid following injection of fresh Krebs-Henseleit's solution. The volume of the chamber with the lid in place was 2.75 ml. This was calculated by incrementally injecting water into the chamber via a syringe until the chamber was full.

A small PTFE-coated stir bar was used in conjunction with the magnet under the oxygen electrode to thoroughly mix the Krebs-Henseleit's solution (Figure 3.1). The muscle chamber was filled with oxygenated Krebs-Henseleit Krebs-Henseleit's solution (concentrations in mmol l^{-1}: 117 NaCl, 4.7 KCl, 2.5 $CaCl_2$, 1.2 $MgSO_4$, 24.8 $NaHCO_3$, 1.2 KH_2PO_4 and 11.1 Glucose, pH 7.59 at 40°C when bubbled with 95% O_2 and 5% CO_2; Burton, 1975). A temperature of 40°C was chosen to replicate the pectoralis muscle's temperature during flight (Ellerby and Askew, 2007a). The temperatures of the Krebs-Henseleit's solution and the oxygen chamber were maintained at approximately 40°C using a refrigerated water bath unit (Model TC120, Grant Instruments Ltd., Cambridge) that circulated temperature controlled water through the chamber's water jacket.

A Clark-type oxygen electrode (Rank Bros Ltd., Cambridge; Figure 3.1) built into the base of the muscle chamber was used for these experiments. The oxygen electrode consisted of an outer silver-silver chloride ring reference electrode and a smaller platinum disc electrode that acted as the cathode and was used to detect changes in the oxygen content of the solution in the chamber. The chamber and lid were washed daily with 100% ethanol and rinsed with distilled water before a period of experimentation to remove microorganisms. The platinum and silver-silver chloride electrodes were soaked with 3M KCl to act as the electrolyte for the electrode and a semi-permeable PTFE membrane was placed across the electrodes through which oxygen could reach the electrode but which prevented mixing of the electrolyte and the Krebs-Henseleit's solution in the chamber. The oxygen electrode was calibrated before each experimental period by ensuring the electrode's control box (Digital Model 10, Rank Bros Ltd., Cambridge) was outputting zero volts when disconnected from the electrode and that the sensitivity of the control box was adjusted to 95% when the 95% O_2, 5% CO_2 Krebs-Henseleit's solution first entered the chamber.

The chamber was tightly sealed except for a thin aperture in the lid (approximately 1.2 mm) through which the ergometer rod fitted and another

aperture (approximately 1.2 mm) in the lid which was used to flush the chamber with oxygenated Krebs-Henseleit's solution and through which a thermocouple (Type T Model BAT-12, Physitemp, NJ, USA) was inserted into the chamber to monitor temperature. The electrode's output in response to changes in oxygen concentration would stabilise within approximately 30 seconds following the injection of oxygenated Krebs-Henseleit's solution through the aperture in the lid.
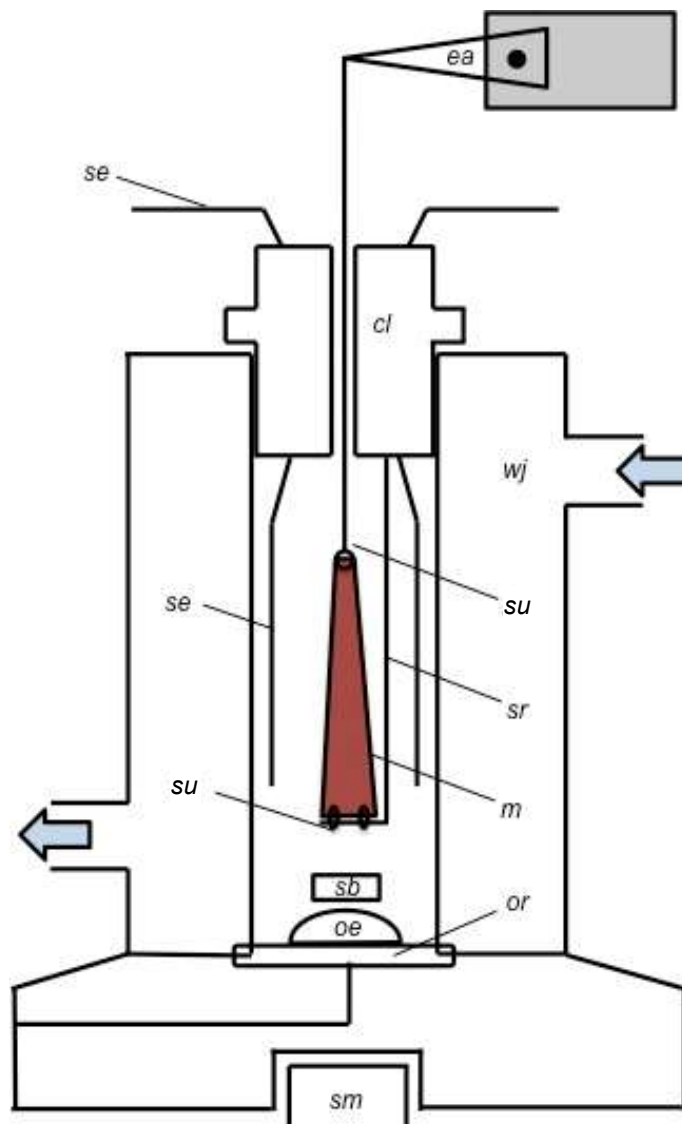
Figure 3.1   Technical diagram of the avian muscle chamber and ergometer setup. Components include stirring magnet (sm), oxygen electrode (oe), O-ring (or), stir-bar (sb), sutures (su), muscle (m), support rod (sr), silver stimulating electrodes (se), water-jacket (wj), chamber lid (cl) and the ergometer arm (ea).

3.3.2 Muscle preparation

Adult budgerigars (*Melopsittacus undulatus*; Shaw, 1805) were housed in a licenced facility and killed by cervical dislocation under terminal isoflurane-induced anaesthesia. Feathers surrounding the incision site on the ventral surface of the bird's chest were removed prior to the incision. An incision was made into the pectoralis muscle on one side of the sternum to access the major flight muscles. A suture was attached to the intramuscular tendon close to the insertion of the deltopectoral crest of the humerus and a section of pectoralis muscle was carefully removed. The sternum was then cut so that a small amount remained attached to the removed muscle section. The muscle was regularly irrigated with chilled oxygenated Krebs-Henseleit's solution during removal. The end with the piece of sternum was sutured on to the support rod that was attached to the chamber lid. The tendon at the other end was sutured on to a hooked rod that was attached to the arm of the ergometer. All air bubbles were carefully removed from the chamber prior to placement of the lid. The chamber lid and mounted muscle were then lowered into the chamber and fitted securely. Once the muscle was secure in the chamber, it was left for a period of 10 minutes to recover from the dissection and to thermoequilibriate.

The high temperature conditions of the muscle chamber and the radius of the muscle limited the diffusion of oxygen to the centre of the muscle. According to Barclay (2005), it can be estimated that the centre of these pectoralis muscle preparations (mean radius 0.86 mm) would have become anoxic after approximately 10 seconds of continuous contraction cycles. To mitigate this, exogenic PO_2 at the muscle surface was kept above 70% at all times, all contraction cycle series were limited to a maximum of 1.4 seconds and muscles were left for at least 10 minutes between contraction sequences to facilitate full metabolic recovery. The contribution of anaerobic metabolism to the production of energy during the contractions is assumed to be negligible based on the findings that anaerobic metabolism (calculated by measurement of accumulated lactate, pyruvate and alanine in a similar muscular respiration chamber) contributed a maximum of 5% of the energy consumed for a

strenuous 15 second tetanus in the mouse soleus in Krebs-Henseleit's solution with a high PO_2 at 20°C (Crow and Kushmerick, 1982).

3.3.3 Ergometer setup

An ergometer (Model 300B-LR; Aurora Scientific Inc., Ontario, Canada) was used to control muscle length and to measure the force and muscle length changes during contraction cycles. The ergometer rod and a support rod built into the underside of the chamber lid were used to secure the muscle in the chamber and to facilitate the manipulation of muscle length via the ergometer (Figure 3.1). The ergometer arm was attached to a vertically-movable platform (C. F. Palmer, London) which was adjusted to remove slack from the muscle and to position it at approximately in vitro resting length. The horizontal position of the ergometer was also adjusted to align the stainless steel rod connected to the muscle directly down the centre of the hole in the chamber lid to minimise interference with force measurements.

3.3.4 Mechanical power measurements

3.3.4.1 Isometric contractile properties

Following the 10 minute recovery period after dissection, a series of isometric twitches were conducted using a supramaximal stimulus with a pulse width of 0.2 ms at increasing muscle lengths (increments of 0.5 mm) to determine the maximum isometric twitch force for the muscle and the associated optimal resting muscle length (L_0). After determining L_0, the length of the muscle was reduced by 7% for the work loop cycles to simulate in vivo muscle length during flight (Ellerby and Askew, 2007a). This reduced length was used for all subsequent experimental contractions.

The muscle was stimulated (applied by a Model S48G Stimulator, Grass Medical Instruments, MA, USA via a Stimulus Isolation Unit, Type 236, Hugo Sachs Elektronik, March-Hugstettem, Germany) which was delivered by the two chloride-coated silver stimulating rods fitted through the lid. The direction of current flow was alternated by changing the polarity of the electrodes with

each stimulus to prevent electrolysis at the stimulating electrodes. A series of control stimulated cycles without a muscle in the chamber were performed to ensure electrolysis was not affecting the oxygen content in the chamber. The muscle length changes and forces produced by muscle contractions were logged to a PC *via* a 12-bit A/D converter (DAS-1801AO, Keithley Metrabyte, OH, USA) and recorded using TestPoint software for calculations of mechanical work (TestPoint Version 7, Capital Equipment Corp, MA, USA).

Control isometric twitches performed immediately before each set of work loops were used to monitor any decline in the muscle's performance. Work loops performed while the muscle was below 65% of peak twitch performance were not used in the analysis. The decline in muscle performance was assumed to be linear (Askew and Marsh, 1997). A recovery period of 1 minute was allotted following each twitch to allow for metabolic recovery. The muscle chamber was re-oxygenated prior to each experimental run by flushing approximately 10 ml of Krebs-Henseleit's solution bubbled with 95% O_2 and 5% CO_2 at 39°C. This ensured the muscle had sufficient exogenous oxygen for recovery metabolism. Excess Krebs-Henseleit's solution exited the chamber through the aperture with the ergometer rod and was captured with tissue paper to prevent any contact between the solution and the electrical components of the electrode.

3.3.4.2 Stimulated contraction cycles

The work loop technique technique (Josephson, 1985, Askew et al., 1997) was used to subject the isolated muscle to cyclical muscle length changes and stimulation patterns in order to generate mechanical work under semi-realistic conditions (Table 3.1). These work measurements allowed the calculation of net work and mechanical power output. To determine the effects of different flight speeds, the muscles were stimulated using three sets of stimulation parameters (phase, duration, cycle frequency and strain) to simulate flight speeds of 4, 10 and 16 m s^{-1} (Figure 3.2). These experiments were carried out at cycle frequencies of 15 and 16 Hz which are representative of budgerigar wingbeat frequency during forward flapping flight; (Ellerby and Askew, 2007a).

These numbers of cycles were chosen as they were predicted to require levels of oxygen consumption that would be detectable by the oxygen electrode, but not promote anaerobic metabolism or muscle fatigue. Following the completion of the work loops or when the performance of a muscle had declined significantly, the muscle preparation was removed from the chamber and the tendon and bone were removed from the ends of the muscle. Any muscle fibres not contributing to force production (i.e. damaged fibres not running the full length of the preparation) were carefully removed and the muscle preparation was blotted lightly with tissue paper before being weighed using an analytical balance (Sartorius, Germany).

Table 3.1   **Muscle strains and stimulation parameters for each simulated flight speed.**

Simulated Flight Speeds (m s^{-1})	4	10	16
Cycles performed	20	20	20
Contraction frequency (Hz)	16	15	16
Total duration (s)	1.25	1.33	1.25
Strain (±%)	7.7	5.8	7.4
Phase (ms)	-0.7	-9.6	-6.1
Stim duration (ms)	18.6	20.7	18.6

Duration = Total time duration between the start and end of contractions

Strain = Amplitude of length change from longest to shortest peak length expressed as a percentage of L_0

Phase = Timing of stimulation, relative to peak length

Stim duration = Duration of stimulation per cycle
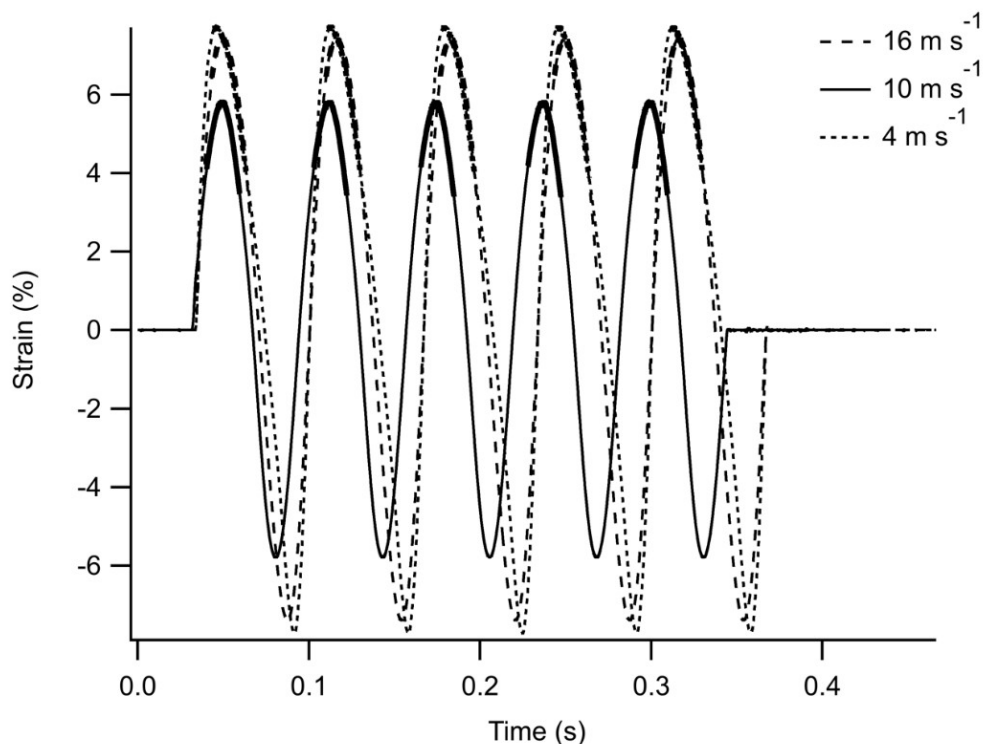
Figure 3.2 **In vivo length trajectories for pectoralis at 4, 10 and 16 m s^{-1}.** Bold sections indicate stimulation duration. Length change and stimulation data provided by Ellerby and Askew (2007a).

3.3.5 Correction for electrode oxygen consumption and leak

When experimental conditions were tested without a muscle present, the oxygen concentration of the chamber decreased over time due to oxygen consumption at the oxygen electrode, potential absorption by materials held within the chamber (e.g. the stir-bar and O-ring) and leak through the chamber lid. There were two narrow holes in the chamber lid through which oxygen could leak and the non-glass components also absorbed oxygen, which resulted in an exponential decline in the oxygen concentration of the chamber over time. This asymptote represents the point at which the combined rate of oxygen decline through chamber leak and oxygen consumption of the electrode equals the rate of oxygen entering the system. A correction to account for this background oxygen consumption was produced by generating a series of oxygen decline curves in the chamber without a muscle and determining the mean coefficients for a double-exponential curve (Equation 2.1). All results refer to the corrected data.

3.3.6 Quantifying O_2 consumption

The metabolic cost of the mechanical work performed by the muscle during the work loops was determined by measuring the O_2 consumed by the muscle during oxidative recovery metabolism. The oxygen concentration in the chamber was continuously sampled at a rate of 20 Hz using LabChart software (LabChart, Version 5.5.6, AD Instruments, Oxford) via a PowerLab data acquisition system (PowerLab Model 4/25, AD Instruments, Oxford) to ensure small or rapid changes were detectable. Once the muscle had been secured in the oxygen chamber, the oxygen concentration was measured for at least 5 minutes to obtain a reliable baseline. Following completion of the work loops, the muscles were left for a period of approximately 5 minutes to fully record the period of recovery oxygen consumption, during which time the rate of oxygen decline in the chamber increased above basal. Following the end of oxidative recovery, the decline in oxygen was recorded for a further 5 minutes to ensure a stable baseline had been reached. Due to the high metabolic rate of the muscle and the size of the muscle preparation, PO_2 declined rapidly in the chamber, limiting the time available to record baselines before re-oxygenation was necessary.

Once the correction for chamber leak and oxygen consumption by the electrode had been applied, linear regressions were fitted to the baselines preceding stimulation and following the completion of oxidative recovery as determined by a period of 1 minute with a stable rate of O_2 consumption (Figure 3.3). The change in the oxygen content of the Krebs-Henseleit's solution (ΔO_2) was calculated as the vertical offset between the two regression lines 30 seconds after the completion of the contraction cycles. This value provided an estimate of active oxygen consumption above basal metabolism that would aptly represent the net oxygen consumed (Trinh and Syme, 2007). ΔO_2 was then multiplied by the chamber volume (2.75 ml) and the oxygen solubility of the Krebs-Henseleit's solution (994.342 nmol O_2 ml^{-1} at a salinity of 8 ‰ at 39°C), which was determined using a standard dissolved oxygen solubility table to obtain the molar oxygen consumption, assuming standard atmospheric pressure (760 Torr / 101.325 kPa; Cameron, 1986). To

standardise the measurements of metabolic and mechanical energy, the oxygen consumption values were converted to Joule equivalents at a rate of 4.79×10^{-4} J $nmol^{-1}$ O_2 (or 20.1 J ml^{-1} O_2). Glucose was the only exogenous fuel source available to the muscle, so a respiratory quotient (RQ) of 1 was assumed (Crow and Kushmerick, 1982). The Joule equivalents of measured oxygen consumption were normalised for muscle mass and expressed as J kg^{-1} for analysis.
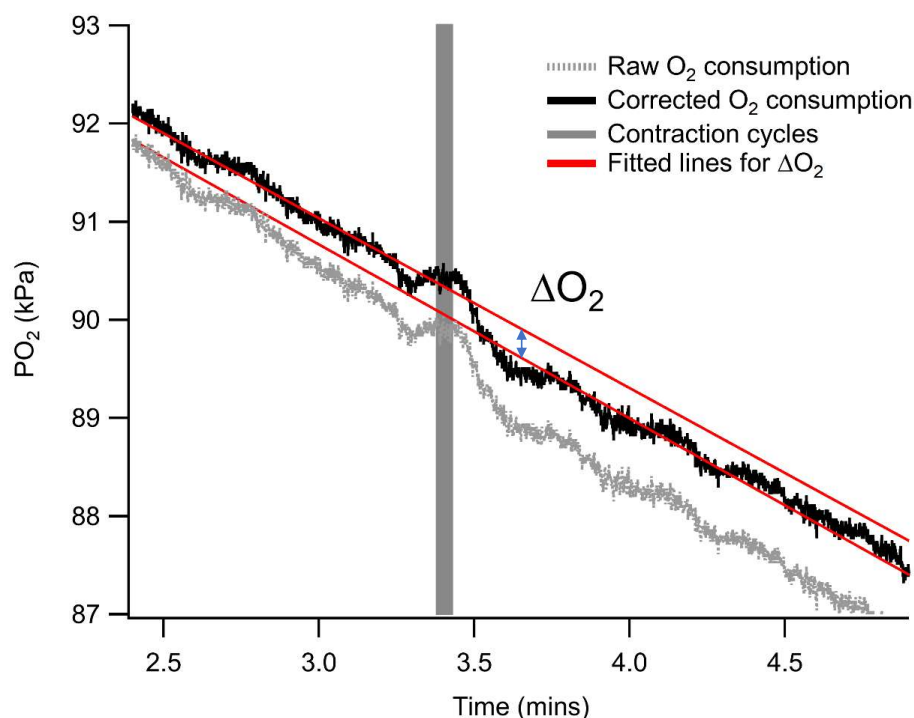
Figure 3.3 **Representative example of O_2 consumption trace.** The corrected trace (black) and uncorrected trace (light grey) are displayed. Dark grey bar indicates period of stimulated contraction cycles. Blue arrow indicates the difference between the pre-contraction and post-contraction resting O_2 consumption (ΔO_2).

3.3.7 Work loop analysis and efficiency calculations

Using force and muscle length measurements from the ergometer, instantaneous mechanical power output was determined for each cycle as the product of force and velocity (IGOR Pro Version 5.01; Wavemetrics, OR, USA).

Velocity was determined as the mathematical derivative of muscle length changes over time. The positive power output during shortening averaged over the whole cycle is equivalent to power generated over the wingbeat cycle, so the shortening mechanical power (shortening P_{mech}) was calculated as our measure of mechanical power generation which also allowed for comparison with published literature.

The shortening power output (shortening P_{mech}) was calculated as the average value of each instantaneous power value for each cycle in the series over the cycle duration. Shortening work (W_{short}) was calculated by multiplying the shortening power by the duration of the entire cycle series. Work loops were produced by plotting force against muscle length to visualise the work done by the muscle per cycle. The net flight muscle efficiency was determined by the following equation:

$$\text{Net } \varepsilon_{\text{fm}} = \frac{W_{short}}{EO_2} \qquad [3.2]$$

where net ε_{fm} is the net flight muscle efficiency, EO_2 is the energetic equivalent of oxygen consumed above basal metabolism and W_{short} is the mechanical work performed by the pectoralis muscle during the downstroke.

3.3.8 Statistical analysis

One-way ANOVAs were used to test for differences in shortening P_{mech}, W_{net}, EO_2 and ε_{net} between the different flight speeds. Bonferroni post-hoc tests were used to identify significant differences between factor categories. All values are reported as the mean average ± SEM unless stated otherwise. All statistical tests were performed in SPSS (Version 20.1, IBM).

3.4 Results

3.4.1 Muscle properties

The contractile properties of the budgerigar pectoralis muscle are reported in Table 3.2. Tetanic contractions were found to reduce the ability of the muscle to generate force which reduced time available for the measurement of O_2 consumption in functioning muscle; therefore, contractile property analysis was limited to peak twitch stress to maintain the longevity of the muscle preparation. Assuming a twitch:tetanus ratio of 0.51 for budgerigar pectoralis muscle (Ellerby and Askew, 2007a), the peak tetanic stress of our muscle preparations was approximately 161 kN m^{-2}, which is 73% of the muscle stresses found by Ellerby and Askew (2007a) (220 kN m^{-2}).

Table 3.2   Muscle properties and mean isometric stress.

Property	Mean ± SEM (n = 12)
Muscle mass [M_m] (mg)	66.9 ± 9.8
Optimal resting length (mm)	25.5 ± 0.4
Muscle radius[1] (mm)	0.86 ± 0.06
Peak isometric twitch stress (kN m^{-2})	82 ± 17.4

[1]Muscle radius was determined using the equation $\sqrt{(\frac{M_m}{\pi \times L_O \times \rho})}$ from Barclay, 2005, where ρ is the density of muscle (1060 kg m^{-3})

3.4.2 Mechanical power and net work

Cycles simulating flight speeds of 4 m s^{-1} produced an average shortening P_{mech} output of 19.5 ± 3.6 W kg^{-1}, 10 m s^{-1} cycles produced 14.4 ± 3.1 W kg^{-1} and 16 m s^{-1} cycles produced 26.2 ± 5.6 W kg^{-1}. These values were then corrected to account for the intermittent flight styles (83% and 61% of raw values for 4 and 10 m s^{-1}, respectively) and relative EMG intensities (85% of raw value for 10 m s^{-1}) recorded in vivo in order to estimate in vivo shortening power (Figure 3.4) using the corrections determined by Ellerby and Askew (2007a). The corrected shortening power outputs were 16.2 ± 3 for 4 m s^{-1}

cycles, 7.4 ± 1.6 for 10 m s^{-1} cycles and 26.2 ± 5.6 for 16 m s^{-1} cycles. Corrected shortening power varied significantly with flight speed ($F_{2,14}$ = 7.82, P = 0.005) but the uncorrected power did not.

Cycles simulating 4 m s^{-1} produced an average W_{short} per cycle of 1.05 ± 0.23 J kg^{-1}, 10 m s^{-1} cycles produced 0.72 ± 0.16 J kg^{-1} and 16 m s^{-1} cycles produced 1.18 ± 0.29 J kg^{-1} (Figure 3.5). The W_{short} generated per cycle did not statistically vary with simulated flight speed ($F_{2,14}$ = 1.7, P = 0.219) but the differences in work loop shape can be seen in Figure 3.6.
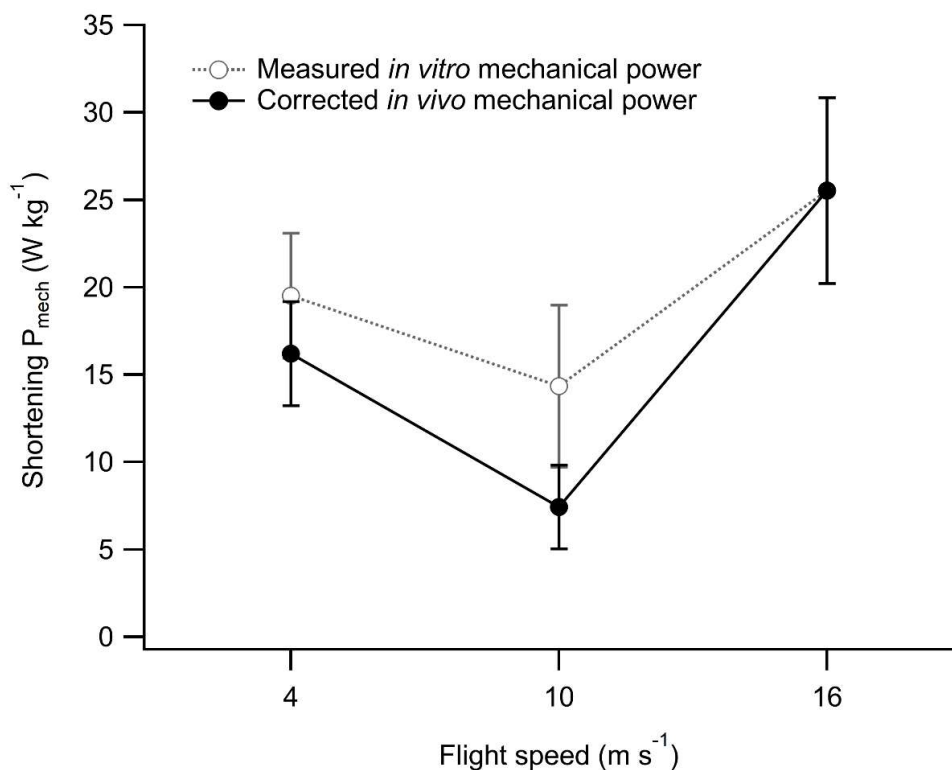
Figure 3.4 **Relationship between shortening P_{met} and flight speed.**
Black lines indicate simulated in vivo mechanical power, generated by correcting the measured in vitro mechanical power (grey lines) for EMG intensity and intermittent flight styles. Data presented as mean ± SEM. n = 5, 7 and 5 for 4, 10 and 16 m s^{-1} respectively.
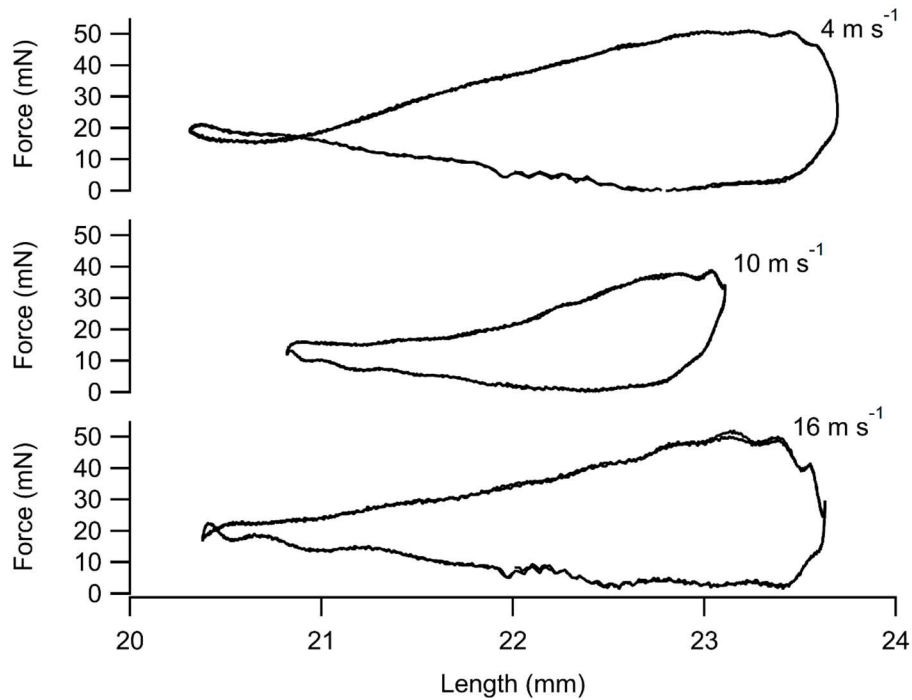
Figure 3.5 **Representative work loops.** Each work loop is representative of the net work generated over a whole cycle for each simulated flight speed. W_{short} is determined as the positive work generated over the descending (in this case, upper right towards lower left) limb of the work loop.

3.4.3 O_2 consumption

The average resting oxygen consumption of a muscle in Krebs-Henseleit's solution at 39°C was 349 ± 50 J min^{-1} kg^{-1}. PO$_2$ declined at this resting rate prior to stimulation, after which the rate of oxygen consumption increased after a delay of between 1 and 10 seconds. This delay is believed to be due to the time it takes for oxygen to diffuse into the muscle (Heglund and Cavagna, 1987). Following the conclusion of oxygen recovery metabolism, the rate of oxygen recovery returned to the same resting oxygen consumption rate as prior to stimulation in most instances. Linear regressions were applied to the oxygen trace before and after oxygen recovery to determine the amount of O_2 consumed during the active consumption period (Figure 3.3).

The oxygen consumption data are presented in J kg^{-1} per cycle to standardise between contraction frequencies and to allow for direct comparison with the W_{short} per cycle. The mean active oxygen consumption following stimulation was 6.54 ± 2.55 J kg^{-1} per cycle when simulating 4 m s^{-1}, 4.56 ± 1.33 J kg^{-1} per cycle when simulating 10 m s^{-1} and 5.52 ± 1.39 J kg^{-1} per cycle when simulating 16 m s^{-1} (Figure 3.5). The energetic equivalent of the oxygen consumption (EO_2) did not statistically vary with simulated flight speed ($F_{2,14} = 0.342$, $P = 0.716$).
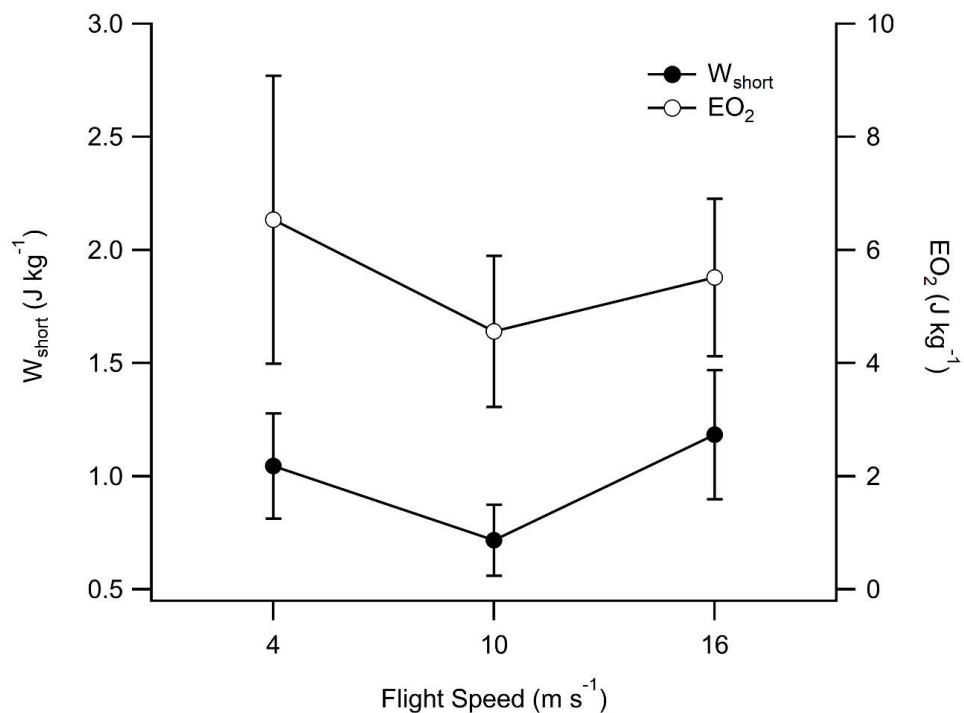
Figure 3.6   Relationship between W_{short} and EO_2 and flight speed. Data presented as mean ± SEM. n = 5, 7 and 5 for 4, 10 and 16 m s^{-1}, respectively.

3.4.4 Net efficiency

ε_{fm} ranged from 19.1 ± 3.1% at 10 m s^{-1} to 24.1 ± 3.8% at 16 m s^{-1} (Figure 3.7), but was independent of simulated flight speed ($F_{2,14} = 0.514$, $P = 0.609$), averaging 20.8 ± 2.1% (n = 17).
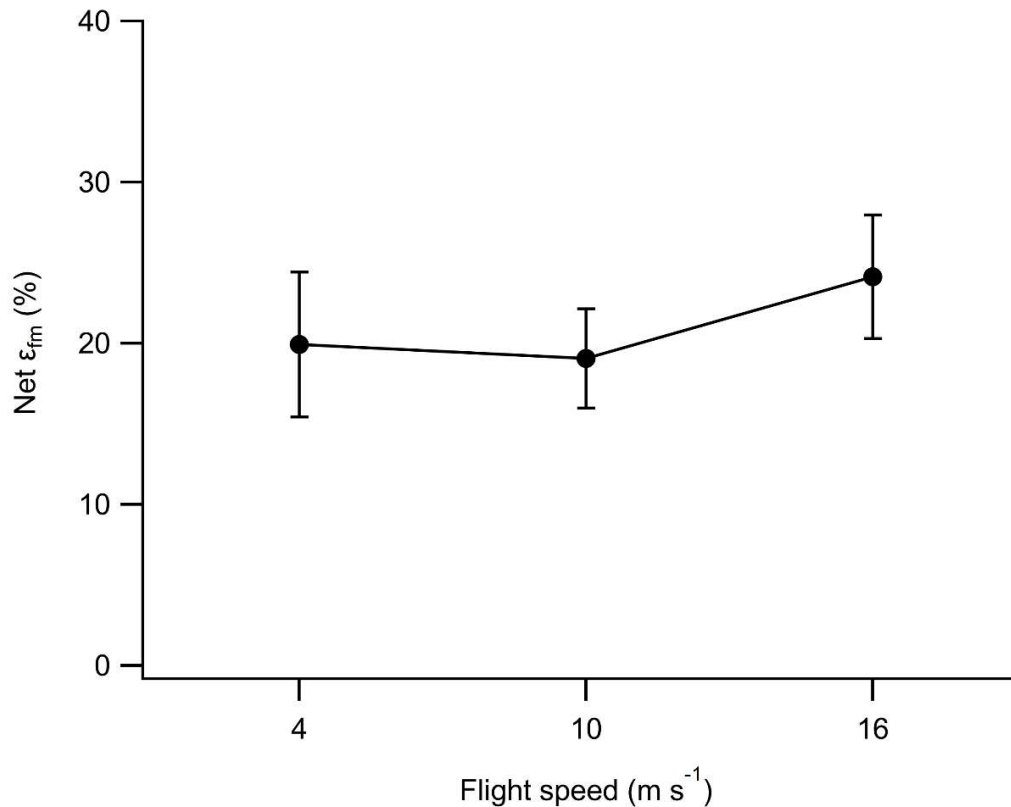
Figure 3.7   Relationship between net ε_{fm} and flight speed. Data presented as mean ± SEM. n = 5, 7 and 5 for 4, 10 and 16 m s^{-1}, respectively.

3.5 Discussion

3.5.1 Mechanical power and flight speed

The relationship between pectoralis mechanical shortening P_{mech} and flight speed was characterised by the typical U-shaped curve, as were the relationships for W_{short} per cycle and O_2 per cycle but these were not significantly distinct between speeds. These relationships are similar to the U-shaped power curves previously reported in budgerigars (Askew and Ellerby, 2007, Ellerby and Askew, 2007a) and other birds (Biewener et al., 1998, Morris and Askew, 2010a), as well as the curves predicted by aerodynamic models based on calculations of lift and drag (Pennycuick, 1968a, Rayner, 1999). The shortening P_{mech} of the muscles in this study was lower than those presented for budgerigars (40-70 W kg^{-1}) by Ellerby and Askew (2007), but these values

were corrected for the reduction in power due to fatigue, which was not performed in this study. Additionally, the subjects of their study were subjected to months of training in a wind tunnel prior to the muscle dissection which may have changed the physiological properties of the flight muscles compared to those used in this study, which were not trained at all (Butler and Turner, 1988).

3.5.2 Metabolic power, $P_{met,pec}$ and flight speed

Currently, there are only estimates of whole-animal metabolic power as the proportion of total metabolic power required by the pectoralis for flight ($P_{met,pec}$) is unknown. By multiplying the measured EO_2 per cycle by the contraction frequency for each speed, we can estimate that the metabolic power requirements of the budgerigar pectoralis range from approximately 68.9 ± 19.63 W kg^{-1} at 10 m s^{-1} to 115.13 ± 19.63 W kg^{-1} at 4 m s^{-1}. Previous whole estimates of the whole-animal metabolic costs of budgerigar flight range between 113.22 to 172.85 W kg^{-1} above resting metabolic rate for level flight at approximately 10 m s^{-1} (Tucker, 1968, Bundle et al., 2007). When our $P_{met,pec}$ values are taken as a proportion of these whole-animal metabolic costs, it suggests that the pectoralis consumes approximately 40-60% of the additional metabolic energy required for flight at 10 m/s. This is similar to previous estimates of $P_{met,pec}$ for the cockatiel (46-64%) (Morris et al., 2010), where they used a predictive model to determine the postural costs of flight (Equation 3.3) and assumed a net flight muscle efficiency of 19%.

$$k_{pos} = \frac{\varepsilon_{fm}(P_{met} - P_{bas})}{P_{mech}}$$
[3.3]

However, as our muscle preparations were not generating mechanical power as high as previously determined (Askew and Ellerby, 2007) and the whole-animal metabolic costs of flight might be overestimated due to the additional costs of wearing respirometry equipment, it is likely that the $P_{met,pec}$ of wild budgerigars may be higher than predicted by this study.

3.5.3 Muscle efficiency and flight speed

The mechanical efficiency of the budgerigar pectoralis is approximately 21% and invariant with flight speed. This result was not unexpected as the variation in cycle frequency, strain, phase and duration of stimulation were similar across all of the simulated flight speeds (Askew and Ellerby, 2007). The practical outcome of attaining a constant net muscle efficiency is that there is no visible trade-off between maintaining a high muscle efficiency and generating the higher mechanical power requirements for flight at substantially faster or slower speeds than the preferred cruising speed. Such trade-offs have been found in the white muscle fibres of dogfish, where mechanical power and net muscle efficiency are optimised at different stimulus duty cycles, allowing one value to be enhanced at the expense of the other (Curtin and Woledge, 1996), but no such trade-off has been found in the net efficiency of mammalian muscle (see Chapter 2 for the mouse soleus muscle; for a review of mammalian muscle efficiency in general, see Smith et al., 2005).

Previous predictions of avian flight muscle efficiency based in aerodynamic models and whole-animal metabolic studies have landed in the range of 10-23% (Wells, 1993, Chai, 1997, Rayner, 1999, Ward et al., 2001, Morris et al., 2010). The use of these untested values in models of the metabolic costs of flight can lead to uninformed conclusions about energy consumption and transformation during exercise at the muscular level. Whilst these predictions appear similar to the findings of this study, those values have been based on data from starlings (Ward et al., 2001) and cockatiels (Morris et al., 2010), which have larger body masses and potentially dissimilar muscle properties from budgerigars, and may also fly with different gaits, so no direct comparisons can yet be made.

The values presented in this study are somewhat higher than observed in similar studies with isolated mammalian muscle, which are typically 10-15% (Smith et al., 2005), and slightly lower than values observed in amphibians, which are typically 20-35% (Heglund and Cavagna, 1987, Trinh and Syme, 2007), although the amphibian muscles were operated under much lower

temperatures than in this study. This difference in efficiency may be due to physiological differences in the muscle such as the optimum contraction velocity for maximizing mechanical power, muscle fibre-type composition and the preferred form of energy storage. The primary fuel metabolised for avian locomotion is lipid-based (Rothe et al., 1987, Jenni and Jenni-Eiermann, 1998), while terrestrial mammalian locomotion is mostly carbohydrate-based (Brooks and Gaesser, 1980, Brooks and Donovan, 1983), producing respiratory quotients of roughly 0.73 and 0.9 respectively. These physiological differences may play a role in the variation found in the net efficiencies of vertebrate muscles, but further work is required to understand why avian flight muscles appear to be more efficient than those of mammals of similar body masses. There has been very little research into the mechanics and energetics of bat flight muscle due to their legal protection, but a future comparison with avian flight muscle may prove insightful in this area.

While the net muscle efficiency of the avian pectoralis may not be likely to change as a function of flight speed, it has been posited that other factors may have significant effects on muscle efficiency. It is a recognized principle in locomotion energetics that muscle efficiency tends to scale positively with body mass in mammals (Heglund et al., 1982, Heglund and Cavagna, 1985) and insects (Wieser and Gnaiger, 1989) and this relationship may also be applicable to flying birds (Alexander, 2005). Indeed, estimates of apparent muscle efficiencies from cardiovascular data by Bishop (2005) suggest that values of flight muscle efficiency are likely to scale strongly with body mass. However, these predictions should be treated with caution as their values for birds with body masses greater than 1 kg reach values previously considered unrealistically high. One of the major aerodynamic factors that changes with body mass is that wing beat frequency tends to decrease in birds with increasing body masses (Pennycuick, 1990), meaning that whilst our results may be representative of budgerigars and similar sized birds, net muscle efficiency and its relationship with flight speed may vary for other species of different body masses that have dissimilar flight styles and power modulation strategies.

While the absolute net efficiency values may be similar, predictions of how avian flight muscle efficiency changes with flight speed tend to differ from our findings. The majority of recent literature suggests that muscle efficiency should increase with increasing flight speed (Ward et al., 2001, Morris et al., 2010) and by their estimates, flight muscle efficiency should increase by approximately 5-10% over a typical range of flight speeds from 6 to 14 m s^{-1}. However, both of these studies predicted muscle efficiency values under the assumption that the postural costs of flight are equivalent to 10% of the energy consumed by the pectoralis during flight and that this value is constant across all flight speeds.

Although the speeds selected for this study represent a sufficiently wide range of flight speeds performable by free-flying budgerigars, we did not include other intermediate speeds or the extremely low and high flight speeds where the mechanical and metabolic flight requirements are considered to be the highest (Tucker, 1968, Ellerby and Askew, 2007b). It is possible that these extreme speeds may show a departure from the unchanging linear relationship between flight speed and efficiency presented in this study, but these extreme speeds are unlikely to be utilised for periods of sustained flight in the wild due to the high metabolic requirements (Pennycuick, 1968a, Schiffner and Srinivasan, 2016).

In order to further validate the measurements reported in this study, it would be valuable to repeat the experiments using a second method for quantifying the energy consumption of the pectoralis undergoing cyclical contractions. While mechanical work and power data were collected consistently, O_2 consumption was much more variable and was occasionally undetectable due to signal fluctuations. In addition to the polarographic electrode respirometry method used in this study, optical O_2 sensors are also a method that could be used. A major benefit of optical O_2 sensors over polarographic electrode sensors is that they don't consume O_2 during measurement, and are also capable of accurate and rapid measurements (Papkovsky and Dmitriev, 2013). It would also be beneficial to repeat these experiments with the pectoralis

muscles of other bird species and using a greater range of flight speeds, to more accurately determine how the efficiency-speed relationship may vary between different birds.

Chapter 4

The metabolic costs of flight in masked lovebirds (*Agapornis personatus*) measured using respirometry, and the validation of accelerometry as a proxy for metabolic energy expenditure during flight

4.1 Abstract

Determining the metabolic costs of flight is an important aspect of avian ecology, providing insights into the energetic requirements of foraging, hunting, migrating and escaping predation. These metabolic costs have been measured directly for a number of bird species through laboratory experiments using a number of methods including respirometry, but in order to estimate the metabolic costs of flight in wild birds, indirect methods have been developed. Tri-axial accelerometry is becoming an increasingly popular tool for indirectly estimating the energy expenditure of birds during flight. While indices of dynamic body acceleration, ODBA and VeDBA, have shown to correlate well with direct metabolic measurements using respirometry in walking birds, there has been no validation of the method during flight. By measuring energy consumption via respirometry and dynamic body acceleration in masked lovebirds (*Agapornis personatus*) during wind tunnel flights at a range of speeds, we determine the metabolic requirements of flight for a new avian species and validate the use of accelerometry for estimating energy expenditure and flight kinematics. We determine that both the metabolic power-speed and dynamic body acceleration-speed relationships of the masked lovebird are U-shaped with flight speed, corresponding to the U-shaped metabolic- and mechanical-speed relationships determined for birds of a similar size. Our results indicate significant correlations between body acceleration and the metabolic costs of flight, validating their use as a predictor of energy expenditure during flight. We also assess the ability of accelerometry to determine flight kinematics such as wingbeat frequency and intermittent flight styles, and discuss the effects of instrumentation on estimates of avian flight energetics.

4.2 Introduction

Avian flight is an energetically expensive activity. During flight, the majority of this energy is most likely consumed by the flight muscles to generate mechanical work to move the wings through the environment, but a certain amount will also be consumed by physiological processes such as the circulatory and respiratory systems (Butler et al., 1988, Ellerby et al., 2005), culminating in the total metabolic costs of flight.

Determining the metabolic costs of flight is crucially important to ecologists and eco-physiologists investigating a range of activities such as migration, foraging, hunting and habitat selection (Butler et al., 2004, Gavrilov, 2011, Elliott, 2016). However, direct measurement of these metabolic costs in wild animals (e.g. via respirometry) is extremely impractical and multiple indirect methods have been developed as proxies for energetic expenditure during free flight. The two most popular techniques are the doubly-labelled water method (DLW) (Butler et al., 2004, Fort et al., 2011, Shaffer, 2011) and the heart-rate (fH) method (Groscolas et al., 2010, Green, 2011, Sakamoto et al., 2013, Hicks et al., 2017) but other less commonly used methods have also been developed, including time-activity budgets and mass loss estimates (Portugal and Guillemette, 2011). While DLW and measurements of fH have been shown to provide useful estimates of energy expenditure during flight, they both have practical limitations. For example, DLW has poor temporal resolution due to its long flight-time requirements (Butler et al., 2004) and the fH method typically requires the invasive implantation of data loggers (Ward et al., 2002). A recent extensive review by Elliott (2016) details the existing techniques used for estimating energetic expenditure during flight, concluding that the measurement of body acceleration via accelerometry is a promising but unproven method for predicting the metabolic costs of flight.

Over the past decade, accelerometry has become an increasingly popular technique for estimating the metabolic costs of locomotion in humans and other animals alike (Halsey et al., 2008a, Brown et al., 2013, Miwa et al., 2015,

White et al., 2016, Mandigout et al., 2017). An accelerometer consists of a spring-like piezoelectric crystal or capacitive plate that generates a voltage proportional to the changes in acceleration it experiences (Dow et al., 2009). The generation of mechanical work by an animal through physical activity can be estimated by measuring this acceleration over time (Bäckman et al., 2017). Given a constant rate of mechanochemical energy conversion, it is therefore logical that this work generation should be proportional to the energy consumed for the activity by the locomotor muscles (Wilson et al., 2006a, Halsey et al., 2008a, Green et al., 2009). A relatively recent review by Brown et al. (2013) demonstrates how quickly this technique has been adopted as a proxy for energy expenditure for a number of modes of locomotion; including avian flight.

Accelerometry is especially well suited to detecting body movement during oscillatory locomotion styles such as undulatory swimming in fish (Murchie et al., 2011, Wilson et al., 2013, Metcalfe et al., 2016) and flapping flight in birds (Wilson et al., 2006b, Halsey et al., 2011, Elliott et al., 2013a, Spivey and Bishop, 2013). During flapping flight, the generation of net positive oscillatory work and associated energy consumption is closely tied to the movement of the limbs, while passive flight styles such as soaring and gliding are supported by largely isometric muscle contractions that consume energy with almost no positive work generation (Williams et al., 2015, Sur et al., 2017).

High resolution accelerometry also shows promise in determining specific kinematic attributes and flight behaviours, which could be useful in estimating the frequency of different flight activities during migratory or foraging flight (Brown et al., 2013). For example, some birds intersperse flapping flight with brief bounds or glides that reduce the instantaneous body acceleration (Rayner, 1985, Tobalske, 2007, 2010, Sachs, 2013). These intermittent flight styles have been found to modulate the mechanical power generation in some species of birds (Ellerby and Askew, 2007b, Morris and Askew, 2010b) and potentially help to reduce the metabolic costs of flight. In order to validate the estimation of kinematic metrics such as wingbeat frequency and relative

flapping duration from accelerometry data, the relevant data needs to be simultaneously extracted from video footage. One of the benefits of wind tunnel studies compared to free-flight is that flight kinematics can be easily determined from calibrated video recordings (Tobalske and Dial, 1996, Tobalske et al., 2003a, Tobalske et al., 2007), allowing wingbeat frequencies to be calculated and compared with accelerometry-derived values using fast Fourier transformations and wave analysis (Yost et al., 1983, Arai et al., 2000, Santoyo et al., 2016).

Overall Dynamic Body Acceleration (ODBA), calculated from tri-axial accelerometry and determined as the absolute sum of acceleration in each axis, has become the most commonly used accelerometry-derived metric for energy expenditure in animal locomotion (Wilson et al., 2006b, Gleiss et al., 2011). However, as acceleration is a vectorial quantity, the acceleration in each axis should not be treated independently, and so Vectorial Dynamic Body Acceleration (VeDBA) has also been investigated to a lesser extent (Qasem et al., 2012). Measurements of both ODBA and VeDBA have been found to correlate strongly with reliable indicators of metabolic energy such as DLW and fH (Jeanniard-Du-Dot et al., 2016, Hicks et al., 2017), and most importantly, O_2 consumption (Wilson et al., 2006a, Halsey et al., 2009).

Respirometry is considered to be the gold standard for measuring organismal metabolic rate and is commonly used to calibrate other estimation techniques such as DLW and fH (Elliott, 2016). Generally, new methods of metabolic estimation should be tested using a "laboratory-to-field" approach for proper calibration (Wilmers et al., 2015), with examples of terrestrial and aquatic locomotion being validated using a combination of accelerometry and respirometry during activity on speed-variable treadmills and swim tunnels, respectively (Williams et al., 2014, Wright et al., 2014). However, there is currently no experimental validation of the relationship between accelerometry and respirometry-derived O_2 consumption for avian flight and there is increasing evidence demonstrating that different modes of locomotion, even within the same species, require different calibrations between accelerometry

and metabolic rate (Hicks et al., 2017), suggesting that applying a walking-based calibration to flight data is likely to be inaccurate (Ward et al., 2002, Wilson et al., 2006a, Green et al., 2009).

Before ODBA and VeDBA can be used to confidently estimate energy expenditure during flight in wild birds, it needs to be properly calibrated at a range of natural flight speeds under the same environmental conditions. While accelerometry-derived metrics have been demonstrated to correlate with O_2 consumption as a measure of energy expenditure in humans and a range of animal species during terrestrial locomotion (Wilson et al., 2006a, Halsey et al., 2008b, Halsey et al., 2009), studies focused on avian flight have used walking calibrations to calculate their metabolic values from accelerometry metrics, despite evidence suggesting that this can underestimate the metabolic costs of flight (Ward et al., 2002). A recent validation test between ODBA and heart rate (fH) during free-flight as an indirect proxy for O_2 consumption exists for European shags (Hicks et al., 2017) which indicates a strong correlation similar to those observed for terrestrial locomotion. However, it is possible that this relationship between fH and ODBA could be somewhat unreliable due physiological and mental stresses that increase fH with no increase in body movement (Hicks et al., 2017) and differences in season between their collection of fH and ODBA data, which may be affected by season variations in BMR (Smit and Mckechnie Andrew, 2010). Additionally, ODBA and VeDBA shouldn't be affected by changes in fitness levels over time as fH might be expected to do, as these fitness changes may possible lower heart rate and increase stroke volume during activity (Turner and Butler, 1988). In order to validate the past and future use of accelerometry for estimating metabolic rate during avian flight, a robust calibration of body acceleration metrics (ODBA and VeDBA) by energetic expenditure using respirometry is urgently required.

In this study, we collected respirometry, accelerometry and video-derived kinematic data from masked lovebirds (*Agapornis personatus*) flying at a range of speeds in a wind tunnel. Masked lovebirds were selected for this

investigation due to their appropriate body size and wingspan for the wind tunnel, as well as their predicted responsiveness to training. Small to medium sized Australian parrots such as budgerigars and cockatiels have repeatedly proven to be suitable candidates for wind-tunnel flight training and respirometry experiments (Ellerby and Askew, 2007b, Morris et al., 2010) but these are the first African parrots to have their metabolic rate determined during flight.

4.3 Methods

4.3.1 Birds and flight training

Eleven masked lovebirds (*Agapornis personatus*; Reichenow, 1887; mean body mass 49.3 ± 0.71 g) were housed in a large aviary within a temperature (19-22°C) and relative humidity (49 – 55 %) controlled room with a 12:12 hour light:dark cycle. Food, water and cuttlebones were available *ad libitum*. The birds were weighed prior to each period of flight training. Their health was monitored over time from their body masses, body condition and behaviour. Multiple perches were constructed from wooden dowels with diameter of 0.48 cm and placed in both the aviary and wind tunnel to encourage the association of those perches as a resting place.

The lovebirds were trained to fly in an Eiffel-type speed-variable wind tunnel with a working section of 52 cm by 52 cm by 95 cm (width x height x length). Vertical nylon wires (0.4 mm diameter) were positioned at the upstream end (15 mm intervals) and downstream end (7.5 mm intervals) of the working section to keep the bird within the working section during flight. A thin mesh netting was also installed to ensure separation of the birds from the fan section without significantly affecting the air flow. The standard velocity of air flow through the wind tunnel (V_{std}) was measured by using a hot wire anemometer (VelociCalc, TSI Inc., MN, USA) and calibrated using Equation 4.1 to determine the actual flow velocity of the air (V_{act}) at different fan rotation speeds.

$$V_{act} = V_{std} \left(\frac{273 + T_a}{273 + T_s}\right)\left(\frac{SP}{BP}\right) \qquad [4.1]$$

where V_{std} is the standard velocity measured by the instrument, T_a is the ambient temperature, T_s is the standard temperature (21.1 °C), BP is the barometric pressure and SP is the standard atmospheric pressure (101.4 kPa).

The birds were initially trained at an airflow velocity of 11 m/s; a comfortable flying speed for small-medium sized parrots in previous wind tunnel experiments (Ellerby and Askew, 2007b, Morris et al., 2010). To initiate training flights, the perch was removed and flights were terminated by returning the perch to the working section and allowing the bird to rest. Initially, the birds were encouraged to keep airborne by tapping on the working section if the bird rested on the floor or the nylon wires. The duration of these flights was increased over the course of the training period until the birds were comfortable flying for at least 3 minutes. At this time, they were introduced to other flight speeds ranging from 4 to 16 m/s that represented the viable flight speed range for other small-medium sized parrots (Morris et al., 2010). The birds were trained in this manner five times a week for approximately 4 months.

Once the birds were able to fly for at least 8 minutes at a range of speeds, the addition of a training respirometry mask was introduced. The birds were trained to fly with the respirometry mask for an additional 2 months, and once the birds were able to fly for at least 5 minutes with the respirometry mask, connective tubing was then added to the mask but left unattached to the gas analysis system. The birds were then trained for a further month with a variety of tubing sizes and materials to determine the most appropriate tubing for the respirometry experiments. Prior to the actual experiments, the tubing was attached to the gas analysis and pump system through the top of the wind tunnel.

4.3.2 Mask respirometry

We used an open-flow respirometry system to measure the O_2 consumption and CO_2 production of birds during flight, which are proportional to metabolic energy consumed during aerobic exercise (Lighton and Halsey, 2011, Welch Jr, 2011).

4.3.2.1 Respirometry setup

The respirometry setup is detailed in Figure 4.1. Baseline fractional gas content was determined through sampling of CO_2-scrubbed and dried outside air by drawing it through columns of soda lime and Drierite, respectively. The CO_2-scrubbed and dried outside air was split into two sets of tubing: one that was pumped towards a switching box and one that was pumped towards the differential O_2 analyser (S-3A/II Model N-37M O_2 Sensor, AMETEK Inc., PA, USA) containing two zirconia electrochemical cells. The switching box allowed for rapid switching of air source between baseline and experimental measurements. The outside air that entered the differential O_2 analyser was used as the reference air sample when calculating the O_2 contents of the air flowing from the mask. Finally, this outside air entered a pump (SS4 Sub-Sampler Pump, Sable Systems International Inc., NV, USA) before flowing out into the room.

Room air was drawn into the mask around the bird's head through small gaps at the bottom and sides of the mask using a vacuum pump controlled by a mass-flow controller (MFC-2 Mass Flow Valve Controller, Sable Systems International Inc., NV, USA) that allowed the air flow to be accurately measured and fixed at a set rate. This air mixture then entered a partially open manifold that allowed some of the air to escape and a sub-sample to be extracted at a different rate. The sub-sample then entered a switching box that was shared with the dried and CO_2-scrubbed outside air.

The air leaving the switching box then entered a relative humidity meter (RH-100 Relative Humidity Meter, Sable Systems International Inc., NV, USA) to determine the H_2O content of the air. The air was then dried by passing through
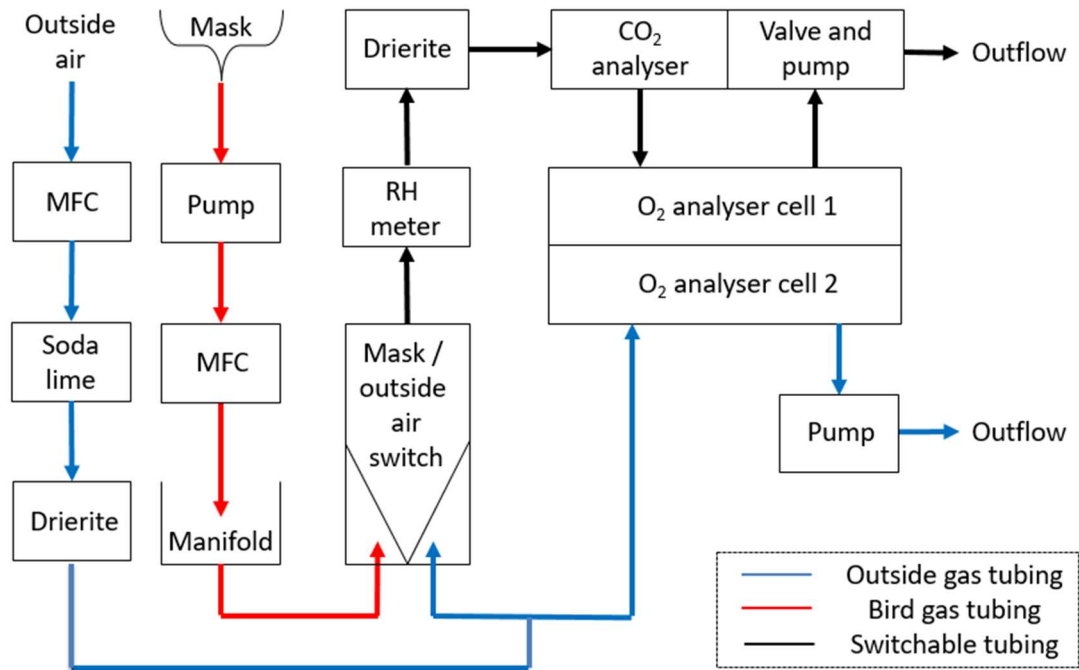
Figure 4.1   Schematic diagram of the respirometry system. Different coloured arrows represent direction of air flow from different sources in respirometry tubing. Components include mass flow controller (MFC) and relative humidity (RH) meter.

a column of Drierite and entered the Foxbox CO_2 analyser (Foxbox O_2/CO_2 Analyser, Sable Systems International Inc., NV, USA) where the CO_2 contents was determined. The air then passed into the differential O_2 analyser and was used as the experimental sample when calculating the O_2 contents of the air flowing from the mask. Finally, the air entered the Foxbox pump before flowing out into the room.

The Foxbox also collected information on barometric pressure and temperature. All fractional gas content, airflow, pressure, temperature and humidity values were output in volts to an analogue-to-digital converter (PowerLab, ADInstruments Inc., CO, USA) which was linked to a computer and recorded using LabChart (Version 8.1.10, ADInstruments Inc., CO, USA). The O_2 and CO_2 contents of the air were converted to percentages, temperature to degrees Celcius, pressure and humidity to kilopascals and flow rate to litres per minute.

4.3.3 Mask design

Respirometry masks were designed to loosely enclose the beak and surrounding facial structure of masked lovebirds in order for room air to be drawn into the mask through gaps at the side of the mask and exhaled air to be withdrawn into the gas analysis system. Two respirometry masks designs were created (Figure 4.2), one hand-made using cellulose acetate as used in previous avian respirometry experiments (Ward et al., 2004, Morris et al., 2010) and one designed using computer-aided drafting (SketchUp, Trimble Inc., CA, USA) and produced using a 3D printer (KLONER3D 140, KLONER3D, Florence, Italy). Unfortunately, due to the limited resolution of the 3D printer (minimum 0.5 mm thickness), the 3D printed masks (Figure 4.2A) were much thicker and heavier than the cellulose acetate masks (0.08 mm thickness). It was also difficult to ensure the masks were sufficiently airtight due to the low resolution of the printing process. The cellulose acetate masks (Figure 4.2B and Figure 4.2C) were used from this point onwards. The metal tubing of a 14-gauge hypodermic needle was filed down and glued through the top of the mask so that the respirometry tubing could easily be attached and detached. These light-weight masks could also be fitted and removed from the birds in a few seconds, minimising handling stress for the birds. A small loop made of cotton thread was attached at the rear of the straps through which the respirometry tubing was slotted to keep the tubing flat against the bird's back and out of the way of the wings during flight. After 5 or fewer training flights with the respirometry mask, all birds were able to fly for at least 1 minute and showed no signs of flight behaviours different to un-instrumented flight.

The masks were connected to the gas analysis system by polyethylene tubing (internal diameter of 1.57 mm, outer diameter of 2.08 mm; Figure 4.2C). This polyethelyne tubing provided excellent gas resistance (Scientific Commodities Inc., AZ, USA) and a flowrate suitable for gas analysis, which was determined by reducing the flowrate further and ensuring that lower flowrates recorded the same volumetric gas contents. This tubing was also light and flexible enough for the bird to fly relatively unencumbered. The total length of the tubing from the mask to the point of exit from the working section was 73 cm and the tubing weighed 1.11 g. The combined mass of the mask and tubing supported by the bird was 1.81 g, equivalent to 3.7% of the mean lovebird body mass.

Figure 4.2   Respirometry masks. (A) 3D printed mask. (B) Cellulose acetate mask. (C) Final cellulose acetate mask with tubing on masked lovebird.

4.3.3.1 Respirometry calculations

The flow rate of air through the mask once attached to the bird was set to be 1.5 L min^{-1}. The actual airflow ($\dot{V}_c$) was calculated using Equation 4.2.

$$\dot{V}_c = \dot{V}_u \frac{BP - WVP}{BP} \qquad [4.2]$$

where $\dot{V}_u$ is the uncorrected air flow in ml s^{-1}, BP is the barometric pressure and WVP is the water vapour pressure of the airflow in kPa. The corrected airflow was then used to calculate the volumetric quantities of O_2 (Equation 4.3) and CO_2 (Equation 4.4).

$$\dot{V}O_2 = \dot{V}_c \frac{(F_iO_2 - F_eO_2) - F_iO_2(F_eCO_2 - F_iCO_2)}{1 - F_iO_2} \qquad [4.3]$$

$$\dot{V}CO_2 = \dot{V}_c \frac{(F_eCO_2 - F_iCO_2) + F_iCO_2(F_iO_2 - F_eO_2)}{1 + F_iCO_2} \dot{V}O_2 \qquad [4.4]$$

where F_i is the incurrent flow into the mask and F_e is the excurrent flow out of the mask. Once $\dot{V}O_2$ and $\dot{V}CO_2$ were determined, the respiratory exchange ratio (RER) of the flights was calculated from the volumetric gas quantities using Equation 4.5.

$$RER = \frac{\dot{V}CO_2}{\dot{V}O_2} \qquad [4.5]$$

For comparisons with published literature on the metabolic (P_{met}) and mechanical power requirements of flight (P_{mech}) in the published literature, an estimate of mass-specific metabolic power in W kg^{-1} was calculated using Equation 4.6 (Romijn, 1961, Brouwer, 1965, Ward et al., 2001).

$$P_{met} = (16.18 * \dot{V}O_2) + (5.02 * \dot{V}CO_2) \qquad [4.6]$$

4.3.3.2 Calibration of gas analysers

In-between each experimental flight, the fractional gas content traces recorded by LabChart were calibrated against dried and CO_2 scrubbed outside air and one of two calibration gases (20% O_2, 1% CO_2 or 12% O_2, 5% CO_2). Following the end of the data collection period, the actual fractional gas contents of both calibration gas cylinders were verified using an ethanol combustion method (Withers, 2001, Lighton, 2008)

An ethanol burner was placed under a hollow pipe, which surrounded the burner and allowed for the inflow of a small amount of air at the bottom (Figure 4.3). First the O_2 analyser was calibrated using nitrogen and outside air, and the CO_2 analyser was zeroed. The burner was then lit and air was drawn

through the flame and into a tube leading into the O_2 analyser. Once the O_2 analyser provided a stable reading, the known ratio of O_2 to CO_2 produced during ethanol combustion (0.677) was used to calculate the rate of CO_2 production. Once the O_2 and CO_2 traces had been calibrated using these values, they were compared to those produced by the calibration gas cylinders and trace corrections were calculated from any differences in the fractional gas contents. All respirometry data refers to data calibrated and corrected by this method.
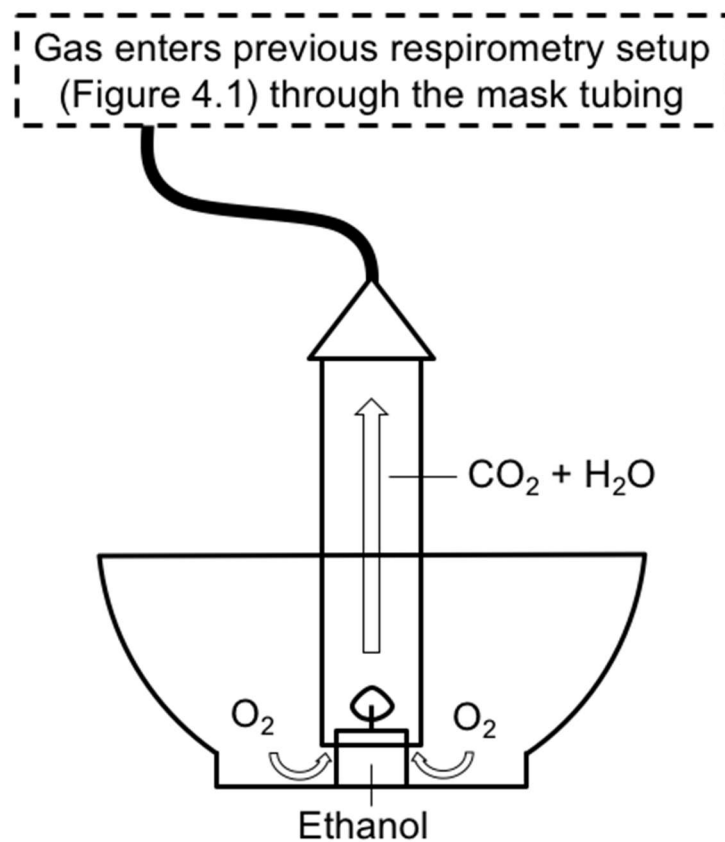
Figure 4.3   Gas flame calibration setup.

4.3.4 Accelerometry

An AXY-3 tri-axial accelerometer (TechnoSmArt s.r.l., Rome, Italy) was carried on the back of the lovebirds (Figure 4.4) to collect instantaneous acceleration data from the lovebirds during flight. With the battery attached, the accelerometer measured 9 by 31 by 4 mm and weighed 1.8 g. The accelerometer captured acceleration information within a range of ± 4 g at a

sample frequency of 100 Hz. This sample frequency allowed for the recording of multiple points per wingbeat cycle (approximate wingbeat of 17 Hz during cruising flight) (Kress et al., 2015).
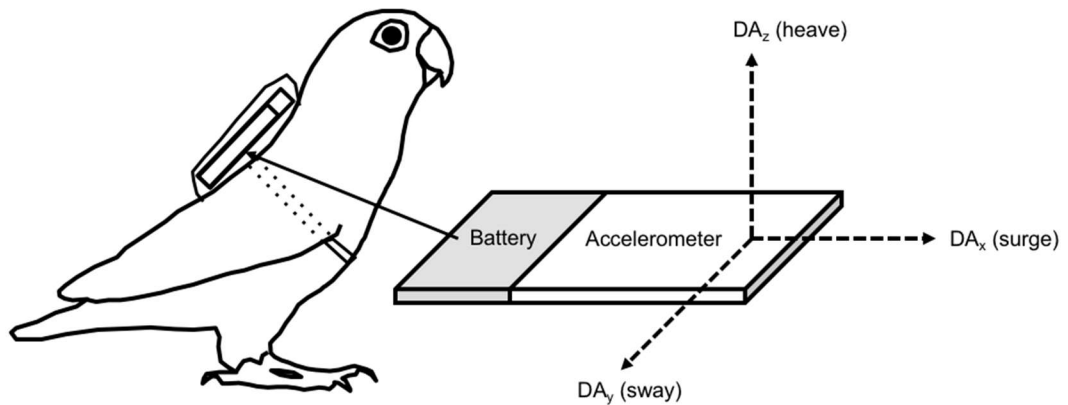
Figure 4.4   Diagram of accelerometer and harness positioning.

To safely house the accelerometer and securely attach it to the bird, three harness designs were constructed: a leg-harness design, a single-strap chest harness and a double-strap chest harness. Each design had a trade-off between impact on the bird's flying performance and the stability of the accelerometer output, and after a series of trials, the single-strap harness proved to be the most reliable harness for data collection (Figure 4.5). When containing the accelerometer, this harness weighed 2.78 g, equivalent to 5.6% of the mean lovebird body mass.

To minimise interruption of natural flight behaviours, the harness was constructed from light-weight materials (thin transparent plastic, paper card, adhesive plasters and flat elastic cord; Figure 4.5), the straps were positioned out of the way of the wings and the front end of the harness was raised slightly off from the bird's back to allow free movement of the shoulders during flight. The accelerometer was activated and deactivated by use of a small magnet attached to a matchstick.

Only one or two training sessions with the final harness were required until the birds were flying comfortably for the required length of time and the harness design appeared to have little impact on the flying performance or behaviour of the lovebirds compared to un-instrumented flight. The harness was placed on the upper back of the bird, approximately above the bird's centre of mass. The centre of mass was determined by hanging a frozen lovebird in a mid-flight pose from two different locations on the body, photographing the positions of the bird and identifying the intersection between the sagittal body axes from each hanging position.

Figure 4.5   Photograph of accelerometer and final harness design.

4.3.5 Data collection

All comparative respirometry and accelerometry data were collected during the same three-week period to minimise differences in body condition or flight behaviour between measurements. A second smaller accelerometry data set was collected simultaneously with high-speed video for the comparison of kinematic data.

4.3.5.1 Respirometry

During data collection sessions, flight speeds were selected in a randomised order. The birds were weighed, fitted with the respirometry mask and introduced to the perch inside working section of the wind tunnel. To determine their resting metabolic rate, the O_2 consumption and CO_2 production of the

birds were measured for a period of at least 3 minutes while they sat on the perch prior to the start of the flights.

At the start of each flight, the air velocity of the wind tunnel was adjusted to simulate the required flight speed and the perch was removed from the working section, prompting the bird to fly. Experimental flights lasted between 2 and 5 minutes depending on the flight speed with shorter flights being recorded at the slowest and fastest speeds. To compare between flights, respirometry data were always collected from the final 1 minute of stable flight after a stable plateau of O_2 consumption and CO_2 production had been reached (Figure 4.6). Following the experimental flight, the perch was returned to the working section of the wind tunnel and the bird was allowed to rest for at least 5 minutes before the next flight. After a maximum of four consecutive flights, the mask was removed from the bird and the bird was removed from the wind tunnel and returned to the aviary.
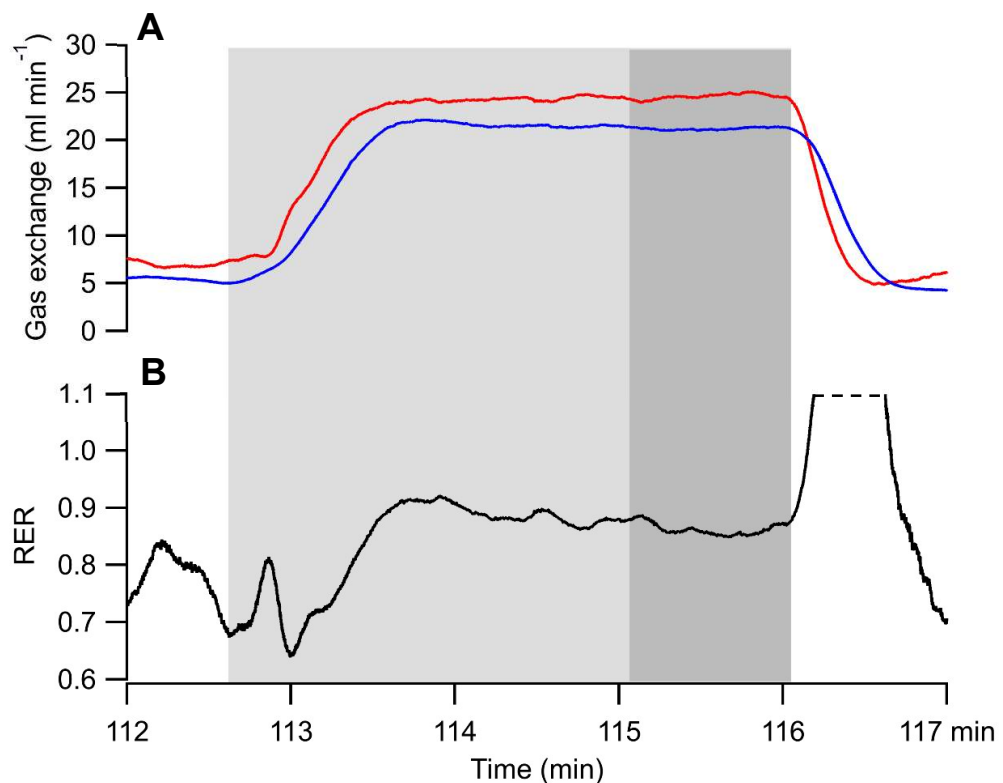
Figure 4.6 **Respirometry traces.** (A) $\dot{V}O_2$ (red) and $\dot{V}CO_2$ (blue) traces recorded during a flight with periods of rest at the start and end. (B) RER during flight. Light grey area represents period spent flying and dark grey indicates last minute of stable flight.

4.3.5.2 Accelerometry

As with the respirometry experiments, flight speeds were selected in a randomised order. The accelerometers were activated prior to the flight session and important events or notes (e.g. activation, take-off, landing and mid-flight interruptions) were timestamped and recorded for analysis.

The birds were weighed, fitted with the harness and introduced to the perch inside working section of the wind tunnel. The air velocity of the wind tunnel was adjusted to simulate the required flight speed and the perch was removed from the working section, prompting the bird to fly. Experimental flights lasted between 10 and 20 seconds in order to gather a large sample of stable and complete wingbeat cycles for data analysis (approximately 170-340 wingbeats) (Kress et al., 2015). The perch was then returned to the working section and the bird was permitted to rest until recovered. The experimental flights were then repeated for all flight speeds. Following the end of an experimental flight session, the accelerometer was removed from the harness and deactivated.

The data were subsequently retrieved from the accelerometer and converted into text files (AXY Manager, TechnoSmArt Europe s.r.l., Rome, Italy) that could be analysed in IGOR Pro. The first and last wingbeats of each flight were omitted from analysis in order to avoid the inclusion of take-off and landing events.

4.3.5.3 Calculating ODBA and VeDBA

The raw accelerometry data consisted of acceleration due to movement along three orthogonal axes (dynamic acceleration, DA) represented as DA_x (surge), DA_y (sway) and DA_z (heave), as well as the acceleration due to the Earth's gravity (static acceleration, SA; 9.81 m s^{-1}). Static acceleration was determined using a two-band low-pass filter between 0.1 and 0.5 Hz across all three axes and subtracting the resulting values from the raw acceleration (Shepard et al., 2008). This method produced a similar effect to subtracting the running mean over a short time from the raw acceleration data (Wilson et al., 2006a).

Dynamic acceleration (DA) in each axis was determined by subtracting the static acceleration from the total raw acceleration. Using the values of DA for each axis, ODBA and VeDBA were calculated using Equations 4.7 and 4.8, respectively.

$$ODBA = |DA_x| + |DA_y| + |DA_z| \qquad [4.7]$$

$$VeDBA = \sqrt{DA_x{}^2 + DA_y{}^2 + DA_z{}^2} \qquad [4.8]$$

where DA_x, DA_y and DA_z are the measures of dynamic acceleration in each axis (g). To normalise ODBA and VeDBA values for flights of varying duration, all traces were integrated and the resulting area values were divided by the time duration of the flight in order to calculate the ODBA and VeDBA generated per second (Figure 4.7). These values were then divided by the body mass of the bird to generate mass-specific ODBA values.

4.3.5.4 Accelerometry-derived flight kinematics

Accelerometry-derived wingbeat frequency (WF_{acc}) was calculated by applying a fast Fourier transformation (FFT) to the DA_z across the flight duration as a representative measurement of vertical acceleration due to the wingbeat. The highest peak from the FFT trace between the frequencies of 10 and 30 Hz was selected as a representative value for the modal average wingbeat frequency (Figure 4.8). Accelerometry-derived relative flapping duration (RFD_{acc}) was calculated by distinguishing the flapping and non-flapping periods of flight from the DA_z across the flight duration. DA values below a certain threshold were set as non-flapping periods and values above the threshold were set as flapping periods (Figure 4.8). After experimenting with a range of threshold values and visually assessing their validity against the DA trace, the final threshold was set as 15% of the maximum DA recorded during each flight

(approximately 0.4 *g*) as this reliably reproduced the separation between flapping and non-flapping periods.
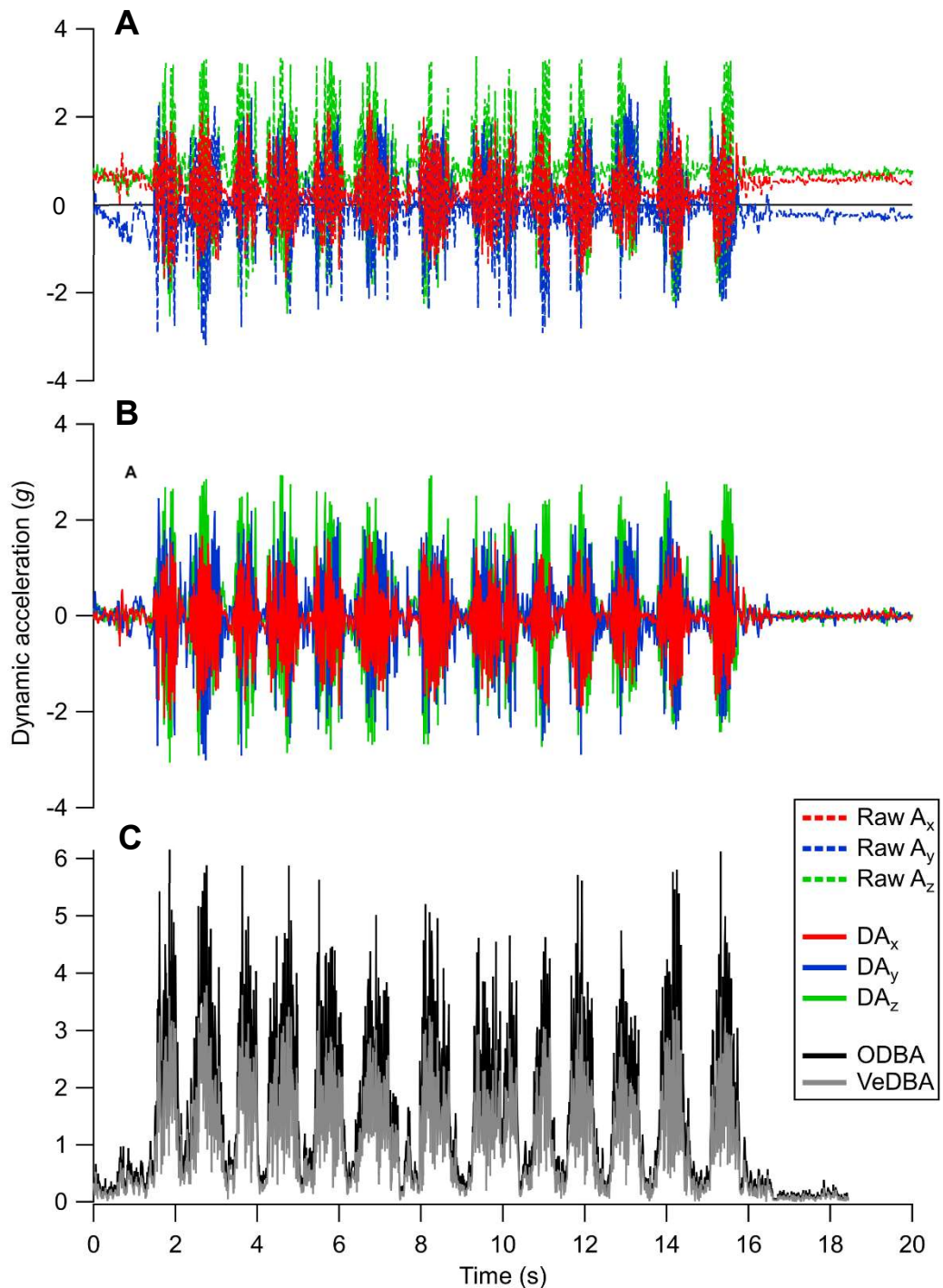
Figure 4.7 **Calculation of dynamic body acceleration.** (A) Raw acceleration values along each of the three axes. (B) Dynamic acceleration with the passive acceleration removed. (C) Overall Dynamic Body Acceleration (black) and Vectorial Dynamic Body Acceleration (dark grey), calculated from the sum of the dynamic acceleration in each axis.
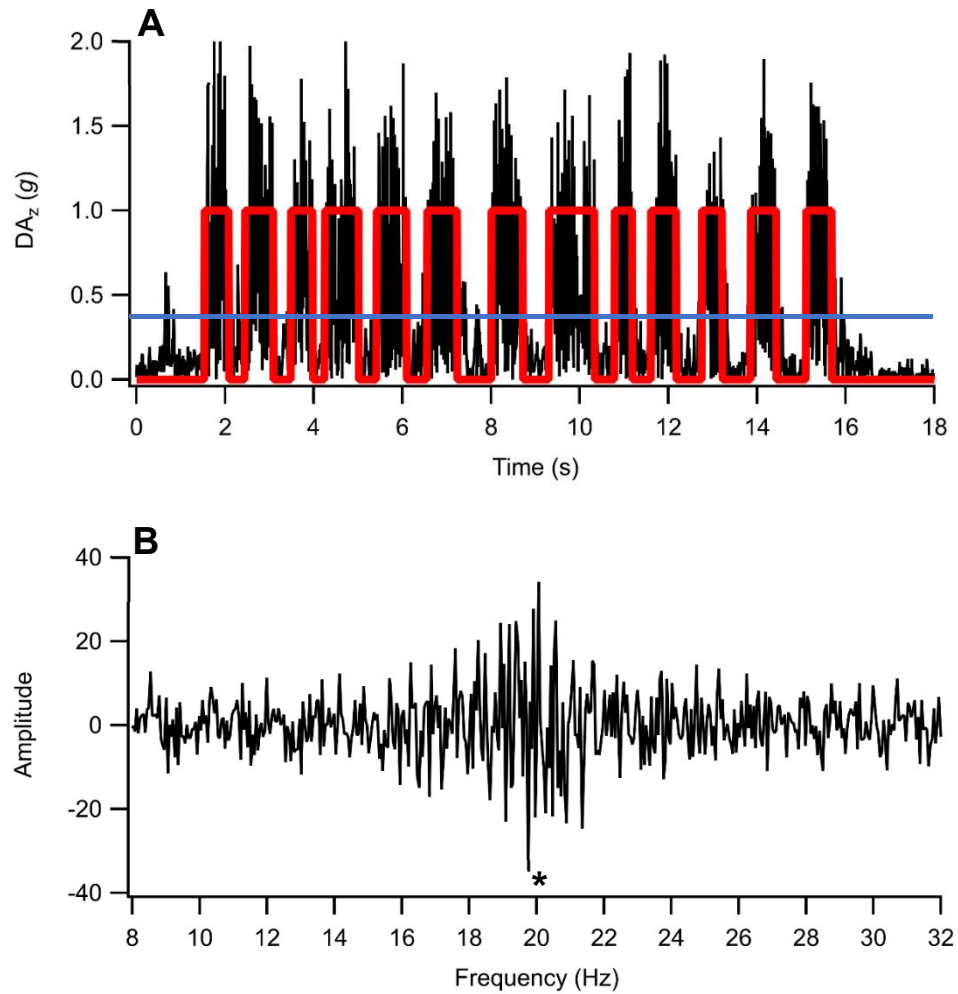
Figure 4.8 **Accelerometry-derived kinematics.** (A) Relative flapping duration (red line) calculated as the mean proportion of time spent above the flapping threshold (blue line). (B) Modal wingbeat frequency determined by Fast Fourier transformation of a full flight trace. * indicates peak at which the modal value was extracted.

4.3.5.5 Combined respirometry and accelerometry

The birds were first fitted with the accelerometry harness and then the respirometry mask as previously described. After this initial setup, the combined experimental procedure did not differ from the independent experimental procedures.

4.3.6 Video capture and digitisation

A high-speed video camera (Fastcam SA3, Photron) was used to the record the kinematics of both instrumented and un-instrumented flights at 500 frames per second with a shutter speed of 0.5 ms, providing approximately 25-30 frames per wingbeat cycle. The camera was positioned perpendicular to the working section of the chamber and the filming volume was calibrated using a wire-frame cube of known dimensions constructed from K'NEX (Basic Fun, USA). The camera recorded continuously and a remote controlled end trigger was used to save the preceding 12 seconds of stored footage of following a successful flight.

The raw images were processed by Saul Avery (SA) using ImageJ (National Institutes for Health, Bethesda, USA) in order to determine the actual flight kinematics including wingbeat frequency (WF_{vid}) and relative flapping duration (RFD_{vid}). Two-dimensional positional data from the videos were extracted by semi-automated tracking the lovebird's pupil using Tracker (Version 4.96, Open Source Physics, Boston USA) as this was easily discernible from the footage. These data were converted from pixels to meters using values determined by the wire-frame calibration object. Digitisation error was calculated by running the semi-automatic tracking procedure across the same 100 frames (1 s) of a candidate video in Tracker 15 times, and the standard error across the pixel coordinates for the 100th frame (converted into mm) was recorded as the digitisation error.

4.3.6.1 Video-derived flight kinematics

The two-dimensional positional data were differentiated twice using Igor Pro and acceleration values were determined using the Pythagorean theorem. Digitised acceleration values were then interpolated to match the accelerometer's sampling frequency (100 Hz) and superimposed with the accelerometer's data for synchronisation using the first mid-downstroke peak in acceleration as the reference point. WF_{vid} was determined as the modal wingbeat frequency using the same Fast Fourier transformation (FFTs)

method as described for the accelerometry analysis. RFD_{vid} was determined as the ratio of time spent flapping to the total time spent in flight.

4.3.7 Statistical analysis

Type 3 GLMs were performed for all statistical tests except for correlations, for which Pearson correlation tests were performed. When appropriate, the individual birds were included as random factors to test for the effects of inter-individual variation. Metabolic and acceleration measurements plotted against flight speed were fitted with third-order polynomial curves. All statistical tests were conducted in SPSS (Version 20.1, IBM).

4.4 Results

4.4.1 Respirometry

Respirometry data across at least 5 flight speeds ranging from 6 to 12 m s^{-1} were collected from 6 birds. In order to compare our results with published measurements of $\dot{V}O_2$, $\dot{V}CO_2$ and P_{met}, the gross metabolic values incorporating the resting metabolic rate are presented.

4.4.1.1 Resting metabolic rate

All of our resting metabolic measurements varied significantly between individual birds, with $\dot{V}O_2$ ranging from 2.37 to 2.92 ml s^{-1} kg^{-1} ($F_{5,32} = 7.24$, P < 0.001), $\dot{V}CO_2$ ranging from 2.46 to 2.83 ml s^{-1} kg^{-1} ($F_{5,32} = 7.43$, P < 0.001) and P_{met} ranging from 48.4 to 59.1 W kg^{-1} ($F_{5,32} = 7.61$, P < 0.001). However, resting RER did not differ significantly between birds ($F_{5,32} = 2.02$, P = 0.103) and was pooled to a mean value of 0.73 ± 0.01.

4.4.1.2 Metabolic costs of flight

All metabolic measurements exhibited a U-shaped relationship with flight speed, with higher values at the lowest (6 m s^{-1}) and highest (12 m s^{-1}) speeds with lower values at the most intermediate speeds (9 to 10 m s^{-1}) (Figure 4.9). $\dot{V}O_2$ ($F_{6,26} = 2.53$, P = 0.046), $\dot{V}CO_2$ ($F_{6,26} = 4.1$, P = 0.005), P_{met} ($F_{6,26} = 2.97$,

P = 0.024) and flight RER ($F_{6,26}$ = 3.33, P = 0.014) all varied significantly as a factor of flight speed. $\dot{V}O_2$ values varied slightly between individual birds ($F_{5,26}$ = 2.6, P = 0.049) but $\dot{V}CO_2$ ($F_{5,26}$ = 1.21, P = 0.332) P_{met} ($F_{5,26}$ = 2.23, P = 0.082) and flight RER ($F_{5,26}$ = 2.23, P = 0.081) did not.

$\dot{V}O_2$ during flight ranged from 7.15 ml s^{-1} kg^{-1} at 10 m s^{-1} to 8.05 ml s^{-1} kg^{-1} at 6 m s^{-1}, constituting a proportional increase of 12% minimum flight $\dot{V}O_2$ between the minimum and maximum mean $\dot{V}O_2$ values across the speed
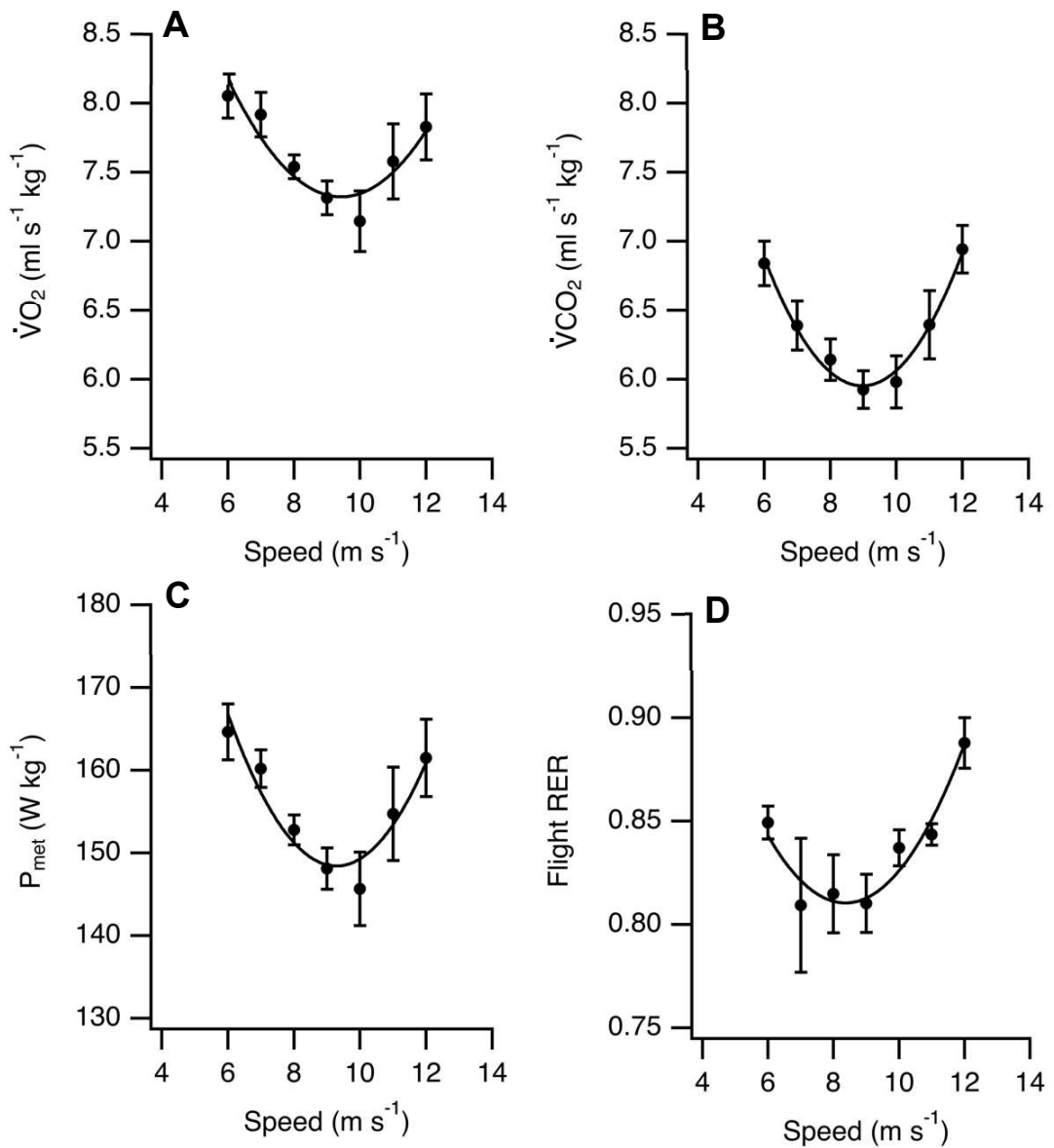
Figure 4.9   Relationships between metabolic measurements and flight speed. (A) $\dot{V}O_2$. (B) $\dot{V}CO_2$. (C) P_{met}. (D) Flight RER. Data presented as mean ± SEM. n = 4, 5, 6, 6, 6, 6 and 5 for 6, 7 8, 9, 10, 11 and 12 m s^{-1} respectively.

range. However, as detailed later in this chapter, this does not cover the full speed range achieved by the birds during the accelerometry experiments. $\dot{V}CO_2$ ranged from 5.93 ml s^{-1} kg^{-1} at 9 m s^{-1} to 6.94 ml s^{-1} kg^{-1} at 12 m s^{-1}, constituting a proportional increase of 17%. P_{met} ranged from 146 W kg^{-1} at 10 m s^{-1} to 165 at 6 m s^{-1}, constituting a proportional increase of 13%. RER ranged from 0.81 at 7 m s^{-1} to 0.89 at 12 m s^{-1}, constituting a proportional increase of approximately 10%.

4.4.2 Accelerometry

Accelerometry data across at least 7 flight speeds ranging from 4 to 14 m s^{-1} were collected from 6 birds. Both respirometry and accelerometer datasets were collected from 5 birds.

4.4.2.1 ODBA and VeDBA

Both ODBA and VeDBA exhibited a U-shaped relationship with flight speed, with higher values at the lowest (4 m s^{-1}) and highest (14 m s^{-1}) speeds with lower values at the most intermediate speeds (8 to 11 m s^{-1}) (Figure 4.10A).
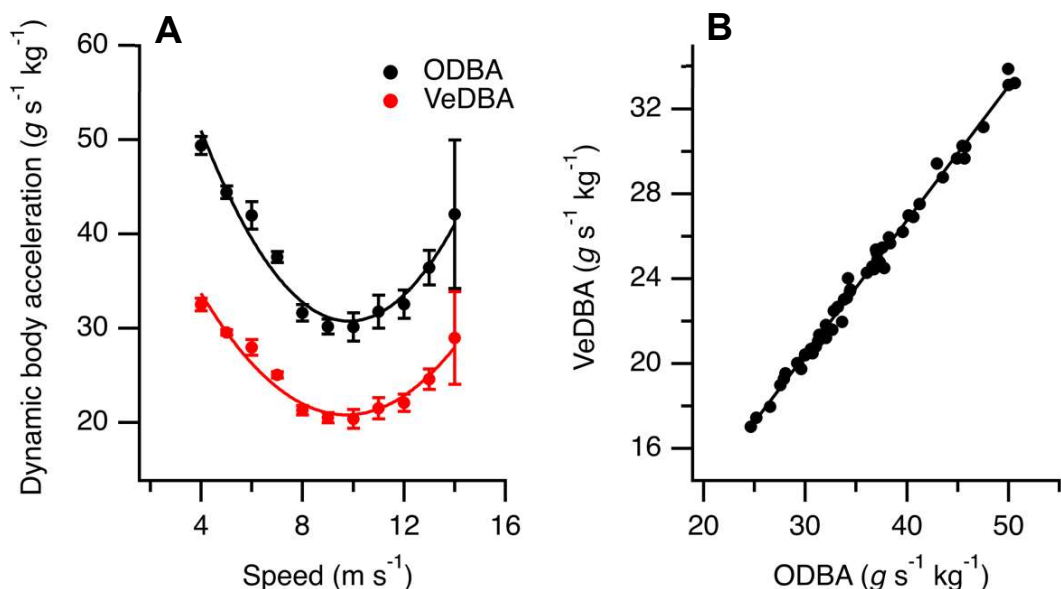
Figure 4.10 Relationships between accelerometry measurements and flight speed. (A) ODBA and VeDBA. Data presented as mean ± SEM. n = 3, 4, 5, 5, 6, 5, 6, 6, 5, 6 and 2 for 4, 5, 6, 7 8, 9, 10, 11, 12, 13 and 14 m s^{-1} respectively. (B) Correlation between ODBA and VeDBA (R^2 = 0.993, n = 53).
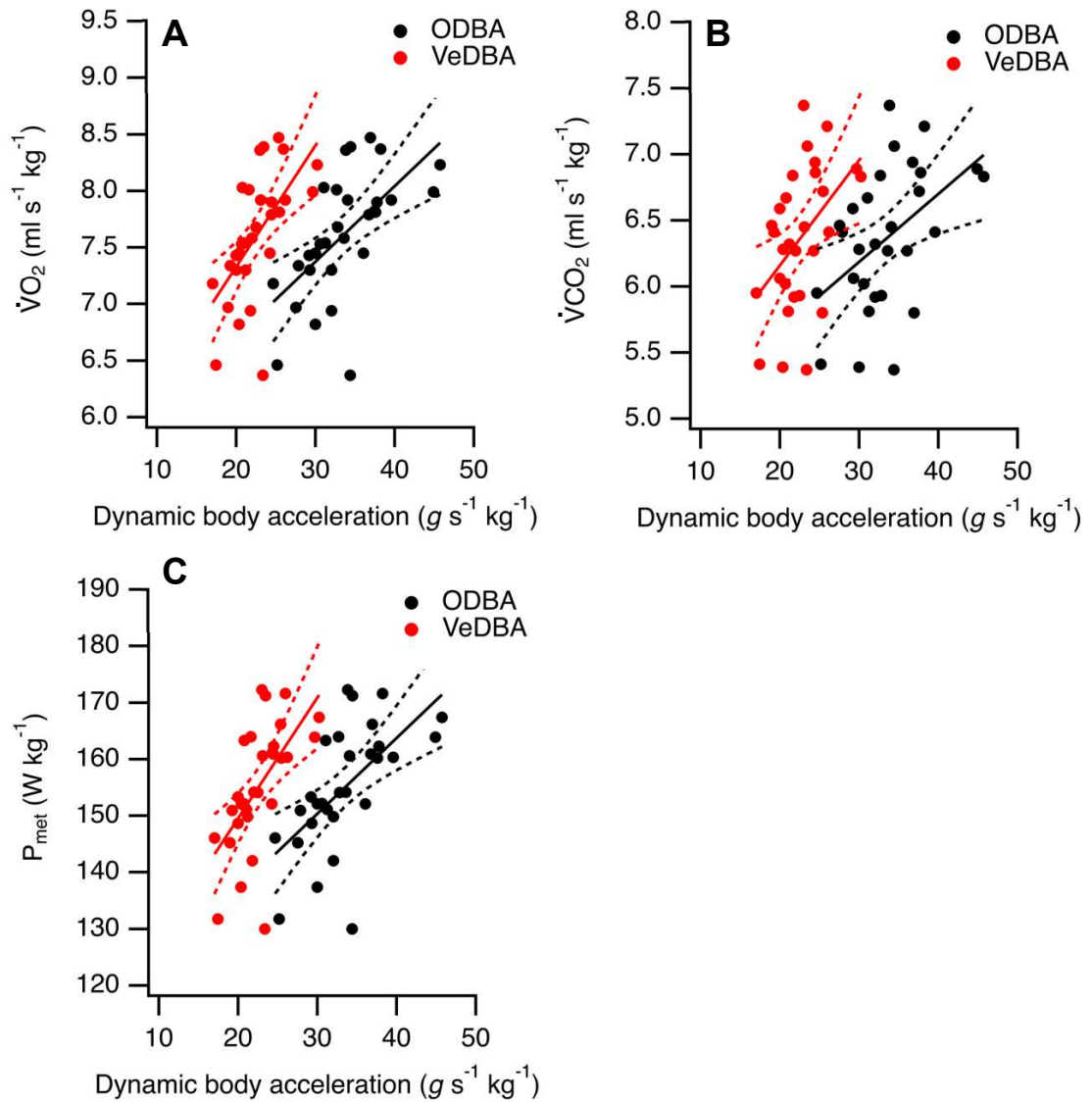
Figure 4.11 Relationships between metabolic and acceleration measurements. Acceleration presented as both ODBA and VeDBA. (A) $\dot{V}O_2$. (B) $\dot{V}CO_2$. (C) P_{met}. Solid lines are fitted linear curves, dotted lines are 95% confidence intervals of the curves. Curve equations and R^2 values are presented in Table 4.1. n = 29 for all plots.

Both ODBA ($F_{10,37}$ = 24, P < 0.001) and VeDBA ($F_{10,37}$ = 24, P < 0.001) varied significantly as a factor of flight speed. Both ODBA ($F_{5,37}$ = 10.2, P < 0.001) and VeDBA ($F_{5,37}$ = 8.67, P < 0.001) also varied significantly between individual birds. ODBA and VeDBA were very strongly correlated (r = 0.996, P < 0.001, R^2 = 0.993) (Figure 4.10B).

In terms of correlations between metabolic and acceleration values, we present the following results. ODBA had a significant positive relationship with all metabolic values, including $\dot{V}O_2$ ($F_{1,23}$ = 5.12, P = 0.032), $\dot{V}CO_2$ ($F_{1,23}$ = 4.98, P = 0.036) and P_{met} ($F_{1,23}$ = 5.75, P = 0.025) (Figure 4.11). Similarly, VeDBA had a significant positive relationship with all metabolic values, including $\dot{V}O_2$ ($F_{1,23}$ = 5.28, P = 0.031), $\dot{V}CO_2$ ($F_{1,23}$ = 4.89, P = 0.037) and P_{met} ($F_{1,23}$ = 5.79, P = 0.025) (Figure 4.11). None of these relationships varied between individual birds.

4.4.2.2 Accelerometry-derived kinematics

To test for temporal differences on the Fast Fourier transformation, WF_{acc} was calculated across both whole flight sessions and just the flapping periods for a subsample of flights (n = 13) and a paired samples T-test found that there was no difference between the methods used to extract WF_{acc} (t_{12} = -0.014, P = 0.989). There did appear to be increased variation when smaller sections of the FFT trace were selected, so data from the whole flight sessions are reported.
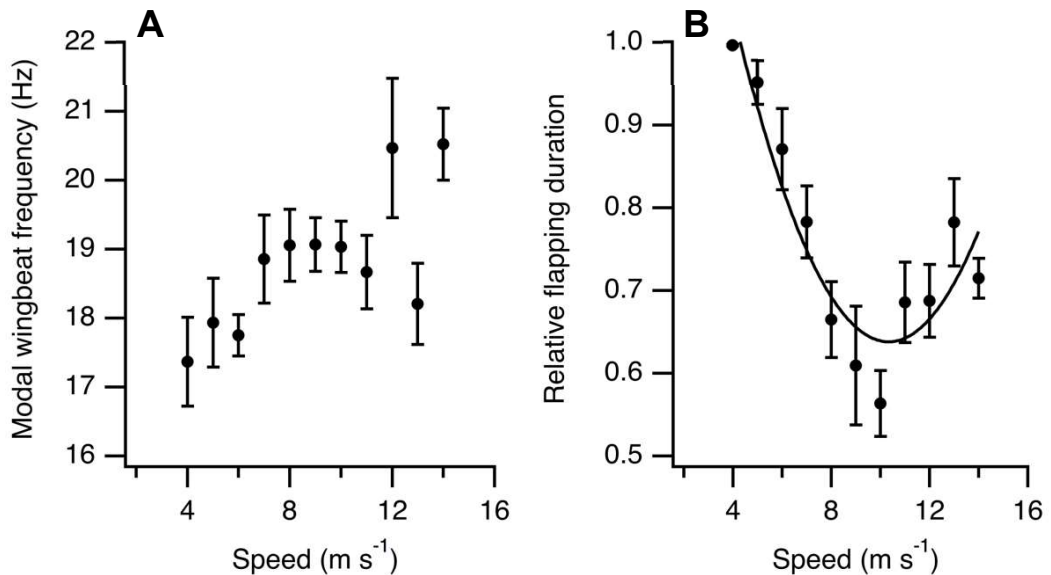
Figure 4.12 Relationships between accelerometry-derived kinematics and flight speed. (A) Wf_{acc}. (B) RFD_{acc}. Data presented as mean ± SEM. n = 3, 4, 5, 5, 6, 5, 6, 6, 5, 6 and 2 for 4, 5, 6, 7 8, 9, 10, 11, 12, 13 and 14 m s^{-1} respectively.

Accelerometry-derived wingbeat frequency (WF_{acc}) did not vary significantly as a factor of flight speed ($F_{10,37}$ = 1.96, P = 0.068) and averaged at 18.8 ± 0.2 Hz (Figure 4.12A).

Relative flap duration (RFD_{acc}) did vary as a factor of flight speed ($F_{10,37}$ = 13.7, P < 0.001) and exhibited an almost U-shaped relationship, with high values at the lowest speed (0.996 at 4 m s^{-1}), lower values at intermediate speeds (0.609 at 9 m s^{-1}) and higher values at higher speeds (0.782 at 13 m s^{-1}) (Figure 4.12B). Individual bird was not a significant factor in any of these relationships.

4.4.3 Video-derived kinematics

The data simultaneously recorded from accelerometry and video were analysed for one bird across a wide range of speeds (4, 6, 8, 10, 12 and 14 m s^{-1}). The data from this individual were used to investigate the similarity of WF_{acc} and RFD_{acc} to the video-derived wingbeat frequency (WF_{vid}) and video-
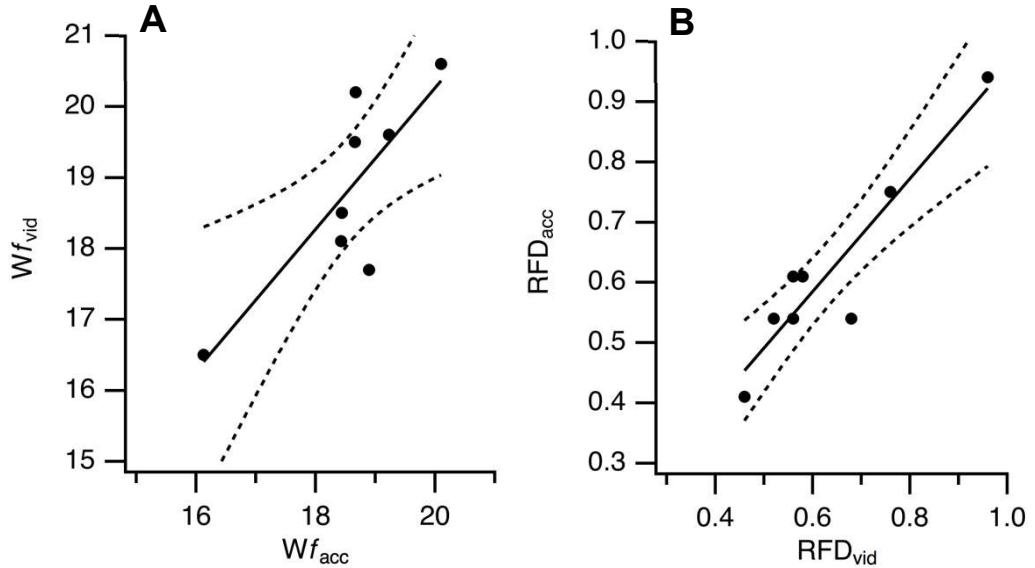
Figure 4.13 Relationships between accelerometry- and video-derived kinematics. (A) Wingbeat frequency (R^2 = 0.661, n = 8). (B) RFD(R^2 = 0.871, n = 8). Solid lines are fitted linear curves, dotted lines are 95% confidence intervals of the curves.

derived relative flapping duration (RFD_{vid}). Digitisation error was found to be 0.08 mm in the vertical axis and 0.38 mm in the horizontal axis (n = 15).

WF_{acc} was significantly positively correlated with WF_{vid} (r = 0.813, P = 0.014; R^2 = 0.661) (Figure 4.13A). RFD_{acc} was significantly positively correlated with RFD_{vid} (r = 0.931, P < 0.001; R^2 = 0.867) (Figure 4.13B).
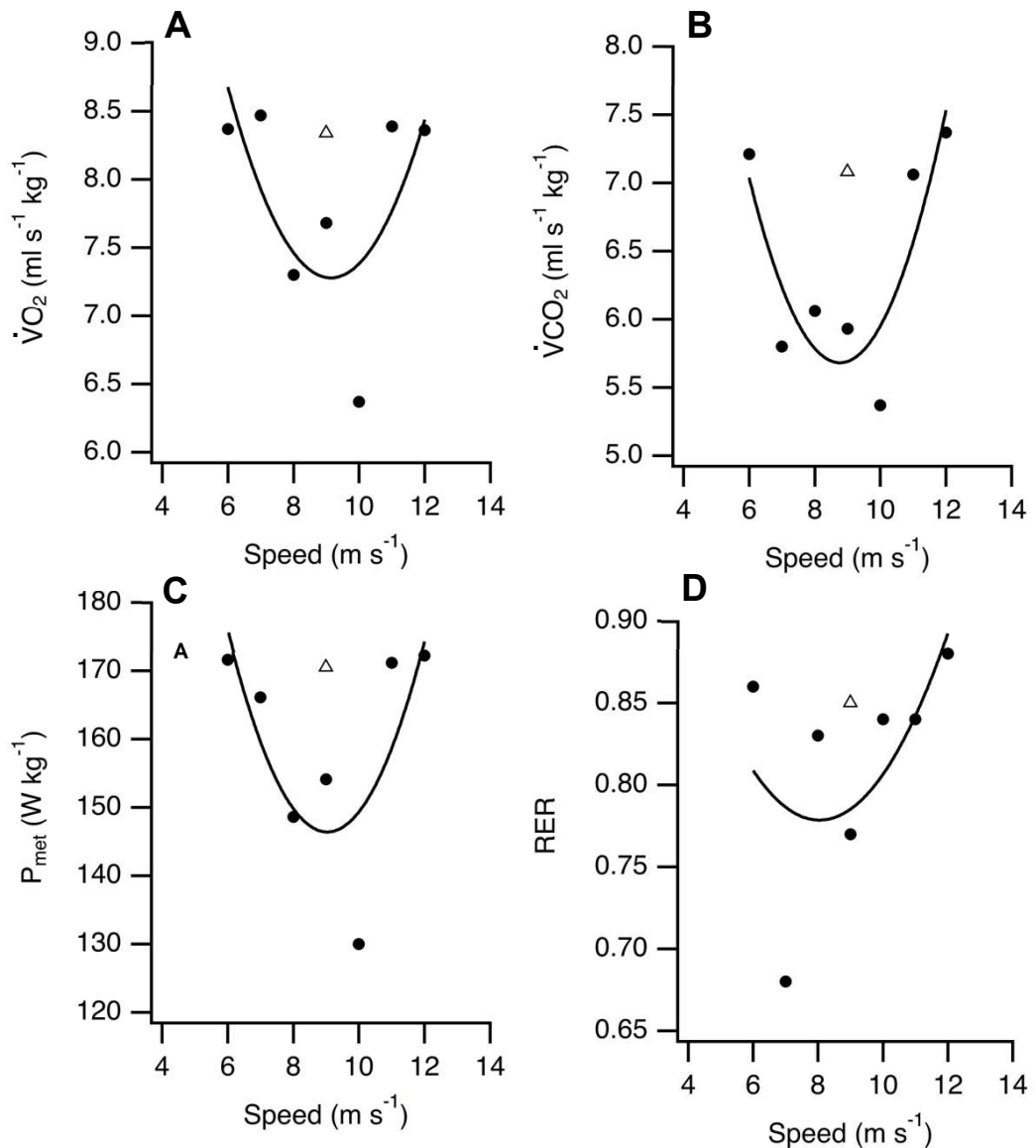
Figure 4.14 Relationship between metabolic measurements and flight speed from a single bird, including combined-equipment flight. (A) $\dot{V}O_2$. (B) $\dot{V}CO_2$. (C) P_{met}. (D) Flight RER. Black circles represent data collected when flying with only the respirometry equipment, hollow triangles represent data collected with both respirometry and accelerometry equipment.
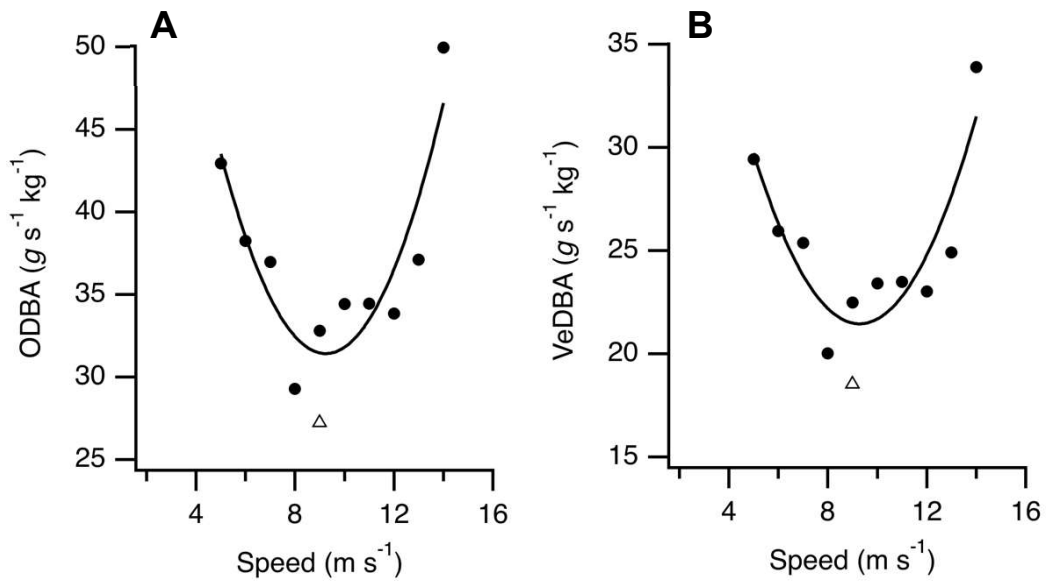
Figure 4.15 Relationship between acceleration measurements and flight speed from a single bird, including combined-equipment flight. (A) ODBA. (B) VeDBA. Black circles represent data collected when flying with only the accelerometer equipment, hollow triangles represent data collected with both respirometry and accelerometry equipment.

4.4.4 Combined respirometry and accelerometry

Only one bird flew for more than 1 minute with both the respirometry equipment and accelerometry harness attached. The O_2 and CO_2 traces remained at a stable plateau for at least 60 seconds and the flight behaviour was consistent with previous flights for that individual, but the bird was observed dropping to the floor of the wind tunnel more often than during the respirometry flights and was visibly ventilating more heavily once the flight was finished. The metabolic (Figures 4.14) and acceleration (Figure 4.15) measurements from this flight are included on all relevant traces and indicated with a triangle, but this point was not included when determining relationships using the fitted curves and statistical analysis cannot be performed using a single datapoint.

4.5 Discussion

4.5.1 Metabolism of lovebirds at rest

The resting metabolic rate (RMR) of the masked lovebirds was relatively high, as they were not recorded under complete resting conditions. There are no comparable published values for the RMR of lovebirds, but the basal metabolic rate (BMR) can be approximated from an allometric scaling relationship between the BMR and body mass of birds (Equation 4.7) (Lasiewski and Dawson, 1967).

$$BMR = 86.4 * M_b^{0.688} \qquad [4.7]$$

The BMR represents the absolute lowest level of metabolic energy consumption that can maintain life for a particular species, and is measured under a specific set of conditions requiring the animal to be in a postabsorptive and nonreproductive state, and at rest in a thermoneutral temperature (Bushuev et al., 2017). Food was not withdrawn prior to flight, and they could have been in an absorptive and actively mobile state, therefore RMR is expected to be higher than predicted BMR. Indeed, Equation 4.8 predicts that the BMR of these masked lovebirds should be approximately 10.7 W kg^{-1}, which is a substantially lower than our RMR values of 53.1 W kg^{-1}. The basal metabolic rate (BMR) of peach-faced lovebirds (*Agapornis roseicollis*; 47.9 ± 0.18 g) under the strict resting conditions mentioned above has been calculated to be approximately 1.84 ml min $^{-1}$ (Bucher and Morgan, 1989), compared to our RMR oxygen consumption values of approximately 7.09 ± 0.12 ml min $^{-1}$. It is not surprising that the RMR of our lovebirds would be substantially lower than these values of BMR as these experimental "rest" periods consisted of a short duration spent in a constant airflow while instrumented and waiting to take-off, which may require energy expenditure much greater than required by the conditions at which SMR and BMR are usually determined. However, a mean RER during rest of 0.728 ± 0.008 indicates that the resting metabolism was aerobic and that mostly fat was being metabolised prior to flight, which is comparable to the RER of great cormorants

(Butler et al., 2000, Wilson et al., 2006a). For comparison with other studies on the metabolic costs of flight (Bundle et al., 2007), the same allometric prediction of BMR will be used.

4.5.2 Metabolism of lovebirds during flight

All of our metabolic measurements ($\dot{V}O_2$, $\dot{V}CO_2$, P_{met} and RER) varied as a factor of flight speed in the characteristic U-shape relationship often observed with both the metabolic and mechanical power requirements of flight (Figure 4.9).

The gross metabolic costs of flight (P_{met}) for masked lovebirds fit reasonably close to the gross values determined for budgerigars and cockatiels (Figure 4.16) (Tucker, 1968, Bundle et al., 2007, Morris et al., 2010), but if based solely on the mass-specific scaling of metabolic power, these costs are slightly higher than should be predicted relative to these other species. This elevated metabolic rate may be due to intraspecific differences in wing shape and flight style. Tobalske et al. (2003a) demonstrated that intraspecific wing morphology and wingbeat kinematics play equally important roles as body mass when determining the metabolic power of flight. Budgerigars and cockatiels have relatively long wings for the body mass, giving them approximate wing loadings of 26.8 N m^{-2} and 23.2 N m^{-2}, respectively (Tobalske et al., 2003a), while these masked lovebirds have relatively short wings for their body mass, giving them an approximate wing loading of 42.4 N m^{-2}. This higher wing loading may require higher wingbeat frequencies or stroke amplitudes to generate the required mechanical power to overcome drag, and in turn, increase the metabolic costs of flight.

Our values for RER during flight (0.809 – 0.888) are similar to those determined for other bird species, including budgerigars (0.88) (Bundle et al., 2007), cockatiels (0.93 – 0.98) (Morris et al., 2010), barnacle geese (0.8 – 1.01) and bar-headed geese (0.89 – 0.98) (Ward et al., 2002) for flights lasting between 1 and 10 minutes. Multiple studies have reported that the RER of birds will rise rapidly at the start of flight and steadily decline over time due to a

constant $\dot{V}O_2$ and slightly declining $\dot{V}CO_2$ indicating a shift in fuel use (Butler et al., 1977, Rothe et al., 1987, Ward et al., 2002) but our flights were limited to a maximum of 4 minutes, suggesting that we captured the higher end of observable RER values for masked lovebirds during flight.
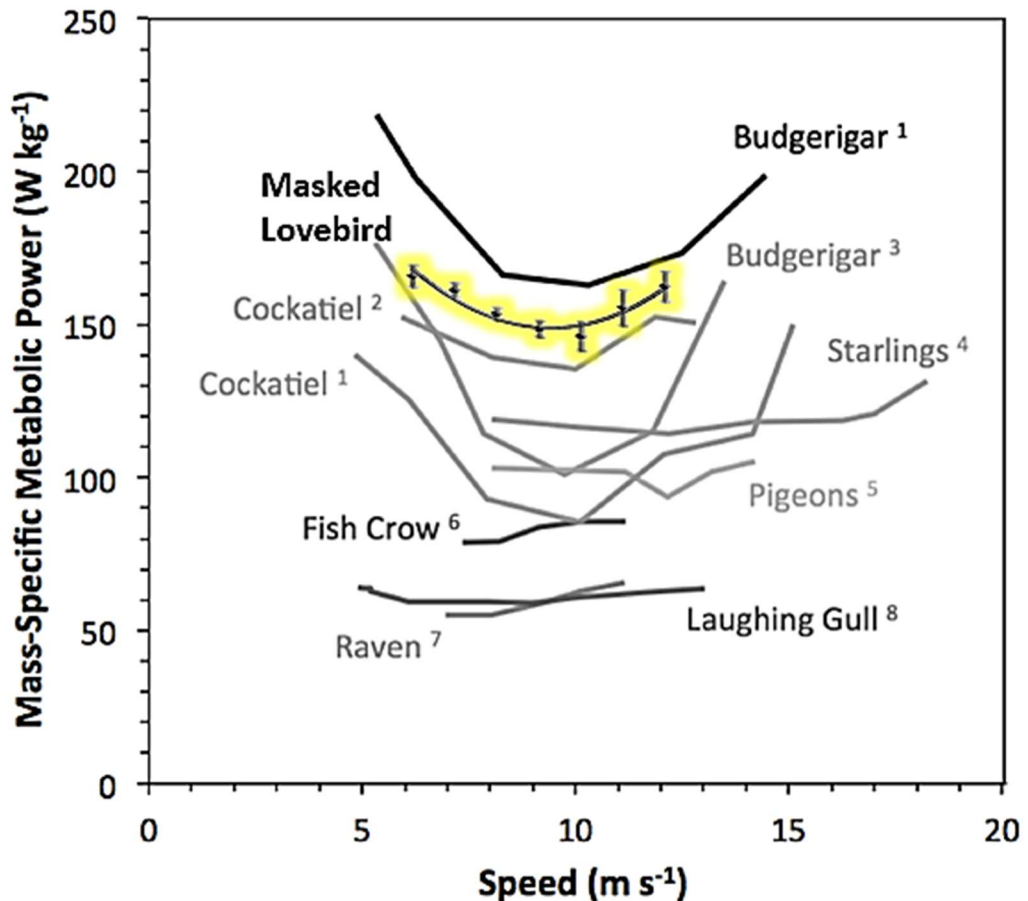
Figure 4.16 Comparison of masked lovebird P_{met} across flight speed with published P_{met}-speed relationships. Masked lovebird highlighted in yellow. Data from [1] Bundle et al. (2007); [2] Morris et al. (2010); [3] Tucker (1968); [4] Ward et al. (2001); [5] Rothe et al. (1987); [6] Bernstein et al. (1973); [7] Hudson (1983) and [8] Tucker (1972).

It is important to consider the additional costs of flying with respirometry equipment above unencumbered flight. The mass of the mask and tubing supported by the lovebirds (3.7%) was similar to that used on cockatiels (4%) by (Morris et al., 2010) and much less than used on cockatiels (11%) by (Bundle et al., 2007). As well as mass, the additional aerodynamic drag

created by the presence of the mask and tubing is likely to affect the costs of flight (Pennycuick et al., 2012). In order to assess the impact of respirometry equipment on the metabolic performance of cockatiels, Morris et al. (2010) performed kinematic analysis on videos taken of both instrumented and un-instrumented birds, finding no differences in wing stroke amplitude, relative shortening duration or stroke plane angle. Using an aerodynamic model (Morris and Askew, 2010a), they concluded that their metabolic power measurements were largely unaffected by the presence of respirometry gear. Even though our respirometry equipment weighed relatively less, we did not perform similar comparative tests with un-instrumented flights and cannot assume the same conclusion. We therefore assume that there is at least a small additional energetic cost to flying with respirometry equipment and attempt to estimate this cost later in the discussion (Chapter 4.5.5).

4.5.3 Accelerometry as a proxy for energy consumption

We present the first ODBA- and VeDBA-speed relationship curves determined for birds (Figure 4.16). Both ODBA and VeDBA displayed the characteristic U-shaped parabolic relationship with flight speed often observed with both the metabolic and mechanical power requirements of flight (Ward et al., 2001, Ward et al., 2004, Askew and Ellerby, 2007, Morris and Askew, 2010b, Morris et al., 2010), which supports our hypothesis and suggests that the slowest and highest speeds require the highest levels of acceleration-related mechanical power generation and associated metabolic costs. Determining the metabolic costs of flight at the widest possible range of speeds is valuable for ensuring that all naturally occurring flight speeds are properly calibrated. It is unlikely that the masked lovebirds will fly at the lowest or highest speeds (potentially beyond the range achieved in these experiments) unless under extreme pressure to do so and the majority of flights are expected to be done close to the minimum power speed (Hedenström and Alerstam, 1995).

As our metabolic values represent the gross energetic costs of flight and not the net costs above resting metabolism, there is an offset between the true costs of activity as estimated by ODBA and VeDBA. This is evident from Figure

4.11, where an extrapolation of acceleration to zero g suggests that there is still a level of EE when there is no acceleration, which represents the basal costs of flight. However, if basal metabolism is relatively constant as we find it to be, then the relationship with net metabolism should be largely proportional to gross metabolism but with a y-intercept closer to zero, representing no net EE when at rest. Indeed, we find that net $\dot{V}O_2$, net $\dot{V}CO_2$, and net P_{met} all produce relationship equations with flight speed that include very similar slopes but have reduced (albeit non-zero) y-intercept values compared to the gross values. Using the net metabolic values also results in slightly higher R^2 values (Table 4.1), inferring a better fitted relationship when net values are used. These non-zero y-intercept values are likely due to additional non-movement related EE above resting levels including increased physiological requirements (e.g. ventilation and circulation) and thermoregulation during flight (Gleiss et al., 2011). As we found resting metabolism to vary significantly between birds, it may be useful to determine net metabolic measurements as well as gross measurements when estimating the flight costs of wild bird populations and examining the effects of inter-individual variation.

Our calibrations of ODBA and VeDBA against $\dot{V}O_2$ and P_{met} were significantly correlated (Figure 4.11), supporting our prediction that accelerometry would be a valuable estimator of energy expenditure. Linear equations were produced to predict energy expenditure variables from both ODBA and VeDBA (Table 4.1). Whilst all relationships were found to be significant, the R^2 values representing the goodness of fit between the equation and the data were all rather low compared to other published R^2 values for metabolic-acceleration relationships (Qasem et al., 2012). However, the majority of these relationships have been determined for terrestrial locomotion where a relatively larger range of body acceleration values can be examined between slow walking (e.g. 0.25 g) to fast running (e.g. 2 g) in humans (Halsey et al., 2008b), compared to the narrower range observed from our masked lovebirds (1.3 – 2.3 g) due to the high minimum body acceleration required for flight. These low R^2 may also be due to the limited dataset including only a single flight per speed for each bird and only sampling from a short bout of flight.

Lower than expected R^2 values between ODBA and fH-derived $\dot{V}O_2$ during flight were also recorded in European shags by Hicks et al. (2017) ($R^2 = 0.21$) and these were also thought to be due the short time scales recorded (Green, 2011, Elliott, 2016). However, even from this limited dataset, the relationships between all of our dynamic body movement metrics and metabolic measurements demonstrate the value of accelerometry as an estimator of energetic expenditure across a wide range of flight speeds.

For $\dot{V}O_2$ and P_{met}, the R^2 values were slightly higher when estimated using VeDBA, but overall there appears to be no real difference in the relationship between body acceleration and EE when either ODBA or VeDBA is used, which corroborates the findings of Halsey et al. (2009). Although Halsey et al. (2009) and other studies have not used mass-specific values for ODBA and VeDBA, they have found significant intra-individual variation in the data between individual that they contribute to differences in body mass (Halsey et al. 2009) and recommend that mass-scaling be included in future metabolic-acceleration relationship models (Halsey et al., 2009; Miwa et al. 2015). Therefore, when validating against mass-specific metabolic measurements, it is important to also incorporate a mass-scaling element into the accelerometry values as we have done in this study.

Table 4.1   Equations for predicting the metabolic requirements of flight from measures of dynamic acceleration.

Target (y-axis	Source (x-axis)	Gross equation	R^2	Net equation	R^2
$\dot{V}O_2$	ODBA	y = 5.37 + 0.07*x	0.367	y = 2.5 + 0.07*x	0.369
	VeDBA	y = 5.19 + 0.11*x	0.371	y = 2.24 + 0.012*x	0.393
$\dot{V}CO_2$	ODBA	y = 4.64 + 0.05*x	0.231	y = 2.46 + 0.06*x	0.297
	VeDBA	y = 4.57 + 0.08*x	0.218	y = 2.33 + 0.09*x	0.292
P_{met}	ODBA	y = 110 + 1.34*x	0.365	y = 52.74 + 1.44*x	0.377
	VeDBA	y = 107 + 2.13*x	0.364	y = 47.87 + 2.35*x	0.395

4.5.4 Combined respirometry and accelerometry

Although only a single bird was able to maintain a stable state for respirometry long enough while wearing both the respirometry and accelerometry equipment due to possible fatigue, it does demonstrate that the experiment is possible and that the dataset could potentially be expanded. However, it may take extensive training with all birds to achieve reliable results and repeating the experiment with larger bird species is more likely to produce a reliable dataset. This single flight provided interesting results, but should be treated with a degree of uncertainty.

While all metabolic values ($\dot{V}O_2$, $\dot{V}CO_2$, P_{met} and RER) measured during this combined-equipment flight were greater than the flight with just the respirometry equipment (Figure 4.14), the accelerometry values were slightly lower during the combined-equipment flight than with just the accelerometry equipment (Figure 4.15). These reductions in ODBA and VeDBA during the combined-equipment flight may be due to the fact that they were measured over a much longer duration in the combined-equipment flight (60 s) compared to the accelerometry flight (9.62 s), while the flight time for the respirometry flight (60 s) was the same as the combined flight time. Indeed, when accelerometry values are determined using the same duration of flight time (first 9.62 seconds after the initial wingbeat), ODBA and VeDBA increased and were much closer to those measured during un-instrumented flight. This suggests that the birds may have generated greater body acceleration towards the start of the flight compared to later in the flight, which resulted in lower measurements of ODBA and VeDBA over the longer flight duration. However, without repeat flights from this bird, it is hard to determine whether these values lie within the range of error around the mean, and so we can't say for sure that these values are distinct from those measured with the un-instrumented bird.

While we have generated reasonable evidence to validate the use of accelerometry for estimating EE during flight across a range of speeds, the one combined-equipment flight recorded from this bird demonstrates that estimating the metabolic costs of flight from accelerometry is not an infallible

method, and that care should be taken when interpreting body acceleration data in the context of EE, especially when dealing with instrumented birds or sampling over uneven timescales.

4.5.5 The energetic costs of instrumentation

By analysing the estimations of energy consumption from respirometry and accelerometry calculated individually and during the combination-equipment flight, it is possible to provide a rough approximation of the relative contribution of additional energy expenditure (EE) of each piece of equipment and predict the costs of un-instrumented flight. From Table 4.2, it is clear that there are likely to be some metabolic costs associated with instrumented flight. These values suggest that the accelerometer is responsible for a higher increase in additional energy expenditure (EE) contributing to P_{met} than the respirometry equipment, accounting for 68% of the increase in P_{met} observed during the combined-equipment flight. This is not a surprising result, as the accelerometer accounted for approximately 60% of the additional load carried by the bird during the combined-equipment flight, however, it is difficult to draw conclusions without more inter- and intra-individual data.

This additional EE is most likely due to the energetic costs of generating more mechanical power in order to overcome the additional aerodynamic drag. The extra mass of the equipment will increase the bird's lift-induced drag and the shape of the equipment will increase the parasite drag, which is likely to increase the energetic requirements to maintain flight (Pennycuick et al., 2012) and push this individual bird close to its energetic ceiling, even at the cruising flight speed of 9 m s^{-1} (Elliott et al., 2014). Previous estimates of the additional P_{met} required to fly encumbered suggests that respirometry may overestimate the true P_{met} by 3-30% (comparable to our 13%) due to the additional work required to overcome the drag provided by the mask and tubing (Tucker, 1972, Rothe et al., 1987, Ward et al., 2001, Ward et al., 2002). Future development of this calibration could include the calculation of aerodynamic drag coefficients from 3D flight kinematics in both instrumented and un-

instrumented flight in order to better estimate the costs of instrumentation (Morris et al., 2010).

Table 4.2 **Estimated energy expenditure (EE) for un-instrumented flight and extra EE required with instrumentation.** $\dot{V}O_2$ and P_{met} are included as representative measures of EE. Observed values from the bird capable of flying with combined-equipment included. Respirometry costs measurements calculated from VeDBA using the equations from Table 4.1.

	Equipment	$\dot{V}O_2$	P_{met}
Gross EE	Un-instrumented	7.05 ml min^{-1} kg^{-1}	124 W kg^{-1}
Extra EE (%)	Respirometry	+ 9.21	+ 13.1
	Accelerometry	+ 9.01	+ 24
	Both	+ 18.2	+ 37.1

4.5.6 Kinematics

We found that accelerometry-derived wingbeat did not vary with flight speed, but that relative flapping duration did. Interestingly, we found a significant inverse correlation between the two kinematic variables, perhaps suggesting that masked lovebirds modulate their mechanical power generation by varying the relative flapping duration of their flights, but this may be a case of pseudo-correlation since wingbeat did not differ significantly between flight speeds, and relative flapping duration may just vary with speed. Other species of birds have been found to modulate their mechanical power output during flight through intermittent flight in addition to varying muscle recruitment, including other parrots such as budgerigars and cockatiels (Bundle et al., 2007; Ellerby and Askew, 2007a, 2007b). In order to validate the estimation of kinematic variables from accelerometry, the same variables were determined simultaneously from video footage of the same flights. We found that both accelerometry-derived WR and RFD were significantly correlated with the video-derived WR and RFD, supporting the use of accelerometry as a technique for determining certain flight kinematics.

In a similar vein of research, accelerometry is also now being used to predict specific activities from three-dimensional body movements (Wright et al., 2014, Angel et al., 2015). Recent examples include the differentiation of flight behaviours in Scopoli's shearwaters (Cianchetti-Benedetti et al., 2017) and razorbills (Chimienti et al., 2016). Building on simple predictive algorithms, increasingly complex methods of accelerometry analysis are being employed to more accurately predict specific behaviours, including the development of neural networks (Resheff et al., 2014), nearest neighbour algorithms (Bidder et al., 2014), and Markov models (Leos-Barajas et al., 2017) to predict flight behaviours.

4.5.7 Development of the respirometry and accelerometry techniques

The respirometry technique used for these experiments is largely similar to the ones used in previous investigations into the metabolic costs of flight (Morris et al., 2010). However, a few of our alterations to the method may help to improve the technique for future use. First, while 3D printed masks were not selected for use in data collection in this study, high-resolution printers combined with appropriate moulding plastic could produce more robust and customisable alternatives to cellulose acetate. Secondly, we determined from comparative gas analysis that the gas cylinders used for calibration of the respirometry setup were very inconsistent in contents, and so we recommend that the gas flame technique of calibration be used as a secondary method for ensuring that the true gas contents of calibration cylinders are known.

The methods of determining ODBA and VeDBA from accelerometry data were also largely unchanged from the published literature (Qasem et al., 2012), but the design process of our small-parrot back-mounted accelerometer harness may provide useful insights for future work. Accelerometers are typically attached to the back of birds (Wilson and Mcmahon, 2006) and this was found to be the most appropriate placement for our lovebirds. The general guidelines suggest that biologgers attached to birds should weigh 3-5% or less of the bird's body mass, but the 3% rule posited by Philips et al. (2003) has primarily

been applied for large seabirds with body masses above 1 kg, and a review by Barron et al. (2010) found that harness attachment method was more likely to affect flight performance than proportional mass increase, and it is more important to suit the design of harnesses to match the locomotor style of the animal (Vandenbeele et al., 2014). They found that a 3% increase in body mass seemed to result in an EE increase of 4.67 – 5.71% without accounting for EE increases due to the extra drag, and this appears to agree with our predicted results for $\dot{V}O_2$ (5.6 g harness predicted to incur a 9.01% EE cost). Additionally, a recent review by Elliott (2016) found that increasing external tag sizes had increasingly large effects and that there was no minimum tag size that didn't alter natural flight behaviour in some way.

The rapid miniaturisation of modern biologging technology (Ropert-Coudert and Wilson, 2005) has rendered this issue less problematic for large birds over 1 kg but there are still issues in attaching these devices to small passerines with body masses of 30 g or less (Bäckman et al., 2017). However, due to the high wingbeat frequency of smaller birds (typically > 12 Hz), oscillatory activity can be determined over a short period of time and measurements of dynamic acceleration can be extracted from bouts of continuous flight lasting only a couple of seconds as long as the accelerometer samples at a high enough frequency (~100 Hz) (Hedenström et al., 2016, Bäckman et al., 2017).

Chapter 5
The effects of Ca^{2+} on the mechanical power output and efficiency of asynchronous insect flight muscle

5.1 Abstract

Asynchronous insect flight muscles (IFMs) are able to contract in disassociation with neural activation, enabling some insects to fly with incredibly high wingbeat frequencies without the energetic costs of rapid calcium cycling. Instead, stretch-activation and myoplasmic calcium ion concentration ([Ca^{2+}]) play important roles in muscle activation during oscillatory contractions. Previous work has demonstrated that varying concentrations of calcium ions strongly affects the development of isometric force in isolated IFMs and there is increasing evidence to suggest that the regulation of myoplasmic calcium ions plays an important role in the modulation of mechanical power during insect flight. However, the effects of varying [Ca^{2+}] on the mechanical and energetic properties of asynchronous IFMs at different contraction frequencies have not yet been determined. By simultaneously measuring the generation of work from isolated muscle fibres undergoing contraction cycles and the rate of ATPase activity via an NADH-linked assay, we investigated the interacting effects of contraction frequency and [Ca^{2+}] on the mechanical power, rate of ATPase activity and myofibrillar efficiency of dorsal-longitudinal flight muscles from the the *Lethocerus indicus* waterbug. Both mechanical power and gross ATPase activity increased in parallel with increasing frequency, but the optimal frequency range differed between activating solutions containing different [Ca^{2+}], suggesting that [Ca^{2+}] plays a role in determining the optimal conditions for cross-bridge mechanics and energetics. Due to the parallel nature of the power-ATPase relationship, gross myofibrillar efficiency varied with frequency bit did not differ between activating solutions, generating a peak mean gross efficiency of 8.06% when oscillating with intermediate contraction frequencies and [Ca^{2+}]. These results are discussed in the context of the Ca^{2+}-release power modulation hypothesis in *Lethocerus* and *Drosophila* flight muscles.

5.2 Introduction

Insects have developed specialised flight muscles to meet their locomotor requirements, including the adaptation of asynchronous muscles that have arisen independently almost a dozen times. The asynchronous flight muscles of many insect species can contract repeatedly at incredibly high frequencies, even as high as 1000 Hz in midges (*Forcipomyia*) (Sotavalta, 1953). While synchronous muscles contract in a 1:1 ratio with neural impulses, asynchronous muscles can contract and relax multiple times per neural impulse (Josephson et al., 2000a). Instead of relying on electrical stimulation and calcium cycling to regulate contraction, asynchronous muscles utilise stretch-activation and shortening-deactivation in order to generate delayed force at a rapid rate (Glasheen et al., 2017). However, calcium ions still play a pivotal role in determining the levels of force developed through cross-bridge cycling.

Many animals modulate the mechanical power generated for locomotion by varying the recruitment of muscle fibres (Enoka, 1995, Altshuler et al., 2010, Morris and Askew, 2010b). However, this may be less viable for insects that have a small number of motor units with a limited ability to fine-tune fibre recruitment (Wang et al., 2011). Furthermore, there is increasing evidence to suggest that insects with asynchronous flight muscles may vary mechanical power generation through the regulation of myoplasmic $[Ca^{2+}]$. The quantity of calcium ion release in insect flight may not be simply binary with low and high levels of calcium release for inactive and active muscles respectively, and there may be more of a graded relationship between myoplasmic $[Ca^{2+}]$ and the generation of power in order to meet the changing aerodynamic requirements of flight (Gordon and Dickinson, 2006).

If the mechanical power output of asynchronous IFM is, at least in part, modulated by varying myoplasmic $[Ca^{2+}]$, there should be evidence of a coupled change in flight kinematics such as wingbeat frequency to drive the variation in aerodynamic power. Indeed, in vivo studies by Gordon and

Dickinson (2006) and Lehmann (2013) have provided simultaneous measurements of relative [Ca^{2+}], wingbeat frequency and aerodynamic power from genetically engineered *Drosophila* IFMs during tethered flight using calcium-dependent fluorescence resonance energy transfer (FRET) (Miyawaki et al., 1997, Truong et al., 2001), revealing closely linked increases in [Ca^{2+}], wingbeat frequency and aerodynamic power. Earlier in vitro work by Steiger and Rüegg (1969) demonstrated that the optimum frequency for power generation and muscle efficiency in glycerol extracted *Lethocerus* DLM fibres were higher in a bathing solution containing a higher [Ca^{2+}] compared to a lower [Ca^{2+}]. However, this set of experiments had severe limitations. Firstly, only two oscillation frequencies were used and each was tested at different temperature ranges (2 Hz at 26 ˚C and 10 Hz at 23-25 ˚C). Secondly, only three fibre bundles were analysed and these varied in size between 4 and 6 myofibrils. A more recent study by Wang et al. (2011) observed that the optimal power generation in *Drosophila* was generated at 100 Hz oscillations in bathing solutions with low [Ca^{2+}], and during 125 Hz oscillations in bathing solutions with high [Ca^{2+}], but did not explore this relationship any further than these two frequencies.

Glycerol extracted *Lethocerus* IFMs have long been a preferred study system for investigating a range of mechanical and energetic properties of insect muscle and have played major roles in the development of the sliding filament theory of muscle contraction (Reedy et al., 1965, Huxley, 1969). Their large and regularly structured fibrillar flight muscles make them relatively easy to manipulate (Pringle, 1977, Reedy and Garrett, 1977) and the glycerination extraction procedure allows just the isolated contractile machinery to be examined (Jewell and Rüegg, 1966). Another benefit of working with glycerol extracted fibres is that they are directly exposed to ionic changes in the extracellular environment, providing ample opportunity to examine the effects of Ca^{2+} on the mechanical and energetic properties of the fibres (Woledge et al., 1985).

While the mechanical properties of IFMs have been extensively studied, studies on the energetic costs and efficiency of contracting these muscles are much less prevalent. The studies that exist confirm a close link between mechanical power generation and ATPase activity and a close relationship between peak mechanical generation power and the mechanochemical efficiency of the muscle (Steiger and Rüegg, 1969). Experimentally determined values of IFM efficiency are relatively small compared to vertebrate muscle but within IFMs, asynchronous muscles are considered to be more efficient than synchronous muscles due to their ability to generate work without the high energetic costs associated with rapid calcium cycling (Josephson et al., 2000a). Published values of net muscle efficiency determined from skinned IFMs range from 3% in locusts (*Schistocerca americana*) (Josephson and Stevenson, 1991) to 11-12% in figeater beetles (*Cotinis mutabilis*) (Josephson et al., 2000b) while gross muscle efficiency values range up to 15-23% in bees (*Bombus* and Euglossini) (Askew et al., 2010).

In order to provide insight into the potential role of $[Ca^{2+}]$ in the modulation of aerodynamic power and the concomitant effect on metabolic energy use, mechanical power generation and ATPase activity of glycerol extracted *Lethocerus* muscles were simultaneously measured across a range of oscillation frequencies and in a range of activating solutions containing different $[Ca^{2+}]$. Hence, the relationships between $[Ca^{2+}]$ and optimum frequency for power, work and myofibrillar efficiency were determined. Based on the limited existing literature based in both in vitro and in vivo experiments, it was hypothesised that the optimal oscillation frequency for mechanical power generation would increase with increasing $[Ca^{2+}]$ and that the associated ATPase activity would increase in parallel, resulting in a relatively constant optimal frequency for muscle efficiency across $[Ca^{2+}]$.

5.3 Methods

5.3.1 Insect dissection

The dorsal-longitudinal flight muscles (DLM) of the giant waterbug, *Lethocerus indicus*, were chosen for this experiment as they are large muscles comprising many long parallel asynchronous muscle fibres whose contractile properties are well established in the literature (Pringle, 1977, Reedy and Garrett, 1977, Boussouf et al., 2007). All of the insect carcasses used in this study were collected in Thailand and shipped live to UK where they were killed and the thoraxes glycerinated (three animals from 2009 and three from 2012 supplied as glycerinated thoraxes by Dr Belinda Bullard).

Prior to the glycerination process, the insects were first immobilised in a freezer and the head, legs, elytra and wings were then removed consecutively. The abdomen was carefully removed from the thorax by cutting the connecting membrane and gently pulling the abdomen. Special care was taken not to rupture the gut and release digestive enzymes as it was pulled from the thorax. Finally, the thorax was split bilaterally down the centre to expose the DLM on both sides, which allowed the fibres to accessed and extracted.

5.3.2 Glycerination protocol

The glycerination process followed the method used by Askew et al. (2010) for the DLM of apid bees. Each pair of hemithoraxes were placed in the first of a series of glycerination solutions and subsequently transferred to the other solutions at precise intervals over the course of three days. The glycerol concentration of the nine solutions increased gradually from 0% to 75%. Protease inhibitors (PMSF and Complete™ mini EDTA-free tablets) were added to the early solutions following muscle dissection to prevent any damage to the contractile proteins by proteases released that were potentially from the gut. The addition of 1% Triton X-100 removed the membranes from the DLM and left only the contractile proteins and the connective tissues. Sodium azide was added to inhibit mitochondrial ATPase. 5 mM DTT was

added during the final stage to absorb oxygen from the solution and further prevent the proliferation of micro-organisms in the solution.

Upon completion of the glycerination process, the final holding solution containing the hemithoraxes was stored at -80°C until required for the experiments. The holding solution consisted of 20 mM phosphate buffer (pH 6.8 at 20°C), 5 mM potassium EGTA, 5 mM sodium azide, 10 mM potassium chloride, 2 mM magnesium chloride and 5 mM magnesium ATP.

5.3.3 Muscle chamber and experimental setup

The mechanochemical experiments were performed in a specialised muscle chamber (Figure 5.1), described in Askew et al. (2010). The solution chamber (approximate capacity 115 µl) was constructed from anodized aluminium with two parallel sides covered by UV-fused silica glass windows (Comar Instruments, Cambridge, UK) that allowed transmission of light between 170-2500 nm. A small well in the base of the chamber held a stir-bar which allowed the solution to be mixed without interfering with the muscle fibres. A combination of a Peltier heating system and a cooling fan were used to maintain the temperature of the chamber at 40 ± 0.3°C, which is the in vivo thoracic temperature for *L. indicus* during flight (Molloy, 1988).

At the start of the experiments, single glycerinated muscle fibres were carefully detached from the bundle of glycerinated muscle fibres with insect pins and were mounted between a force transducer (AE801, Kronex Technologies Corporation, Oakland, CA, USA) and a mechanical vibrator (V201, Ling Dynamic Systems Ltd, Royston, Herts, UK). Glue composed of cellulose nitrate dissolved in acetone was used to secure the muscle fibres in place. Muscle fibre length and oscillation parameters (frequency and strain) were controlled using a custom-built function generator (Gilmour and Ellington, 1993). The equipment used for ultraviolet spectroscopy is detailed later in this chapter (Chapter 5.3.8).
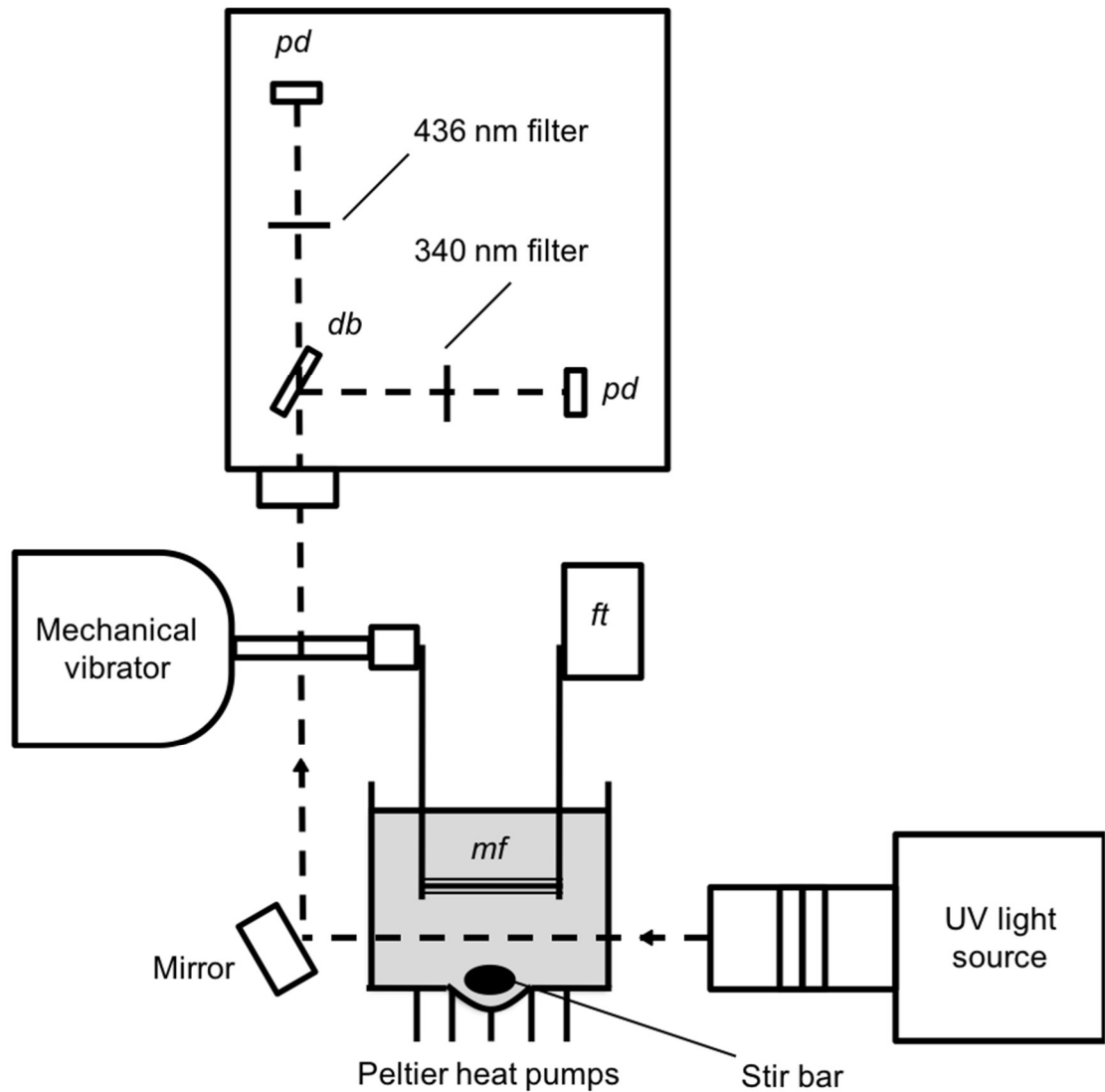
Figure 5.1   Muscle chamber and experimental setup. (mf) muscle fibre, (ft) force transducer, (db) dichroic beamsplitter, (pd) photodiode. Shaded volume represents the diluted activating solution ($A_\%$).

5.3.4 Relaxing and activating solutions

The Ca^{2+} concentration ($[Ca^{2+}]$) in the experimental solutions was varied by producing a range of activating solutions ($A_\%$) containing different ratios of the activating (A) and relaxing (R) solution components (Table 5.1). The activating solution consisted of 20mM Pipes buffer (pH 7.0 at 20°C), 20 mM Ca EGTA, 5 mM NaN_3, 2 mM $MgCl_2$ and 10 mM MgATP. The relaxing solution consisted of 20mM Pipes buffer (pH 7.0 at 20°C), 5 mM K EGTA, 5 mM NaN_3, 10 mM KCl, 2 mM $MgCl_2$ and 10 mM MgATP. Approximately 8 mmol l^{-1}

phosphoenolpyruvate (PEP), 1.7 units pyruvate kinase (PK) and 3.1 units lactate dehydrogenase (LDH) were added to both the relaxing and activating solutions. The concentrations of these substrates and enzymes were kept consistent across all solutions.

Table 5.1   Ionic composition of relaxing and activation solutions.

Sol.	[CaCl$_2$] (mM)	[Free Ca^{2+}] (μM)	pCa	[MgATP^{2-}] (mM)	[Free Mg^{2+}] (mM)	Ionic strength (mM)
R	0	-	-	8.4	0.625	136
A$_{10\%}$	0.1	2	5.7	8.4	0.632	137
A$_{20\%}$	0.2	2.6	5.59	8.4	0.634	138
A$_{40\%}$	0.4	3.8	5.42	8.4	0.639	140
A$_{60\%}$	0.6	5.8	5.24	8.4	0.645	142
A$_{70\%}$	0.7	7.5	5.13	8.4	0.638	143
A$_{80\%}$	0.8	10	5	8.4	0.653	144

5.3.5 Isometric properties and [Ca^{2+}]-force relationship

In order to determine an appropriate range of [Ca^{2+}] for the activating solutions, a number of muscle fibres were subjected to increasing [Ca^{2+}] and the resulting peak isometric force for each solution was recorded. Force data were then normalised to the maximum force attained. Throughout the relevant literature discussed in this chapter, force and tension are seemingly treated as synonymous but all references to force and tension in this chapter will be presented as force for clarity.

5.3.6 Mechanical contraction properties

Net mechanical power (net P_{mech}) output and net work (W_{net}) production by the muscle were determined during cyclical contractions using the work loop technique (Josephson, 1985, Askew et al., 1997). The mechanical contraction parameters were selected in part to generate measurable quantities of NADH depletion as determined through preliminary experiments, and also to approximately represent the in vivo conditions of the *Lethocerus* DLM during flight, as detailed below.

The length trajectory of the muscle was sinusoidal around the mean length, shortening and lengthening the muscle to a set strain. Due to a lack of evidence for in vivo muscle length changes, preliminary experiments were performed at a range of strains between 1% and 5% peak-peak amplitude in order to determine the optimal power-producing strain for these fibres, which was 4%. This value corresponds to similar optimal strains used by other studies of *Lethocerus* IFM (Rüegg and Stumpf, 1968, Tregear, 1969, Molloy, 1988).

While the wingbeat frequency of *L. indicus* during flight has been determined to be approximately 20-30 Hz (Molloy, 1988), the range of cycle frequencies used in these experiments is somewhat lower. Optimal frequency for contraction is negatively correlated with strain amplitude, and the relatively high strains used in these experiments may explain this reduction in optimal frequency. The reduction in optimal cycle frequency for generating work and power in skinned muscle fibres compared to whole fibres is also a previously reported phenomenon (Gilmour and Ellington, 1993, Askew et al., 2010).

5.3.7 Experimental work loops

Once the fibre was attached and placed in the chamber, a short set of reference work loops was carried out at in order to assess the initial mechanical performance of the muscle fibre. These reference work loops were all carried out at 8 Hz, which produced large positive-work generating work

loops across most of the range of activating solutions during preliminary experiments. Work loops that collapsed to zero net work generation during the contraction cycles, potentially due to fibre damage during paring or oscillation (Gilmour and Ellington, 1993), were removed from analysis.

During each experimental run, the muscle was cycled for a period of between 80 and 120 seconds. Occasionally, the mean length of the muscle would be slightly adjusted during the cycles in order to maintain a consistent level of work generation, but was otherwise left untouched. Upon completion of the first set of work loops in a single solution, the muscle fibre remained in the solution for another 40-60 seconds before being moved to the relaxing solution. While the muscle fibre was in the relaxing solution, the activating solution was removed and the experimental chamber was washed out first with deionized water and then ethanol before a different activating solution was added. The muscle fibre was then brought back into the experimental chamber and new reference work loops were performed prior to the next run of experimental contractions.

When all experimental work loops were completed, the muscle fibre was removed from the solution chamber and acetone was applied to dissolve the cellulose nitrate glue and release the fibre. Following this, the experimental chamber was emptied and washed out repeatedly with deionized water before the new solution was added for the next fibre.

5.3.8 Ultraviolet absorption spectroscopy

The rate of ATPase activity in the chamber solutions was determined using an NADH-linked spectroscopic assay. A 75 W xenon arc lamp was used as an ultraviolet light source and was positioned perpendicular to the muscle energetics chamber in order to direct a narrow beam of light through the chamber windows and into the solution. After passing out through the other side of the chamber, the light was reflected towards a dichroic beamsplitter which produced two beams: a transmitted beam in the visible region (390 to 700 nm), and a reflected beam with a wavelength range of 340-390 nm.

Bandpass interference filters restricted the beams to wavelengths of 435.8 nm and 340 nm, respectively. These beams both terminated at separate UV enhanced 100 mm² photodiodes, where the intensity of the beams was used to determine the absorption of UV light by the solution in the muscle chamber. Specifically, the intensity of the 340 nm beam was used to measure the concentration of NADH in the solution and the 435.8 nm beam acted as a 'reference beam' with which the 340 nm 'experimental beam' could be corrected for intensity fluctuations and stirring artefacts.

5.3.9 Measuring NADH depletion

From the intensity of the beams measured by the photodiodes, the ATPase activity within the solution could be determined by calculating the rate of NADH depletion.

During ATP hydrolysis, high-energy phosphate bonds release chemical energy, as well as producing ADP and inorganic phosphate P_i (Equation 5.1). ADP is rephosphorylated to ATP by PEP and the enzyme pyruvate kinase (PK) which produces pyruvate (Equation 5.2). In a coupled reaction catalysed by lactate dehydrogenase (LDH), pyruvate is reduced to L-Lactate and NADH is oxidized to NAD⁺ (Equation 5.3).

$$ATP \xrightarrow{ATPase} ADP + P_i \qquad\qquad [5.1]$$

$$PEP + ADP \xrightarrow{PK} Pyruvate + ATP \qquad\qquad [5.2]$$

$$Pyruvate + NADH + H^+ \xrightarrow{LDH} Lactate + NAD^+ \qquad [5.3]$$
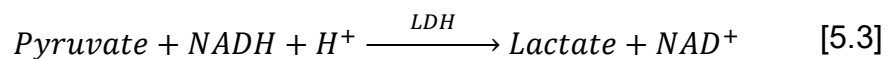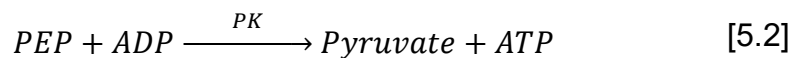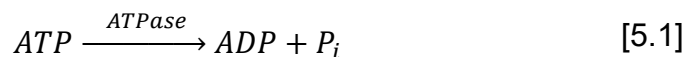
NADH absorbs light at a wavelength of 340 nm but NAD⁺ does not. Measuring the absorbance of light at 340 nm by the solution in which the muscle is situated allows the rate of NADH depletion, and therefore ATP hydrolysis, to be determined. The quantity of NADH (q; in moles) in the solution was calculated using the Beer-Lambert law (Equation 5.4).

$$q = -\frac{v_{sol}}{EL}\log\left(\frac{I_t R_0}{R_t I_0}\right) \qquad\qquad [5.4]$$

where V_{sol} is the volume of solution in the chamber (litres), E is the extinction coefficient for NADH at 340 nm (6.22×10^{-3} mol l^{-1} cm^{-1}; Askew et al. (2010)), l is the path length (cm), I_t is the intensity of the 340 nm beam at time t, R_t is the intensity of the reference beam at time t, I_0 is the intensity of the 340 nm beam with no NADH present, R_0 is the intensity of the reference beam with no NADH present. All beam intensities were reported in volts.
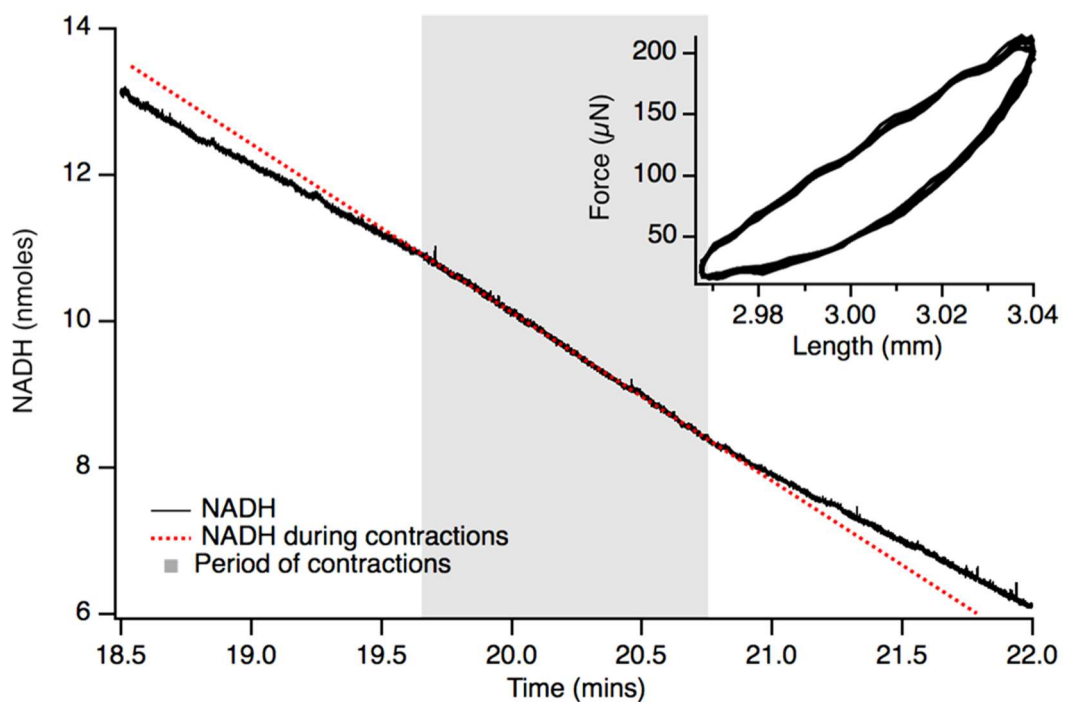
Figure 5.2   **Representative trace of the NADH depletion over time.**
Black trace represents the quantity of NADH in the solution and red trace represents the increased depletion during oscillatory contractions (grey area). The work loop associated with these oscillatory contractions is included inset.

5.3.10   Calculating mechanical power and net work per cycle

Using force and muscle length measurements from the force transducer and mechanical vibrator, mechanical power output was determined for each cycle as the product of force and velocity (IGOR Pro Version 7; Wavemetrics, OR,

USA). Velocity was determined as the mathematical derivative of muscle length change over time. Net P_{mech} was calculated as the average value of each instantaneous power value for each cycle in the series. W_{net} per cycle (W_{net}) was calculated by dividing the net P_{mech} by the cycle frequency.

5.3.11 Calculating ATPase rate, MC and efficiency

To determine the rate of ATPase activity during contraction cycles and during isometric periods, linear regressions were fitted to the NADH concentration (nmol) against time. The ratio of the net P_{mech} output to the rate of ATP hydrolysis, referred to as the gross mechanochemical coefficient (MC_{gross}; kJ mol^{-1}), was calculated using Equation 5.5.

$$MC_{gross} = \frac{P_{mech}}{ATP_{gross}} \qquad [5.5]$$

where P_{mech} is the net mechanical power and ATP_{gross} is the gross ATPase rate.

Additionally, some of the previously published work on glycerinated insect asynchronous flight muscles has investigated the ratio of mechanical power output to the rate of ATP hydrolysis during contraction cycles minus the rate of ATP hydrolysis during the isometric phase, referred to as extra ATPase (ATP_{extra}) (Steiger and Rüegg, 1969). Using this value of extra ATPase, the apparent MC was calculated using Equation 5.6.

$$MC_{apparent} = \frac{P_{mech}}{ATP_{extra}} \qquad [5.6]$$

The gross (η_{gross}) and apparent (η_{app}) efficiencies were calculated as the ratio of their respective MC values to the free energy released by ATP hydrolysis during muscle contraction, which was assumed to be 48 kJ mol^{-1} (Kushmerick and Davies, 1969, Barclay, 1998).

5.3.12   Statistical analysis

Type 3 GLMs were used to test for differences in all of test variables between different cycle frequencies and activating solutions with different $[Ca^{2+}]$. Both factors were included as main effects and the interaction between the two factors was included as an additional term in the model. All values are reported as the mean average ± SEM unless stated otherwise. Statistical tests were performed in SPSS (Version 20.1, IBM) and R (Version 3.5.0, R-Project).

5.4 Results

Data from 122 experimental runs were collected from 31 fibres. Heat maps are included as alternative data plots for most of the results presented in this chapter (Figure 5.12), but these include additional dimensions of data interpolation and serve to visualise trends and patterns in the data rather than to discern statistical differences.

5.4.1 Calcium-force relationship

Normalised force developed by the isolated fibres increased with increasing free $[Ca^{2+}]$ as a sigmoidal relationship (Figure 5.3). The data were plotted against both molecular concentration of Ca^{2+} and pCa (a commonly used logarithmic index of $[Ca^{2+}]$) and a Hill-equation curve was fitted to the data.

The activation solutions used for the rest of the experiments were selected from various points across this curve to represent a range of $[Ca^{2+}]$ between those that generated no isometric force through to those that generated maximum isometric force. Although an $A_{80\%}$ activating solution was included in the experiments, the vast majority of fibres subjected to this $[Ca^{2+}]$ seemingly became damaged shortly after the start of the contraction cycles, pulling the muscle apart and producing unusable work loops. Therefore, these data were excluded from the dataset and $A_{70\%}$ was treated as the highest $[Ca^{2+}]$ activating solution.

Pre-oscillatory isometric force recorded during the experiments were significantly different between different activating solutions ($F_{4,117}$ = 14.4, P < 0.001) with isometric force rose with increasing [Ca^{2+}] until plateauing between $A_{40\%}$ and $A_{60\%}$, at which point force began to decline through to $A_{70\%}$.
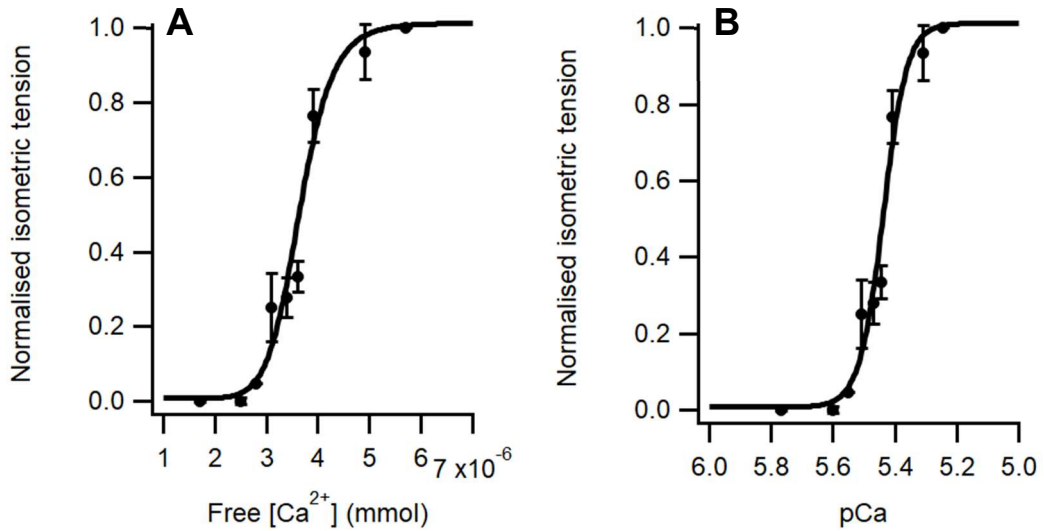
Figure 5.3 **Isometric force-calcium relationship.** Force normalised to a proportion of maximum isometric force attained for each fibre. (A) [Ca^{2+}] presented as a molecular concentration. (B) [Ca^{2+}] represented as pCa. Error bars are ± SEM.

5.4.2 Mechanical power and work per cycle

For all activating solutions, the net P_{mech} output of the fibres during contraction cycles was low at both the lowest frequency (4 Hz) and the highest frequency (20 Hz), with the $A_{20\%}$, $A_{40\%}$ and $A_{60\%}$ solutions achieving greater net P_{mech} at intermediate frequencies (8, 12 and 16 Hz). For fibres immersed in the $A_{10\%}$ solution, net P_{mech} generation was always negative and became even more negative with increasing frequency. For fibres in the $A_{70\%}$ solution, net P_{mech} generation was negative at lower frequencies, before becoming slightly positive at 12 Hz and then declining back to a negative P_{mech} at higher frequencies. Net P_{mech} was significantly different between different frequencies ($F_{4,97}$ = 9.44, P < 0.001) and activating solutions ($F_{4,97}$ = 22, P < 0.001), and there was an interacting effect between frequency and solution ($F_{4,97}$ = 2.7, P = 0.001). The highest mean net P_{mech}, 22.1 nW cm^{-1}, was generated at a frequency of 12 Hz in the $A_{40\%}$ solution (Figure 5.4). The optimum frequency

for generating peak P_{mech} tended to increase with increasing $[Ca^{2+}]$ activating solutions (Appendix 2).

Similar to P_{mech}, the net work performed (W_{net}) was also significantly different between cycle frequencies ($F_{4,97} = 4.25$, $P = 0.003$) and activating solutions ($F_{4,97} = 8.53$, $P < 0.001$) with a comparable increase at intermediate frequencies compared to low and high frequencies. (Figure 5.5). Compared to P_{mech}, the relationship between W_{net} and frequency is down-shifted, resulting in lower optimal frequencies for generating W_{net}. However, W_{net} was not significantly affected by the interaction between frequency and solution ($F_{4,97} = 1.23$, $P = 0.22$). The highest mean W_{net} of 1.34 nJ cm^{-1} was generated at a frequency of 8 Hz in the $A_{20\%}$ solution (Figure 5.4). The shape of the work loops also differed greatly between different experimental conditions (Figure 5.6). As

Figure 5.4   Relationship between net P_{mech} and oscillation frequency, grouped by $A_\%$. Data presented as mean ± SEM. n for $A_{10\%}$ is 5, 5, 4, 4 and 4; $A_{20\%}$ is 4, 5, 6, 5 and 4; $A_{40\%}$ is 6, 5, 6, 6 and 6; $A_{60\%}$ is 4, 5, 5, 5 and 5; $A_{70\%}$ is 4, 5, 5, 5 and 4 for 4, 8, 12, 16 and 20 Hz.

with P_{mech}, the optimum frequency for generating peak W_{net} tended to increase with increasing $[Ca^{2+}]$ activating solutions but peaked at different frequencies than P_{mech} (Appendix 2).

Figure 5.5 **Relationship between W_{net} and oscillation frequency, grouped by $A_\%$.** Data presented as mean ± SEM. n for $A_{10\%}$ is 5, 5, 4, 4 and 4; $A_{20\%}$ is 4, 5, 6, 5 and 4; $A_{40\%}$ is 6, 5, 6, 6 and 6; $A_{60\%}$ is 4, 5, 5, 5 and 5; $A_{70\%}$ is 4, 5, 5, 5 and 4 for 4, 8, 12, 16 and 20 Hz.
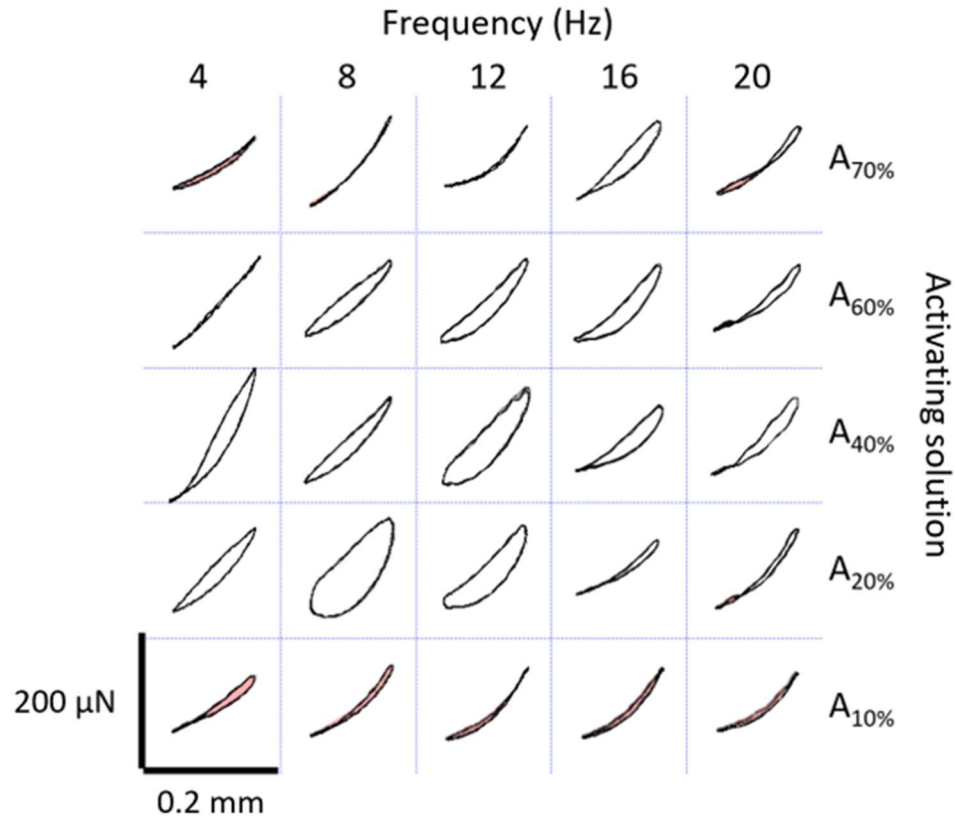
Figure 5.6 **Work loop shape at different contraction conditions.**
Each loop is force (y axis) plotted against length (x axis). White areas indicate positive work and pink areas indicate negative work. Work loops generating the greatest mechanical power for each frequency-solution pairing are presented as representations of peak performance.

5.4.3 ATPase

Multiple preliminary tests confirmed that there was no detectable ATP consumption in the absence of a fibre and that ATPase activity was initiated as soon as the fibre entered the chamber, representing the ATPase rate during isometric contractions (ATP_{iso}). The isometric ATPase increased with increasing $[Ca^{2+}]$ activating solutions until $A_{60\%}$, at which point the ATPase began to decrease. ATP_{iso} was significantly different between activating solutions ($F_{4,73} = 0.067$, $P < 0.001$) but not between frequencies ($F_{4,73} = 1.31$, $P = 0.275$) was not affected by a solution-frequency interaction ($F_{4,73} = 0.467$, $P = 0.95$). The ATP_{iso} was closely correlated with pre-cycle isometric force across the different activating solutions ($r = 0.512$, $P < 0.001$).

The ATPase rate of the fibres during oscillatory contraction cycles (ATP_{gross}) was similarly affected by activating solution ($F_{4,94} = 15.7$, $P < 0.001$) but not by frequency ($F_{4,94} = 1.36$, $P = 0.255$) or the interaction ($F_{4,94} = 0.949$, $P = 0.518$) (Figure 5.7), exhibiting a more than three-fold increase between $A_{10\%}$ and $A_{20\%}$. Interestingly, the ATPase rate of the fibres during sinusoidal contraction cycles above the isometric rate, often referred to as "extra" ATP (ATP_{extra}), was affected by neither frequency ($F_{4,73} = 1.67$, $P = 0.166$) or activating solution ($F_{4,73} = 1.16$, $P = 0.336$), but was affected by the interaction between the two ($F_{4,73} = 2.4$, $P = 0.007$) and peaks in ATP_{extra} can indeed be observed occurring at different frequencies with different activating solutions (Figure 5.8). Net P_{mech} was strongly correlated in positive relationships with both gross ATPase activity ($r = 0.605$, $P < 0.001$) and extra ATPase activity ($r = 0.406$, $P < 0.001$) (Figure 5.10B).
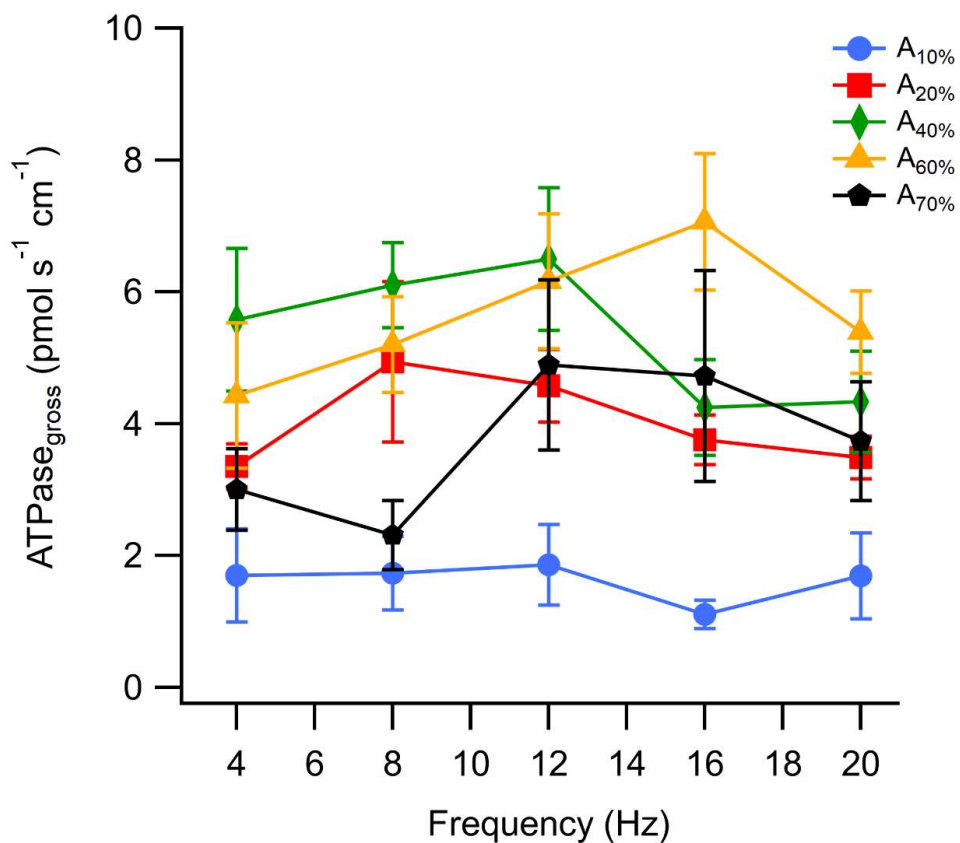
Figure 5.7   Relationship between ATPase$_{gross}$ and oscillation frequency, grouped by A$_\%$. Data presented as mean ± SEM. n for $A_{10\%}$ is 5, 5, 4, 4 and 3; $A_{20\%}$ is 4, 5, 5, 5 and 4; $A_{40\%}$ is 6, 5, 6, 6 and 6; $A_{60\%}$ is 4, 5, 5, 5 and 5; $A_{70\%}$ is 4, 5, 4, 5 and 4 for 4, 8, 12, 16 and 20 Hz.
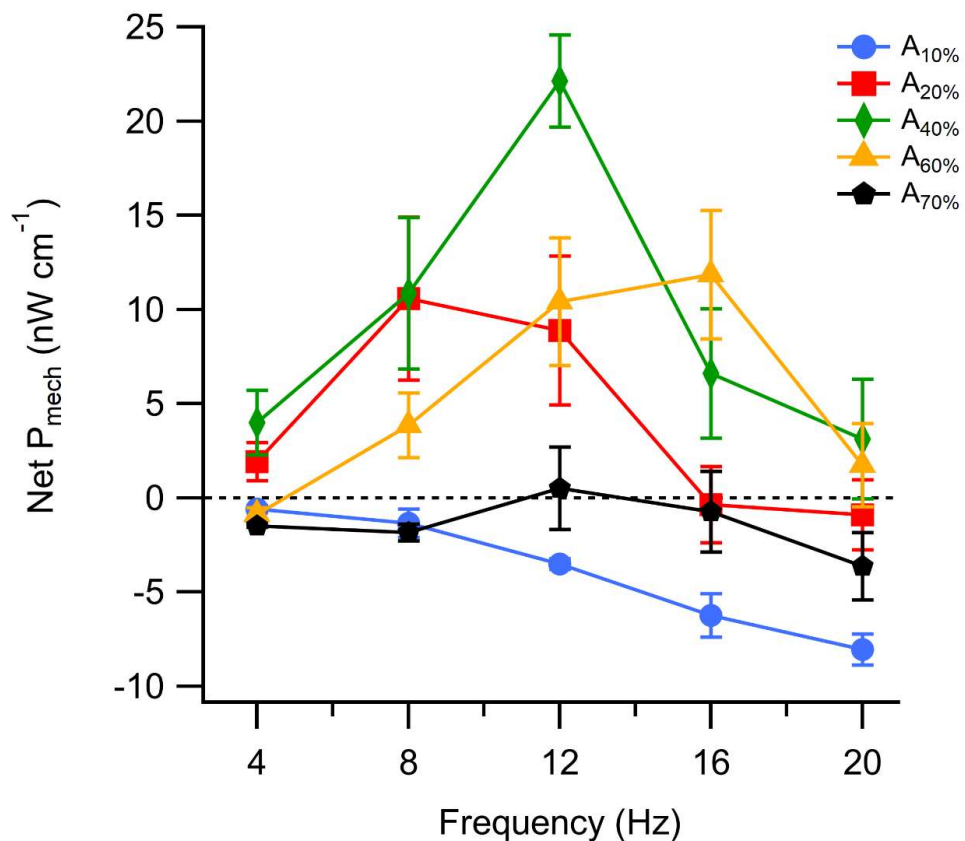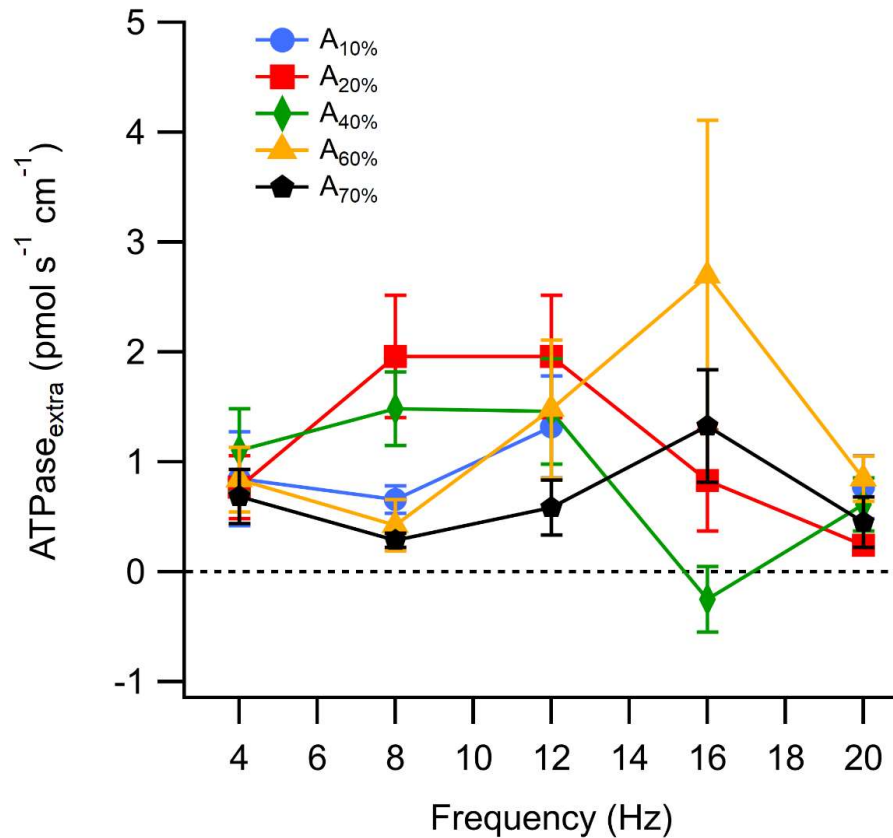
Figure 5.8   Relationship between ATPase$_{extra}$ and oscillation frequency, grouped by A$_{\%}$. Data presented as mean ± SEM. n for A$_{10\%}$ is 4, 4 and 2; A$_{20\%}$ is 4, 5, 5, 5 and 3; A$_{40\%}$ is 5, 4, 6, 4 and 5; A$_{60\%}$ is 3, 4, 4, 3 and 4; A$_{70\%}$ is 3, 5, 4, 3 and 4 for 4, 8, 12, 16 and 20 Hz.

5.4.4 Efficiency

Similar to the relationships between P$_{mech}$ and W$_{net}$ with frequency and activating solution, the "gross" efficiency (η_{gross}) of the fibres during oscillatory contraction cycles was generally low at the low and high frequencies but rose during the intermediate frequencies. η_{gross} was significantly different between different frequencies (F$_{4,94}$ = 7.7, P < 0.001) and activating solutions (F$_{4,94}$ = 38.6, P < 0.001), as well being affected by an interaction between frequency and solution (F$_{4,94}$ = 3.86, P < 0.001). The highest mean efficiency, 8.06%, was generated at a frequency of 12 Hz in the A$_{40\%}$ solution (Figure 5.9) and interestingly, the optimum frequency for generating mechanical power appeared to be 12 Hz for all activating solutions except A$_{10\%}$ which only generated positive work at 4 Hz.
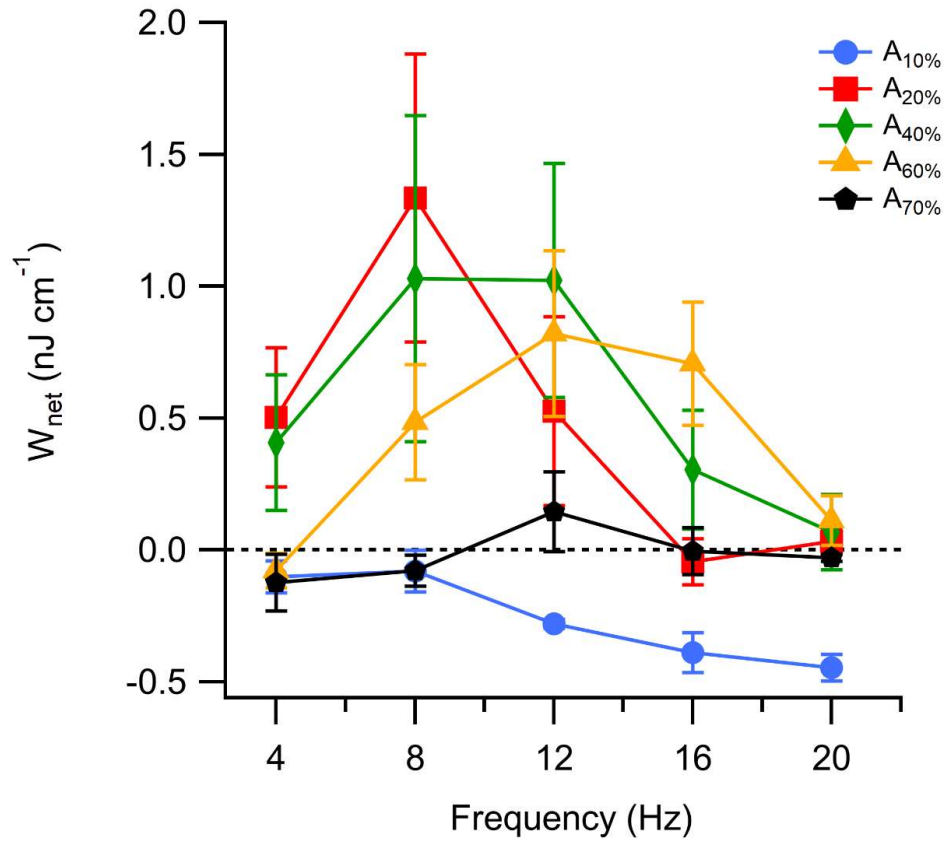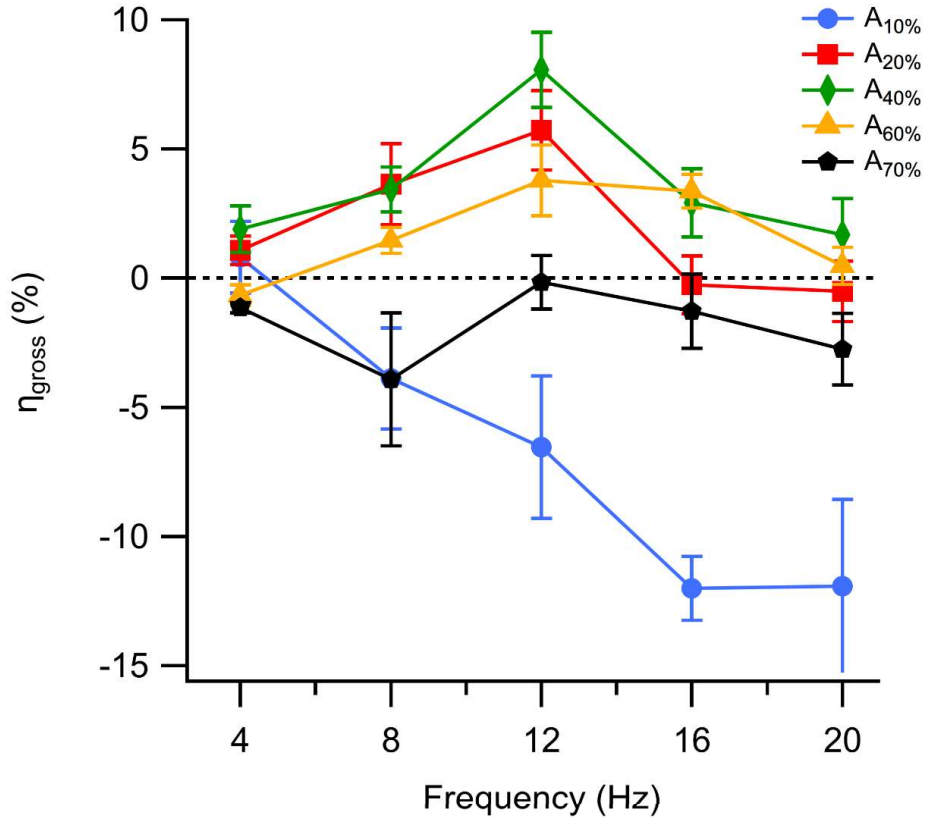
Figure 5.9   Relationship between η_{gross} and oscillation frequency, grouped by $A_\%$. Data presented as mean ± SEM. n for $A_{10\%}$ is 5, 5, 4, 4 and 3; $A_{20\%}$ is 4, 5, 5, 5 and 4; $A_{40\%}$ is 6, 5, 6, 6 and 6; $A_{60\%}$ is 4, 5, 5, 5 and 5; $A_{70\%}$ is 4, 5, 4, 5 and 4 for 4, 8, 12, 16 and 20 Hz.
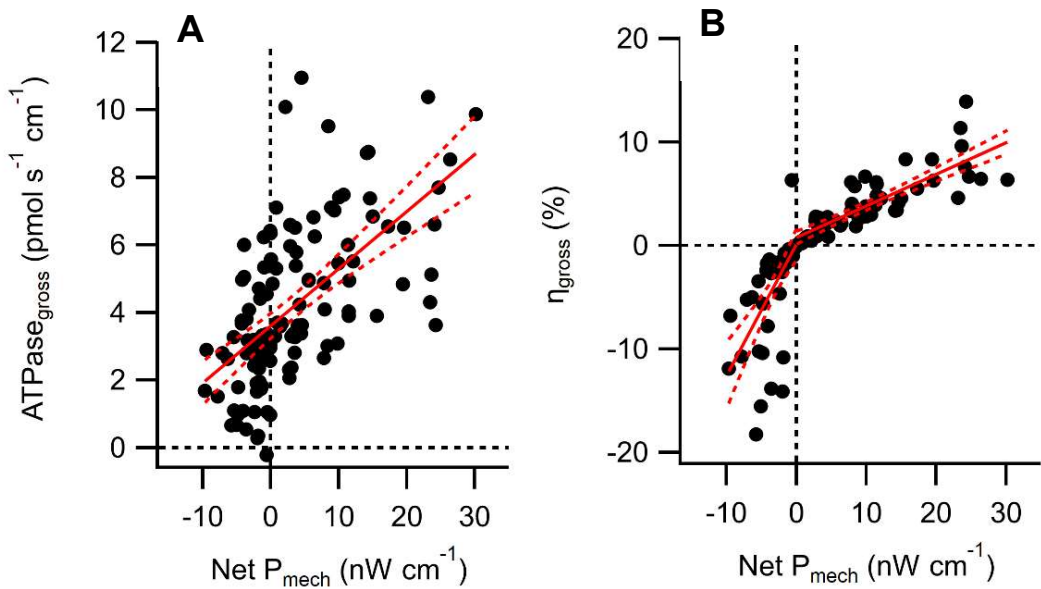

Figure 5.10   Relationships between $ATPase_{gross}$ and η_{gross} with net P_{met}. (A) $ATPase_{gross}$. (B) η_{gross}. Solid lines are fitted linear curves, dotted lines are 95% confidence intervals of the curves. n = 117.
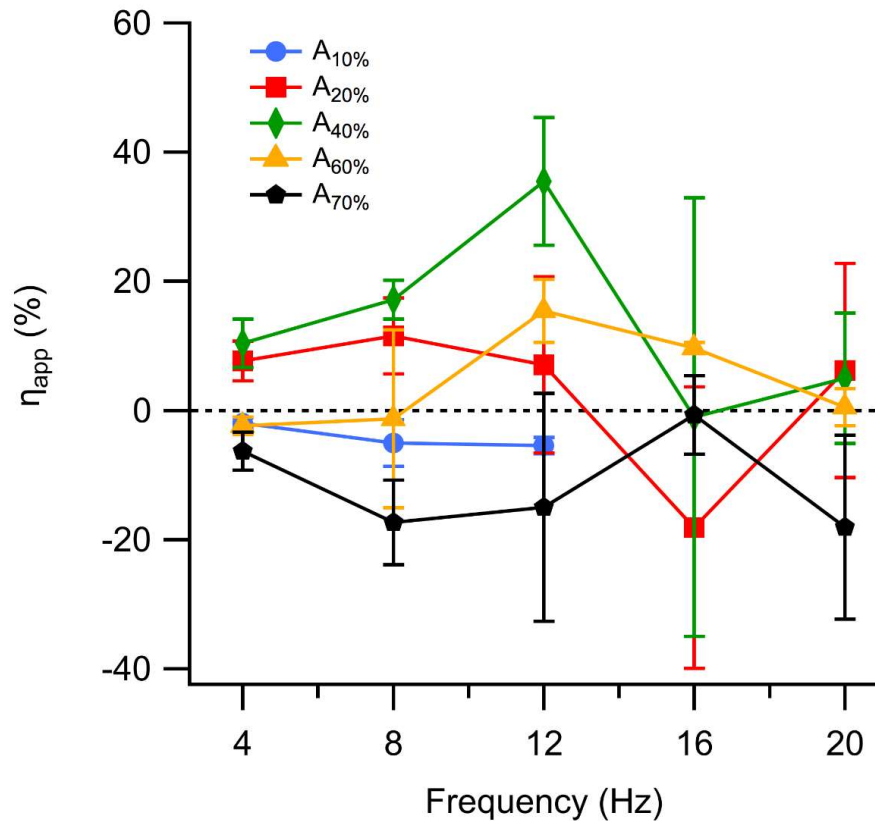
Figure 5.9   Relationship between η_{app} and oscillation frequency, grouped by A%. Data presented as mean ± SEM. n for $A_{10\%}$ is 4, 4 and 2; $A_{20\%}$ is 4, 5, 5, 5 and 3; $A_{40\%}$ is 5, 4, 6, 4 and 5; $A_{60\%}$ is 3, 4, 4, 3 and 4; $A_{70\%}$ is 3, 5, 4, 3 and 4 for 4, 8, 12, 16 and 20 Hz.

The "apparent" efficiency of the fibres during oscillatory contraction cycles differed significantly between activating solution ($F_{4,67} = 5.4$, P = 0.001) but was not significantly affected by frequency ($F_{4,67} = 2.25$, P = 0.073) or the frequency-solution interaction ($F_{4,67} = 1.22$, P = 0.278) (Figure 5.11). Net P_{mech} was strongly correlated in a positive relationship with both gross efficiency (r = 0.785, P < 0.001) and apparent efficiency (r = 0.49, P < 0.001) (Figure 5.10A). The relationship between net P_{mech} and gross efficiency ($R^2 = 0.616$) differed in slope at approximately net P_{mech} values of zero (Davies, 2002, Muggeo, 2008). This relationship was then split to represent the different relationships with efficiency depending whether net P_{mech} the values were positive or negative. From these relationships, positive power exhibited a tighter relationship with gross efficiency ($R^2 = 0.702$) than negative power ($R^2 = 0.392$).
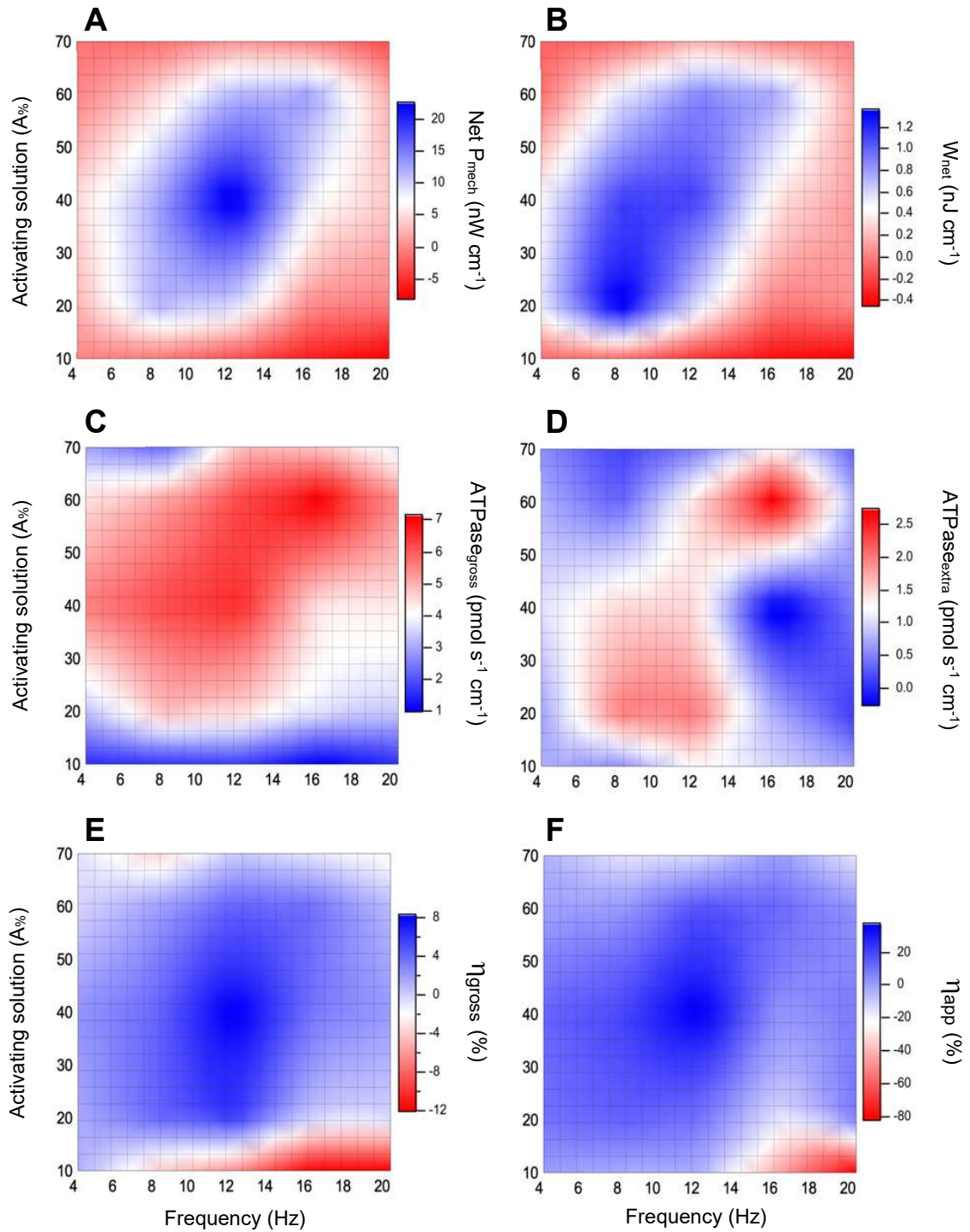
Figure 5.10 Heat map of all variables plotted against frequency and A%.
Colour variation represents range of values. (A) Net P_{mech}. (B) W_{net}. (C) ATPase$_{gross}$. (D) ATPase$_{extra}$. (E) η_{gross}. (F) η_{app}.

5.5 Discussion

5.5.1 Effect of calcium on the optimal frequency for net mechanical power and work

Our results support our hypothesis that increasing myoplasmic $[Ca^{2+}]$ above a sub-activating level not only increases mechanical power, but also the optimal frequency at which mechanical power is generated (Figure 5.4; Appendix 2). This supports the in vivo coupled calcium-frequency-power relationship observed in *Drosophila* IFM by Gordon and Dickinson (2006) in theory, but no in vivo studies of $[Ca^{2+}]$ in *Lethocerus* IFM have yet been conducted and the absolute range by which myoplasmic calcium ion concentration varies is unknown. Our results found a peak mean P_{met} (22.125 nW cm^{-1}) that is similar to the peak values recorded for *Lethocerus* IFM (~ 30 nW cm^{-1}) by Steiger and Rüegg (1969) using 10 Hz oscillations with a 4% peak-peak strain between 23 and 25°C. Positive net P_{mech} was generated between pCa 5.59 and pCa 5.13, which overlaps with the range of $[Ca^{2+}]$ found to yield positive net power by Wang et al. (2011) in *Drosophila* IFM (pCa 5.8 to 5.25) and their fibres generated negative power at $[Ca^{2+}]$ below approximately pCa 5.7-5.8, which also agrees with our results. Our results also indicate that net work exhibits a similar pattern as net mechanical power but with lower optimal frequencies (Figure 5.6), which is to be expected as power increases relatively more with frequency as more cycles are performed per second (Stevenson and Josephson, 1990). Positive net work in *Lethocerus* IFM was generated over a wider pCa range than ours in a study by Kržič et al. (2010) IFM (pCa 6.5 to 4.5), but the mechanical work of their fibres similarly deteriorated at relatively high $[Ca^{2+}]$.

In agreement with our results, studies of *Lethocerus* IFM by Steiger and Rüegg (1969) and Kržič et al. (2010) both experienced a decrease in mechanical power and work generated at high $[Ca^{2+}]$, which they both attributed to the increases in calcium-induced force (F_0) and a proportional reduction in stretch-activated force (F_{SA}), which may increase force generation during lengthening and reduce net mechanical power. This reduction of net mechanical power and

work at high frequency and [Ca^{2+}] is likely not due to the diffusion limitation of ATP as all our IFM preparations were pared down to single fibres and all $A_\%$ had generous non-limiting ATP regeneration systems in place, which is also true for the results found by Kržič et al. (2010). However, Wang et al. (2011) found no such decrease in the mechanical power generated by *Drosophila* and found it to remain high at [Ca^{2+}] above pCa 5.25, suggesting a contrary relationship. To add to the uncertainty surrounding this calcium-power relationship, Lehmann et al. (2013) incorrectly describes the relationship between mechanical power generation and [Ca^{2+}] while interpreting the results of Wang et al. (2011). They state that *Drosophila* IFM starts to generate positive power at pCa 5.0 and becomes saturated above pCa 5.8, but this is the inverse of the expected physiological response. It is unclear whether this error is due to a typographical mistake or a fundamental misunderstanding about the calcium-power relationship in IFM, but they also repeatedly describe the range of [Ca^{2+}] as "small", even though this range contains more than a 6-fold increase in calcium ions and covers a range greater than is predicted to occur in *Drosophila* during flight (Wang et al., 2011).

5.5.2 Effect of calcium on ATPase activity and efficiency

Our results demonstrate that gross myofibrillar efficiency varies significantly in a range of myoplasmic [Ca^{2+}] which supports our hypothesis, and also that the optimum frequency for efficiency does not change with increasing [Ca^{2+}], which also supports our hypothesis.

As observed in previous studies of glycerol extracted *Lethocerus* IFM and our own, both positive power generation and ATPase activity (Figure 5.7) increase in parallel and subsequently decrease in parallel beyond the optimal frequency for each $A_\%$ solution (Steiger and Rüegg, 1969). However, mechanical power tends to increase proportionally more than ATPase activity, which creates measurable changes in efficiency, which is what we find in our correlations between mechanical power and both gross and apparent efficiency. The peak efficiency values presented here for *Lethocerus* IFMs are similar to those previously estimated for *Lethocerus* and asynchronous IFM from other insect

species. The highest gross efficiency value recorded from an individual fibre (13.9%) was generated at 12 Hz in $A_{40\%}$, which were the same conditions that generated the highest average gross efficiency from our fibres (approximately 8.1%).

Although Steiger and Rüegg (1969) did not publish values of gross efficiency from their *Lethocerus* fibres, they did calculate the "apparent" mechano-chemical coefficient (MC_{app}) values from the "extra" ATPase activity above that measured at isometric levels. Oscillating with a 4% peak-peak amplitude strain at 20°C, they found MC_{app} to peak at approximately 12 to 17 kJ of work per mole of extra ATP. Similarly, Pybus and Tragear (1975) found peak MC_{app} values of 16 to 17 kJ mol^{-1} during similar 4% strain oscillations at 30°C. The apparent values of MC_{app} calculated from this study also peak at approximately 17 kJ mol^{-1} during 4% strain oscillations at 40°C, suggesting that temperature has seemingly little effect on the mechano-chemical efficiency and that 17 kJ mol^{-1} represents a value close to the maximum achievable MC_{app} with skinned *Lethocerus* fibres.

According to the results of Casey and Ellington (1989) and Askew et al. (2010), the efficiency of insect IFM is likely to scale intraspecifically with body mass, but it can be difficult to compare inter-specifically as a variety of methodologies and definitions of IFM efficiency have been published, and it may not be correct to assume that the same scaling relationship applies to different groups of insects. Our values of peak gross efficiency of *Lethocerus* are lower than determined for bumblebees and euglossine bees (15-23%) (Askew et al., 2010), suggesting that our values may lie outside of the range predicted purely by mass-scaling. However, as these experiments weren't designed to optimise power, it is unsurprising that muscle efficiency values below those predicted by body mass scaling were recorded during non-optimal contraction conditions including low $[Ca^{2+}]$ and low frequencies. Our mean efficiency values remained at a similar level (3-8%) across the intermediate range of oscillation frequencies and $[Ca^{2+}]$ with lower or "negative" efficiency values occurring at the extremes of those parameter ranges. This is similar to the relationships

observed in isolated muscle preparations where high velocity contractions appear to consume more ATP per unit of work performed than those at a slower velocity, creating a reduction in efficiency at high frequency (Kushmerick and Davies, 1969, Steiger and Rüegg, 1969).

Due to the absorption of work at non-optimal oscillation frequencies and $[Ca^{2+}]$, some efficiency values are presented as negative values. Logically, a negative muscle efficiency is thermodynamically impossible, and these values instead represent the energetic costs of the muscles absorbing work during oscillation. The cost of absorbing work is always less energetically costly than generating positive work (Holt et al., 2014) and the difference in costs between generating positive and negative work has been reported to increase with increasing contraction velocities (Abbott and Aubert, 1952). This would help to explain the high negative efficiency values generated by fibres in the $A_{10\%}$ solution at high frequency oscillations, as this negative work can be generated for a relatively small energetic cost.

If there is a proportional relationship between mechanical power and ATPase activity, it could be surmised that variation in gross efficiency is due to variation in the amount of force-generating cross-bridge cycling performed per oscillation. Steiger and Rüegg (1969) suggested that the observed reduction in the efficiency of *Lethocerus* IFM contractions with changes in frequency may be caused by a decrease in the phase angle of sinusoidal force development and length changes. For example, at sub-optimal frequency, the slow oscillation may shift the delayed rise in force following stretch towards a phase angle closer to zero, generating zero net work. If the frequency is supra-optimal, then there may not be sufficient time for the optimal number of cross-bridges to form and the muscle will be sub-optimally activated. If $[Ca^{2+}]$ is sub-optimal, then there may not be enough cross-bridges formation and force generation to generate a net positive power. If $[Ca^{2+}]$ is supra-optimal, then there may be too many force-generating cross-bridges formed during lengthening to produce a net positive power. All of these conditions may work

to reduce the ratio of mechanical power and work generation to the associated energetic costs.

It has been argued that the relatively low efficiency of IFM is compensated by the presence of elastic energy storage mechanisms (Dickinson and Lighton, 1995) but the true role of these mechanisms remains unknown. A number of previous studies of IFM efficiency have assumed either perfect or zero elastic energy storage during contraction, producing efficiency values that are 2-3 fold higher when no elastic energy storage is assumed compared to perfect elastic energy storage (Ellington, 1984, 1985). However, a revised aerodynamic analysis by Askew et al., 2010 indicated that assumptions about elastic energy storage didn't make much difference to overall efficiency.

In order to further determine the relationship between calcium ion concentration and the optimal frequency for gross efficiency, the data must be analysed at a more fundamental level by teasing apart the cross-bridge mechanics during shortening and lengthening. Determining work generation during shortening, the peak rates of force development (PRFD) during lengthening and force reduction during shortening may reveal more about the molecular mechanisms at work (Yue, 1987). These factors have not yet been investigated during oscillatory contractions in *Lethocerus* and novel work may elucidate how [Ca^{2+}] and frequency interact with the mechanics and energetics of IFM at the molecular level.

5.5.3 The calcium-force relationship

We found that increases in [Ca^{2+}] tended to increase the pre-oscillation isometric force until it plateaued between the $A_{40\%}$ and $A_{60\%}$ solutions. This result is not surprising as a greater concentration of free Ca^{2+} should lead to greater muscle activation and the formation of more cross-bridges, enabling a greater development of force. However, our results also indicated an interesting reduction in the pre-oscillation isometric force at the highest [Ca^{2+}], which was coupled with a faster reduction in isometric force over time and an increased likelihood of fibre breakage. When fibres entered the chamber

containing the A_{80}% solution, almost all of the fibres developed high isometric tension without stretch and immediately began to rapidly lose force after reaching a brief plateau of peak isometric force. At the start of oscillation, these fibres typically began producing positive work but the work loops quickly collapsed and would be producing zero net work within 60 seconds. Upon closer inspection of the fibres post-oscillation, they appeared to be damaged and were almost always torn apart when removed from the chamber. Moving fibres through the surface tension of a solution-air interface has been known to damage and tear fibres (Swank, 2012), but this level of damage was not observed with any other activating solution. While we can't separate out the F_{SA} and F_0 from the overall force generated, it is reasonable to assume from the existing literature that the vast majority of the isometric force generated at high [Ca^{2+}] was from calcium ions binding to the available sites on the myosin heads and encouraging constant high-force isometric contraction. If this is so, then the large strain amplitude of the oscillations and high levels of eccentric force generation during lengthening may have caused increasing levels of damage to the sarcomeres with increasing calcium ion saturation, leading to fibre breakage.

We found that the relationship between [Ca^{2+}] and peak force observed in glycerol extracted *Lethocerus* fibres between pCa 5.6 and pCa 5.2 conform to the sigmoidal relationship described by the Hill equation (Walker et al., 2010). Generally, studies of isolated *Lethocerus* IFM fibres have shown that fibres are activated by stretch at low [Ca^{2+}] and activated proportionally more by isometric force with increasing [Ca^{2+}] (Kuhn et al., 1985, Loxdale and Tregear, 1985, Agianian et al., 2004, Linari et al., 2004), suggesting a complementary and competitive mechanism for myosin head recruitment. However, the true nature of the relationship between tension development and calcium ion concentration in IFM remains a controversial area of discussion. While those studies found stretch-activated force generation to be maximal at intermediate [Ca^{2+}] in *Lethocerus* IFM, other studies have found contrary results, suggesting F_{SA} is maximal at saturating [Ca^{2+}] in *Lethocerus* (Glasheen et al., 2017) and

Drosophila (Iwamoto, 2009, Wang et al., 2011, Glasheen et al., 2017). IFMs, suggesting an additive relationship between F_{SA} and calcium-induced force.

5.5.4 Assessing the Ca^{2+}-release power modulation hypothesis

While our results demonstrate a shifting relationship between $[Ca^{2+}]$ and mechanical power generation, it is difficult to apply these in support of the Ca^{2+}-release power modulation hypothesis. Gordon (2006) demonstrated that the modulation of mechanical power output of *Drosophila* IFM during flight could not be adequately explained by differential recruitment of separately innervated motor units alone, and that $[Ca^{2+}]$ was more tightly linked to the two-fold increase in wingbeat frequency and aerodynamic power generation. However, the absolute $[Ca^{2+}]$ of IFMs during flight remains unknown and while varying $[Ca^{2+}]$ may play an important role in mechanical power modulation, this two-fold increase may not reach saturating $[Ca^{2+}]$ if inactive IFMs maintain low levels of calcium ions. Indeed, Wang et al. (2011) predicted that the in vivo myoplasmic $[Ca^{2+}]$ of *Drosophila* during flight is likely to be pCa 5.7 to pCa 5.4, which is well below the saturating $[Ca^{2+}]$ (pCa ~ 4.5) (Wang et al., 2011).

Wang et al. (2011) concluded from their results that the response of stretch activated tension to $[Ca^{2+}]$ was likely to be the main mechanism for power modulation during flight. If this is the case, intra-specific structural differences in IFM may explain the discrepancies in how F_{SA} varies with $[Ca^{2+}]$ between studies of *Lethocerus* and *Drosophila* IFM. Specifically, *Lethocerus* IFMs are comprised of ~1000 times more fibres than *Drosophila* IFMs (Peckham, 1990) and are potentially innervated by more motor units compared to the 8 observed in Drosophila IFM (Wang et al., 2011), which may make fibre recruitment a more feasible mechanism for power modulation and reduce the reliance of *Lethocerus* IFMs on maintaining a high level of F_{SA} at high $[Ca^{2+}]$. This is compared to *Drosophila* IFMs which have relatively few fibres and may rely more heavily on the generation of F_{SA} at high $[Ca^{2+}]$ to modulate their mechanical power output. Another major difference in the mechanics between these two IFMs is the in vivo wingbeat frequency, with *Lethocerus* reaching ~30 Hz during flight (Molloy, 1988, Kržič et al., 2010) and *Drosophila* reaching

~200 Hz (Hyatt and Maughan, 1994), which may affect the requirements for calcium-linked power modulation.

While a shift in the optimal frequency for power generation may theoretically support the $[Ca^{2+}]$-linked power modulation hypothesis, in order to be convinced that varying $[Ca^{2+}]$ plays a driving role in asynchronous IFM power modulation, the time course of calcium ion release and responsiveness of mechanical power generation needs to be determined. Given the much reduced SR of asynchronous IFM, the task of driving rapid modulations in power through changes in myofibrillar $[Ca^{2+}]$ seems difficult due to the slower rate of $[Ca^{2+}]$ release and sequestering compared to synchronous muscles.

5.5.5 The consideration of experimental limitations

By using standardised work loops, we aimed to ensure a consistent level of fibre quality across the experiments, but these type of experiments are known for exhibiting high levels of intra-fibre variation in performance (Gilmour and Ellington, 1993). Additionally, the muscle fibres used in this study had been in storage for approximately nine years before these experiments occurred, and there have been no studies on the effects of such long term storage on the quality of glycerol extracted IFMs. Gilmour and Ellington (1993) found that while freshly glycerinated muscle fibres (<48 hours) produced significantly higher levels of oscillatory work than fibres stored for longer periods of time, this was only examined up to 45 days post-glycerination.

While this study aimed to replicate the in vivo physiological conditions of *Lethocerus* IFM during flight, there were a number of parameters that had to be compromised. For example, the true in vivo oscillatory strain amplitude for *Lethocerus* IFMs is currently unknown. The optimal peak-to-peak strains for glycerol extracted *Lethocerus* IFM fibres range between 3 to 9% (Rüegg and Stumpf, 1968, Tregear, 1969, Molloy, 1988), and so values within this range were tested and 4% was selected for optimal performance. Additionally, as discussed in Chapter 5.3.6, the wingbeat frequency range used in these experiments is lower than those measured in vivo (Molloy, 1988). This may be

due to the relatively high oscillatory strain, which is correlated with reduced optimal frequencies for power generation (Askew et al., 2010), and indeed Glasheen et al. (2017) demonstrated that they could reproduce positive power generation at in vivo frequencies in skinned *Lethocerus* fibres, but only when using an incredibly small peak-peak strain amplitude of 0.25% that is likely to be much less than the operating strain during flight.

Chapter 6
General discussion

6.1 Coupling the mechanics and energetics of flight

The central theme of this thesis is the integration of experiments investigating the mechanics and energetics of animal flight. One of the most pivotal determinants in the relationship between locomotor mechanics and energetics is the mechano-chemical efficiency of the muscles. In Chapter 2, I measured the net efficiency of the mouse soleus muscle at different length trajectories and revealed that it changed proportionally with the initial mechanical efficiency as determined by Holt and Askew (2012), suggesting a relatively constant oxidative recovery efficiency. Similarly, in Chapter 3, I determined the net efficiency of the major avian flight muscle and revealed that it did not vary with flight speed. Finally, in Chapter 5, I demonstrated how the gross efficiency of a major flight muscle in *Lethocerus* waterbugs changed with varying wingbeat frequency and myoplasmic Ca^{2+} concentration. These investigations into how muscle efficiency is affected by physiological and behavioural factors helps to improve our understanding of the requirements and limitations of animal flight, as well as the mechanics and energetics of locomotor muscles in general. However, one of the biggest difficulties in comparing muscle efficiencies between studies is that a range of vague, inconsistent and non-mutually exclusive definitions are often used for studies of both vertebrate and invertebrate muscles. In order to maintain comparable values, both intra- and inter-specifically, I recommend that the equations and definitions laid out by Smith et al. (2005) should serve as the guidelines for the appropriate terminology and application of various measurements of efficiency.

While I examine the effects of a few contractile parameters (length trajectory and frequency) on muscle efficiency in this thesis, there are many more that may interact with not only the net and gross efficiencies, but also the efficiencies of constituent mechanical and energetic processes. As observed by the different effects of fast and slow fibre-types on the initial and net muscle

efficiencies (Barclay and Weber, 2004), some factors that appear to affect net muscle efficiency may only be having an effect on the mechanical efficiency or the metabolic recovery efficiency without affecting the other, and factors that don't appear to affect net muscle efficiency may be affecting those two processes in an inversely proportional way.

The benefits of performing experiments that couple mechanics and energetics are demonstrated and explained throughout this thesis, but it should be noted that there are situations where it may be more suitable to measure the mechanics and energetics of flight separately. For example, the measurement of in vitro muscular mechanical power can be compromised if subjected to sub-optimal conditions during the experiment. However, these sub-optimal conditions may be necessary for energetic measurements, such as the out-of-solution contractions required by a muscle when using a thermopile, or the longer inter-experimental waiting durations required to measure the O_2 consumption of substrate regeneration following contraction. Alternatively, as demonstrated in Chapter 4, the simultaneous use of accelerometers and respirometry masks is likely to affect the measurement of mechanical and energetic factors from whole organisms more than the use of a single piece of measurement equipment. I still recommend that coupled experiments be pursued where possible, but these factors should be taken into consideration during the development of hypotheses and experimental design processes.

6.2 Impact and application of this research

Chapters 2 and 3 both present new information that is essential for the development of improved predictive models of the metabolic costs of flight. A clear issue with estimating values of muscle efficiency and the postural costs of flight using predictive models is largely the result of disparate experimental methodologies that can't be directly compared. Even when mechanical and energetic experiments are performed with the same species, the effects of individual variation between animals and different equipment, techniques and research environments between institutions means that it is difficult to ensure

we're comparing like with like, which serves to support the integration of mechanical and energetic experiments. This is highlighted in Chapter 2 in the large differences in reported metabolic measurements from two previously published experiments with budgerigars, which generates large differences in estimated muscle efficiency when each is included in predictive models. As neither of these experiments also measured mechanical power output, these values were drawn from a third source, introducing more opportunity for error in the model. In order to develop useful predictive models, more integrated experiments need to be performed.

The integrative nature of the experiments presented in this thesis express the core ideologies of the 3 Rs of animal research (Guhad, 2005): replacement, reduction and refinement. Combined investigations into the mechanics and energetics of animal flight allows not only for improved data, but also leads to the reduction of animals that would be required for separate experiments. These experiments emphasise the benefits of reducing the number of experimental animals and reusing animals for simultaneous data acquisition.

6.3 Recommendations for early career researchers working with laboratory birds

The following reflections and recommendations are intended to inform and aid future early career researchers that intend to work with laboratory birds. Importantly, these issues also affect the ethical integrity of the research institution and government body that regulates them.

6.3.1 Open communication and access

Open and clear communication between researchers, institution support staff and governmental bodies is crucial to the generation of quality research and the welfare of the animals involved. It is vital that the researchers and animal unit staff agree on the role and responsibilities of each party in regards to the welfare of animals and the financial costs of any services rendered, prior to the induction of animals to prevent disputes that may result in needless termination

of animals. The priorities and expectations of each party should be acknowledged, and in cases of disagreements involving animal welfare, issues should be quickly clarified and solved together rationally through agreed upon lines of communication. Often these can take a long time to resolve, which can lead to scheduling and payment issues between researchers and the housing institution.

For researchers working with laboratory birds, and especially those that frequently remove the birds from a central animal housing location, all-hours access to the animals should be granted immediately. It is essential that no situation should occur where animals cannot be retrieved from, or returned to, the aviary, and therefore needlessly terminated.

6.3.2 Housing regulations

The current laboratory bird housing space regulations only apply to a small number of named bird species, with little guidance for birds outside of these few. The regulations for the species that are included are taken directly from Hawkins et al. (2001), which recommends housing space requirements for many other bird species beyond those cited in the regulations. For example, there are regulations related to the space requirements for lovebirds (Hawkins et al., 2001), but instead of recommending these guidelines for the work presented in this thesis, regulations for zebra finches were invoked, despite the fact that they are almost 5 times smaller than lovebirds, belong to a different taxonomic order, require different aviary-mesh properties and are endemic to a different continent (Home Office, 2014). It seems highly counter-intuitive for a governing body to recommend the advice of experts and then disregard the advice provided.

Additionally, many of the legal regulations are adapted from tables within this handbook quoting appropriate housing space requirements without acknowledging the accompanying text which explains the context for these values. For example, the original guidelines specifies that the housing guidelines are appropriate only for birds that don't get flight-time outside of the

aviary (Hawkins et al., 2001), but these stipulations don't apply to the legal regulations and flight-time outside of the aviary is not taken into consideration (Office, 2014).

Finally, while there are strict rules for the dimensions required to house a number of bird species, there are only vague guidelines for aviary mesh spacing. This is arguably a bigger welfare concern than space sizing, as although space sizing is important for maintaining the psychological and physical health of the birds, picking appropriate mesh sizes for individual species is essential in order to ensure hazard-free captivity that could otherwise lead to serious bird injury or death. Additionally, while the large flight-style aviaries currently required offer a generous amount of space for the birds to fly, no guidance is provided regarding the safe catching of birds in these environments beyond using nets with padded rims (Home Office, 2014). Catching birds with a net can take repeated attempts with risk of injury to the birds, especially with small, fast-accelerating species. These catching sessions may possibly contribute to increased physiological stress that may confound the very behavioural or physiological investigations for which the birds are being caught (Hawkins et al., 2001). In the event that aviary size requirements cannot be changed, alternative solutions to this issue may involve the use of larger nets or dimmed lighting when catching the birds, although these come with their own risks to bird safety.

6.4 Future directions of work

All experimental Chapters may benefit from the collection of additional data, but this is most importantly the case for Chapter 3, in which a comparison of methodologies through a replication of the experiments may help to validate the values determined, or provide evidence supporting alternative measures of efficiency. The efficiency of the avian flight muscle is an important piece of missing knowledge with the potential to greatly improve future predictive models of flight energetics, so measurement using a secondary method such as the optical electrode suggested in Chapter 3 should help to develop our

understanding of avian flight muscle efficiency and how it changes with flight speed. If there are differences in the efficiency values estimated by each of these methods, it would be valuable to find out why this is the case, and determine which method is most suitable for future work.

In Chapter 4, only one masked lovebird was able to fly for the required amount of time with both respirometry and accelerometry equipment attached. Given more training time, or a larger bird species, it would be very beneficial to collect more combined respirometry and accelerometry data in order to confidently estimate the contributing additional metabolic costs of these data collection methods from simultaneously instrumented birds.

As touched upon in Chapter 5, a deeper analysis of the comparative cross-bridge mechanics during the shortening and lengthening periods of oscillatory contractions in *Lethocerus* IFM is required to determine why the optimal frequency for net mechanical power generation and muscle efficiency increases with increasing $[Ca^{2+}]$. Chapter 5 currently provides a novel investigation into the relationships between mechanical power, energy consumption and efficiency and presents , but further investigation into the ratio of positive and negative work generation during muscle shortening and lengthening will help to explain why we observe these relationships and their significance at the cross-bridge level. These data are available but a substantial amount of additional time is required to fully extract this information. It is hoped that this will be achieved in the near future.

Appendices

Appendix 1: **Summary of studies testing the energy-saving hypothesis for formation flight.** Also included is their support for the energy-saving hypothesis. (Aero calc.) refers to aerodynamic calculations. * indicates values estimated from figures.

Study	Species	Number of birds	Estimation method	Average induced power savings	Maximum induced power savings	Average total power savings	Supports energy saving hypothesis
Lissaman (1970)	Branta canadensis	Infinite	Aero calc.	-	71%	-	Yes
May (1979)	B. canadensis	Infinite	Aero calc.	-	10%	-	No
Badgerow (1981)	B. canadensis	Nine	Aero calc.	-	51%	-	Yes
Hainsworth (1987)	B. canadensis	Fifty-five	Aero calc.	10%	36%	-	Yes
Cutts and Speakman (1994)	Anser brachyrhynchus	Nine	Aero calc.	14%	51%	2.4-5.5%	No
Speakman and Banks (1998)	Anser anser	Fifteen	Aero calc.	26.5%	-	4.5-8.9%	Yes
Weimerskirch (2001)	Pelecanus onocrotalus	Eight	Heart-rate	≈ 30% *	≈ 72% *	11.4-14%	Yes
Portugal (2014)	Geronticus eremita	Fourteen	Positional data loggers	-	-	-	Yes

Appendix 2: **Optimum frequencies for peak mean mechanical power, work and efficiency of *Lethocerus* DLM within each activating solution.**

Parameter	$A_{10\%}$	$A_{20\%}$	$A_{40\%}$	$A_{60\%}$	$A_{70\%}$
P_{mech}	4 Hz	8 Hz	12 Hz	16 Hz	12 Hz
W_{net}	8 Hz	8 Hz	8 Hz	12 Hz	12 Hz
η_{gross}	4 Hz	12 Hz	12 Hz	12 Hz	12 Hz
$\eta_{apparent}$	4 Hz	8 Hz	12 Hz	12 Hz	16 Hz

Appendix 3: **Optimum contraction parameters for the mechanical power, work and efficiency of *Lethocerus* DLM.**

Parameter	Opt. solution	Opt. frequency	Mean value
P_{mech}	A40	12	22.125 nW cm^{-1}
W_{net}	A20	8	1.335 nJ cm^{-1}
η_{gross}	A40	12	8.06%
$\eta_{apparent}$	A40	12	35.44%

References

Abbott, B. C. & Aubert, X. M. 1952. The force exerted by active striated muscle during and after change of length. *The Journal of physiology,* 117**,** 77-86.

Adams, G. R., Duvoisin, M. R. & Dudley, G. A. 1992. Magnetic resonance imaging and electromyography as indexes of muscle function. *Journal of Applied Physiology,* 73**,** 1578-1583.

Agianian, B., Kržič, U., Qiu, F., Linke, W. A., Leonard, K. & Bullard, B. 2004. A troponin switch that regulates muscle contraction by stretch instead of calcium. *The European Molecular Biology Organization Journal,* 23**,** 772-779.

Akos, Z., Nagy, M., Leven, S. & Vicsek, T. 2010. Thermal soaring flight of birds and unmanned aerial vehicles. *Bioinspiration & Biomimetics,* 5**,** Article No. 045003.

Alerstam, T. 1991. Bird flight and optimal migration. *Trends in Ecology & Evolution,* 6**,** 210-215.

Alexander, D. E. 2002. *Nature's flyers: Birds, insects, and the biomechanics of flight,* The John Hopkins University Press, Baltimore.

Alexander, R. M. 1991. Energy-saving mechanisms in walking and running. *Journal of Experimental Biology,* 160**,** 55-69.

Alexander, R. M. 1999. Bioenergetics: One price to run, swim or fly? *Nature,* 397**,** 651-653.

Alexander, R. M. 2005. Models and the scaling of energy costs for locomotion. *Journal of Experimental Biology,* 208**,** 1645-1652.

Altshuler, D. L., Welch, K. C., Cho, B. H., Welch, D. B., Lin, A. F., Dickson, W. B. & Dickinson, M. H. 2010. Neuromuscular control of wingbeat kinematics in Anna's hummingbirds (*Calypte anna*). *Journal of Experimental Biology,* 213**,** 2507-2514.

Andersson, M. & Wallander, J. 2004. Kin selection and reciprocity in flight formation? *Behavioral Ecology,* 15**,** 158-162.

Angel, L., Jeanniard-Du-Dot, T., Speakman, J. & Arnould, J. 2015. Determining activity-specific energy expenditure in a large seabird using accelerometry. *Factors influencing foraging behaviour in the Australasian gannet***,** 46.

Arai, N., Kuroki, M., Sakamoto, W. & Naito, Y. 2000. Analysis of diving behavior of Adélie penguins using acceleration data logger. 13, 95-100.

Askew, G. N. & Ellerby, D. J. 2007. The mechanical power requirements of avian flight. *Biology Letters,* 3**,** 445-448.

Askew, G. N. & Marsh, R. L. 1997. The effects of length trajectory on the mechanical power output of mouse skeletal muscles. *Journal of Experimental Biology,* 200**,** 3119-3131.

Askew, G. N. & Marsh, R. L. 2001. The mechanical power output of the pectoralis muscle of blue-breasted quail (*Coturnix chinensis*): The in vivo length cycle and its implications for muscle performance. *Journal of Experimental Biology,* 204**,** 3587-3600.

Askew, G. N., Tregear, R. T. & Ellington, C. P. 2010. The scaling of myofibrillar actomyosin ATPase activity in apid bee flight muscle in relation to hovering flight energetics. *The Journal of Experimental Biology,* 213**,** 1195-1206.

Askew, G. N., Young, I. S. & Altringham, J. D. 1997. Fatigue of mouse soleus muscle, using the work loop technique. *The Journal of Experimental Biology,* 200**,** 2907-2912.

Bäckman, J., Andersson, A., Pedersen, L., Sjöberg, S., Tøttrup, A. P. & Alerstam, T. 2017. Actogram analysis of free-flying migratory birds: New perspectives based on acceleration logging. *Journal of Comparative Physiology A,* 203**,** 543-564.

Badgerow, J. P. 1988. An analysis of function in the formation flight of Canada geese. *The Auk,* 105**,** 749-755.

Bajec, I. L. & Heppner, F. H. 2009. Organized flight in birds. *Animal Behaviour,* 78**,** 777-789.

Barclay, C. 2015. Energetics of contraction. *Comprehensive Physiology*.

Barclay, C. J. 1994. Efficiency of fast- and slow-twitch muscles of the mouse performing cyclic contractions. *The Journal of Experimental Biology,* 193**,** 65-78.

Barclay, C. J. 1996. Mechanical efficiency and fatigue of fast and slow muscles of the mouse. *The Journal of physiology,* 497**,** 781-794.

Barclay, C. J. 1998. Estimation of cross-bridge stiffness from maximum thermodynamic efficiency. *Journal of Muscle Research & Cell Motility,* 19**,** 855-864.

Barclay, C. J. 2005. Modelling diffusive O_2 supply to isolated preparations of mammalian skeletal and cardiac muscle. *Journal of Muscle Research & Cell Motility,* 26**,** 225-235.

Barclay, C. J. 2017. Energy demand and supply in human skeletal muscle. *Journal of Muscle Research and Cell Motility,* 38**,** 143-155.

Barclay, C. J. & Weber, C. L. 2004. Slow skeletal muscles of the mouse have greater initial efficiency than fast muscles but the same net efficiency. *The Journal of Physiology,* 559**,** 519-533.

Barclay, C. J., Woledge, R. C. & Curtin, N. A. 2010. Is the efficiency of mammalian (mouse) skeletal muscle temperature dependent? *The Journal of Physiology,* 588**,** 3819-3831.

Barron, D., G., Brawn, J., D. & Weatherhead, P., J. 2010. Meta-analysis of transmitter effects on avian behaviour and ecology. *Methods in Ecology and Evolution,* 1**,** 180-187.

Beaufrere, H. 2009. A review of biomechanic and aerodynamic considerations of the avian thoracic limb. *Journal of Avian Medicine and Surgery,* 23**,** 173-185.

Bejan, A. & Marden, J. H. 2006. Unifying constructal theory for scale effects in running, swimming and flying. *Journal of Experimental Biology,* 209**,** 238-248.

Bennet-Clark, H. C. 1975. The energetics of the jump of the locust *Schistocerca gregaria. The Journal of Experimental Biology,* 63**,** 53.

Berger, M. 1972. Formationsflug ohne phasenbeziehung der flugelschlage. *Journal of Ornithology,* 113**,** 161-169.

Bernstein, M. H., Thomas, S. P. & Schmidt-Nielsen, K. 1973. Power input during flight of the fish crow, *Corvus ossifragus. Journal of Experimental Biology,* 58**,** 401-410.

Bevan, R., Woakes, A., Butler, P. & Boyd, I. 1994. The use of heart rate to estimate oxygen consumption of free-ranging black-browed albatrosses *Diomedea melanophrys. Journal of Experimental Biology,* 193**,** 119-137.

Bidder, O. R., Campbell, H. A., Gomez-Laich, A., Urge, P., Walker, J. & Cai, Y. 2014. Love thy neighbour: Automatic animal behavioural classification of acceleration data using the k-nearest neighbour algorithm. *PLOS ONE,* 9, Article No. e88609

Biewener, A. A. 1998. Muscle function in vivo: A comparison of muscles used for elastic energy savings versus muscles used to generate mechanical power. *American Zoologist,* 38**,** 703-717.

Biewener, A. A. 2011. Muscle function in avian flight: Achieving power and control. *Philosophical Transactions of the Royal Society B: Biological Sciences,* 366**,** 1496-1506.

Biewener, A. A., Corning, W. R. & Tobalske, B. W. 1998. In vivo pectoralis muscle force-length behavior during level flight in pigeons (*Columba livia*). *Journal of Experimental Biology,* 201**,** 3293-3307.

Biewener, A. A., Dial, K. P. & Goslow, G. E. 1992. Pectoralis muscle force and power output during flight in the starling. *Journal of Experimental Biology,* 164**,** 1-18.

Bill, R. G. & Herrnkind, W. F. 1976. Drag reduction by formation movement in spiny lobsters. *Science,* 193**,** 1146-1148.

Bishop, C. M. 2005. Circulatory variables and the flight performance of birds. *Journal of Experimental Biology,* 208**,** 1695-1708.

Bishop, C. M., Ward, S., Woakes, A. J. & Butler, P. J. 2002. The energetics of barnacle geese (*Branta leucopsis*) flying in captive and wild conditions. *Comparative Biochemistry and Physiology Part A: Molecular & Integrative Physiology,* 133**,** 225-237.

Boggs, D. F. & Dial, K. P. 1993. Neuromuscular organization and regional emg activity of the pectoralis in the pigeon. *Journal of Morphology,* 218**,** 43-57.

Boussouf, S. E., Agianian, B., Bullard, B. & Geeves, M. A. 2007. The regulation of myosin binding to actin filaments by *Lethocerus* troponin. *Journal of Molecular Biology,* 373**,** 587-598.

Brooks, G. A. & Donovan, C. M. 1983. Effect of endurance training on glucose kinetics during exercise. *American Journal of Physiology-Endocrinology And Metabolism,* 244**,** 505-512.

Brooks, G. A. & Gaesser, G. A. 1980. End points of lactate and glucose metabolism after exhausting exercise. *Journal of Applied Physiology,* 49**,** 1057-1069.

Brouwer, E. 1965. Report on sub-committee on constants and factors. In: Blaxter, K. L., (Ed.) Proceedings of the 3rd Symposium on Energy Metabolism, Academic Press, London, 441-443

Brown, D. D., Kays, R., Wikelski, M., Wilson, R. & Klimley, A. P. 2013. Observing the unwatchable through acceleration logging of animal behavior. *Animal Biotelemetry,* 1**,** 1-16.

Bucher, T. L. & Morgan, K. R. 1989. The effect of ambient temperature on the relationship between ventilation and metabolism in a small parrot (*Agapornis roseicollis*). *Journal of Comparative Physiology B,* 159**,** 567.

Bundle, M. W., Hansen, K. S. & Dial, K. P. 2007. Does the metabolic rate–flight speed relationship vary among geometrically similar birds of different mass? *Journal of Experimental Biology,* 210**,** 1075-1083.

Burton, R. F. 1975. *Ringer solutions and physiological salines*, Wright's Scientechnica, Bristol.

Bushuev, A., Tolstenkov, O., Zubkova, E., Solovyeva, E. & Kerimov, A. 2017. Basal metabolic rate in free-living tropical birds: The influence of phylogenetic, behavioral, and ecological factors. *Current Zoology*, 64, 1, 33-43.

Butler, P. J., Green, J. A., Boyd, I. L. & Speakman, J. R. 2004. Measuring metabolic rate in the field: The pros and cons of the doubly labelled water and heart rate methods. *Functional Ecology,* 18**,** 168-183.

Butler, P. J. & Turner, D. L. 1988. Effect of training on maximal oxygen uptake and aerobic capacity of locomotory muscles in tufted ducks, *Aythya fuligula*. *The Journal of Physiology,* 401**,** 347-359.

Butler, P. J., Turner, D. L., Al-Wassia, A. & Bevan, R. M. 1988. Regional distribution of blood flow during swimming in the tufted duck (*Aythya fuligula*). *Journal of Experimental Biology,* 135**,** 461-472.

Butler, P. J., West, N. H. & Jones, D. R. 1977. Respiratory and cardiovascular responses of the pigeon to sustained, level flight in a wind-tunnel. *The Journal of Experimental Biology,* 71**,** 7-26.

Butler, P. J., Woakes, A. J., Bevan, R. M. & Stephenson, R. 2000. Heart rate and rate of oxygen consumption during flight of the barnacle goose, *Branta leucopsis*. *Comparative Biochemistry and Physiology Part A: Molecular & Integrative Physiology,* 126**,** 379-385.

Cameron, J. 1986. *Principles of physiological measurement*. Academic Press Inc., London.

Cannon, D. T., Bimson, W. E., Hampson, S. A., Bowen, T. S., Murgatroyd, S. R., Marwood, S., Kemp, G. J. & Rossiter, H. B. 2014. Skeletal muscle atp turnover by 31P magnetic resonance spectroscopy during moderate and heavy bilateral knee extension. *The Journal of Physiology,* 592**,** 5287-5300.

Cao, J., Currie, K., Carry, P., Maddox, G., Nino, S. & Ipaktchi, K. 2017. Smartphone-based thermal imaging: A new modality for tissue temperature measurement in hand and upper extremity surgeries. *HAND,* 13**,** 350-354.

Casey, T. M. & Ellington, C. P. 1989. Energetics of insect flight. *Energy transformations in cells and organisms.* In: Weiser, W. & Gnaiger, E., Proceedings of the 10th Conference of the European Society for Comparative Physiology and Biochemistry, Thieme, Madison. 200-210.

Chai, P. 1997. Hummingbird hovering energetics during moult of primary flight feathers. *Journal of Experimental Biology,* 200**,** 1527-1536.

Chimienti, M., Cornulier, T., Owen, E., Bolton, M., Davies, I. M., Travis, J. M. & Scott, B. E. 2016. The use of an unsupervised learning approach for characterizing latent behaviors in accelerometer data. *Ecology and Evolution,* 6**,** 727-741.

Cianchetti-Benedetti, M., Catoni, C., Kato, A., Massa, B. & Quillfeldt, P. 2017. A new algorithm for the identification of dives reveals the foraging ecology of a shallow-diving seabird using accelerometer data. *Marine Biology,* 164**,** 77.

Crow, M. T. & Kushmerick, M. J. 1982. Chemical energetics of slow- and fast-twitch muscles of the mouse. *The Journal of General Physiology,* 79**,** 147-166.

Curtin, N. & Woledge, R. 1996. Power at the expense of efficiency in contraction of white muscle fibres from dogfish *Scyliorhinus canicula*. *The Journal of Experimental Biology,* 199**,** 593-601.

Curtin, N. A. & Woledge, R. C. 1993. Efficiency of energy-conversion during sinusoidal movement of white muscle-fibers from the dogfish *Scyliorhinus-canicula*. *Journal of Experimental Biology,* 183**,** 137-147.

Cutts, C. & Speakman, J. 1994. Energy savings in formation flight of pink-footed geese. *Journal of Experimental Biology,* 189**,** 251-261.

Davies, R. B. 2002. Hypothesis testing when a nuisance parameter is present only under the alternative: Linear model case. *Biometrika***,** 89, 484-489.

Dial, K. P. 1992. Activity patterns of the wing muscles of the pigeon (*Columba livia*) during different modes of flight. *Journal of Experimental Zoology,* 262**,** 357-373.

Dial, K. P. & Biewener, A. A. 1993. Pectoralis muscle force and power output during different modes of flight in pigeons (*Columba livia*). *Journal of Experimental Biology,* 176**,** 31-54.

Dial, K. P., Biewener, A. A., Tobalske, B. W. & Warrick, D. R. 1997. Mechanical power output of bird flight. *Nature,* 390**,** 67-70.

Dickinson, M. & Lighton 1995. Muscle efficiency and elastic storage in the flight motor of drosophila. *Science,* 268**,** 87-90.

Dimock, G. & Selig, M. 2003. The aerodynamic benefits of self-organization in bird flocks. *41st aerospace sciences meeting and exhibit.* American Institute of Aeronautics and Astronautics.

Dow, C., Michel, K. E., Love, M. & Brown, D. C. 2009. Evaluation of optimal sampling interval for activity monitoring in companion dogs. *American Journal of Veterinary Research,* 70**,** 444-448.

Ellerby, D. J. & Askew, G. N. 2007a. Modulation of flight muscle power output in budgerigars *Melopsittacus undulatus* and zebra finches *Taeniopygia guttata*: In vitro muscle performance. *Journal of Experimental Biology,* 210, 3780-3788.

Ellerby, D. J. & Askew, G. N. 2007b. Modulation of pectoralis muscle function in budgerigars *Melopsittacus undulatus* and zebra finches *Taeniopygia guttata* in response to changing flight speed. *Journal of Experimental Biology,* 210**,** 3789-3797.

Ellerby, D. J., Henry, H. T., Carr, J. A., Buchanan, C. I. & Marsh, R. L. 2005. Blood flow in guinea fowl *Numida meleagris* as an indicator of energy expenditure by individual muscles during walking and running. *The Journal of Physiology,* 564**,** 631-648.

Ellington, C. P. 1984. The aerodynamics of hovering insect flight. Vi. Lift and power requirements. *Philosophical Transactions of the Royal Society of London. B, Biological Sciences,* 305**,** 145-181.

Ellington, C. P. 1985. Power and efficiency of insect flight muscle. *Journal of Experimental Biology,* 115**,** 293-304.

Ellington, C. P. 1991. Limitations on animal flight performance. *Journal of Experimental Biology,* 160**,** 71-91.

Elliott, K. H. 2016. Measurement of flying and diving metabolic rate in wild animals: Review and recommendations. *Comparative Biochemistry and Physiology Part A: Molecular & Integrative Physiology,* 202**,** 63-77.

Elliott, K. H., Le Vaillant, M., Kato, A., Gaston, A. J., Ropert-Coudert, Y., Hare, J. F., Speakman, J. R. & Croll, D. 2014. Age-related variation in energy expenditure in a long-lived bird within the envelope of an energy ceiling. *Journal of Animal Ecology,* 83**,** 136-146.

Elliott, K. H., Le Vaillant, M., Kato, A., Speakman, J. R. & Ropert-Coudert, Y. 2013a. Accelerometry predicts daily energy expenditure in a bird with high activity levels. *Biology Letters,* 9, Article No. 20120919

Elliott, K. H., Ricklefs, R. E., Gaston, A. J., Hatch, S. A., Speakman, J. R. & Davoren, G. K. 2013b. High flight costs, but low dive costs, in auks support the biomechanical hypothesis for flightlessness in penguins. *Proceedings of the National Academy of Sciences,* 110**,** 9380-9384.

Enoka, R. M. 1995. Morphological features and activation patterns of motor units. *Journal of clinical neurophysiology: official publication of the American Electroencephalographic Society,* 12**,** 538-559.

Fenwick, A. J., Wood, A. M. & Tanner, B. C. W. 2017. Effects of cross-bridge compliance on the force-velocity relationship and muscle power output. *PLOS ONE,* 12**,** Article No. e0190335.

Fort, J., Porter, W. P. & Grémillet, D. 2011. Energetic modelling: A comparison of the different approaches used in seabirds. *Comparative Biochemistry and Physiology Part A: Molecular & Integrative Physiology,* 158**,** 358-365.

Gavrilov, V. M. 2011. Energy expenditures for flight, aerodynamic quality, and colonization of forest habitats by birds. *Biology Bulletin,* 38**,** 779-788.

Gessaman, J. A. & Nagy, K. A. 1988. Transmitter loads affect the flight speed and metabolism of homing pigeons. *The Condor,* 90**,** 662-668.

Gibbs, C. L. & Barclay, C. J. 1995. Cardiac efficiency. *Cardiovascular Research,* 30**,** 627-634.

Gibbs, C. L. & Chapman, J. B. 1974. Effects of stimulus conditions, temperature, and length on energy output of frog and toad sartorius. *American Journal of Physiology,* 227**,** 964-971.

Gilmour, K. M. & Ellington, C. P. 1993. Power output of glycerinated bumblebee flight muscle. *The Journal of Experimental Biology,* 183**,** 77-100.

Girgenrath, M. & Marsh, R. L. 1999. Power output of sound-producing muscles in the tree frogs *Hyla versicolor* and *Hyla chrysoscelis*. *Journal of Experimental Biology,* 202**,** 3225-3237.

Glasheen, B. M., Eldred, C. C., Sullivan, L. C., Zhao, C., Reedy, M. K., Edwards, R. J. & Swank, D. M. 2017. Stretch activation properties of *Drosophila* and *Lethocerus* indirect flight muscle suggest similar calcium-dependent mechanisms. *American Journal of Physiology - Cell Physiology,* 313**,** C621-c631.

Gleiss, A. C., Wilson, R. P. & Shepard, E. L. C. 2011. Making overall dynamic body acceleration work: On the theory of acceleration as a proxy for energy expenditure. *Methods in Ecology and Evolution,* 2**,** 23-33.

Gordon, A. M., Huxley, A. F. & Julian, F. J. 1966. The variation in isometric tension with sarcomere length in vertebrate muscle fibres. *The Journal of Physiology,* 184**,** 170-192.

Gordon, S. & Dickinson, M. H. 2006. Role of calcium in the regulation of mechanical power in insect flight. *Proceedings of the National Academy of Sciences of the United States of America,* 103**,** 4311-4315.

Green, J. A. 2011. The heart rate method for estimating metabolic rate: Review and recommendations. *Comparative Biochemistry and Physiology Part A: Molecular & Integrative Physiology,* 158**,** 287-304.

Green, J. A., Halsey, L. G., Wilson, R. P. & Frappell, P. B. 2009. Estimating energy expenditure of animals using the accelerometry technique: Activity, inactivity and comparison with the heart-rate technique. *Journal of Experimental Biology,* 212**,** 471-482.

Greenewalt, C. H. 1975. The flight of birds: The significant dimensions, their departure from the requirements for dimensional similarity, and the effect on flight aerodynamics of that departure. *Transactions of the American Philosophical Society,* 65**,** 1-67.

Griffiths, R. 1987. Ultrasound transit time gives direct measurement of muscle fibre length in vivo. *Journal of Neuroscience Methods,* 21**,** 159-165.

Groscolas, R., Viera, V., Guerin, N., Handrich, Y. & Côté, S. D. 2010. Heart rate as a predictor of energy expenditure in undisturbed fasting and

incubating penguins. *The Journal of Experimental Biology,* 213**,** 153-160.

Guhad, F. 2005. Introduction to the 3Rs (refinement, reduction and replacement). *Journal of the American Association for Laboratory Animal Science,* 44**,** 58-59.

Habicht, G. S. 1981. Body temperature in normal and endotoxin-treated mice of different ages. *Mechanisms of Ageing and Development,* 16**,** 97-104.

Hainsworth, F. R. 1987. Precision and dynamics of positioning by Canada geese flying in formation. *Journal of Experimental Biology,* 128**,** 445-462.

Hainsworth, F. R. 1988. Induced drag savings from ground effect and formation flight in brown pelicans. *Journal of Experimental Biology,* 135**,** 431-444.

Halsey, L., Green, J., Wilson, R. & Frappell, P. 2008a. Accelerometry to estimate energy expenditure during activity: Best practice with data loggers. *Physiological And Biochemical Zoology,* 82**,** 396-404.

Halsey, L. G., Shepard, E. L. C., Hulston, C. J., Venables, M. C., White, C. R., Jeukendrup, A. E. & Wilson, R. P. 2008b. Acceleration versus heart rate for estimating energy expenditure and speed during locomotion in animals: Tests with an easy model species, homo sapiens. *Zoology,* 111**,** 231-241.

Halsey, L. G., Shepard, E. L. C., Quintana, F., Gomez Laich, A., Green, J. A. & Wilson, R. P. 2009. The relationship between oxygen consumption and body acceleration in a range of species. *Comparative Biochemistry and Physiology Part A: Molecular & Integrative Physiology,* 152**,** 197-202.

Halsey, L. G., White, C. R., Enstipp, M. R., Wilson, R. P., Butler, P. J., Martin, G. R., Gremillet, D. & Jones, D. R. 2011. Assessing the validity of the accelerometry technique for estimating the energy expenditure of diving double-crested cormorants phalacrocorax auritus. *Physiological and Biochemical Zoology,* 84**,** 230-237.

Hambly, C. & Voigt, C. C. 2011. Measuring energy expenditure in birds using bolus injections of 13C-labelled Na-bicarbonate. *Comparative Biochemistry and Physiology Part A: Molecular & Integrative Physiology,* 158**,** 323-328.

Harwood, C. L., Young, I. S. & Altringham, J. D. 2002. How the efficiency of rainbow trout (*Oncorhynchus mykiss*) ventricular muscle changes with cycle frequency. *Journal of Experimental Biology,* 205**,** 697-706.

Hawkins, P., Morton, D., Cameron, D., Cuthill, I., Francis, R., Freire, R., Gosler, A., Healy, S., Hudson, A. & Inglis, I. 2001. Laboratory birds:

Refinements in husbandry and procedures. *Laboratory Animals,* 35**,** 1-163.

Hedenström, A. & Alerstam, T. 1995. Optimal flight speed of birds. *Philosophical Transactions of the Royal Society of London. Series B: Biological Sciences,* 348**,** 471-487.

Hedenström, A., Norevik, G., Warfvinge, K., Andersson, A., Bäckman, J. & Åkesson, S. 2016. Annual 10-month aerial life phase in the common swift *Apus apus*. *Current Biology,* 26**,** 3066-3070.

Hedenström, A., Rosén, M. & Spedding, G. R. 2006. Vortex wakes generated by robins *Erithacus rubecula* during free flight in a wind tunnel. *Journal of The Royal Society Interface,* 3**,** 263-276.

Hedrick, T. L., Tobalske, B. W. & Blewener, A. A. 2003. How cockatiels (*Nymphicus hollandicus*) modulate pectoralis power output across flight speeds. *Journal of Experimental Biology,* 206**,** 1363-1378.

Heglund, N. C. & Cavagna, G. A. 1985. Efficiency of vertebrate locomotory muscles. *Journal of Experimental Biology,* 115**,** 283-292.

Heglund, N. C. & Cavagna, G. A. 1987. Mechanical work, oxygen consumption, and efficiency in isolated frog and rat muscle. *American Journal of Physiology - Cell Physiology,* 253**,** C22-C29.

Heglund, N. C., Fedak, M. A., Taylor, C. R. & Cavagna, G. A. 1982. Energetics and mechanics of terrestrial locomotion. IV. Total mechanical energy changes as a function of speed and body size in birds and mammals. *Journal of Experimental Biology,* 97**,** 57-66.

Herskin, J. & Steffensen, J. F. 1998. Energy savings in sea bass swimming in a school: Measurements of tail beat frequency and oxygen consumption at different swimming speeds. *Journal of Fish Biology,* 53**,** 366-376.

Hicks, O., Burthe, S., Daunt, F., Butler, A., Bishop, C. & Green, J. A. 2017. Validating accelerometry estimates of energy expenditure across behaviours using heart rate data in a free-living seabird. *Journal of Experimental Biology,* 220**,** 1875-1881.

Hill, A. V. 1938. The heat of shortening and the dynamic constants of muscle. *Proceedings of the Royal Society of London. Series B - Biological Sciences,* 126**,** 136-195.

Hill, D. L., Lindström, J., Mccafferty, D. J. & Nager, R. G. 2014. Female but not male zebra finches adjust heat output in response to increased incubation demand. *The Journal of Experimental Biology,* 217**,** 1326-1332.

Hill, R. R., Wyse, G. A. & Anderson, M. 2012. *Animal Physiology*. Sinauer Associates, Inc.

Holt, N. C. & Askew, G. N. 2012. The effects of asymmetric length trajectories on the initial mechanical efficiency of mouse soleus muscles. *Journal of Experimental Biology,* 215**,** 324-330.

Holt, N. C., Roberts, T. J. & Askew, G. N. 2014. The energetic benefits of tendon springs in running: Is the reduction of muscle work important? *The Journal of Experimental Biology,* 217**,** 4365-4371.

Home Office 2014. Code of practice for the housing and care of animals bred, supplied or used for scientific purposes. Williams Lea Group London.

Hummel, D. 1973. The power reduction in flight formations. *Journal fuer Ornithologie,* 114**,** 259-282.

Hummel, D. 1983. Aerodynamic aspects of formation flight in birds. *Journal of Theoretical Biology,* 104**,** 321-347.

Huxley, H. E. 1969. The mechanism of muscular contraction. *Science,* 164**,** 1356-1366.

Hyatt, C. J. & Maughan, D. W. 1994. Fourier analysis of wing beat signals: Assessing the effects of genetic alterations of flight muscle structure in Diptera. *Biophysical Journal,* 67**,** 1149-1154.

Iwamoto, H. 2009. Evidence for unique structural change of thin filaments upon calcium activation of insect flight muscle. *Journal of Molecular Biology,* 390**,** 99-111.

James, R. S., Altringham, J. D. & Goldspink, D. F. 1995. The mechanical properties of fast and slow skeletal muscles of the mouse in relation to their locomotory function. *The Journal of Experimental Biology,* 198**,** 491-502.

James, R. S., Young, I. S., Cox, V. M., Goldspink, D. F. & Altringham, J. D. 1996. Isometric and isotonic muscle properties as determinants of work loop power output. *Pflügers Archiv,* 432**,** 767-774.

Jeanniard-Du-Dot, T., Guinet, C., Arnould, J. P. Y., Speakman, J. R. & Trites, A. W. 2016. Accelerometers can measure total and activity-specific energy expenditures in free-ranging marine mammals only if linked to time-activity budgets. *Functional Ecology***,** 31, 377-386

Jenni, L. & Jenni-Eiermann, S. 1998. Fuel supply and metabolic constraints in migrating birds. *Journal of Avian Biology,* 29**,** 521-528.

Jewell, B. R. & Rüegg, J. C. 1966. Oscillatory contraction of insect fibrillar muscle after glycerol extraction. *Proc. R. Soc. Lond. B,* 164**,** 428-459.

Josephson, R. K. 1985. Mechanical power output from striated muscle during cyclic contraction. *Journal of Experimental Biology,* 114**,** 493-512.

Josephson, R. K., Malamud, J. G. & Stokes, D. R. 2000a. Asynchronous muscle: A primer. *Journal of Experimental Biology,* 203**,** 2713-2722.

Josephson, R. K., Malamud, J. G. & Stokes, D. R. 2000b. Power output by an asynchronous flight muscle from a beetle. *Journal of Experimental Biology,* 203**,** 2667-2689.

Josephson, R. K. & Stevenson, R. D. 1991. The efficiency of a flight muscle from the locust *Schistocerca americana. The Journal of physiology,* 442**,** 413-429.

Kemp, G. J., Meyerspeer, M. & Moser, E. 2007. Absolute quantification of phosphorus metabolite concentrations in human muscle in vivo by 31p mrs: A quantitative review. *NMR in Biomedicine,* 20**,** 555-565.

Kleiber, M. 1961. The fire of life. An introduction to animal energetics. Wiley.

Kokshaysky, N. V. 1979. Tracing the wake of a flying bird. *Nature,* 279**,** 146-148.

Kosan, R. L. & Burton, A. C. 1966. Oxygen consumption of arterial smooth muscle as a function of active tone and passive stretch. *Circulation Research,* 18**,** 79-88.

Kress, D., Van Bokhorst, E. & Lentink, D. 2015. How lovebirds maneuver rapidly using super-fast head saccades and image feature stabilization. *PLOS ONE,* 10**,** Aticle No. e0129287.

Kržič, U., Rybin, V., Leonard, K. R., Linke, W. A. & Bullard, B. 2010. Regulation of oscillatory contraction in insect flight muscle by troponin. *Journal of Molecular Biology,* 397**,** 110-118.

Kshatriya, M. 1990. *Optimum bird flock size in formation flight.* MSc thesis, The University of British Columbia.

Kuhn, H. J., Bletz, C., Güth, K. & Rüegg, J. C. 1985. The effect of mgatp on forming and breaking actin-myosin linkages in contracted skinned insect flight muscle fibres. *Journal of Muscle Research & Cell Motility,* 6**,** 5-27.

Kushmerick, M. J. & Davies, R. E. 1969. *The chemical energetics of muscle contraction. II. The chemistry, efficiency and power of maximally working sartorius muscles. Proceedings of the Royal Society B,* 174, 315-347.

Kushmerick, M. J. & Paul, R. J. 1976. Aerobic recovery metabolism following a single isometric tetanus in frog sartorius muscle at 0 degrees C. *The Journal of Physiology,* 254**,** 693-709.

Lasiewski, R. C. & Dawson, W. R. 1967. A re-examination of the relation between standard metabolic rate and body weight in birds. *The Condor,* 69**,** 13-23.

Lefebvre, E. A. 1964. The use of D_2O^{18} for measuring energy metabolism in columba livia at rest and in flight. *The Auk,* 81**,** 403-416.

Lehmann, F.-O., Skandalis, D. A. & Berthé, R. 2013. Calcium signalling indicates bilateral power balancing in the *Drosophila* flight muscle

during manoeuvring flight. *Journal of The Royal Society Interface,* 10, Article No. 20121050

Leos-Barajas, V., Photopoulou, T., Langrock, R., Patterson, T. A., Watanabe, Y. Y., Murgatroyd, M. & Papastamatiou, Y. P. 2017. Analysis of animal accelerometer data using hidden markov models. *Methods in Ecology and Evolution,* 8**,** 161-173.

Lighton, J. R. B. 2008. *Measuring metabolic rates: A manual for scientists*, Oxford University Press.

Lighton, J. R. B. & Halsey, L. G. 2011. Flow-through respirometry applied to chamber systems: Pros and cons, hints and tips. *Comparative Biochemistry and Physiology Part A: Molecular & Integrative Physiology,* 158**,** 265-275.

Linari, M., Reedy, M. K., Reedy, M. C., Lombardi, V. & Piazzesi, G. 2004. Ca-activation and stretch-activation in insect flight muscle. *Biophysical Journal,* 87**,** 1101-1111.

Lisa Lofland, G. & Heppner, F. 1974. The vee formation of Canada geese. *The Auk,* 91**,** 494-506.

Lissaman, P. B. S. & Shollenberger, C. A. 1970. Formation flight of birds. *Science,* 168**,** 1003-1005.

Loxdale, H. D. & Tregear, R. T. 1985. Dissociation between mechanical performance and the cost of isometric tension maintenance inlethocerus flight muscle. *Journal of Muscle Research & Cell Motility,* 6**,** 163-175.

Mandigout, S., Lacroix, J., Ferry, B., Vuillerme, N., Compagnat, M. & Daviet, J.-C. 2017. Can energy expenditure be accurately assessed using accelerometry-based wearable motion detectors for physical activity monitoring in post-stroke patients in the subacute phase? *European Journal of Preventive Cardiology,* 24**,** 2009-2016.

Marsh, R. L. 1999. How muscles deal with real-world loads: The influence of length trajectory on muscle performance. *Journal of Experimental Biology,* 202**,** 3377-3385.

Mccafferty, D. J., Gilbert, C., Paterson, W., Pomeroy, P. P., Thompson, D., Currie, J. I. & Ancel, A. 2011. Estimating metabolic heat loss in birds and mammals by combining infrared thermography with biophysical modelling. *Comparative Biochemistry and Physiology Part A: Molecular & Integrative Physiology,* 158**,** 337-345.

Mendez, J. & Keys, A. 1960. Density and composition of mammalian muscle. *Metabolism-Clinical and Experimental,* 9**,** 184-188.

Metcalfe, J. D., Wright, S., Tudorache, C. & Wilson, R. P. 2016. Recent advances in telemetry for estimating the energy metabolism of wild fishes. *Journal of Fish Biology,* 88**,** 284-297.

Miwa, M., Oishi, K., Nakagawa, Y., Maeno, H., Anzai, H., Kumagai, H., Okano, K., Tobioka, H. & Hirooka, H. 2015. Application of overall dynamic body acceleration as a proxy for estimating the energy expenditure of grazing farm animals: Relationship with heart rate. *PLOS ONE,* 10**,** Article No. e0128042.

Miyawaki, A., Llopis, J., Heim, R., Mccaffery, J. M., Adams, J. A., Ikura, M. & Tsien, R. Y. 1997. Fluorescent indicators for Ca^{2+} based on green fluorescent proteins and calmodulin. *Nature,* 388**,** 882.

Molloy, J. E. 1988. Active insect fibrillar flight muscle, its mechanical performance and cross-bridge kinetics. PhD thesis, University of York.

Morris, C. R. & Askew, G. N. 2010a. Comparison between mechanical power requirements of flight estimated using an aerodynamic model and in vitro muscle performance in the cockatiel (*Nymphicus hollandicus*). *The Journal of Experimental Biology,* 213**,** 2781-2787.

Morris, C. R. & Askew, G. N. 2010b. The mechanical power output of the pectoralis muscle of cockatiel (*Nymphicus hollandicus*): The in vivo muscle length trajectory and activity patterns and their implications for power modulation. *The Journal of Experimental Biology,* 213**,** 2770-2780.

Morris, C. R., Nelson, F. E. & Askew, G. N. 2010. The metabolic power requirements of flight and estimations of flight muscle efficiency in the cockatiel (*Nymphicus hollandicus*). *The Journal of Experimental Biology,* 213**,** 2788-2796.

Muggeo, V. M. 2008. Segmented: An R package to fit regression models with broken-line relationships. *R news,* 8**,** 20-25.

Muijres, F. T., Johansson, L. C., Bowlin, M. S., Winter, Y. & Hedenstrom, A. 2012. Comparing aerodynamic efficiency in birds and bats suggests better flight performance in birds. *PLOS One,* 7, Article No. e37335.

Murchie, K. J., Cooke, S. J., Danylchuk, A. J. & Suski, C. D. 2011. Estimates of field activity and metabolic rates of bonefish (*Albula vulpes*) in coastal marine habitats using acoustic tri-axial accelerometer transmitters and intermittent-flow respirometry. *Journal of Experimental Marine Biology and Ecology,* 396**,** 147-155.

Nachtigall, W. 1970. Phasenbeziehungen der flügelschläge von gänsen während des verbandflugs in keilformation. *Journal of Comparative Physiology A,* 67**,** 414-422.

Norberg, U. 1996. Energetics of flight. *In:* Carey, C. (Ed.) *Avian energetics and nutritional ecology.* Springer US.

Norberg, U. M. L. 2002. Structure, form, and function of flight in engineering and the living world. *Journal of Morphology,* 252**,** 52-81.

O'Malley, J. & Evans, M. R. 1982. Flock formation in white pelicans. *Canadian Journal Of Zoology,* 60, 1024-1031.

Papkovsky, D. B. & Dmitriev, R. I. 2013. Biological detection by optical oxygen sensing. *Chemical Society Reviews,* 42, 8700-8732.

Pennycuick, C. J. 1968a. Power requirements for horizontal flight in the pigeon *Columba livia. Journal of Experimental Biology,* 49, 527-555.

Pennycuick, C. J. 1968b. A wind-tunnel study of gliding flight in the pigeon *Columba livia. Journal of Experimental Biology,* 49, 509-526.

Pennycuick, C. J. 1989. *Bird flight performance: A practical calculation manual,* Oxford University Press, New York.

Pennycuick, C. J. 1990. Predicting wingbeat frequency and wavelength of birds. *Journal of Experimental Biology,* 150, 171-185.

Pennycuick, C. J. 2008. *Modelling the flying bird,* Massachusetts, Academic Press, Elsevier.

Pennycuick, C. J., Fast, P. F., Ballerstädt, N. & Rattenborg, N. 2012. The effect of an external transmitter on the drag coefficient of a bird's body, and hence on migration range, and energy reserves after migration. *Journal of Ornithology,* 153, 633-644.

Phillips, R. A., Jose, C. X. & Croxall, J. P. 2003. Effects of satellite transmitters on albatrosses and petrels. *The Auk,* 120, 1082-1090.

Portugal, S. J., & Guillemette, M. 2011. The use of body mass loss to estimate metabolic rate in birds. *Comparative Biochemistry and Physiology Part A: Molecular & Integrative Physiology,* 158, 329-336.

Portugal, S. J., Hubel, T. Y., Fritz, J., Heese, S., Trobe, D., Voelkl, B., Hailes, S., Wilson, A. M. & Usherwood, J. R. 2014. Upwash exploitation and downwash avoidance by flap phasing in ibis formation flight. *Nature,* 505, 399-402.

Pringle, J. W. S. 1977. The mechanical characteristics of insect fibrillar muscle. *In: Proceedings of the Oxford Symposium: Insect Flight Muscle,* 177-196.

Proske, U. & Morgan, D. L. 1999. Do cross-bridges contribute to the tension during stretch of passive muscle? *Journal of Muscle Research & Cell Motility,* 20, 433-442.

Pybus, J. & Tregear, R. T. 1975. The relationship of adenosine triphosphatase activity to tension and power output of insect flight muscle. *The Journal of Physiology,* 247, 71-89.

Qasem, L., Cardew, A., Wilson, A., Griffiths, I., Halsey, L. G. & Shepard, E. L. 2012. Tri-axial dynamic acceleration as a proxy for animal energy expenditure; should we be summing values or calculating the vector? *PLOS ONE,* 7. Article No. e31187.

Rayner, J., M., V. 1994. Aerodynamic corrections for the flight of birds and bats in wind tunnels. *Journal of Zoology,* 234, 537-563.

Rayner, J. M. 1999. Estimating power curves of flying vertebrates. *Journal of Experimental Biology,* 202**,** 3449-3461.

Rayner, J. M. V. 1979a. A new approach to animal flight mechanics. *Journal of Experimental Biology,* 80**,** 17-54.

Rayner, J. M. V. 1979b. A vortex theory of animal flight. Part 2. The forward flight of birds. *Journal of Fluid Mechanics,* 91**,** 731-763.

Rayner, J. M. V. 1982. Avian flight energetics. *Annual Reviews of Physiology*, 44, 109-119.

Rayner, J. M. V. 1985. Bounding and undulating flight in birds. *Journal of Theoretical Biology,* 117**,** 47-77.

Reedy, M. K. & Garrett, W. E. 1977. Electron microscope studies of *Lethocerus* flight muscle in rigor. *In: Proceedings of the Oxford Symposium: Insect Flight Muscle***,** 115-136.

Reedy, M. K., Holmes, K. C. & Tregear, R. T. 1965. Induced changes in orientation of the cross-bridges of glycerinated insect flight muscle. *Nature,* 207**,** 1276.

Reger, M., Peterman, J. E., Kram, R. & Byrnes, W. C. 2012. Exercise efficiency of low power output cycling. *Scandinavian Journal of Medicine & Science in Sports,* 23**,** 713-721.

Resheff, Y. S., Rotics, S., Harel, R., Spiegel, O. & Nathan, R. 2014. Accelerater: A web application for supervised learning of behaviour modes from acceleration measurements. *Movement Ecology,* 2, 27.

Robertson, A. M. B. & Biewener, A. A. 2012. Muscle function during takeoff and landing flight in the pigeon (*Columba livia*). *The Journal of Experimental Biology,* 215**,** 4104-4114.

Romijn, C. 1961. Some aspects of energy metabolism in birds. Proceedings of 2nd symposium on energy metabolism. *Wageningen***,** 49-58.

Ropert-Coudert, Y. & Wilson, R., P. 2005. Trends and perspectives in animal-attached remote sensing. *Frontiers in Ecology and the Environment,* 3**,** 437-444.

Rosser, B. W. C. & George, J. C. 1986. The avian pectoralis: Histochemical characterization and distribution of muscle fiber types. *Canadian Journal of Zoology,* 64**,** 1174-1185.

Rosser, B. W. C., Waldbillig, D. M., Wick, M. & Bandman, E. 1994. Muscle-fiber types in the pectoralis of the white pelican, a soaring bird. *Acta Zoologica,* 75**,** 329-336.

Rothe, H. J., Biesel, W. & Nachtigall, W. 1987. Pigeon flight in a wind tunnel. *Journal of Comparative Physiology B,* 157**,** 99-109.

Rüegg, J. C. & Stumpf, H. 1968. The coupling of poweroutput and myofibrillar atpase activity in glycerol-extracted insect fibrillar muscle at varying amplitude of ATP-driven oscillation. *Pflügers Archiv,* 305**,** 21-33.

Sachs, G. 2013. Wind effects on bounding flight. *Journal of Theoretical Biology,* 316**,** 35-41.

Sakamoto, K. Q., Takahashi, A., Iwata, T., Yamamoto, T., Yamamoto, M. & Trathan, P. N. 2013. Heart rate and estimated energy expenditure of flapping and gliding in black-browed albatrosses. *Journal of Experimental Biology,* 216, 3175-3182.

Santoyo, J., Azarcoya, W., Valencia, M., Torres, A. & Salas, J. 2016. Frequency analysis of a bumblebee (*Bombus impatiens*) wingbeat. *Pattern Analysis and Applications,* 19**,** 487-493.

Schiffner, I. & Srinivasan, M. V. 2016. Budgerigar flight in a varying environment: Flight at distinct speeds? *Biology Letters,* 12, Article No. 20160221.

Seebacher, F., Tallis, J. A. & James, R. S. 2014. The cost of muscle power production: Muscle oxygen consumption per unit work increases at low temperatures in *Xenopus laevis. The Journal of Experimental Biology,* 217**,** 1940.

Shaffer, S. A. 2011. A review of seabird energetics using the doubly labeled water method. *Comparative Biochemistry and Physiology Part A: Molecular & Integrative Physiology,* 158**,** 315-322.

Shepard, E. L. C., Wilson, R. P., Halsey, L. G., Quintana, F., Gómez Laich, A. & Gleiss, A. C. 2008. Derivation of body motion via appropriate smoothing of acceleration data. *Aquatic Biology,* 4, 235-241.

Smit, B. & Mckechnie Andrew, E. 2010. Avian seasonal metabolic variation in a subtropical desert: Basal metabolic rates are lower in winter than in summer. *Functional Ecology,* 24**,** 330-339.

Smith, N. P., Barclay, C. J. & Loiselle, D. S. 2005. The efficiency of muscle contraction. *Progress in Biophysics and Molecular Biology,* 88**,** 1-58.

Soman, A., Hedrick, T. L. & Biewener, A. A. 2005. Regional patterns of pectoralis fascicle strain in the pigeon *Columba livia* during level flight. *Journal of Experimental Biology,* 208**,** 771-786.

Sotavalta, O. 1953. Recordings of high wing-stroke and thoracic vibration frequency in some midges. *Biological Bulletin,* 104**,** 439-444.

Speakman, J. R. & Banks, D. 1998. The function of flight formations in greylag geese anser anser; energy saving or orientation? *Ibis,* 140**,** 280-287.

Spedding, G. R. 1986. The wake of a jackdaw (*Corvus monedula*) in slow flight. *Journal of Experimental Biology,* 125**,** 287-307.

Spedding, G. R. 1987a. The wake of a kestrel (*Falco tinnunculus*) in flapping flight. *Journal of Experimental Biology,* 127**,** 59-78.

Spedding, G. R. 1987b. The wake of a kestrel (*Falco tinnunculus*) in gliding flight. *Journal of Experimental Biology,* 127**,** 45-57.

Spedding, G. R., Rosén, M. & Hedenström, A. 2003. A family of vortex wakes generated by a thrush nightingale in free flight in a wind tunnel over its entire natural range of flight speeds. *Journal of Experimental Biology,* 206**,** 2313-2344.

Spivey, R. J. & Bishop, C. M. 2013. Interpretation of body-mounted accelerometry in flying animals and estimation of biomechanical power. *Journal of The Royal Society Interface,* 10, Article No. 20130404.

Steiger, G. J. & Rüegg, J. C. 1969. Energetics and "efficiency" in the isolated contractile machinery of an insect fibrillar muscle at various frequencies of oscillation. *Pflügers Archiv,* 307**,** 1-21.

Stevens, E. D. 1992. Use of plastic materials in oxygen-measuring systems. *Journal of Applied Physiology,* 72, 801-804.

Stevenson, R. D. & Josephson, R. K. 1990. Effects of operating frequency and temperature on mechanical power output from moth flight muscle. *Journal of Experimental Biology,* 149**,** 61-78.

Sur, M., Suffredini, T., Wessells, S. M., Bloom, P. H., Lanzone, M., Blackshire, S., Sridhar, S. & Katzner, T. 2017. Improved supervised classification of accelerometry data to distinguish behaviors of soaring birds. *PLOS ONE,* 12**,** Article No. e0174785.

Swank, D. M. 2012. Mechanical analysis of *Drosophila* indirect flight and jump muscles. *Methods,* 56**,** 69-77.

Tatner, P. & Bryant, D. M. 1986. Flight cost of a small passerine measured using doubly labeled water: Implications for energetics studies. *The Auk,* 103**,** 169-180.

Tobalske, B. & Dial, K. 1996. Flight kinematics of black-billed magpies and pigeons over a wide range of speeds. *Journal of Experimental Biology,* 199**,** 263-280.

Tobalske, B. W. 2000. Biomechanics and physiology of gait selection in flying birds. *Physiological And Biochemical Zoology,* 73**,** 736-750.

Tobalske, B. W. 2007. Biomechanics of bird flight. *Journal of Experimental Biology,* 210**,** 3135-3146.

Tobalske, B. W. 2010. Hovering and intermittent flight in birds. *Bioinspiration & Biomimetics,* 5**,** Article No. 045004.

Tobalske, B. W., Biewener, A. A., Warrick, D. R., Hedrick, T. L. & Powers, D. R. 2010. Effects of flight speed upon muscle activity in hummingbirds. *Journal of Experimental Biology,* 213**,** 2515-2523.

Tobalske, B. W. & Dial, K. P. 2000. Effects of body size on take-off flight performance in the Phasianidae (Aves). *Journal of Experimental Biology,* 203**,** 3319.

Tobalske, B. W., Hedrick, T. L. & Biewener, A. A. 2003a. Wing kinematics of avian flight across speeds. *Journal of Avian Biology,* 34**,** 177-184.

Tobalske, B. W., Hedrick, T. L., Dial, K. P. & Biewener, A. A. 2003b. Comparative power curves in bird flight. *Nature,* 421**,** 363-366.

Tobalske, B. W., Puccinelli, L. A. & Sheridan, D. C. 2005. Contractile activity of the pectoralis in the zebra finch according to mode and velocity of flap-bounding flight. *Journal of Experimental Biology,* 208**,** 2895-2901.

Tobalske, B. W., Warrick, D. R., Clark, C. J., Powers, D. R., Hedrick, T. L., Hyder, G. A. & Biewener, A. A. 2007. Three-dimensional kinematics of hummingbird flight. *Journal of Experimental Biology,* 210**,** 2368-2382.

Torre-Bueno, J. R. & Larochelle, J. 1978. The metabolic cost of flight in unrestrained birds. *Journal of Experimental Biology,* 75**,** 223-229.

Tregear, R. T. 1969. Mechanical properties of insect fibrillar muscle at large amplitudes of oscillation. *Proceedings of the Royal Society B,* 174**,** 33-50.

Trinh, M. & Syme, D. A. 2007. Effects of stretch on work and efficiency of frog (*Rana pipiens*) muscle. *Journal of Experimental Biology,* 210**,** 2843-2850.

Truong, K., Sawano, A., Mizuno, H., Hama, H., Tong, K. I., Mal, T. K., Miyawaki, A. & Ikura, M. 2001. Fret-based in vivo Ca^{2+} imaging by a new calmodulin-GFP fusion molecule. *Nature Structural and Molecular Biology,* 8**,** 1069.

Tucker, V. 1972. Metabolism during flight in the laughing gull, *Larus atricilla*. *American Journal of Physiology -- Legacy Content,* 222**,** 237-245.

Tucker, V. A. 1966. Oxygen consumption of a flying bird. *Science,* 154**,** 150-151.

Tucker, V. A. 1968. Respiratory exchange and evaporative water loss in the flying budgerigar. *Journal of Experimental Biology,* 48**,** 67-87.

Tucker, V. A. 1973. Bird metabolism during flight: Evaluation of a theory. *Journal of Experimental Biology,* 58**,** 689-709.

Turner, D. L. & Butler, P. J. 1988. The aerobic capacity of locomotory muscles in the tufted duck, *Aythya fuligula*. *Journal of Experimental Biology,* 135**,** 445-460.

Usherwood, J. R., Hedrick, T. L. & Biewener, A. A. 2003. The aerodynamics of avian take-off from direct pressure measurements in canada geese (*Branta canadensis*). *Journal of Experimental Biology,* 206**,** 4051-4056.

Usherwood, J. R., Hedrick, T. L., Mcgowan, C. P. & Biewener, A. A. 2005. Dynamic pressure maps for wings and tails of pigeons in slow, flapping flight, and their energetic implications. *Journal of Experimental Biology,* 208**,** 355-369.

Vandenabeele, S. P., Grundy, E., Friswell, M. I., Grogan, A., Votier, S. C. & Wilson, R. P. 2014. Excess baggage for birds: Inappropriate placement of tags on gannets changes flight patterns. *PLOS ONE,* 9, Article No. e92657.

Vigoreaux, J. 2007. *Nature's versatile engine: Insect flight muscle inside and out*, Springer Science & Business Media.

Walker, J. S., Li, X. & Buttrick, P. M. 2010. Analysing force–pCa curves. *Journal of Muscle Research and Cell Motility,* 31**,** 59-69.

Wang, Q., Zhao, C. & Swank, Douglas m. 2011. Calcium and stretch activation modulate power generation in drosophila flight muscle. *Biophysical Journal,* 101**,** 2207-2213.

Ward, S., Bishop, C. M., Woakes, A. J. & Butler, P. J. 2002. Heart rate and the rate of oxygen consumption of flying and walking barnacle geese (*Branta leucopsis*) and bar-headed geese (*Anser indicus*). *Journal of Experimental Biology,* 205**,** 3347-3356.

Ward, S., Möller, U., Rayner, J. M. V., Jackson, D. M., Bilo, D., Nachtigall, W. & Speakman, J. R. 2001. Metabolic power, mechanical power and efficiency during wind tunnel flight by the european starling *Sturnus vulgaris*. *Journal of Experimental Biology,* 204**,** 3311-3322.

Ward, S., Möller, U., Rayner, J. M. V., Jackson, D. M., Nachtigall, W. & Speakman, J. R. 2004. Metabolic power of european starlings *Sturnus vulgaris* during flight in a wind tunnel, estimated from heat transfer modelling, doubly labelled water and mask respirometry. *Journal of Experimental Biology,* 207**,** 4291-4298.

Warrick, D., Hedrick, T., Fernandez, M. J., Tobalske, B. & Biewener, A. 2012. Hummingbird flight. *Current Biology,* 22**,** 472-477.

Weimerskirch, H., Martin, J., Clerquin, Y., Alexandre, P. & Jiraskova, S. 2001. Energy saving in flight formation. *Nature,* 413**,** 697-698.

Welch Jr, K. C. 2011. The power of feeder-mask respirometry as a method for examining hummingbird energetics. *Comparative Biochemistry and Physiology Part A: Molecular & Integrative Physiology,* 158**,** 276-286.

Welch, K. C. & Altshuler, D. L. 2009. Fiber type homogeneity of the flight musculature in small birds. *Comparative Biochemistry and Physiology B-Biochemistry & Molecular Biology,* 152**,** 324-331.

Wells, D. J. 1993. Muscle performance in hovering hummingbirds. *Journal of Experimental Biology,* 178**,** 39-57.

White, T., Westgate, K., Wareham, N. J. & Brage, S. 2016. Estimation of physical activity energy expenditure during free-living from wrist accelerometry in UK adults. *PLOS ONE,* 11**,** Article No. e0167472.

Wieser, W. & Gnaiger, E. 1989. *Energy transformations in cells and organisms*, Thieme, Stuttgart.

Williams, H. J., Shepard, E. L. C., Duriez, O. & Lambertucci, S. A. 2015. Can accelerometry be used to distinguish between flight types in soaring birds? *Animal Biotelemetry,* 3**,** 1-11.

Williams, T. M., Wolfe, L., Davis, T., Kendall, T., Richter, B., Wang, Y., Bryce, C., Elkaim, G. H. & Wilmers, C. C. 2014. Instantaneous energetics of puma kills reveal advantage of felid sneak attacks. *Science,* 346**,** 81.

Williamson, M. R., Dial, K. P. & Biewener, A. A. 2001. Pectoralis muscle performance during ascending and slow level flight in mallards (*Anas platyrhynchos*). *Journal of Experimental Biology,* 204**,** 495-507.

Wilmers, C. C., Nickel, B., Bryce, C. M., Smith, J. A., Wheat, R. E. & Yovovich, V. 2015. The golden age of bio-logging: How animal-borne sensors are advancing the frontiers of ecology. *Ecology,* 96**,** 1741-1753.

Wilson, R. P. & Mcmahon, C. R. 2006. Measuring devices on wild animals: What constitutes acceptable practice? *Frontiers in Ecology and the Environment,* 4**,** 147-154.

Wilson, R. P., White, C. R., Quintana, F., Halsey, L. G., Liebsch, N. & Martin, G. R. 2006a. Moving towards acceleration for estimates of activity-specific metabolic rate in free-living animals: The case of the cormorant. *Journal of Animal Ecology,* 75, 1081-1090.

Wilson, R. P., White, C. R., Quintana, F., Halsey, L. G., Liebsch, N., Martin, G. R. & Butler, P. J. 2006b. Moving towards acceleration for estimates of activity-specific metabolic rate in free-living animals: The case of the cormorant. *Journal of Animal Ecology,* 75**,** 1081-1090.

Wilson, S. M., Hinch, S. G., Eliason, E. J., Farrell, A. P. & Cooke, S. J. 2013. Calibrating acoustic acceleration transmitters for estimating energy use by wild adult pacific salmon. *Comparative Biochemistry and Physiology Part A: Molecular & Integrative Physiology,* 164**,** 491-498.

Withers, P. C. 1977. Measurement of VO_2, VCO_2, and evaporative water loss with a flow-through mask. *Journal of Applied Physiology,* 42**,** 120-123.

Withers, P. C. 2001. Design, calibration and calculation for flow-through respirometry systems. *Australian Journal of Zoology,* 49**,** 445-461.

Woledge, R. C. 1968. The energetics of tortoise muscle. *The Journal of Physiology,* 197**,** 685-707.

Woledge, R. C., Curtain, N. A. & Homsher, E. 1985. *Energetic aspects of muscle contraction,* London, Academic Press.

Wright, S., Metcalfe, J. D., Hetherington, S. & Wilson, R. 2014. Estimating activity-specific energy expenditure in a teleost fish, using accelerometer loggers. *Marine Ecology Progress Series,* 496**,** 19-32.

Yost, M., Cooper, R. A. & Bremner, F. J. 1983. Fourier analyses: A mathematical and geometric explanation. *Behavior Research Methods & Instrumentation,* 15**,** 258-261.

Yue, D. T. 1987. Intracellular [Ca^{2+}] related to rate of force development in twitch contraction of heart. *American Journal of Physiology-Heart and Circulatory Physiology,* 252**,** 760-770.